

Effects of Geosynthetic Reinforcement Spacing on the Performance of Mechanically Stabilized Earth Walls

PUBLICATION NO. FHWA-RD-03-048

SEPTEMBER 2003



U.S. Department of Transportation
Federal Highway Administration

Research, Development, and Technology @ Seismicisolation
Turner-Fairbank Highway Research Center
6300 Georgetown Pike
McLean, VA 22101-2296

FOREWORD

This report is part of an effort to refine the design of Mechanically Stabilized Earth (MSE) walls with modular block facing. The study simulated the construction of a reinforced soil wall up to failure with two-dimensional finite difference computer program. Results of the study indicate that reinforcement spacing controls the failure mechanism and affects considerably the performance and internal stability of MSE walls. The results of the study infer that the beneficial effects of reinforcement spacing in MSE systems should be considered as a component of sound design.

Terry B. Chase
for T. Paul Teng, P.E.
Director, Office of Infrastructure
Research and Development

NOTICE

This document is disseminated under the sponsorship of the Department of Transportation in the interest of information exchange. The United States Government assumes no liability for its contents or use thereof. This report does not constitute a standard, specification, or regulation.

The United States Government does not endorse products or manufacturers. Trade and manufacturers' names appear in this report only because they are considered essential to the object of the document.

Technical Report Documentation Page

1. Report No. FFHWA-RD-03-048	2. Government Accession No.	3. Recipient's Catalog No.	
4. Title and Subtitle EFFECTS OF GEOSYNTHETIC REINFORCEMENT SPACING ON THE PERFORMANCE OF MECHANICALLY STABILIZED EARTH WALLS		5. Report Date September 2003	6. Performing Organization Code
7. Author(s) Christina Vulova and Dov Leshchinsky		8. Performing Organization Report No.	
9. Performing Organization Name and Address Department of Civil and Environmental Engineering University of Delaware Newark, DE 19711		10. Work Unit No.	
		11. Contract or Grant No.	
12. Sponsoring Agency Name and Address Office of Infrastructure Research and Development Federal Highway Administration 6300 Georgetown Pike McLean, VA 22101-2296		13. Type of Report and Period Covered Final Report, Feb. 1999-August 2000	
		14. Sponsoring Agency Code	
15. Supplementary Notes Contracting Officer's Technical Representative (COTR): M. T. Adams , HRDI-06			
<p>16. Abstract The behavior of mechanically stabilized earth walls (MSEW) with modular block facing and geosynthetic reinforcement was investigated with numerical models that simulate construction of the wall, layer by layer, until it fails under gravity loading. The two-dimensional finite difference program Fast Lagrangian Analysis of Continua (FLAC), version 3.4, Itasca 1998, was used to carry out the numerical analysis. The material properties were based on data reported in the literature, which represent typical values used in design practice. Failure mechanisms of MSEWs were identified as a function of geosynthetic spacing considering the effects of soil strength, reinforcement stiffness, connection strength, secondary reinforcement layers, and foundation stiffness. The effects of reinforcement length on reinforcement stresses and wall stability were also investigated. FLAC predictions were compared with the American Association of State Highway and Transportation Officials (AASHTO) design method. Additional numerical experiments were carried out to investigate the effects of some modeling parameters on wall response.</p> <p>Four failure modes of MSEW were identified: external, deep-seated, compound, and connection. The reinforcement spacing was identified as a major factor controlling the behavior of MSEWs. Two types of spacing were considered in studying the effects of spacing: small (less than or equal to 0.4 m) and large (larger than 0.4 m). Increasing reinforcement spacing decreased the wall stability and changed the predominant failure mode from external or deep-seated to compound and connection mode. Similar effects were identified when the soil strength, reinforcement stiffness, or foundation stiffness were decreased. Connection strength appeared to affect only the behavior of walls with large reinforcement spacing, i.e., increased connection strength, decreased wall displacements, improved wall stability, and changed failure mode. Similar effects were identified when secondary reinforcement layers were introduced in a model with large reinforcement spacing. Increased reinforcement length improved wall stability and decreased wall displacements and reinforcement forces.</p> <p>A comparison between FLAC predictions and AASHTO calculations demonstrated a good agreement. The comparisons indicated that the existing design method could distinguish the modes of failure identified by FLAC analysis, especially those due to external stability. However, AASHTO disregards the effect of reinforcement spacing and thus, considers an external wedge always to develop internally.</p>			
17. Key Words block walls, external stability, failure mechanism, FLAC, geosynthetic reinforcement, interface effects, internal stability, MSE walls		<p>18. Distribution Statement No restrictions. This document is available to the public through the National Technical Information Service, Springfield, VA 22161.</p>	
19. Security Classif. (of this report) Unclassified	20. Security Classif. (of this page) Unclassified	21. No of Pages 226	22. Price

SI* (MODERN METRIC) CONVERSION FACTORS

APPROXIMATE CONVERSIONS TO SI UNITS

APPROXIMATE CONVERSIONS FROM SI UNITS

Symbol	When You Know	Multiply By	To Find	Symbol	When You Know	Multiply By	To Find	Symbol
LENGTH								
AREA								
in	inches	25.4	millimeters	mm	mm	millimeters	0.039	inches
ft	feet	0.305	meters	m	m	meters	3.26	feet
yd	yards	0.914	meters	m	m	meters	1.09	yards
mi	miles	1.61	kilometers	km	km	kilometers	0.621	miles
VOLUME								
in ³	square inches	645.2	square millimeters	mm ²	mm ²	square millimeters	0.0016	square inches
ft ³	square feet	0.093	square meters	m ²	m ²	square meters	10.764	square feet
yd ³	square yards	0.636	square meters	m ²	m ²	square meters	1.195	square yards
ac	acres	0.405	hectares	ha	ha	hectares	2.47	acres
mi ³	square miles	2.59	square kilometers	km ²	km ²	square kilometers	0.366	square miles
MASS								
oz	ounces	26.35	milliliters	ml	ml	milliliters	0.034	fluid ounces
lb	pounds	0.454	liters	L	L	liters	0.264	gallons
T	short tons (2000 lb)	0.907	cubic meters	m ³	m ³	cubic meters	35.71	cubic feet
			cubic meters	m ³	m ³	cubic meters	1.307	cubic yards
TEMPERATURE (exact)								
°F	Fahrenheit temperature	5(F-32)/9 or (F-32)/1.8	Celcius temperature	°C	°C	Celcius temperature	1.8C + 32	Fahrenheit temperature
ILLUMINATION								
fc	foot-candles	10.76	lux	lx	lx	lux	0.0929	foot-candles
fl	foot-Lamberts	3.426	candela/m ²	cd/m ²	cd/m ²	candela/m ²	0.2919	foot-Lamberts
FORCE and PRESSURE or STRESS								
lbf	poundforce	4.45	newtons	N	N	newtons	0.225	poundforce
lbf/in ²	poundforce per square inch	6.89	kilopascals	kPa	kPa	kilopascals	0.145	poundforce per square inch ,
FORCE and PRESSURE or STRESS								

* SI is the symbol for the International System of Units. Appropriate rounding should be made to comply with Section 4 of ASTM E380.

(Revised September 1993)

TABLE OF CONTENTS

LIST OF FIGURES	v
LIST OF TABLES.....	xiii

Chapter

1 INTRODUCTION	1
2 BACKGROUND	3
2.1 Review of Current Design Practice of MSEWs with Respect to Reinforcement Spacing.....	3
2.2 Program FLAC: Theoretical Background and General Features.....	7
2.3 Literature Review	8
3 NUMERICAL ANALYSIS.....	11
3.1 Scope	11
3.2 Numerical Model.....	11
3.2.1 Modeling Methodology	11
3.2.2 Model Description	12
3.2.3 Material Properties	16
3.3 Scope of Parametric Studies	18
4 RESULTS.....	45
4.1 Failure Mechanisms of MSEWs.....	45
4.1.1 Description of Identified Failure Mechanisms	46
4.1.1.1 External Mode of Failure.....	46
4.1.1.2 Deep-Seated Mode of Failure.....	47
4.1.1.3 Compound Mode of Failure	48
4.1.1.4 Connection Mode of Failure.....	48
4.1.1.5 Mixed Modes of Failure	49
4.1.2 Effects of Geosynthetic Spacing on Failure Mechanisms	51
4.1.3 Effects of Soil Strength on Failure Mechanisms as Function of Geosynthetic Spacing.....	52
4.1.4 Effects of Reinforcement Stiffness on Failure Mechanisms as Function of Geosynthetic Spacing	52
4.1.4.1 High Strength Soil	53
4.1.4.2 Medium Strength Soil.....	53
4.1.4.3 Low Strength Soil.....	54

4.1.5	Effects of Connection Strength on Failure Mechanisms as Function of Geosynthetic Spacing.....	56
4.1.5.1	Cases with Small Reinforcement Spacing	56
4.1.5.2	Cases with Large Reinforcement Spacing	57
4.1.6	Effects of Foundation Stiffness on Failure Mechanisms as Function of Geosynthetic Spacing.....	58
4.2	Effects of Reinforcement Length on Reinforcement Stresses and Wall Stability.....	61
4.3	Effects of Secondary Reinforcement Layers on Connection Loads and Wall Stability	62
4.4	Influence of Soil Dilatancy on Model Response	64
5	COMPARISON WITH EXISTING DESIGN PRACTICE.....	165
5.1	Analysis of Baseline Cases using AASHTO	165
5.2	Slope of Slip Planes.....	168
5.3	Stresses	168
6	IMPLICATIONS TO DESIGN	187
7	CONCLUSIONS AND RECOMMENDATIONS	189
	APPENDIX: TYPICAL INPUT DATA FILE.....	195
	REFERENCES	211

LIST OF FIGURES

Figure

3.1	Numerical Model Components.....	20
3.2	Schematic of Modeling of Construction Sequence of Wall with Reinforcement Spacing Equal to 0.4 m.....	21
3.3	Definition of: (a) Failure State; (b) Critical State; (c) Stable State	22
3.4	Typical Numerical Grid.....	23
3.5	Grid Definition: (a) Model Zones with Respect to Grid Generation; (b) Grid of Modular Blocks in the Current Model; (c) Grid of Modular Blocks in Early Versions of the Model.	24
3.6	Boundary Effects on Model Response: Horizontal Displacements along Vertical Section A Located 0.1 m behind the Facing.....	25
3.7	Boundary Effects on Model Response: Stress Distributions along Vertical Section A Located 0.15 m behind the Facing.....	26
3.8	Types of Interfaces at the Blocks.....	27
3.9	Baseline Cases: (a) Number of Calculation Steps Necessary to Equilibrate Each Layer; (b) Maximum Cumulative Displacement during Wall Construction	28
3.10	Effects of FLAC Equilibrium Ratio Limit on Model Response of Case 1 ($s=0.2$ m, $l=1.5$ m): (a) Number of Calculation Steps; (b) Maximum Cumulative Displacement.	29
3.11	Effects of FLAC Step Limit on Model Response of Case 12 ($s=0.2$ m, $l=1.5$ m): (a) Number of Calculation Steps; (b) Maximum Cumulative Displacement.	30
3.12	Reinforcement Layout with Primary and Secondary Layers for Case 7 ($s=0.6/0.2$ m).	31
3.13	Some of the Executed Numerical Runs.....	32

4.1	Critical Wall Height and Prevailing Mode of Failure: (a) Cases with Very Stiff Foundation; (b) Cases with Baseline Foundation.....	65
4.2	Change of Critical Wall Height with Respect to Soil Strength: (a) Cases with Very Stiff Foundation; (b) Cases with Baseline Foundation.....	67
4.3	Slip Surface Types: (a) External Slip Surface; (b) Deep-Seated Slip Surface; (c) Compound Slip Surface; (d) Internal Slip Surface	68
4.4	Definition of Vertical Sections A, B, and C along which Stress and Displacement Distributions Were Investigated.	69
4.5	State of Soil for Case 1 ($s=0.2$ m, $l=1.5$ m): (a) Failure State ($h=8.6$ m, $l/h=0.17$); (b) Critical State ($h=6.6$ m, $l/h=0.23$).	70
4.6	Displacement Vectors for Case 1 ($s=0.2$ m, $l=1.5$ m): (a) Failure State ($h=8.6$ m, $l/h=0.17$); (b) Critical State ($h=6.6$ m, $l/h=0.23$).	71
4.7	Distorted Grid for Case 1 ($s=0.2$ m, $l=1.5$ m): (a) Failure State ($h=8.6$ m, $l/h=0.17$); (b) Critical State ($h=6.6$ m, $l/h=0.23$).	72
4.8	Cumulative Horizontal Displacements for Case 1 ($s=0.2$ m, $l=1.5$ m): (a) Failure State ($h=8.6$ m, $l/h=0.17$); (b) Critical State ($h=6.6$ m, $l/h=0.23$).	73
4.9	Axial Force Distribution in Reinforcement for Case 1 ($s=0.2$ m, $l=1.5$ m): (a) Failure State ($h=8.6$ m, $l/h=0.17$); (b) Critical State ($h=6.6$ m, $l/h=0.23$).	74
4.10	State of Soil for Case 1 ($s=0.4$ m, $l=1.5$ m): (a) Failure State ($h=8.2$ m, $l/h=0.18$); (b) Critical State ($h=6.0$ m, $l/h=0.25$).	76
4.11	State of Soil for Case 4 ($s=0.2$ m, $l=1.5$ m): (a) Failure State ($h=7.0$ m, $l/h=0.21$); (b) Critical State ($h=5.6$ m, $l/h=0.27$).	77
4.12	State of Soil for Case 9 ($s=0.2$ m, $l=1.5$ m): (a) Failure State ($h=8.2$ m, $l/h=0.18$); (b) Critical State ($h=6.6$ m, $l/h=0.23$).	78
4.13	State of Soil for Case 11 ($s=0.2$ m, $l=1.5$ m): (a) Failure State ($h=7.2$ m, $l/h=0.21$); (b) Critical State ($h=6.0$ m, $l/h=0.25$).	79
4.14	State of Soil for Case 12 ($s=0.2$ m, $l=1.5$ m): (a) Failure State ($h=9.4$ m, $l/h=0.16$); (b) Critical State ($h=6.6$ m, $l/h=0.23$).	80

4.15	State of Soil for Case 10 ($s=0.2$ m, $l=1.5$ m): (a) Failure State ($h=4.4$ m, $l/h=0.34$); (b) Critical State ($h=3.2$ m, $l/h=0.47$).	81
4.16	Displacement Vectors for Case 10 ($s=0.2$ m, $l=1.5$ m): (a) Failure State ($h=4.4$ m, $l/h=0.34$); (b) Critical State ($h=3.2$ m, $l/h=0.47$).	82
4.17	Distorted Grid for Case 10 ($s=0.2$ m, $l=1.5$ m): (a) Failure State ($h=4.4$ m, $l/h=0.34$); (b) Critical State ($h=3.2$ m, $l/h=0.47$).	83
4.18	Horizontal Displacements for Case 10 ($s=0.2$ m, $l=1.5$ m) at Failure State ($h=4.4$ m, $l/h=0.34$) and Critical State ($h=3.2$ m, $l/h=0.47$).	84
4.19	Axial Force Distribution in Reinforcement for Case 10 ($s=0.2$ m, $l=1.5$ m): (a) Failure State ($h=4.4$ m, $l/h=0.34$); (b) Critical State ($h=3.2$ m, $l/h=0.47$).	85
4.20	State of Soil for Case 5 ($s=0.2$ m, $l=1.5$ m): (a) Failure State ($h=5.4$ m, $l/h=0.28$); (b) Critical State ($h=4.2$ m, $l/h=0.36$).	87
4.21	State of Soil for Case 8–1 ($s=0.4$ m, $l=1.5$ m): (a) Failure State ($h=8.0$ m, $l/h=0.19$); (b) Critical State ($h=5.0$ m, $l/h=0.30$).	88
4.22	Displacement Vectors for Case 8–1 ($s=0.4$ m, $l=1.5$ m): (a) Failure State ($h=8.0$ m, $l/h=0.19$); (b) Critical State ($h=5.0$ m, $l/h=0.30$).	89
4.23	Distorted Grid for Case 8–1 ($s=0.4$ m, $l=1.5$ m): (a) Failure State ($h=8.0$ m, $l/h=0.19$); (b) Critical State ($h=5.0$ m, $l/h=0.30$).	90
4.24	Horizontal Displacements for Case 8–1 ($s=0.4$ m, $l=1.5$ m) at Failure ($h=8.0$ m, $l/h=0.19$) and Critical State ($h=5.0$ m, $l/h=0.30$).	91
4.25	Axial Force Distribution in Reinforcement for Case 8–1 ($s=0.4$ m, $l=1.5$ m): (a) Failure State ($h=8.0$ m, $l/h=0.19$); (b) Critical State ($h=5.0$ m, $l/h=0.30$).	92
4.26	State of Soil for Case 2 ($s=0.4$ m, $l=1.5$ m): (a) Failure State ($h=6.0$ m, $l/h=0.25$); (b) Critical State ($h=4.4$ m, $l/h=0.34$).	94
4.27	State of Soil for Case 3 ($s=0.2$ m, $l=1.5$ m): (a) Failure State ($h=4.2$ m, $l/h=0.36$); (b) Critical State ($h=4.0$ m, $l/h=0.38$).	95
4.28	State of Soil for Case 7 ($s=0.6/0.2$ m, $l=1.5$ m): (a) Failure State ($h=6.0$ m, $l/h=0.25$); (b) Critical State ($h=5.0$ m, $l/h=0.30$).	96

4.29	State of Soil for Case 8–2 ($s=0.4$ m, $l=1.5$ m): (a) Failure State ($h=5.4$ m, $l/h=0.28$); (b) Critical State ($h=3.2$ m, $l/h=0.47$).	97
4.30	State of Soil for Case 8–3 ($s=0.2$ m, $l=1.5$ m): (a) Failure State ($h=5.0$ m, $l/h=0.30$); (b) Critical State ($h=2.2$ m, $l/h=0.68$).	98
4.31	State of Soil for Case 12 ($s=0.6$ m, $l=1.5$ m): (a) Failure State ($h=6.0$ m, $l/h=0.25$); (b) Critical State ($h=4.6$ m, $l/h=0.33$).	99
4.32	State of Soil for Case 2 ($s=0.6$ m, $l=1.5$ m): (a) Failure State ($h=4.6$ m, $l/h=0.33$); (b) Critical State ($h=2.6$ m, $l/h=0.58$).	100
4.33	Displacement Vectors for Case 2 ($s=0.6$ m, $l=1.5$ m): (a) Failure State ($h=4.6$ m, $l/h=0.33$); (b) Critical State ($h=2.6$ m, $l/h=0.58$).	101
4.34	Distorted Grid for Case 2 ($s=0.6$ m, $l=1.5$ m): (a) Failure State ($h=4.6$ m, $l/h=0.33$); (b) Critical State ($h=2.6$ m, $l/h=0.58$).	102
4.35	Horizontal Displacements for Case 2 ($s=0.6$ m, $l=1.5$ m) at Failure State ($h=4.6$ m, $l/h=0.33$) and Critical State ($h=2.6$ m, $l/h=0.58$).	103
4.36	Axial Force Distribution in Reinforcement for Case 2 ($s=0.6$ m, $l=1.5$ m): (a) Failure State ($h=4.6$ m, $l/h=0.33$); (b) Critical State ($h=2.6$ m, $l/h=0.58$).	104
4.37	State of Soil for Case 4 ($s=0.6$ m, $l=1.5$ m): (a) Failure State ($h=5.4$ m, $l/h=0.28$); (b) Critical State ($h=3.8$ m, $l/h=0.39$).	106
4.38	Case 1 ($s=0.4$ m, $l=1.5$ m, $h=5.0$ m): (a) State of Soil; (b) Axial Force Distribution in Reinforcement.	107
4.39	Connection Force and Maximum Force in Reinforcement for Case 1 ($s=0.4$ m, $h=5.0$ m, BR) and Case 8–1 ($s=0.4$ m, $h=5.0$ m, DR): Effects of Reinforcement Stiffness.	109
4.40	Horizontal Displacements along Section A: Comparison with Respect to Reinforcement Stiffness.	110
4.41	State of Soil for Cases 2 and 8–2 ($s=0.4$ m, $h=3.2$ m, $l=1.5$ m): (a) Case 2 (BR); (b) Case 8–2 (DR).	111
4.42	Axial Force Distributions in Reinforcement for Cases 2 and 8–2 ($s=0.4$ m, $h=3.2$ m, $l=1.5$ m): (a) Case 2 (BR); (b) Case 8–2 (DR).	112

4.43	Connection Force and Maximum Force in Reinforcement for Case 2 ($s=0.4$ m, $h=3.2$ m, BR) and Case 8–2 ($s=0.4$ m, $h=3.2$ m, DR): Effects of Reinforcement Stiffness.....	114
4.44	State of Soil for Cases 3 and 8–3 ($s=0.2$ m, $h=2.2$ m, $l=1.5$ m): (a) Case 3 (BR); (b) Case 8–3 (DR).	115
4.45	Axial Force Distributions in Reinforcement for Cases 3 and 8–3 ($s=0.2$ m, $h=2.2$ m, $l=1.5$ m): (a) Case 3 (BR); (b) Case 8–3 (DR).....	116
4.46	Connection Force and Maximum Force in Reinforcement for Case 3 ($s=0.2$ m, $h=2.2$ m, BR) and Case 8–3 ($s=0.2$ m, $h=2.2$ m, DR): Effects of Reinforcement Stiffness.....	118
4.47	Effects of Connection Strength on Connection Force for Cases with Small Reinforcement Spacing ($s=0.2$ m).....	119
4.48	Effects of Connection Strength on Maximum Force in Reinforcement for Cases with Small Reinforcement Spacing ($s=0.2$ m).	120
4.49	Effects of Connection Strength on Horizontal Displacements along Section A for Cases with Small Reinforcement Spacing ($s=0.2$ m).....	121
4.50	Effects of Connection Strength on Connection Force and Maximum Force in Reinforcement for Cases with Large Reinforcement Spacing ($s=0.6$ m).	122
4.51	Axial Force Distribution in Reinforcement for Case 12 ($l=1.5$ m): (a) $s=0.2$ m, $h=6.6$ m; (b) $s=0.6$ m, $h=2.6$ m.	123
4.52	Effects of Connection Strength on Horizontal Displacements along Section A for Cases with Large Reinforcement Spacing ($s=0.6$ m).....	125
4.53	Effects of Foundation Strength on Critical Wall Height.	126
4.54	Effects of Foundation Strength for Cases 1, 4, and 10 ($s=0.2$ m, $l=1.5$ m $h=3.2$ m) on: (a) Horizontal Displacements along Section A; (b) Connection Force and Maximum Axial Force in Reinforcement; (c) Stresses along Section A.	128
4.55	Stress Distributions along Section A for Critical and Stable States of Case 1 ($s=0.2$ m, $h=6.6$ m, $l/h=0.23$ –0.5).....	131

4.56	Stress Distributions along Section C for Critical and Stable States of Case 1 ($s=0.2$ m, $h=6.6$ m, $l/h=0.23-0.5$).....	132
4.57	Horizontal Displacements along Sections A and B for Critical and Stable States of Case 1 ($s=0.2$ m, $h=6.6$ m, $l/h=0.23-0.5$).....	133
4.58	Maximum Axial Force in Reinforcement for Critical and Stable States of Case 1 ($s=0.2$ m, $h=6.6$ m, $l/h=0.23-0.5$).....	134
4.59	Connection Force for Critical and Stable States of Case 1 ($s=0.2$ m, $h=6.6$ m, $l/h=0.23-0.5$).....	135
4.60	Stress Distributions along Section A for Critical and Stable States of Case 8-1 ($s=0.4$ m, $h=5.0$ m, $l/h=0.3-0.5$).....	136
4.61	Stress Distributions along Section C for Critical and Stable States of Case 8-1 ($s=0.4$ m, $h=5.0$ m, $l/h=0.3-0.5$).....	137
4.62	Horizontal Displacements along Sections A and B for Critical and Stable States of Case 8-1 ($s=0.4$ m, $h=5.0$ m, $l/h=0.3-0.5$).....	138
4.63	Connection Force and Maximum Axial Force in Reinforcement for Critical and Stable States of Case 8-1 ($s=0.4$ m, $h=5.0$ m, $l/h=0.3-0.5$).....	139
4.64	Stress Distributions along Section A for Critical and Stable States of Case 10 ($s=0.2$ m, $h=3.2$ m, $l/h=0.47-0.7$).....	140
4.65	Stress Distributions along Section C for Critical and Stable States of Case 10 ($s=0.2$ m, $h=3.2$ m, $l/h=0.47-0.7$).....	141
4.66	Horizontal Displacements along Sections A and B for Critical and Stable States of Case 10 ($s=0.2$ m, $h=3.2$ m, $l/h=0.47-0.7$).....	142
4.67	Connection Force and Maximum Axial Force in Reinforcement for Critical and Stable States of Case 10 ($s=0.2$ m, $h=3.2$ m, $l/h=0.47-0.7$).....	143
4.68	Effects of Secondary Reinforcement: Axial Force Distribution in Reinforcement for Case 7 ($s=0.6/0.2$ m), (a) $h=2.6$ m; (b) $h=5.0$ m.....	144
4.69	Effects of Secondary Reinforcement: State of Soil for Case 7 ($h=2.6$ m, $s=0.6/0.2$ m).....	146

4.70	Effects of Secondary Reinforcement: Horizontal Displacements along Section A for Cases 2 and 7 ($h=2.6$ m).....	147
4.71	Effects of Secondary Reinforcement: Connection Force and Maximum Axial Force in Reinforcement for Cases 2 and 7 ($h=2.6$ m).....	148
5.1	Maximum Force in Reinforcement: Comparison of FLAC and AASHTO Results for Case 1 ($s=0.4$ m) and Case 2 ($s=0.6$ m).....	170
5.2	Maximum Force in Reinforcement: Comparison of FLAC and AASHTO Results for Case 8–1 ($s=0.4$ m) and Case 10 ($s=0.2$ m).....	171
5.3	Comparison of FLAC and AASHTO Results for Case 8–1 ($s=0.4$ m, $h=5.0$ m, $l=1.5$ m): (a) MSEW 1.1 Analysis: Critical Slip Surface from Compound Stability Analysis; (b) FLAC Analysis: Failure Zones Distribution at the Critical State.....	172
5.4	Comparison of FLAC and AASHTO Results for Case 10 ($s=0.2$ m, $h=3.2$ m, $l=1.5$ m): (a) MSEW 1.1 Analysis: Critical Slip Surface from Deep-Seated Stability Analysis; (b) FLAC Analysis: Failure Zones Distribution at the Critical State.....	173
5.5	Stress Distributions along Sections A and C for Failure State of Case 1 ($s=0.2$ m, $h=8.6$ m, $l/h=0.17$).....	174
5.6	Stress Distributions along Sections A and C for Critical State of Case 1 ($s=0.2$ m, $h=8.6$ m, $l/h=0.17$).....	175
5.7	Stress Distributions along Sections A and C for Failure State of Case 2 ($s=0.6$ m, $h=4.6$ m, $l/h=0.33$).....	176
5.8	Stress Distributions along Sections A and C for Critical State of Case 2 ($s=0.6$ m, $h=4.6$ m, $l/h=0.33$).....	177
5.9	Stress Distributions along Sections A and C for Failure State of Case 8–1 ($s=0.4$ m, $h=8.0$ m, $l/h=0.19$).....	178
5.10	Stress Distributions along Sections A and C for Critical State of Case 8–1 ($s=0.4$ m, $h=8.0$ m, $l/h=0.19$).....	179
5.11	Stress Distributions along Sections A and C for Failure State of Case 10 ($s=0.2$ m, $h=4.4$ m, $l/h=0.34$).....	180

5.12	Stress Distributions along Sections A and C for Critical State of Case 10 ($s=0.2$ m, $h=4.4$ m, $l/h=0.34$).....	181
------	--	-----

LIST OF TABLES

Table

3.1	List of Model Variables.....	33
3.2	Major Results for Case 1 ($s=0.2$ m, $h=6.6$ m, $l=1.5$ m) for Different FLAC Equilibrium Ratio Limits.....	34
3.3	Properties of Modeled Soil: Strength and Elastic Values.....	34
3.4	Properties of Modeled Soil Stiffness.....	35
3.5	Model Parameters and Properties of Facing.....	35
3.6	Modeling of Reinforcement Stiffness.....	36
3.7	Modeling of Block-Block and Block-Reinforcement Interfaces.....	37
3.8	Parametric Study Cases.....	38
3.9	General Information for Runs Corresponding to Failure States.....	40
3.10	General Information for Runs Corresponding to Critical States.....	42
4.1	Summary of Results Identifying Failure Modes.....	149
4.2	Critical Wall Height and Prevailing Mode of Failure.....	152
4.3	Maximum Axial Force in Reinforcement.....	153
4.4	Maximum Connection Force.....	155
4.5	Effects of Reinforcement Stiffness on Model Response: Comparison of Case 1 ($s=0.4$ m) and Case 8–1 ($s=0.4$ m).	157
4.6	Effects of Reinforcement Stiffness of Model Response: Comparison of Case 2 ($s=0.4$ m) and Case 8–2 ($s=0.4$ m).	158
4.7	Effects of Reinforcement Stiffness on Model Response: Comparison of Case 3 ($s=0.2$ m) and Case 8–3 ($s=0.2$ m).	159

4.8	Effects of Connection Strength on Model Response: Cases with Small Reinforcement Spacing ($s=0.2$ m)	160
4.9	Effects of Connection Strength on Model Response: Cases with Large Reinforcement Spacing ($s=0.6$ m)	161
4.10	Effects of Foundation Stiffness on Model Response: Comparison of Cases 1, 4, and 10 ($s=0.2$ m)	162
4.11	Effects of Secondary Reinforcement on Model Response.....	163
4.12	Effects of Soil Dilatancy on Model Response: Comparison of Case 1 ($s=0.2$ m) and Case 11 ($s=0.2$ m).	164
5.1	Input Data for AASHTO Analysis Using MSEW 1.1 Program.	182
5.2	Results from AASHTO Analysis Using MSEW 1.1 Program.	183
5.3	Slope of Slip Planes.....	184

CHAPTER 1. INTRODUCTION

Mechanically stabilized earth walls (MSEWs) are retaining structures constructed of a facing and selected fill material that is stabilized with embedded reinforcement elements. The interaction of the backfill material and the reinforcement form a flexible, coherent block that can sustain significant loads and movements. In principle, the reinforced soil is analogous to the reinforced concrete, and it is logical to assume that the behavior of reinforced soil will depend on the “soil-reinforcement ratio,” expressed in terms of reinforcement spacing.

The existing American Association of State Highway and Transportation Officials (AASHTO) design methodology of MSEWs is based on internal and external stability analysis using limit equilibrium methods. Internal stability calculations are based on the assumption that the most critical slip surface will develop through the reinforced soil. Therefore, in many cases, the internal stability analysis controls the wall design, because of the unnecessarily large reinforcement length specified in the preliminary sizing of the wall. This sizing corresponds to a length-to-height ratio of at least 0.7. However, internal failure can occur only when the reinforcement spacing is relatively large. The relation between the reinforcement spacing and the failure mode is not considered in current design, although there is ample evidence that closely spaced reinforcement may lead to a composite material. That is, no soil plasticity (or failure) develops within the reinforced zone. This may lead to an overly conservative design of MSEWs with continuous facing. Conversely, it may lead to a nonconservative design of MSEWs with modular block facing. The effects of reinforcement stiffness, connection strength, secondary reinforcement layers, and foundations stiffness on failure mechanisms are not involved directly in the current design of MSEWs.

Presented are the results of numerical analysis on the behavior of MSEWs with modular block facing and geosynthetic reinforcement, considering the effects of reinforcement spacing, soil strength, reinforcement stiffness, connection strength, reinforcement length, secondary reinforcement layers, and foundation stiffness. The two-dimensional finite difference program Fast Langrangian Analysis of Continua (FLAC) (Version 3.40, Itasca 1998) was used to conduct the numerical analysis. The material properties are based on data reported in the literature, which represent typical values used in design practice. A set of computer runs was conducted to identify failure mechanisms of MSEWs as a function of geosynthetic spacing. The effects of soil strength, reinforcement stiffness, connection strength, secondary reinforcement layers, and foundation stiffness on failure mechanisms were identified with respect to geosynthetic spacing. Numerical analysis also was conducted to investigate the effects of reinforcement length on reinforcement stresses and wall stability. FLAC

predictions were compared with AASHTO design method. Additional numerical experiments were conducted to investigate the effects of some modeling parameters on the wall response.

The wall behavior was investigated for all relevant reinforcement spacings in the range of 0.2–1.0 m. Soil properties were changed with respect to soil strength (three types: high, medium, and low strength soil) and soil stiffness (two types: baseline and very stiff soil). Three types of connection strength were modeled: frictional connection with low strength, frictional connection with baseline strength, and structural connection. Reinforcement stiffness was modeled to represent baseline reinforcement (BR) and ductile reinforcement (DR).

The results of this work should be viewed only qualitatively. They represent a comprehensive numerical analysis of various idealized cases. However, this work provides a perspective on the effects of reinforcement spacing with clear design implications. Before applying the results to design, the numerical observation must be determined. Therefore, results can be viewed as important guidance toward more focused research.

CHAPTER 2. BACKGROUND

2.1 Review of Current Design Practice of MSEWs with Respect to Reinforcement Spacing

In this chapter, an outline of the design methodology of MSEWs with geosynthetic reinforcement under static conditions is presented in accordance with AASHTO, Section 5.8, 1998 (AASHTO 98). The details of AASHTO design are given in "Demonstration Project No. 82: Mechanically Stabilized Earth Walls and Reinforced Soil Slopes, Design and Construction Guidelines," Federal Highway Administration (FHWA), 1997.

Current design of an MSEW is a multistep process based on limit equilibrium analysis (AASHTO 1998, Elias and Christopher 1997). Based on a detailed analysis of specific site constraints and project requirements (such as wall geometry, performance requirements, constructability, aesthetic, and environmental issues), a particular MSEW system is selected. The most important input design parameters of an MSEW are the type of reinforcing elements and facing. Design of a particular MSEW consists of the following steps:

- Specification of the design input data.
- Preliminary sizing.
- External stability analysis.
- Internal stability analysis.
- Connection design.
- Deformation and settlement calculations.
- Specifications based on the design output.

The following input information is necessary to start the design:

- Wall Parameters: total height (H); face inclination (i); type of facing (modular blocks, precast concrete, wrapped reinforcement, etc.); type of reinforcing elements (metal strips, bar mats, geogrid, geotextile, etc.).
- Soil Parameters: layout/geology of the construction site; angle of internal friction (ϕ) and unit weight (γ) of the backfill material; shear strength parameters and unit weight of the retained soil; shear strength parameters and unit weight of the foundation soil.
- Design Criteria: settlement requirements; factors of safety; design life; construction sequence; etc.

Preliminary Sizing

Based on field observations of existing MSEWs, the prescribed minimum length of the reinforcement is:

$$L \geq \begin{cases} 0.7H \\ 2.5 \text{ m} \end{cases} \quad (2.1)$$

It is used as a preliminary width of a MSEW in the stability analysis.

External Stability Analysis

External stability analysis of an MSEW is similar to the stability analysis of conventional retaining walls. It verifies whether the dimensions of an MSEW ensure its global stability under the loads induced by the retained soil. The reinforced mass is considered as a solid block, and only failure surfaces through the adjacent retained soil are considered. For a given wall, the external stability checks and the corresponding minimum factors of safety are as follows:

- Direct sliding along the interface with the foundation soil ($FS_{sl} \geq 1.5$).
- Eccentricity ($e \leq L/6$ or $L/4$) or overturning ($FS_o \geq 2.0$).
- Bearing capacity (Meyerhof approach, $FS_{bc} \geq 2.0$).
- Deep-seated stability ($FS_{ds} \geq 1.3$).

The direct sliding, eccentricity, and bearing capacity checks are based on the wedge failure mechanism. Deep-seated stability check is based on the rotational failure mechanism. As a result of external stability analysis, the total length of the reinforcement is verified and may be increased if necessary.

Internal Stability Analysis

Internal stability analysis investigates the possibility of collapse within the reinforced soil due to insufficient strength or embedment length of the reinforcement. Planar slip surfaces developed through the toe and the reinforcement are investigated. If the wall front batter is greater than 10 degrees, the inclination of the slip surfaces is defined by Coulomb's earth pressure theory. If the wall front batter is less than or equal to 10 degrees, the inclination of the slip surfaces is defined by Rankine's earth pressure theory. Internal stability analysis yields the spacing and strength parameters of reinforcement necessary to ensure the integrity and internal stability of the reinforced soil. The major calculations are:

- Check against reinforcement strength
- Check against reinforcement pullout.

The check against reinforcement breakage is done at each level of reinforcement. It must ensure that the required tensile resistance of the reinforcement is less than the allowable long-term strength:

$$T_{\max} \leq T_{al} R_c \quad (2.2)$$

where: T_{\max} is the maximum required tensile force needed to resist the active lateral earth pressure at the face of the wall; T_{al} is the allowable tensile capacity per unit width of reinforcement; R_c is the coverage ratio. The allowable long-term tensile strength is calculated according to the type of the reinforcement. For geosynthetic reinforcement, the allowable tensile strength takes into account the reduction of the ultimate strength due to creep, degradation, and installation damage.

The capacity of the reinforcement to develop the required tensile resistance depends on its pullout resistance. The pullout resistance of the reinforcement is defined by the soil-reinforcement interaction and the anchorage length into stable soil. The check against reinforcement pullout is:

$$T_{\max} \leq \frac{P_r \cdot R_c}{FS_{po}} \quad (2.3)$$

$$P_r = F^* \cdot \alpha \cdot \sigma'_v \cdot L_e \cdot C \quad (2.4)$$

where: T_{\max} is the maximum required tensile force needed to resist the active lateral earth pressure at the face of the wall; P_r is the pullout resistance; R_c is the coverage ratio; FS_{po} is the safety factor against pullout; F^* is a pullout resistance factor, defined by the soil-reinforcement interaction; α is a scale effect correction factor taking into account the nonuniform mobilization of the pullout resistance along the length of the reinforcement; σ'_v is the effective vertical stress at the reinforcement level; L_e is the anchorage length of reinforcement; and C is the effective perimeter of reinforcement.

Usually in design, both calculations (against reinforcement breakage and pullout) are satisfied iteratively. First, the reinforcement layout and strength characteristics are specified based on constructability requirements or experience with similar structures, and then the anchorage length is checked. Equations (2.2)–(2.4) are combined as follows:

$$L_e \geq \frac{T_{\max} \cdot FS_{po}}{F^* \cdot \alpha \cdot \sigma'_v \cdot R_c} \geq 1 \text{ m}, \quad L = L_a + L_e \quad (2.5)$$

where: L_e is the anchorage or embedment length of the reinforcement, that extends behind the adopted slip surface; L_a is the length of the reinforcement between the facing and the critical slip surface; L is the total length of the reinforcement.

The internal stability checks are made at each level of reinforcement, and the most critical state defines the final length, spacing and strength parameters of the reinforcement.

Connection Design

Connection design ensures that the forces at the connections can be sustained by both the reinforcement and the connection. The connection force in reinforcement is expressed by the active lateral earth pressure acting on the tributary area at the face of the wall.

Deformations and Settlement Calculations

The settlements and lateral displacements of MSEWs influence their serviceability and long-term performance. Since the limit equilibrium analysis is unable to predict displacements, their evaluation in design is often based on semi-empirical relations and field observations on existing structures. Usually it is assumed that the adequate selection of material properties and safety factors in design ensure acceptable displacements.

The design ends up with the following information (in addition to the design input):

- Reinforcement: spacing; total length; allowable and ultimate strength.
- Facing: connection design.
- Material specifications.

According to the presented design methodology (AASHTO 1998), the internal stability calculations control the total dimensions of the wall and the reinforcement characteristics in most of the cases. This is due to the assumption that an internal slip surface always develops without taking into account the reinforcement spacing, reinforcement stiffness, and other factors that influence the behavior of MSEWs.

2.2 Program FLAC: Theoretical Background and General Features

The program FLAC (Itasca Consulting Group, Inc., 1998) is a two-dimensional explicit finite difference program best suited to simulate the behavior of materials that may undergo plastic flow and large deformations when these materials' yield limits are reached. It is a powerful tool for solving a wide range of complex problems in continuum mechanics, due to its formulation based on dynamic equations of motion that use an explicit Lagrangian calculation scheme and a mixed-discretization zoning technique. FLAC's ability to model plastic collapse and flow of highly nonlinear materials such as soil and rock very accurately makes it a useful tool for numerical analysis in geotechnical and mining engineering. In addition to the basic ability to represent the mechanical response of various materials, including the ability to model groundwater flow and pore pressure dissipation, there are optional modules for dynamic analysis, thermal analysis and modeling of creep material behavior. Some of the program's major features are: 10 built-in material models; plane-strain (basic formulation), plane stress and axisymmetric geometry modes; 4 structural element models simulating structural support; interface elements simulating distinct planes along which slip or separation can occur; built-in programming language FISH; and an extensive facility for generating plots and slideshow movies. The built-in programming language, FISH, offers unique capabilities to tailor the analysis to the user, ranging from implementing user-defined constitutive models to overriding some of the FLAC calculation modules and replacing them with user-written ones.

FLAC formulation is based on the dynamic equations of motion using an explicit time-marching method to solve the algebraic equations that correspond to a given set of governing differential equations, and initial and boundary conditions. The calculation scheme follows two-step calculation cycles. The first step of each cycle uses the equations of motion (equilibrium equation) to derive new velocities and displacements from stresses and forces. At the second step, the stress-strain relation (constitutive equation) is applied, and the velocities calculated during the first step are used to derive new strain rates, and new stresses from strain rates. One cycle occupies one calculation timestep, which is small enough to ensure that the information cannot pass physically from one element to another in the chosen interval. The central concept of the calculation scheme is that the disturbances will propagate across the elements numerically as they would propagate physically; however, the calculational wave speed always keeps ahead of the physical wave speed. Major advantages of FLAC formulation are: numerical scheme is stable when the physical system is unstable; plastic collapse and flow are modeled very accurately; large two-dimensional models can be analyzed without excessive memory requirements (matrices are not formed, iterations are not necessary to compute stresses from strains); objects of any shape and different properties can be modeled; the material can yield and flow, and in

large-strain mode, the grid deforms and moves with the represented material. However, FLAC solution requires many steps because of the typically small timestep.

In current study, the program FLAC (Version 3.40) was chosen to analyze the behavior of geosynthetic reinforced earth block wall up to failure because of its many advantages compared to other commercial programs, and particularly because of its ability to model accurately unstable states of soil systems.

2.3 Literature Review

The literature review is based on references relevant to the following aspects of the current study: design methodology of MSEWs; failure mechanisms of MSEW with modular block facing; and FLAC application in MSEW analysis.

The design methodology of MSEWs with geosynthetic reinforcement and modular block facing has been published in several FHWA and AASHTO documents (Elias and Christopher 1997, AASHTO 1998). Relevant issues are discussed in chapter 2.1. However, none of the existing methods considers the effects of reinforcement spacing on wall stability.

Leshchinsky et al. (1994) conducted a series of pullout experiments employing one and two reinforcement layers. The results demonstrated that the behavior of single- and double-layered systems was different and implied the idea of MSEW with closely spaced reinforcement. The experiments investigated the pullout response of multilayered systems with reference to single-layered systems. The most important observations were: the pullout resistance of single- and double-layered systems was nearly the same for confining pressures typical for actual walls; the front-end displacement corresponding to the maximum pullout force was much smaller for double-layered systems than for single-layered systems; and the displacement field of double-layered systems showed no differential movements within the soil confined between the reinforcement, except near the back end. The test results and observations implied that the material confined between the geogrid layers (double-layered systems) was stiffened for overburden pressures typical for actual walls and moved as a block. The study acknowledged the importance of reinforcement spacing in design with respect to the critical slip surface and critical failure mechanism. The major conclusion was that, if the reinforcement layers are closely spaced and are sufficiently stiff and strong, the reinforced soil can be treated as a composite mass, and the critical slip surface will develop behind it. The current numerical study was designed to investigate further the effects of reinforcement spacing on wall behavior using sophisticated numerical methods.

Bathurst and Hatami (1998) reported results of extensive numerical analysis of seismic response of a MSEW wall with continuous facing panel using FLAC. The effects of dynamic loading on reinforced soil structure, and the influence of reinforcement stiffness, number of reinforcement layers, base condition, and wall geometry on the earthquake response of the system were investigated. The numerical model of a continuous panel wall was 6 meters (m) high with 6 uniformly spaced reinforcement layers. The wall facing was modeled as a continuous concrete panel with a thickness of 0.14 m. The foundation soil was not modeled, and its effect on model response was investigated by specifying different boundary conditions along the base. The reinforcement layers were modeled using FLAC cable elements that were attached to a grid point of the continuous panel region (corresponding to unbreakable structural connections). The soil was modeled as a frictional material with a Mohr-Coulomb failure criterion. The elastic modulus of soil was kept constant using the values calculated at the end of construction before prop removal. The properties of the FLAC model were chosen to correspond to a reference finite element model (FEM) and represent values commonly used in design. The FLAC model represented the following construction sequence: the soil and reinforcement elements were constructed in layers, while the continuous panel was braced horizontally using external rigid supports; at the end of construction, the panel supports were released in sequence from top to bottom; and dynamic loading was applied. The FLAC model response under static loading was compared with the response of a similar model analyzed with FEM. The following parameters were analyzed: dynamic excitation; base conditions; type and location of the right-edge boundary; material dumping ratio; reinforcement stiffness; reinforcement length; and toe restraint condition. Important observations relevant to the current analysis were: for the given reinforcement layout and model properties, interior slip surfaces intersecting all reinforcement layers were not observed during all simulations; the accuracy of dynamic analysis was sufficient if the developed slip surface did not reach the right-edge boundary. The reported results are a major contribution to the analysis of dynamic response of precast facing MSEWs.

Hatami and Bathurst (1999) reported results from a numerical investigation of the influence of wall height, reinforcement stiffness, reinforcement length and toe restrained condition on the frequency response of MSEWs. This study used the same numerical model reported by Bathurst and Hatami (1998) in addition to equivalent models with wall heights equal to 3 m and 9 m. The numerical simulations results showed that the reinforcement stiffness, reinforcement length, and toe-restrained condition did not affect the fundamental frequency of the models. Some effects of the input ground motion were recorded. The stronger of the two input acceleration records gave lower fundamental frequencies of the models. As noted by the authors, the results are relevant only to the rigid foundation condition.

Lee (1999) reported strain and force distributions in reinforcement as results of FLAC analysis of the FHWA test walls built in Algonquin, IL. However, the model was not described. The focus of the analysis was on the earth pressure distribution within the reinforced soil and the corresponding earth pressure coefficient.

Leshchinsky (1997, 1999) proposed four failure mechanisms to be investigated in the design of geosynthetic reinforced steep slopes using the limit equilibrium method: two-part wedge mechanism (direct sliding analysis); rotational mechanism (deep-seated stability analysis and compound stability analysis); and log-spiral failure mechanism (internal stability or tieback analysis). These mechanisms closely correspond to the four failure modes identified numerically in the current study: external, deep-seated, compound, and connection mode.

Leshchinsky (1999) proposed a new concept related to the safety factor in stability analysis of reinforced steep slopes. The safety factor is directly related to the reinforcement strength, based on the fact that reinforced steep slopes are stable because of the reinforcement tensile resistance (i.e., the soil shear strength is fully mobilized, and stability is dependent entirely on reinforcement strength). The peak shear strength of soil is reduced, accounting for possible large deformations and progressive failure. This approach is implemented in the program MSEW 1.1 (ADAMA Engineering 1998) as an L-method for compound or deep-seated stability analysis. Compound stability analysis using the L-method demonstrated very good agreement with relevant FLAC predictions.

CHAPTER 3. NUMERICAL ANALYSIS

3.1 Scope

The purpose of the current study is to investigate the behavior of MSEWs with modular block facing and geosynthetic reinforcement using the two-dimensional finite difference program FLAC (Version 3.40, Itasca 1998). A set of computer runs identified failure mechanisms of MSEWs as function of geosynthetic spacing, considering the effects of soil strength, reinforcement stiffness, connection strength, secondary reinforcement layers, and foundation stiffness. Numerical analysis also was conducted to investigate the effects of reinforcement length on reinforcement stresses and wall stability. FLAC predictions were compared with the existing design method (AASHTO 98) using the MSEW 1.1 program (ADAMA Engineering 1998). Additional numerical experiments investigated the effect of some modeling parameters on the predicted wall response.

3.2 Numerical Model

The behavior of MSEW with modular block facing and geosynthetic reinforcement was investigated with numerical models that simulate construction of the wall, layer by layer, until it fails under gravity loading. Various responses during wall construction such as displacement accumulation, stress histories, and tensile load in reinforcement, can be recorded. The components and basic geometry of the model are shown in figure 3.1.

3.2.1 Modeling Methodology

The numerical model is updated continuously by adding soil and geosynthetic layers up to failure in stages, which represent the construction sequence of actual walls. The first reinforcement layer is always installed at elevation 0.2 m on top of the first soil layer and the first block. Next, reinforcement layers are installed according to the reinforcement spacing. For example, the modeling sequence of a wall with reinforcement spacing equal to 0.4 m consists of the following stages (figure 3.2):

- Stage 1: Foundation modeling (equilibrium under self-weight is achieved; elastic modulus of soil is updated).
- Stage 2: Installation of a modular block of layer 1.
- Stage 3: Placement of a layer of reinforced and backfill soil (equilibrium under self-weight is achieved; elastic modulus of soil is updated).
- Stage 4: Installation of first layer of reinforcement.
- Stage 5: Installation of a modular block of layer 2.

- Stage 6: Placement of a layer of reinforced and backfill soil (equilibrium under self-weight is achieved; elastic modulus of soil is updated). NOTE: For the given reinforcement spacing $s=0.4$ m, a reinforcement layer is not installed at that elevation (it would be installed only for the reinforcement spacing $s=0.2$ m).
- Stage 7: Installation of a modular block of layer 3.
- Stage 8: Placement of a layer of reinforced and backfill soil (equilibrium under self-weight is achieved; elastic modulus of soil is updated).
- Stage 9: Installation of a layer of reinforcement.
- Stage 10: Installation of a modular block of layer 4.
- Stage 11: Placement of a layer of reinforced and backfill soil (equilibrium under self-weight is achieved; elastic modulus of soil is updated). NOTE: For the given reinforcement spacing $s=0.4$ m, a reinforcement layer is not installed at that elevation (it would be installed in case the reinforcement spacing requires).
- Stage 12: Installation of a modular block of layer 5.

Wall construction continues up to failure following the same pattern.

The construction using the numerical model continues until the program stops due to excessive deformations in a certain element (bad geometry). At this stage, the deformations in the system were large and corresponded essentially to a failed wall. Numerical and physical parameters such as slip surface development, maximum displacement of the system accumulated during wall construction, number of calculation steps necessary to equilibrate the system after placement of each layer, and history of maximum unbalanced force, were used to define a critical wall height. This height corresponds to a wall at the verge of failure (figure 3.3–b). All states corresponding to a height larger than the critical one are considered as failure states (figure 3.3–a). To investigate the effects of reinforcement length on wall stability, the wall height of certain numerical tests was kept equal to the critical one, while the length of reinforcement was increased. For these tests, the states that correspond to walls with length-to-height ratio larger than the critical one are considered as stable states (figure 3.3–c).

3.2.2 Model Description

The major components of the model are foundation, modular blocks, reinforced soil, retained soil (backfill), and reinforcements layers (figure 3.1). A set of model variables (listed in table 3.1) was implemented to allow change of geometry and material properties according to the purpose of the analysis.

A typical numerical grid and dimensions to discretize the problem are shown in figure 3.4. The wall and the adjacent backfill with uniform grid density form

a ‘kernel’ of the numerical model. Its dimensions can be changed accordingly (zones 1 and 2 in figure 3.5). The grid around that kernel models the foundation soil and the end part of the backfill adjacent to model boundaries (zones 3 to 6 in figure 3.5). The foundation depth and width of end backfill were fixed to 5.0 m for all simulations.

Grid density of the model is shown on figure 3.5. The grid in zone 1 (figure 3.5-a) represents the wall facing constructed from separate modular blocks. The block-block, block-soil, and block-reinforcement interaction is modeled interfacing with properties that can be changed accordingly. In the final version of the model, the modular blocks are divided into rectangular elements with dimensions 0.05×0.1 m (uniform density in both directions of zone 1) (figure 3.5-b). In early parametric studies, the modular blocks were represented either by one element or divided into square elements with dimensions 0.1×0.1 m (figure 3.5-c); however, to represent the interaction at the connections more accurately, numerical sensitivity analysis indicated that horizontal grid density should be increased. Zone 2 consists of 2 parts (figure 3.5-a). Part 2-a corresponds to the reinforced soil, and part 2-b corresponds to a part of the retained soil adjacent to the reinforced soil. Both parts of zone 2 can change their global horizontal dimension by changing the model variables “length of reinforcement, l ” (zone 2-a) or “length of adjacent backfill, L ” (table 3.1). The grid density of zone 2 is uniform in both directions and can be changed by changing the model variable “number of sublayers within a height of 0.2 m (fixed height of a modular block), n_{sl} ” (table 3.1). In the final version of the model, the elements of zone 2 are squares with dimensions $a \times a$ m, where a is defined as follows:

$$a = \frac{\text{height of modular block}}{\text{number of sublayers}} = \frac{0.2}{n_{sl}} = \frac{0.2}{2} = 0.1 \text{ m} \quad (3.1)$$

However, in the current analysis, the influence of grid density in zone 2 less than 0.1×0.1 m resulted in numerical instability. Numerical tests were done with grid density in zone 2 corresponding to element size 0.05×0.05 m and numerical instability constantly occurred at a wall height of about 2 m. Because of the encountered numerical instability at such small dimensions, the grid density in zone 2 was kept constant, corresponding to the smallest stable element size of 0.1×0.1 m. In zone 3 (end part of the backfill), grid density is uniform vertically and changes gradually in horizontal direction. The element size changes from left to right from 0.1×0.1 m to 0.5×0.1 m. In zone 5 (middle part of foundation), grid density is uniform in horizontal direction and changes gradually in vertical direction. The element size changes from top to bottom from 0.1×0.1 m to 0.1×0.5 m. In zones 4 and 6 (left and right parts of the foundation), grid density changes gradually in both directions. The element size changes from 0.1×0.1 m to 0.5×0.5 m. Grid density of the model was defined with respect to the modular block height ($h_{bl} = 0.2$ m), with ability to be

changed within the zone 2 (figure 3.5). In all numerical tests, the smallest stable element size was used— 0.05×0.1 m in zone 1 (facing) and 0.1×0.1 m in the soil. Figure 3.4 shows a typical grid in all zones.

Boundary conditions of the model consist of prescribed zero velocities (corresponding to zero displacements) perpendicular to the boundaries (figure 3.5). Boundary effects on model response were investigated with respect to the distance of the wall to the right model boundary. In the final version of the model, the total width of backfill is 15.0 m (the width of zone 2–b is 10.0 m, and the width of zone 3 is 5.0 m, figure 3.5). For all numerical simulations, this backfill width ensured that the deformed zone behind the wall was not close to the model boundary. Several numerical simulations varied the width of backfill from 5.2 m to 15.0 m ($L=0.2\text{--}10.0$ m). It was proved that boundary affected the results significantly when the active zone that developed behind the wall was close to or reached the right model boundary. Close boundary effects increased wall stability because of the restraint horizontal displacements along the right model boundary. To avoid boundary effects on model response, additional tests were done for a model (case 1, $s=0.2$ m, $h=6.6$ m, $l=1.5$ m), varying the width L of the adjacent backfill (zone 2–b on figure 3.5). The distributions of stresses and horizontal displacements along a vertical section 0.1 m behind the facing are shown on figure 3.7 for $L=6$, 8 and 10 m. The differences were less than 5 percent. In all consequent numerical tests, the width of the backfill was 15.0 m ($L=10$ m).

Wall facing was specified as concrete modular blocks with a fixed height of 0.2 m and a fixed thickness of 0.2 m. Each new block was placed precisely on top of the previous one. As construction progressed, the facing tilted outward as a result of cumulative displacements. Block-block, block-reinforcement, and block-soil interaction was modeled with interfaces along which sliding or separation can occur.

During construction, reinforcement layers were placed, following the scheme set by the specified spacing (figures 3.2 and 3.8). Each reinforcement layer was designed with two parts, using beam and cable structural elements available in FLAC. The reinforcement section confined between the facing blocks was modeled using a FLAC beam element. The reinforcement section embedded in soil was modeled using a FLAC cable element. The beam and cable elements were linked at a common node. FLAC beam elements are two-dimensional elements with three degrees of freedom at each end node (x-translation, y-translation and rotation). These elements represent structural members in which bending resistance is important. Beam elements can be joined together with each other and the grid, directly or through interface elements. FLAC cable elements are one-dimensional axial elements that may be anchored at a specific point in the grid or grouted so that the cable elements develop forces along its length as the grid deforms. They cannot sustain bending moments and

are used to model supports for which tensile capacity is important. Cable elements interact with the confining material only when they are grouted. To represent the frictional connection between the modular blocks and the reinforcement correctly, the reinforcement was modeled in two parts using beam and cable elements. Beam elements represent the block-reinforcement interaction. Because beam elements can interact with the grid only through interfaces or explicitly specified links, they were not used to model the reinforcement-soil interaction. Cable elements were used to represent the soil-reinforcement interaction, because they cannot be used with the interfaces that model the block-reinforcement interaction.

Each wall was modeled to reach failure by increasing its height in layers while keeping the reinforcement length equal to 1.5 m. In the process of numerical simulation, the wall reached the verge of failure, but its construction continued until the failure was detected numerically. The state that corresponds to a wall at the verge of failure was called a critical state. A critical state is defined by analyzing numerical and physical parameters such as slip surface development, number of calculation steps necessary to equilibrate the system after placement of each layer (figures 3.9-a, 3.10-a, 3.11-a) maximum cumulative displacement of the system during construction (figures 3.9-b, 3.10-b, 3.11-b), and history of maximum unbalanced force. In the current studies, a critical state was identified when at least three of the following events occurred simultaneously: (1) a slip surface was developed fully, (2) the maximum cumulative displacement increases nonlinearly, (3) the number of calculation steps per layer increased rapidly, and (4) the history of maximum unbalanced force indicated an abrupt change of the unbalanced force. Figures 3.9–3.11 provide typical plots showing the maximum cumulative displacements and the number of calculation steps (necessary to equilibrate the system after the placement of each layer).

The height and length-to-height ratio at the critical state are called critical height (h_{cr}) and critical length-to-height ratio (l/h_{cr}), respectively. States of a model that correspond to walls higher than the wall at the critical state are called failure states. Stable states correspond to walls with a height equal to the critical height and a length-to-height ratio larger than the critical length-to-height ratio. The definition of failure, critical, and stable states of a numerical model is illustrated on figure 3.3.

In the process of numerical simulation, the wall is constructed until the failure is detected numerically (i.e., the model construction stops). The model stops in the following two cases:

- If excessive deformations (causing bad geometry) in a certain element are detected.
- If model reaches the specified final height of the wall, and equilibrium is achieved.

The equilibrium state in FLAC is identified when one of the following happens: (1) the number of calculation steps¹ reaches the specified limit (default value is 100,000); or (2) the largest ratio of maximum unbalanced force² to average applied force is below a specified limit called “equilibrium ratio” (default value is 0.001). Computer runs investigated the influence of these model response limits. Typical results are presented on figures 3.9–3.11, and in table 3.2. The presented results proved that the model response is not influenced when the equilibrium ratio was changed from 0.001 (default value) to 0.01, and when the maximum number of steps was changed from 100,000 (default value) to 200,000. In all numerical simulations, the equilibrium ratio was *srat*=0.01 (10 times larger than the default value), and the maximum number of calculation steps was 100,000 (default value).

3.2.3 Material Properties

The material properties used in the analysis were based on data reported in the literature. They represent typical values used in design practice (Das 1999).

The soil was modeled as a cohesionless material using a FLAC plastic constitutive model that corresponds to a Mohr-Coulomb failure criterion with a hyperbolic stress-strain relationship. The elastic modulus of soil was updated after placement and equilibration of each soil layer using the following hyperbolic stress-strain relationship (Wong and Duncan 1974):

$$\frac{E_s}{P_a} = K \left(\frac{\sigma_3}{P_a} \right)^m \quad (3.2)$$

where: E_s = elastic modulus of soil; P_a = atmospheric pressure; σ_3 = minor principal effective stress; and K and m are the hyperbolic model coefficients. For all numerical simulations, the hyperbolic model coefficient m was kept constant equal to 0.5 (Bathurst and Hatami 1999, Ling et al. 2000). The soil properties were changed to

¹ Because FLAC is an explicit code, the solution to a problem requires a number of computational steps. During computational stepping, the information associated with the phenomenon under investigation is propagated across the zones in the finite difference grid. A certain number of steps is required to arrive at an equilibrium or steady flow state for a static solution (FLAC User’s Guide, Itasca 1998).

² The unbalanced force indicates when a mechanical equilibrium state (or the onset of plastic flow) is reached for a static analysis. A model is in exact equilibrium if the net nodal force vector at each gridpoint is zero. The maximum nodal force vector is monitored in FLAC (called the unbalanced force) and will never reach exactly zero for a numerical analysis. The model is considered to be in equilibrium when the maximum unbalanced force is small compared to the total applied forces in the problem (FLAC User’s Guide, Itasca 1998).

investigate different aspects of wall behavior. The soil properties that were used in different numerical tests are summarized in tables 3.3 and 3.4.

The modular blocks were modeled using a linear elastic constitutive model. The geometry, parameters, and properties of the facing were kept constant for all numerical runs and are given in table 3.5.

The reinforcement layers were modeled using beam and cable structural elements available in FLAC. The properties of the cable and beam elements used in different numerical tests are summarized in table 3.6.

The block-block, block-reinforcement, and block-soil interaction was modeled using interfaces available in FLAC. Three types of interfaces were used in the model: between two facing blocks (block-block interface), between a facing block and the part of reinforcement modeled by a beam element (block-beam interface or block-reinforcement interface), and between a facing block and the adjacent soil (block-soil interface). The interfaces are sketched in figure 3.8. They represent planes along which sliding or separation can occur and are characterized by the Coulomb shear-strength criterion:

$$F_{s\max} = cL_e + F_n \tan \delta \quad (3.3)$$

where: $F_{s\max}$ = maximum shear force, c = cohesion along the interface, L_e = effective contact length, F_n = normal force, and δ = friction angle of interface surfaces. If shear forces in interfaces are less than the maximum shear strength defined by Equation (3.3), sliding or separation occurs.

The properties of block-block and block-reinforcement interfaces were changed to simulate different connection strengths between the reinforcement and the modular blocks. Frictional connection was represented by interfaces with no cohesion, and the interface angle of friction was changed to investigate its influence on wall behavior. Structural connection was represented by interfaces characterized with both cohesion and friction. Block-soil interfaces were always modeled with no cohesion. Interface properties used in analysis are summarized in table 3.7. To ensure numerical stability, the normal and shear stiffness of the interfaces were modeled following the guidelines given in the FLAC manual (Itasca 1998). The normal stiffness of interfaces was assigned to correspond to the bulk modulus of concrete. The shear stiffness of interfaces was assigned to correspond to the initial shear modulus of reinforced soil.

The interaction between reinforcement layers and soil is represented by grout-soil interface defined as a part of the cable element definition. Properties of grout as part of the cable elements definition are given in table 3.6.

3.3 Scope of Parametric Studies

Parametric studies investigated the behavior of MSEWs with modular block facing and geosynthetic reinforcement using a numerical model that can simulate construction sequence layer by layer up to failure. A set of runs identified failure mechanisms of MSEWs as function of geosynthetic spacing, considering the effects of soil strength, reinforcement stiffness, connection strength, use of secondary reinforcement layers, and foundation. A second set of numerical runs investigated the effects of reinforcement length on reinforcement stresses and wall stability. FLAC predictions were compared with an existing design method (AASHTO 98) using the MSEW 1.1 program (ADAMA Engineering 1998). Additional numerical runs investigated the effect of some model parameters on the predicted wall response. All numerical runs were grouped into cases according to the set of properties used in the analysis. Within each case, numerical runs with different reinforcement spacing were performed. Summary of all parametric studies is given in table 3.8.

Cases 1, 2, and 3 represent models with very stiff foundation and soil strength of reinforced and retained soil decreasing from case 1 (high strength soil) to case 3 (low strength soil). Cases 4, 5, and 6 represent models with soil properties that are the same for the entire model, with soil strength decreasing from case 4 (high strength soil) to case 6 (low strength soil). For cases 1 to 6, the connection between the reinforcement and facing is frictional (baseline strength, table 3.7), and reinforcement properties correspond to typical design values (baseline reinforcement (BR), table 3.6). All relevant reinforcement spacings within the range of 0.2 to 1.0 m were investigated.

Cases 7 to 12 were designed to investigate certain aspects of wall behavior complementing the first six cases. Case 7 was designed to assess the effects of secondary reinforcement layers (figure 3.12). Model properties of case 7 were the same as the model properties of case 2, with the exception of reinforcement layout, which consists of primary reinforcement layers at every 0.6 m ($l=1.5$ m) and secondary reinforcement layers in between at every 0.2 m ($l=0.3$ m). Cases 8–1, 8–2, and 8–3 were designed to investigate the effects of reducing the reinforcement stiffness on wall response. The effect of connection strength was investigated with cases 9 (low strength frictional connection) and case 12 (structural connection). Case 10 was designed to investigate the wall behavior considering weak foundation. Case 11 was designed to investigate the effect of soil dilatancy on wall behavior.

Additional runs were carried out to investigate the effect of grid density, boundary distance (i.e., boundary effects), and values of FLAC equilibrium limits.

Four numerical models corresponding to different failure mechanisms were investigated with respect to failure and stable states, and are called baseline cases. The set of numerical experiments for case 1 and some of the corresponding modified cases is represented with an organizational chart in figure 3.13.

Thirty-seven runs were directly involved in the analysis (table 3.8). The runs were performed on three personal computers. One of the runs was completed with an Intel® x86 Processor, 384 MB RAM, 800 MHz; the other two runs were completed with Pentium® II Processor Intel MMX™, 128 MB RAM, 550 MHz. The total time of these 37 runs was about 900 hours, or 106 working days. General information about the runs of all cases (at failure and critical states) is given in table 3.9 and table 3.10. Typical input file is given in the appendix.

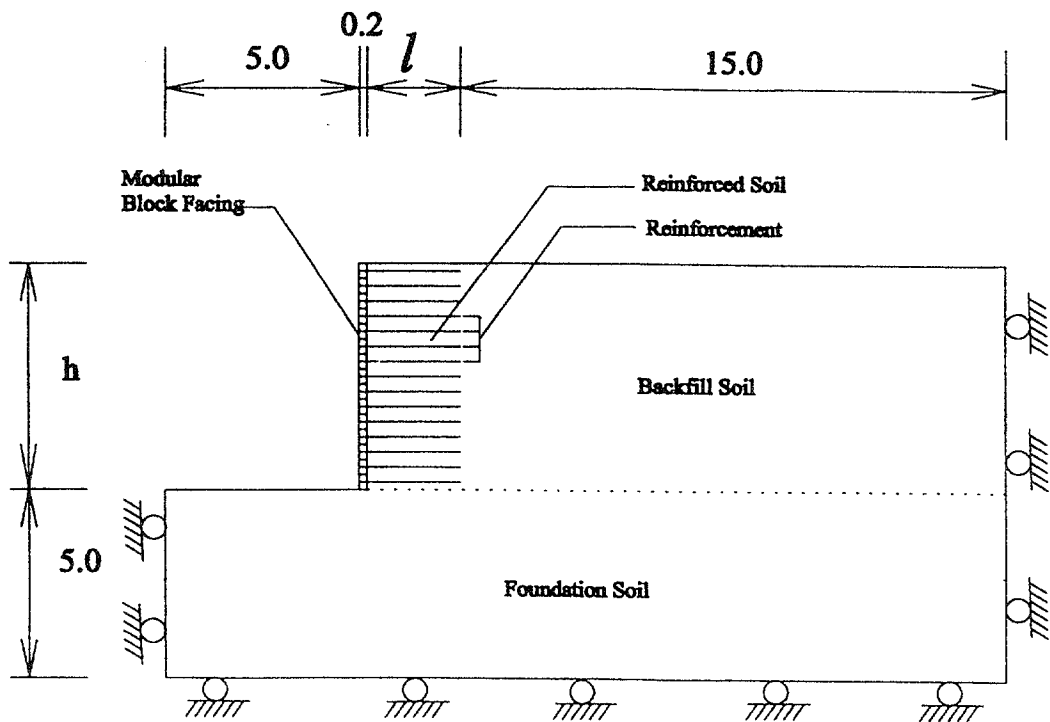


Figure 3.1 Numerical Model Components.

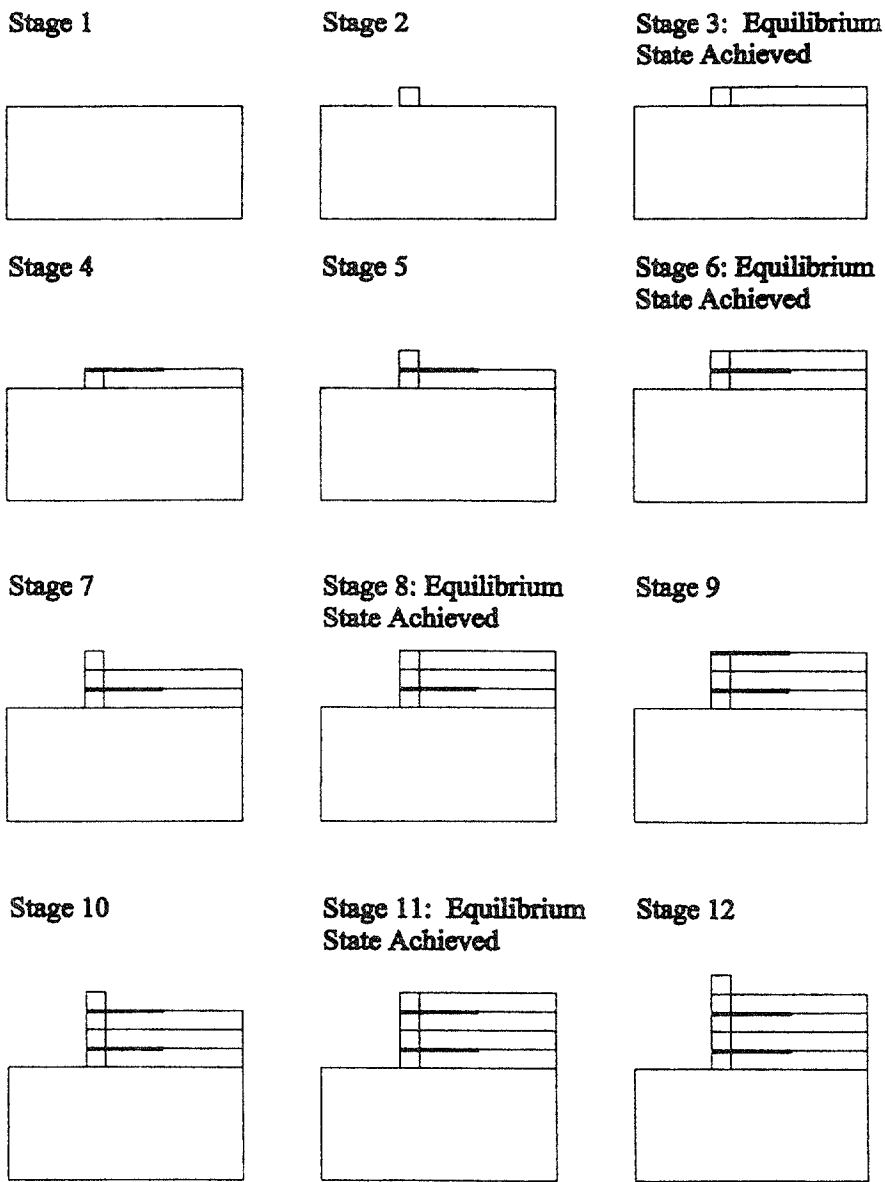


Figure 3.2 Schematic of Modeling of Construction Sequence of Wall with Reinforcement Spacing Equal to 0.4 m.

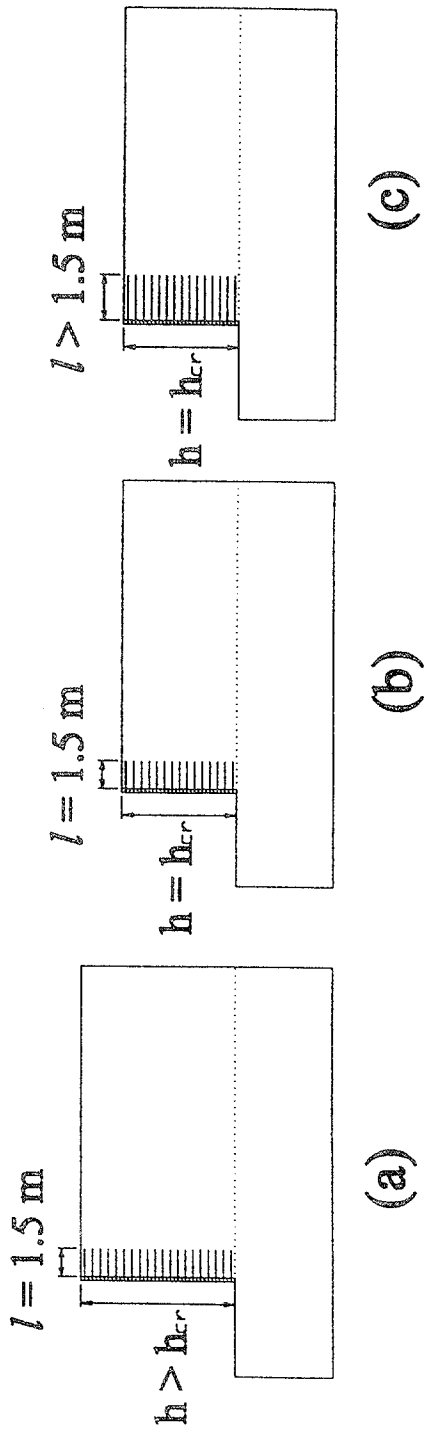
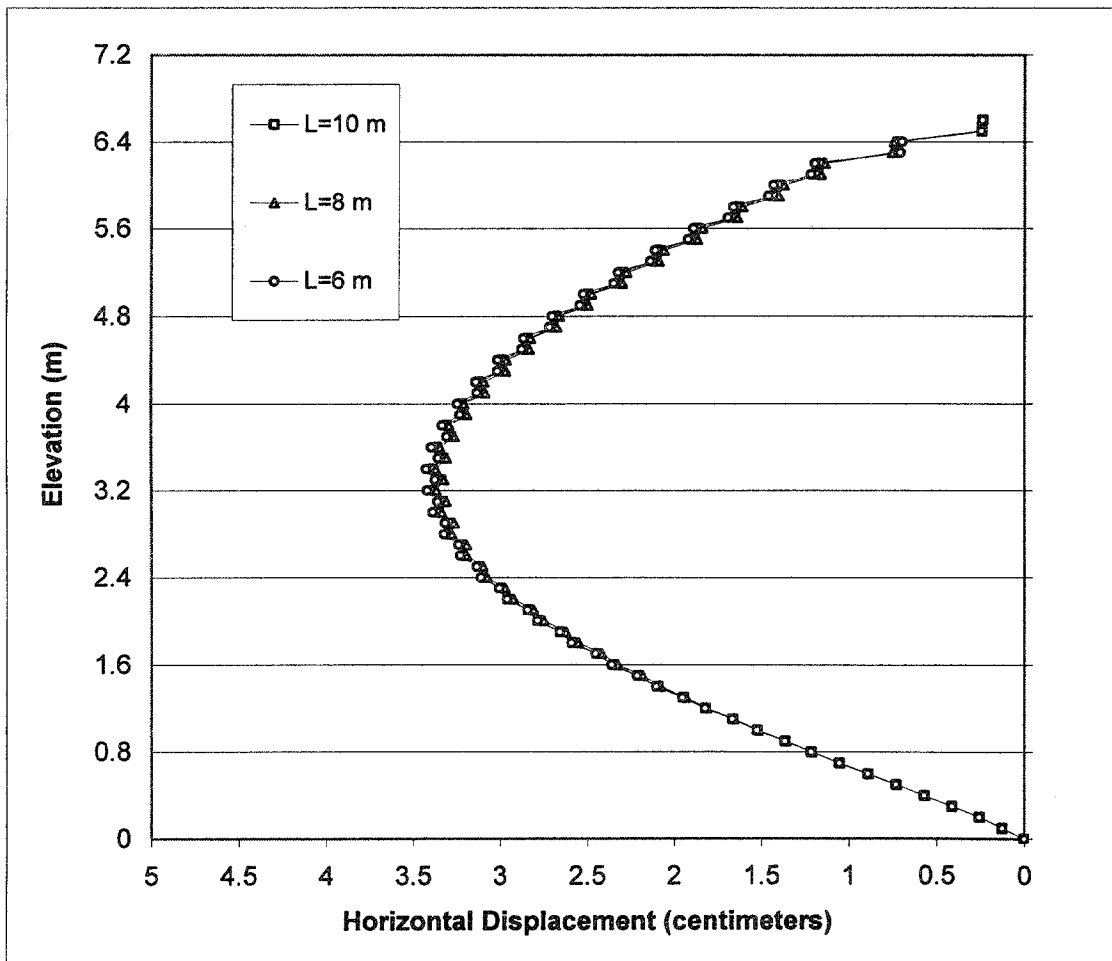
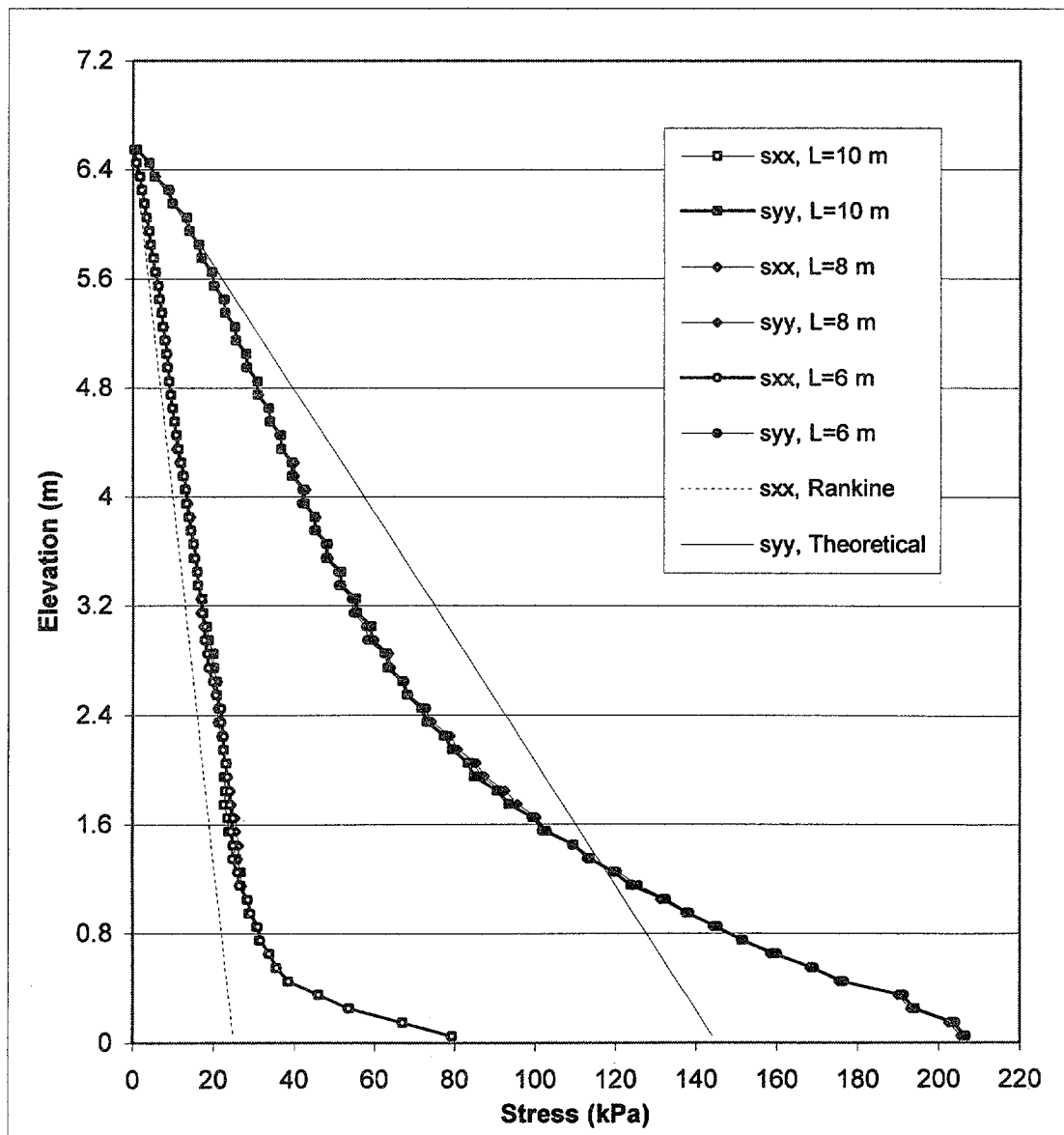


Figure 3.3 Definition of: (a) Failure State; (b) Critical State; (c) Stable State.



NOTE: L=Width of adjacent backfill grid (figure 3.5).

Figure 3.6 Boundary Effects on Model Response: Horizontal Displacements along Vertical Section A Located 0.1 m behind the Facing.



NOTE: L=Width of adjacent backfill (zone 2-a, figure 3.5).

Figure 3.7 Boundary Effects on Model Response: Stress Distributions along Vertical Section A Located 0.15 m behind the Facing.

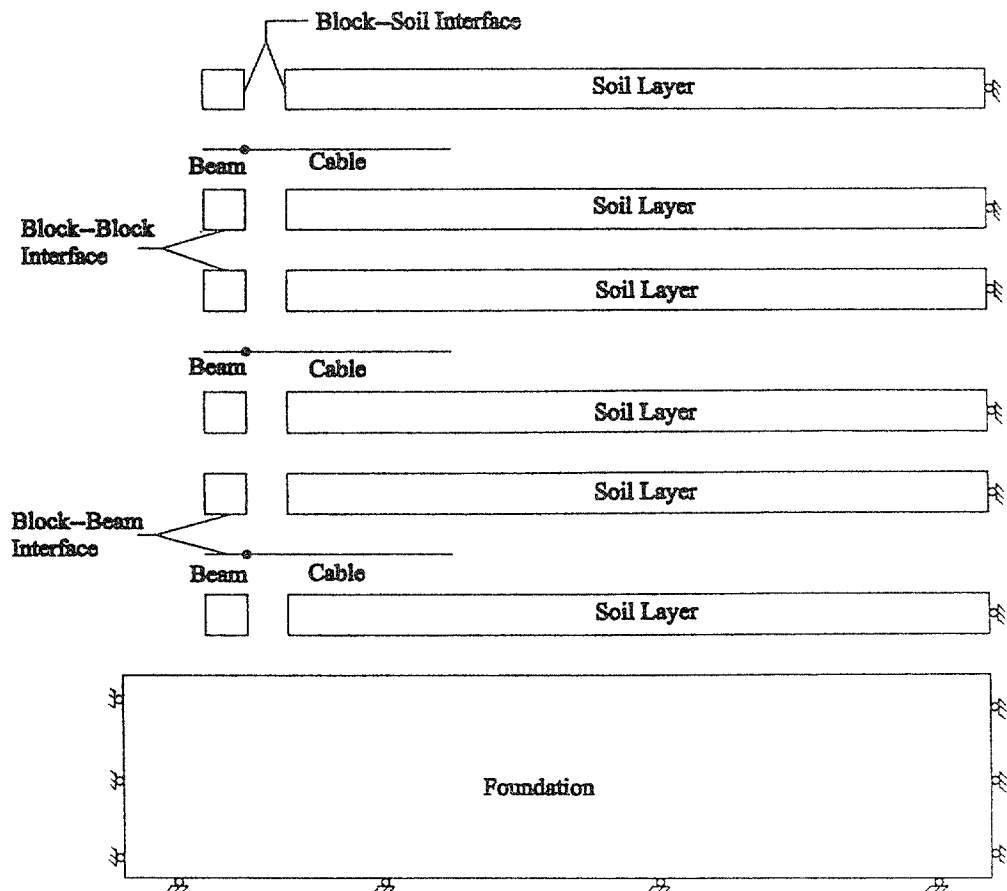
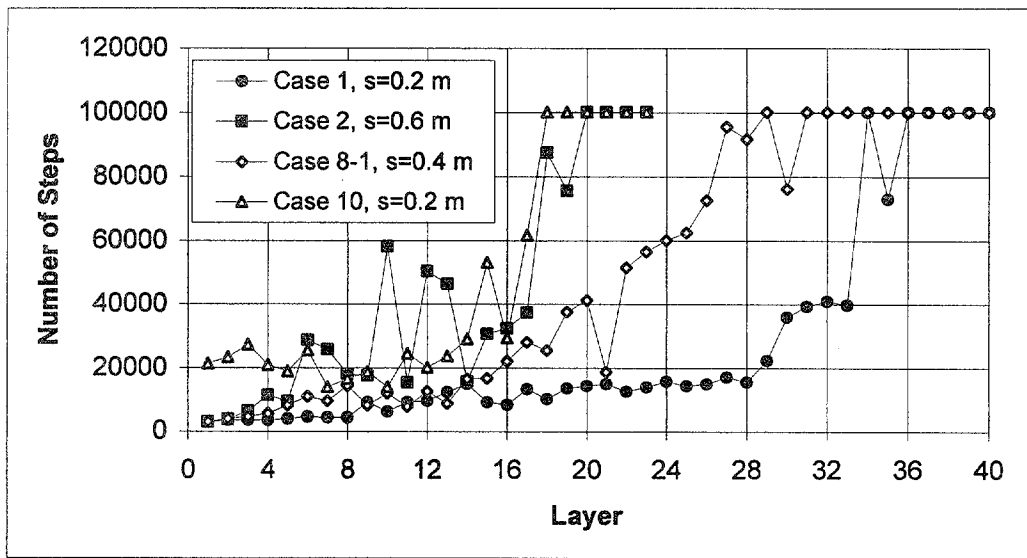


Figure 3.8 Types of Interfaces at the Blocks.

(a)



(b)

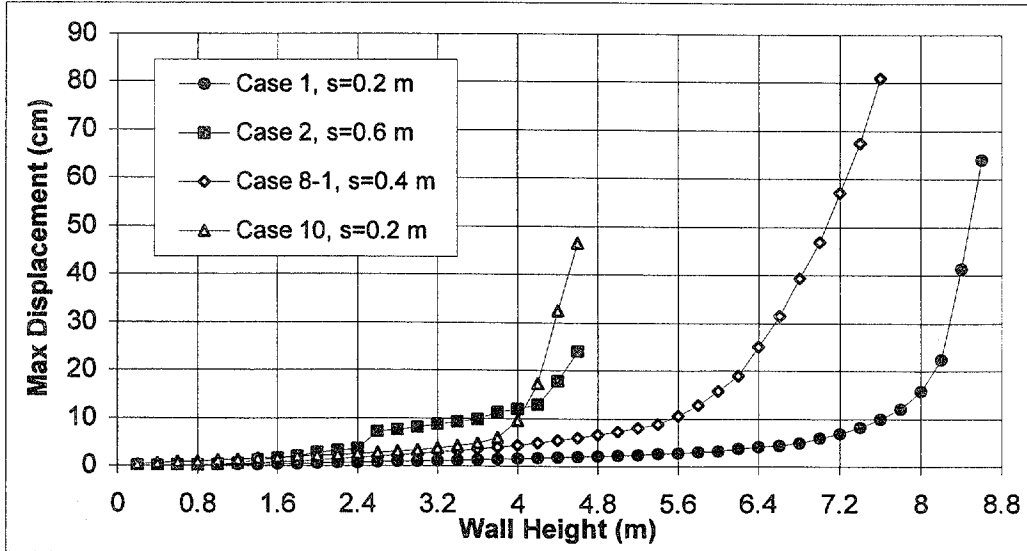


Figure 3.9 Baseline Cases: (a) Number of Calculation Steps Necessary to Equilibrate Each Layer; (b) Maximum Cumulative Displacement during Wall Construction.

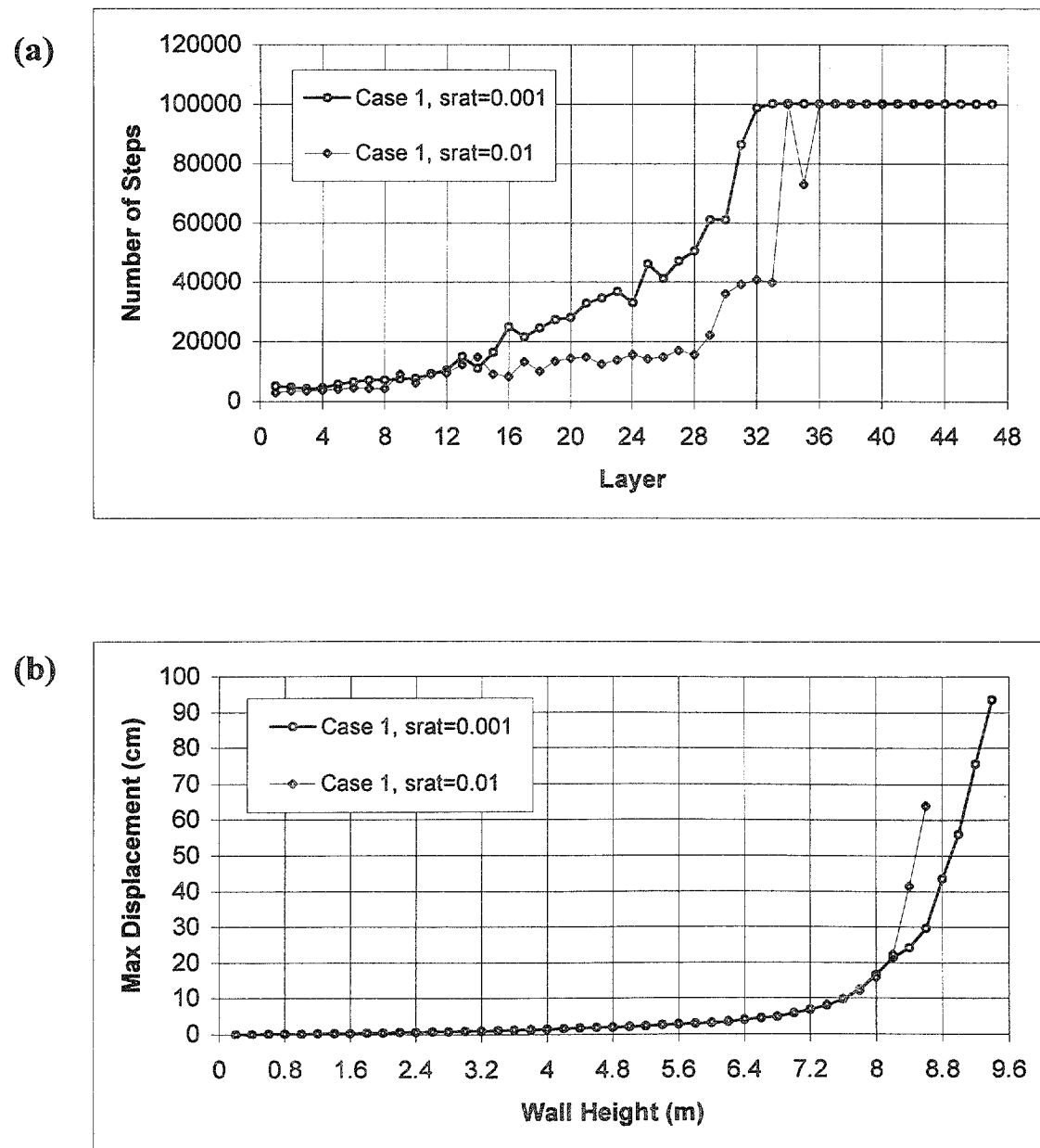


Figure 3.10 Effects of FLAC Equilibrium Ratio Limit on Model Response of Case 1 ($s=0.2$ m, $t=1.5$ m): (a) Number of Calculation Steps; (b) Maximum Cumulative Displacement.

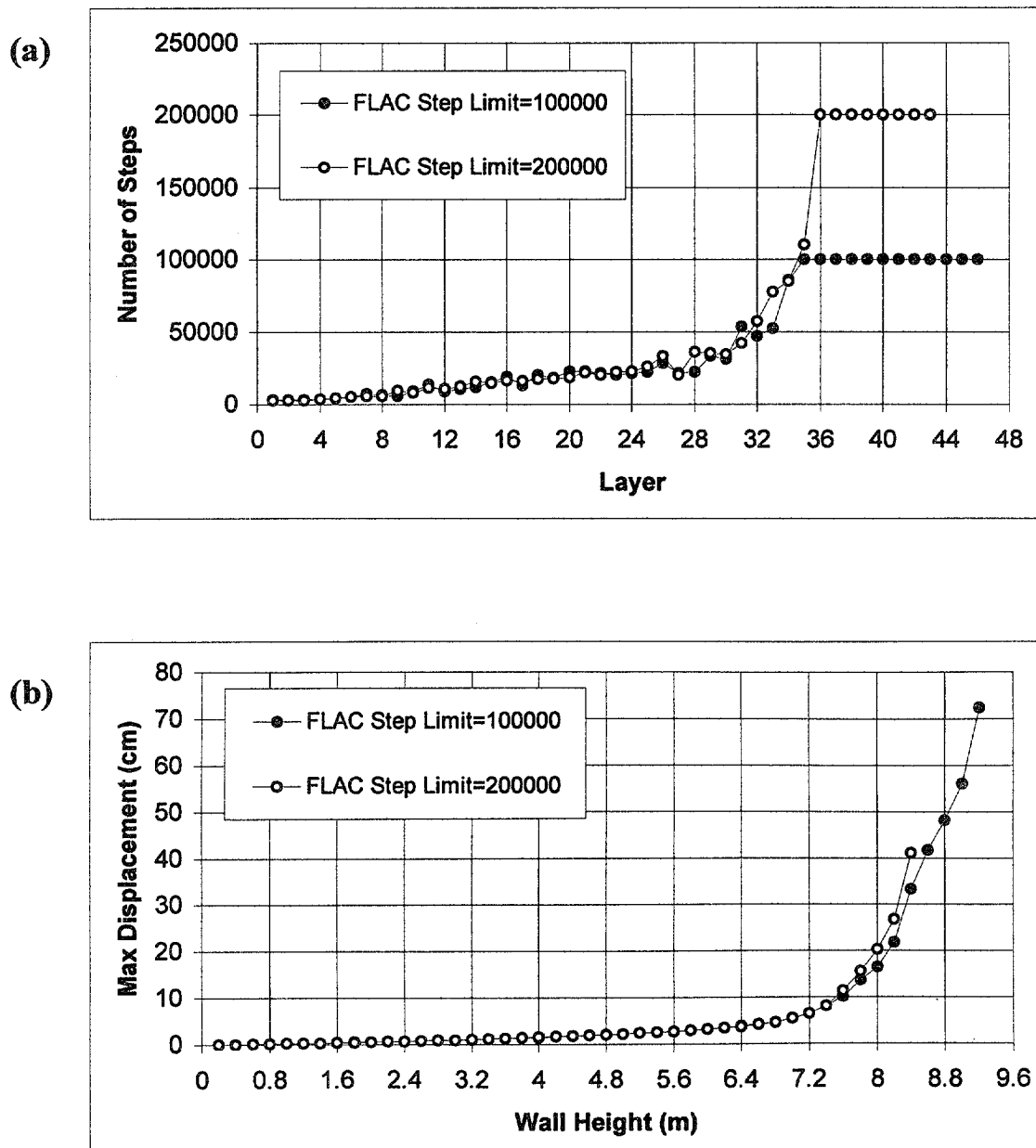


Figure 3.11 Effects of FLAC Step Limit on Model Response of Case 12 ($s=0.2$ m, $l=1.5$ m): (a) Number of Calculation Steps; (b) Maximum Cumulative Displacement.

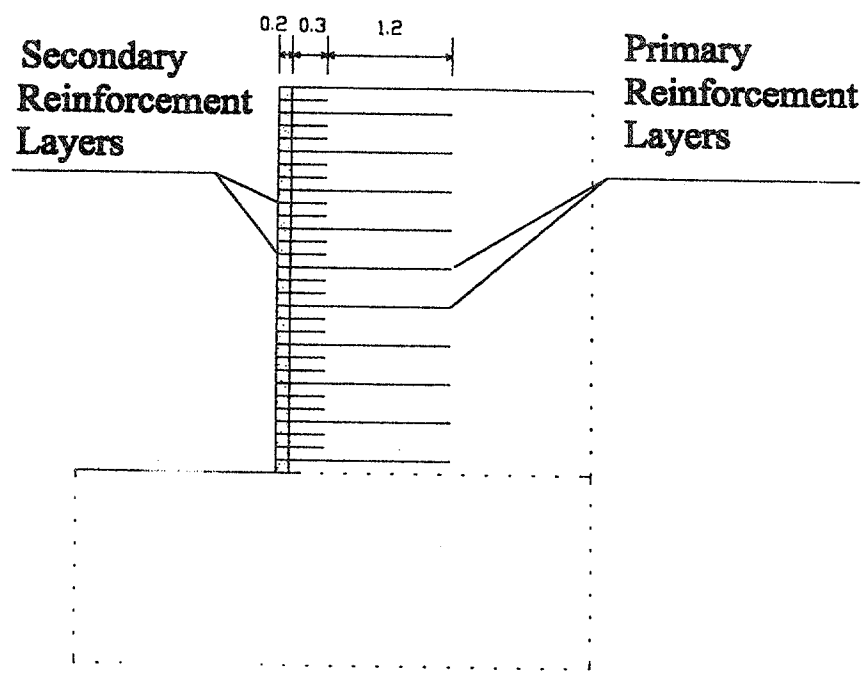


Figure 3.12 Reinforcement Layout with Primary and Secondary Layers for Case 7 ($\delta=0.6/0.2$ m).

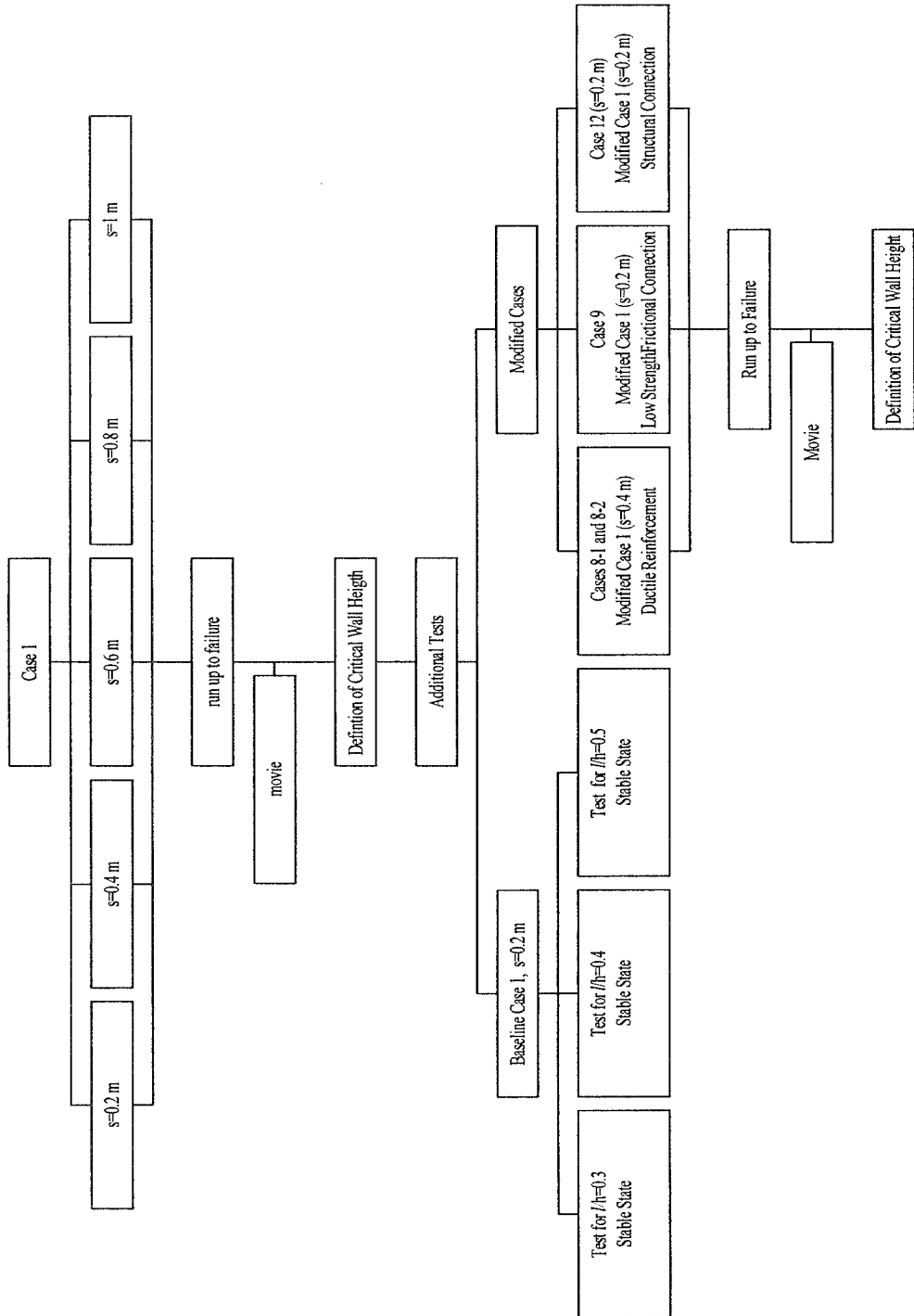


Figure 3.13 Some of the Executed Numerical Runs.

Table 3.1 List of Model Variables.

Model Variable		Notation	Comments
Wall dimensions and grid density	Wall height	h	Multiple of 0.2 m
	Length-to-height ratio	l/h	Must correspond to wall height multiple of 0.2 m
	Length of reinforcement	l	Multiple of 0.1 m
	Length of adjacent backfill	L	Multiple of 0.1 m
	Number of blocks between two reinforcement layers	n_{bl}	Defines the reinforcement spacing. For example, if $n_{bl}=4$, the corresponding reinforcement spacing is $s=n_{bl}*0.2=0.8$ m (0.2 m is a fixed height of a modular block)
	Number of sublayers within a height of 0.2 m	n_{sl}	Defines grid density in reinforced soil and the adjacent backfill
Soil	Friction angle	ϕ_s	Different values for soil in foundation, wall and backfill can be specified
	Poisson's ratio	ν_s	
	Initial elastic modulus	E_{is}	
Facing blocks	Elastic modulus	E_{ib}	It is recommended that this value does not exceed the elastic modulus of soil more than 10 times (Itasca 1998)
	Poisson's ratio	ν_b	—
Reinforcement	Cable elastic modulus	E_c	—
	Grout shear stiffness	k_{bond}	—
	Grout cohesive strength	s_{bond}	—
	Beam elastic modulus	E_b	—
Interfaces	Normal stiffness	k_n	If these values are not derived from tests on real joints, it is recommended that they are less than ten times the equivalent stiffness of interacting materials (Itasca 1998)

Table 3.2 Major Results for Case 1 ($s=0.2$ m, $h=6.6$ m, $l=1.5$ m) for Different FLAC Equilibrium Ratio Limits.

FLAC Equilibrium Ratio Limit	Number of Steps	Maximum Displacement (cm)	Maximum Axial Force		Maximum Connection Force	
			Value (kN)	at Elevation (m)	Value (kN)	at Elevation (m)
0.01	419538	4.4	6.02	1.2	4.83	1.2
0.001	882890	4.38	6.04	0.8	4.58	0.8

Table 3.3 Properties of Modeled Soil: Strength and Elastic Values.

Parameter	Soil Type			Comments
	High Strength Soil (HS)	Medium Strength Soil (MS)	Low Strength Soil (LS)	
Friction angle (deg)	45	35	25	Model variable
Dilation angle (deg)	15	7	0	–
Cohesion (kPa)	0	0	0	–
Initial modulus of elasticity (MPa)	60	60	60	Model variable
Poisson's ratio	0.3	0.3	0.3	Model variable
Density (kg/m ³)	2200	2200	2200	–

Table 3.4 Properties of Modeled Soil Stiffness.

Parameter	Soil Type		Comments	
	Baseline Stiff Soil (BSt)	Very Stiff Soil (VSt)		
Initial modulus of elasticity (MPa)	60	60	Model variable	
Stress-strain relationship	Hyperbolic constitutive model	Hyperbolic constitutive model	See equation (3.2)	
Hyperbolic model parameters: K m	K	270.2	270200	(Ling et al. 2000)
	m	0.5	0.5	
Cohesion (kPa)	0	1000	-	

Table 3.5 Model Parameters and Properties of Facing.

Parameter	Value	Comments
Height (m)	0.2	Fixed
Thickness (m)	0.2	Fixed
Density (kg/m ³)	2200	Corresponds to dry cast concrete
Elastic modulus (MPa)	600	Model variable; ten times larger than initial elastic modulus of soil; linear elastic stress-strain relationship used
Poisson's ratio	0.15	Model variable

Table 3.6 Modeling of Reinforcement Stiffness.

FLAC Modeling Element	Parameter	Reinforcement Type		Comments
		Baseline Reinforcement (BR)	Ductile Reinforcement (DR)	
Cable	Area (m^2)	0.002	0.002	Corresponds to rectangular cross section 0.002x1.0 m
	Perimeter (m)	2.0	2.0	—
	Cable elastic modulus ($\text{kN}/\text{m}^2/\text{m}$)	10^6 (EA=2000 kN/m)	10^5 (EA=200 kN/m)	Model variable
	Cable tensile yield strength (kN/m)	200	200	—
	Grout shear stiffness (kPa)	23077 (Equal to Initial Shear Modulus of Soil)	2307.7 (Equal to 1/10 of Initial Shear Modulus of Soil)	Model variable, characterizes soil-reinforcement interaction
	Grout cohesive strength (kN/m)	100	100	Model variable, characterizes soil-reinforcement interaction
	Grout frictional resistance (deg)	35	35	Characterizes soil-reinforcement interaction
Beam	Area (m^2)	0.002	0.002	—
	Elastic modulus (MPa)	1000	100	Model variable
	Moment of inertia (m^4)	6.67×10^{-10}	6.67×10^{-10}	Corresponds to cross section 0.002x1.0 m

Table 3.7 Modeling of Block-Block and Block-Reinforcement Interfaces.

Parameter	Connection Type			Comments
	Frictional Connection: Low Strength (FCon-L)	Frictional Connection: Baseline Strength (FCon-N)	Structural Connection (SCon)	
Interface friction angle (deg)	20	30	30	—
Interface cohesion (kPa)	0	0	20	—
Interface normal stiffness (kPa/m)	285714	285714	285714	Model variable, corresponds to bulk modulus of concrete blocks
Interface shear stiffness (kPa/m)	23077	23077	23077	Model variable, corresponds to initial shear modulus of soil

Table 3.8 Parametric Study Cases.

Case	Spacing (m)	Soil Type in			Reinforcement Type	Connection Type	Comments
		Foundation	Backfill	Wall			
1	0.2 0.4 0.6 0.8 1.0	HS VSt	HS BSt	HS BSt	BR	FCon-B	Baseline case, $s=0.2$ m
2	0.2 0.4 0.6 0.8	MS VSt	MS BSt	MS BSt	BR	FCon-B	Baseline case, $s=0.6$ m
3	0.2 0.4 0.6 0.8	LS VSt	LS BSt	LS BSt	BR	FCon-B	—
4	0.2 0.4 0.6 0.8	HS BSt	HS BSt	HS BSt	BR	FCon-B	—
5	0.2 0.4 0.6 0.8	MS BSt	MS BSt	MS BSt	BR	FCon-B	—
6	0.2 0.4	LS BSt	LS BSt	LS BSt	BR	FCon-B	—
7	0.2/0.6	MS VSt	MS BSt	MS BSt	BR	FCon-B	Primary and secondary reinforcement
8-1	0.4	HS VSt	HS BSt	HS BSt	DR	FCon-B	Baseline case; modified case 1, $s=0.4$ m

Table 3.8 Parametric Study Cases continued.

Case	Spacing (m)	Soil Type in			Reinforcement Type	Connection Type	Comments
		Foundation	Backfill	Wall			
8-2	0.4	MS VSt	MS BSt	MS BSt	DR	FCon-B	Modified case 2, s=0.4 m
8-3	0.2	LS VSt	LS BSt	LS BSt	DR	FCon-B	Modified case 3, s=0.2 m
9	0.2	HS VSt	HS BSt	HS BSt	BR	FCon-L	Modified case 1, s=0.2 m
10	0.2 0.4 0.6 0.8 1.0	LS BSt	HS BSt	LS BSt	BR	FCon-B	Baseline case, s=0.2 m
11	0.2	HS VSt	HS BSt	HS BSt	BR	FCon-B	Zero dilation in soil, modified case 1, s=0.2 m
12	0.2	HS VSt	HS BSt	HS BSt	BR	SC	Modified case 1, s=0.2 m
	0.6	MS VSt	MS BSt	MS BSt	BR	SC	Modified case 2, s=0.6 m

Table 3.9 General Information for Runs Corresponding to Failure States.

Case	Spacing (m)	Height h_f (m)	Ratio l/h_f	Maximum Displacement (cm)	Grid	Run Time (h:min)	Number of Steps
1	0.2	8.6	0.17	64.0	159x321	50:28***	1333201
	0.4	8.2	0.18	35.8	159x321	31:02	1388425
	0.6	6.2	0.24	7.2	159x321	21:28	726459
	0.8	4.0	0.38	20.3	159x321	14:26	595810
	1	2.0	0.75	30.2	76x121	14:09	363452
2	0.2	6.6	0.23	45.6	159x321	31:55*	823024
	0.4	6.0	0.25	19.3	159x321	28:47*	816555
	0.6	4.6	0.33	23.9	159x321	22:38	874558
	0.8	1.8	0.83	41.5	159x321	9:39*	425868
3	0.2	4.2	0.36	12.8	159x321	7:06*	277551
	0.4	3.8	0.39	32.3	159x321	11:49*	397624
	0.6	2.0	0.75	25.5	159x321	5:37*	229014
	0.8	1.0	1.50	36.5	159x61	1:23	116916
4	0.2	7.0	0.21	17.0	159x321	61:38*	1335795
	0.4	6.0	0.25	8.1	159x321	44:50*	1470381
	0.6	5.4	0.28	16.9	159x321	36:44*	1417394
	0.8	1.8	0.83	24.9	159x321	9:37	478677
5	0.2	5.4	0.28	83.2	159x321	25:54*	1139619

* Run on a computer with Pentium II Processor Intel MMX, 128 MB RAM, 550 MHz.

** Run with FLAC Step Limit=200000.

*** This number is not representative because other runs were running simultaneously on the computer.

Table 3.9 General Information for Runs Corresponding to Failure States Continued.

Case	Spacings (m)	Height h_f (m)	Ratio I/h_f	Maximum Displacement (cm)	Grid	Run Time (h:min)	Number of Steps
5	0.4	3.8	0.39	7.6	159x321	20:25*	765764
	0.6	2.4	0.63	18.9	159x321	14:33	689682
	0.8	1.2	1.25	14.9	159x81	2:38	261182
6	0.2	2.4	0.63	10.8	159x321	9:28*	398764
	0.4	2.6	0.58	33.6	159x321	15:47	732546
7	0.6/0.2	6.0	0.25	46.2	159x181	20:58*	677419
8-1	0.4	8.0	0.19	122.7	159x221	53:32*	1884540
8-2	0.4	5.4	0.28	61.5	159x181	15:18*	999224
8-3	0.2	5.0	0.30	100.8	159x141	28:30*	1073006
9	0.2	8.2	0.18	37.8	159x201	38:07*	1018026
10	0.2	4.4	0.34	32.5	159x321	25:29*	852497
	0.4	4.4	0.34	33.8	159x321	29:44*	1081140
	0.6	2.8	0.54	15.1	159x321	24:00	645318
	0.8	1.0	1.50	16.5	159x321	3:45*	187674
11	0.2	7.2	0.21	41.8	159x321	34:27	1056557
12	0.2	9.4	0.16	90.9	159x321	109:21**	2447030
	0.6	6.0	0.25	59.7	159x221	30:30*	985702

* Run on a computer with Pentium II Processor Intel MMX, 128 MB RAM, 550 MHz.

** Run with FLAC Step Limit=200000.

*** This number is not representative because other runs were running simultaneously on the computer.

Table 3.10 General Information for Runs Corresponding to Critical States.

Case	Spacings (m)	Heigh $t h_{cr}$ (m)	Ratio l/h_{cr}	Maximum displacement		Run time (h:min)	Number of steps
				d_{max} (cm)	d_{max}/h_{cr} (%)		
1	0.2	6.6	0.23	4.4	0.65	26:05***	419538
	0.4	6.0	0.25	4.3	0.72	13:17	440688
	0.6	4.6	0.33	3.1	0.67	7:31	270338
	0.8	2.6	0.58	2.2	0.85	3:46	164679
	1	1.0	1.50	0.3	0.30	0:08	26118
2	0.2	5.4	0.28	4.9	0.91	11:53*	321545
	0.4	4.4	0.34	3.3	0.74	9:21*	286447
	0.6	2.6	0.58	7.1	2.73	5:46	248497
	0.8	1.2	1.25	1.4	1.17	3:29*	158139
3	0.2	4.0	0.38	6.6	1.65	7:36*	227274
	0.4	2.8	0.54	3.7	1.32	4:14*	149751
	0.6	1.6	0.94	3.1	1.94	2:43*	111089
	0.8	0.8	1.88	0.3	0.38	0:12*	16816
4	0.2	5.6	0.27	5.2	0.93	22:42*	740862
	0.4	5.2	0.29	5.5	1.06	29:32*	1055180
	0.6	3.8	0.39	5.4	1.42	15:29*	668768
	0.8	1.6	0.94	2.4	1.50	7:31*	378577
5	0.2	4.2	0.36	5.5	1.31	10:05*	561957

* Run on a computer with Pentium II Processor Intel MMX, 128 MB RAM, 550 MHz.

** Run with FLAC Step Limit=200000.

*** This number is not representative because other runs were running simultaneously on the computer.

3.10 General Information for Runs Corresponding to Critical States Continued.

Case	Spacings (m)	Height h_{cr} (m)	Ratio l/h_{cr}	Maximum displacement		Run time (h:min)	Number of steps
				d_{max} (cm)	d_{max}/h_{cr} (%)		
5	0.4	2.8	0.54	4.1	1.46	10:57*	446741
	0.6	1.2	1.25	1.5	1.25	2:03	101856
	0.8	1.0	1.50	8.5	8.50	1:36	161082
6	0.2	2.0	0.75	3.0	1.50	5:49*	259212
	0.4	1.4	1.08	8.9	6.36***	4:01	203273
7	0.6/0.2	5.0	0.30	5.8	1.16	8:00*	284651
8-1	0.4	5.0	0.30	7.3	1.46	13:50*	485049
8-2	0.4	3.2	0.47	5.2	1.63	3:54*	173555
8-3	0.2	2.2	0.68	2.4	1.09	1:43*	90776
9	0.2	6.6	0.23	5.6	0.85	12:22*	375455
10	0.2	3.2	0.47	3.7	1.16	9:28*	360838
	0.4	3.2	0.47	4.8	1.50	12:48*	514337
	0.6	1.4	1.07	4.3	3.07	4:05	212266
	0.8	0.8	1.88	1.0	1.25	1:39*	87574
11	0.2	6.0	0.25	5.2	0.87	14:13	455957
12	0.2	6.6	0.23	4.2	0.64	10:34**	573009
	0.6	4.6	0.33	4.2	0.64	10:54*	388763

* Run on a computer with Pentium II Processor Intel MMX, 128 MB RAM, 550 MHz.

** Run with FLAC Step Limit=200000.

*** This number is not representative because other runs were running simultaneously on the computer.

@Seismicisolation

CHAPTER 4. RESULTS

The results are divided into two major sets. The first set includes results related to identification of failure mechanisms and influence of soil strength, reinforcement stiffness, foundation stiffness, and secondary reinforcement layers on wall behavior. The second set of results illustrates the influence of reinforcement length, secondary reinforcement layers, and soil dilatancy on wall stability. All tables and figures of chapter 4 are grouped at the end of the chapter in the order of their citing.

All results are presented with reference to three basic states of the modeled wall: failure, critical, and stable states. These states reflect the response of the model during the numerical simulations of construction. Each wall was modeled to reach failure by increasing its height in layers while keeping the reinforcement length equal to 1.5 m. In the process of numerical simulation, the wall reached the verge of failure, but its construction continued until the complete collapse was detected numerically. The state that corresponded to a wall at the verge of failure was termed a critical state. It was defined by analyzing numerical and physical parameters such as slip surface development, maximum cumulative displacement of the system during construction, number of calculation steps necessary to equilibrate the system after placing each layer, and history of maximum unbalanced force. The critical state was identified when at least three of the following events occurred simultaneously: (1) a slip surface was fully developed; (2) the maximum cumulative displacement increased nonlinearly; (3) the number of calculation steps per layer increased rapidly; and (4) the history of maximum unbalanced force indicated an abrupt change of the unbalanced force. The height and length-to-height ratio at the critical state were termed critical height (h_{cr}) and critical length-to-height ratio (l/h_{cr}). The critical wall height with respect to the prevailing mode of failure and soil strength for all cases are shown in figures 4.1 and 4.2. States corresponding to walls higher than the wall at the critical state were termed failure states. Stable states corresponded to walls with a height equal to the critical height but having a length-to-height ratio larger than the critical length-to-height ratio. The definition of failure, critical, and stable states of the numerical modeling is illustrated in figure 3.3. General information about runs corresponding to failure and critical states for all cases are given in table 3.9 and table 3.10.

4.1 Failure Mechanisms of MSEWs

The main purpose of this study was to investigate the behavior of MSEWs with modular block facing and geosynthetic reinforcement simulating construction sequence up to failure. It was important practically to identify the failure mechanisms

as a function of geosynthetic spacing, the effects of soil strength, reinforcement stiffness, foundation stiffness, and secondary reinforcement layers. All numerical simulations used in the analysis are summarized in table 3.8.

4.1.1 Description of Identified Failure Mechanisms

Failure mechanisms were identified by monitoring the development of local plastic (or failure) zones in soil during wall construction, which were recorded incrementally by FLAC on plots in the form of movies. The observed displacement configuration and the type of the developed slip surface defined a failure mechanism. Four failure mechanisms were identified: external mode (direct sliding/toppling); deep-seated mode; compound mode; and connection mode. The slip surface types that corresponded to the identified failure mechanisms are shown in figure 4.3. A summary of results identifying the failure modes of all cases is given in table 4.1. The critical wall height and the prevailing mode of failure of all cases are given in table 4.2. Maximum forces in reinforcement (connection forces and maximum axial forces) for all cases at the critical and failure states are given in tables 4.3 and 4.4.

To gain further insight of wall behavior, stresses, and horizontal displacements at certain vertical sections of the wall were extracted and analyzed. The location of sections A, B, and C is shown in figure 4.4. These vertical sections were defined as Section A (0.1 or 0.15 m behind the facing), Section B (within the reinforced soil, 0.1 m apart from the end of reinforcement), and Section C (within the backfill soil, 0.1 or 0.15 m apart from the end of reinforcement).

The following models were considered as representative cases to illustrate each identified mode of failure:

- External mode: case 1, $s=0.2$ m
- Deep-seated mode: case 10, $s=0.2$ m
- Compound mode: case 8–1, $s=0.4$ m
- Connection mode: case 2, $s=0.6$ m

Figure 3.9 shows the number of calculation steps per layer and the maximum cumulative displacements during wall construction that defined the critical wall height for these cases.

4.1.1.1 External Mode of Failure

The major characteristic of this failure mode was the development of a sliding wedge behind the reinforced mass (figure 4.3-a). When failure was approached, some plastic zones developed within the bottom of reinforced mass.

For cases with foundation soil that was stronger and stiffer than the reinforced soil, the slip surface at failure passed through the bottom of reinforced mass, and the lower reinforcement layers were overstressed. The reinforced mass behaved as a coherent block and failed by toppling against the toe or sliding along the base. This failure mechanism corresponded to toppling or direct sliding. The cases with identified external failure mode are shown in figure 4.1 and given in table 4.2. External failure mode was observed for cases with close reinforcement spacing, stronger reinforced soil, and stiffer foundation and reinforcement.

The model of case 1 ($s=0.2$ m, high strength soil, very stiff foundation) experienced external mode of failure, and the critical state was identified at wall height $h=6.6$ m. At the critical state, the failure zones defined an external slip surface that had developed only in the backfill soil (figure 4.5). The displacement field (figure 4.6) and the distorted grid (figure 4.7) confirmed the observation that the wall was toppling against the toe. The horizontal displacements along sections A and B demonstrated that the reinforced soil was moving as a block (figure 4.8). The axial force distribution along reinforcement layers showed that the reinforcement layers at the wall bottom were overstressed (figure 4.9). However, the forces in the first reinforcement layer were smaller than the forces of adjacent layers, because of a very stiff foundation.

Failure zone distributions of other models that experienced external mode of failure are shown on figures 4.10–4.14.

4.1.1.2 Deep-Seated External Mode of Failure

Deep-seated external mode of failure was characterized by a slip surface developed outside the reinforced mass and through the foundation soil (figure 4.3–b). As failure developed, plastic zones evolved within the bottom of the reinforced mass. This mode of failure was observed for cases with close reinforcement spacing and relatively weak foundation (table 4.2, figure 4.1–b). This failure mechanism corresponded to deep-seated sliding.

The model of case 10 ($s=0.2$ m, high strength reinforced soil, low strength backfill and foundation soil) experienced deep-seated mode of failure, and the critical state was identified at wall height $h=3.2$ m. At the critical state, the failure zones defined an external slip surface that developed outside the reinforced soil (figure 4.15). The displacement field (figure 4.16) and the distorted grid (figure 4.17) confirmed the observation that the wall was first sliding and then toppling against the toe as a result of the foundation's insufficient bearing capacity. The horizontal displacements along sections A and B demonstrated that the reinforced soil was moving as a block (figure 4.18). At the critical state, the displacements at the base of the wall were larger because of the sliding, while at failure, the displacements at the top were larger as a

result of toppling. The axial force distribution along reinforcement layers showed that the forces in reinforcement layers increased with depth (figure 4.19). With the progress of failure, the forces in the bottom layers increased rapidly.

Case 5 ($s=0.2$ m, low strength soil, baseline foundation) also experienced deep-seated mode of failure, and the failure zones' distribution is shown on figure 4.20.

4.1.1.3 Compound Mode of Failure

The compound mode of failure was characterized by a slip surface that developed through the reinforced soil and the backfill (figure 4.3-c). Plastic zones developed within the reinforced soil during early stages of construction. Significant deformations developed as failure approached. The reinforced mass did not behave as a coherent block. The walls failed due to sliding of a mass, defined by a compound slip surface. Compound mode of failure was observed for all cases with DR, and for cases with very stiff foundation and reinforcement spacing that varied from 0.2 m to 0.6 m.

The model of case 8-1 ($s=0.4$ m, high strength soil, very stiff foundation, DR) experienced compound mode of failure, and the critical state was identified at wall height $h=5.0$ m. At the critical state, the failure zones defined a compound slip surface that developed through the reinforced soil (figure 4.21). The displacement field (figure 4.22) and the distorted grid (figure 4.23) indicated significant deformations within the wall, particularly the bottom. The horizontal displacements along sections A and B demonstrated that the reinforced soil was not moving as a coherent block (figure 4.24). The axial force distribution along reinforcement layers (figure 4.25) showed that the forces in reinforcement layers increased with depth and reached their maximum values in the wall section intersecting the compound slip surface. The forces in the bottom reinforcement layer were smaller than the forces of the adjacent layers because of the effects of a very stiff foundation.

Failure zone distributions of models that also experienced compound mode of failure are shown on figures 4.26–4.31.

4.1.1.4 Connection Mode of Failure

Connection mode of failure was characterized by a slip surface that developed entirely within the reinforced soil (figure 4.3-d). Plastic zones and significant deformations within the reinforced soil developed from the beginning of construction. The reinforced mass did not behave as a coherent mass. Due to the large

deformations at the facing, a sliding wedge in the retained soil was observed in some cases. This failure mechanism corresponded to reinforcement pulled out of the facing.

The model of case 2 ($s=0.6$ m, medium strength soil, very stiff foundation) experienced connection mode of failure, and the critical state was identified at wall height $h=2.6$ m. At the critical state, the failure zone was defined by a slip surface that developed entirely within the reinforced soil (figure 4.32). The displacement field (figure 4.33) and the distorted grid (figure 4.34) indicated significant deformations within the wall, and particularly at facing. The horizontal displacements along sections A and B confirmed that there were significant differential movements between the facing blocks, and the reinforced soil was not moving as a block (figure 4.35). The axial force distribution along reinforcement layers showed that the forces in reinforcement layers increased with depth (figure 4.36). The force in the bottom reinforcement layer was smaller than forces in the adjacent layers as a result of the effects of a very stiff foundation.

Case 4 ($s=0.6$ m, high strength soil, baseline foundation) also experienced connection mode of failure, and the failure zones' distribution is shown in figure 4.37.

4.1.1.5 Mixed Modes of Failure

Mixed failure modes were observed for certain combinations of soil and reinforcement properties (table 4.1). In the current analysis, only the predominant mode of failure was considered.

The critical wall height and the predominant mode of failure for all cases are summarized in figures 4.1 and 4.2, and table 4.2.

The identified failure modes (external, deep-seated, compound, and connection mode) closely correspond to the following failure mechanisms investigated in the design of geosynthetic reinforced steep slopes using limit equilibrium method: two-part wedge mechanism (direct sliding analysis); rotational mechanism (deep-seated stability analysis and compound stability analysis); and log-spiral failure mechanism (internal stability or tieback analysis) (Leshchinsky 1997, 1999).

4.1.2 Effects of Geosynthetic Spacing on Failure Mechanisms

The reinforcement spacing was identified as a major factor controlling all aspects of wall behavior. The effects of reinforcement spacing on failure mechanisms were identified with respect to the critical wall height and the mode of failure.

All numerical simulations confirmed the general conclusion that wall stability increases as reinforcement spacing decreases. The critical wall height was defined as a general characteristic of wall stability. It was identified numerically and corresponded to the critical state when the wall was at the verge of failure. Analysis of all relevant cases showed that the critical wall height always increased when the reinforcement spacing decreased. The only exception was observed for case 10 (figure 4.1–b), when the failure was controlled by the strength of the foundation soil, and the wall failed as a result of deep-seated sliding. For this case, the critical wall height remained the same $h=3.2$ m for both models, with reinforcement spacing equal to 0.2 m and 0.4 m.

The numerical analysis confirmed that the reinforcement spacing also controlled the identified modes of failure. In general, it was observed that the mode of failure changed from external or deep-seated to compound and then to connection when the reinforcement spacing increased (figure 4.1, table 4.2). Most of the cases with reinforcement spacing at $s=0.2$ m experienced external or deep-seated modes of failure, and the reinforced soil moved as a solid body, showing no plasticity within the reinforced soil zone. Most of the cases with reinforcement spacing equal to 0.6 m or larger experienced connection mode of failure, and the reinforced soil did not move as a coherent mass. Most of the cases with reinforcement spacing equal to 0.4 m experienced a mixed mode of failure (table 4.1).

In the current analysis, the reinforcement spacing equal to 0.4 m was considered as a specific value that divided the reinforcement spacing range into two categories, with respect to wall behavior. Reinforcement spacing less than or equal to 0.4 m was considered “small” reinforcement spacing. The reinforcement spacing larger than 0.4 m was considered “large” reinforcement spacing. The walls with small reinforcement spacing were more stable than the walls with large reinforcement spacing. The failure of walls with large reinforcement spacing was always accompanied by some degree of instability within the reinforced soil mass.

The behavior of walls with small reinforcement spacing was similar to the behavior of a conventional gravity retaining wall. The identified modes of failure were external or deep-seated (table 4.2). At the critical state, a small number of local failure zones within the bottom part of the reinforced soil mass was observed (figures 4.5, 4.10–4.15, 4.26). The analysis of displacement fields (figures 4.6, 4.16), grid distortions (figures 4.7, 4.17) and horizontal displacement distributions along sections A and B (figures 4.8, 4.18) confirmed that the reinforced soil was internally stable and moved as a coherent mass. The analysis of axial force distributions in reinforcement showed a smooth change of force without abrupt differences within the reinforcement layers or within the wall, which is another indication of internal stability (figures 4.9, 4.19).

All walls with large reinforcement spacing experienced internal instability to some degree. The predominant mode of failure was the connection mode. The reinforced mass did not move as a solid block. Analysis of failure zone distributions (observed by movies produced by FLAC) showed that failure zones evolved first in the reinforced soil, initiating large deformations that led to connection breakage. At the critical state, the predominant part of the reinforced soil was at yield in shear or volume, while the backfill was affected minimally (figures 4.31, 4.32, and 4.37). At failure states, the failure zones propagated to the backfill because of the large deformations at the facing. The analysis of displacement fields (figure 4.33), grid distortions (figure 4.34) and horizontal displacement distributions along sections A and B (figure 4.35) of case 2 ($s=0.6$ m) confirmed that there were significant deformations in the reinforced soil.

The reinforcement spacing appears to control the failure mechanisms of MSEWs. In the subsequent discussion, all effects on wall behavior were identified with respect to reinforcement spacing.

4.1.3 Effects of Soil Strength on Failure Mechanisms as Function of Geosynthetic Spacing

Cases 1 to 6 were designed to investigate the effects of soil strength on failure mechanisms. For cases 1 to 3, the soil strength decreased from case 1 to case 3, and the foundation soil was modeled to represent a very stiff foundation (tables 3.2 and 3.7). The foundation soil of cases 4 to 6 was modeled to be the same as the reinforced and backfill soil. Soil properties were the same as those of cases 1 to 3, respectively.

The effect of soil strength on wall stability is illustrated in figures 4.1 and 4.2 by the change of critical wall height with respect to soil strength. The critical wall height decreased as soil strength decreased. An important observation was that, with smaller reinforcement spacing, the same or higher critical wall height can be achieved with lower strength soil. For example, the critical wall height of case 5 ($s=0.2$ m, medium strength soil) was 4.2 m, while the critical wall height of case 4 ($s=0.6$ m, high strength soil) was 3.8 m.

The effects of soil strength on failure mechanisms were different for the cases with very stiff foundations and the cases with baseline foundations. For very stiff foundations (cases 1–3), the deep-seated mode of failure was not identified. The decrease of soil strength changed the mode of failure from external to compound mode, or from compound to connection mode (table 4.2, figure 4.1-a). For the cases with baseline stiffness of the foundation soil (cases 4–6), all four modes of failure

were observed. For cases 5 and 6 with reinforcement spacing of 0.2 m, and case 4 with reinforcement spacing of 0.2 m and 0.4 m, the decrease of soil strength changed the mode of failure from external to deep-seated. All models experienced connection mode of failure when the reinforcement spacing was equal to 0.6 m or larger.

For a given reinforcement spacing, soil strength affected the stability and, to some extent, the failure mechanism. A decrease of soil strength corresponded to a decrease of the critical wall height. A decrease of soil strength, however, did not always change the identified failure mechanism.

4.1.4 Effects of Reinforcement Stiffness on Failure Mechanisms as Function of Geosynthetic Spacing

Effects of reinforcement stiffness on failure mechanisms were investigated by comparing cases with different reinforcement stiffness. The reinforcement stiffness characteristics of cases 1 ($s=0.4$ m), 2 ($s=0.4$ m), and 3 ($s=0.2$ m) were decreased 10 times, and new models were defined: case 8–1 ($s=0.4$ m), case 8–2 ($s=0.4$ m) and case 8–3 ($s=0.2$ m). Cases 1, 2, and 3 represented models with very stiff foundations and low, medium, and high strength soils, respectively. The largest reinforcement spacing corresponding to models experiencing mainly external mode of failure was chosen for each (table 4.1). The modes of failure of cases 1–3 were mixed. For case 1 ($s=0.4$ m), the external mode was predominant. For cases 2 ($s=0.4$ m) and 3 ($s=0.2$ m), the compound mode was predominant. The reinforcement of the modified cases 8–1, 8–2 and 8–3 was termed DR. The reinforcement of all other cases was termed BR. Material properties of the reinforcement are given in table 3.5.

The effects of reinforcement stiffness on wall response were identified by comparison between cases 1 ($s=0.4$ m, BR) and 8–1 (DR), cases 2 ($s=0.4$ m, BR) and 8–2 (DR), and cases 3 ($s=0.2$ m, BR) and 8–3 (DR). All comparisons were made for a wall height equal to the smaller critical height of the compared cases.

4.1.4.1 High Strength Soil

The effects of reinforcement stiffness on wall response in models with high strength soil and very stiff foundation were investigated by comparing case 1 ($s=0.4$ m, BR) and case 8–1 (DR). The most significant results are given in table 4.5.

For case 1, an external mode of failure prevailed, and the critical wall height was 6.0 m. The plastic zone distribution for wall height $h=5.0$ m (the critical height of case 8–1) shows that plasticity occurred at the bottom of the reinforced soil and behind it, but the slip surface was not developed fully yet (figure 4.38-a). The first plastic zones occurred within the backfill soil at wall height of 3.2 m, and the first

slip surface was external and fully developed at a wall height of 5.8 m (table 4.1). For wall height $h=5.0$ m, the maximum forces in reinforcement were not at the connections (figure 4.38–b). They increased almost linearly with depth, reaching a maximum value of 6.46 kN at elevation 1.0 m, and then decreased in the lower reinforcement layers (figure 4.39). The connection force followed a similar pattern. Maximum horizontal displacement of 2.9 cm was observed at elevation of 2 to 2.5 m (figure 4.40).

For case 8–1, a compound mode of failure was identified, and the critical wall height was 5.0 m. At the critical wall height, a compound slip surface was fully developed, and plastic zones were located not only along the surface, but also within the reinforced soil (figure 4.21). The first plastic zone occurred within the reinforced soil at wall height of 1.6 m, and the first slip surface was internal and fully developed at wall height of 1.8 m. Maximum forces in reinforcement were at the connections (figure 4.25). They increased almost linearly with depth, reaching a maximum value of 5.51 kN at elevation 1.4 m, and then decreased in the lower reinforcement layers (figure 4.39). Maximum horizontal displacement of 7.3 cm was observed at an elevation 2 to 2.5 m (figure 4.40).

Comparing cases 1 and 8–1 (high strength soil) showed that the lower reinforcement stiffness allowed larger deformations within the reinforced soil and, as a consequence, failure mode changed from mixed (predominant external mode) to compound, critical wall height decreased, and plastic zones first occurred within the reinforced soil at much lower wall height. For case 8–1 (DR), the maximum reinforcement forces were lower and always located at the connections. The decrease of reinforcement forces at the bottom of the wall was a result of the effects of a very stiff foundation.

4.1.4.2 Medium Strength Soil

The effects of reinforcement stiffness on wall response in models with medium strength soil and very stiff foundations were investigated by comparing case 2 ($s=0.4$ m, BR) and case 8–2 ($s=0.4$ m, DR). The most significant results are given in table 4.6.

For case 2, the compound mode of failure prevailed, and the critical wall height was 4.4 m. The plastic zone distribution for wall height $h=3.2$ m (the critical height of case 8–2) shows that the plastic zones were located at the bottom of the reinforced soil and within a wedge of backfill soil (figure 4.41). The first plastic zone developed within the reinforced soil at wall height of 1.4 m, and the first slip surface was compound and fully developed at wall height of 2.8 m (table 4.6). For wall height $h=3.2$ m, the maximum forces in reinforcement were not at the connections (figure

4.42). They increased almost linearly with depth until they reached the maximum value of 4.51 kN at elevation 0.6 m, and then decreased in the first reinforcement layer (figure 4.43). Maximum horizontal displacement of 1.7 cm was observed at an elevation of 1.5 to 2.0 m (figure 4.40).

For case 8–2, a compound mode of failure was identified, and the critical wall height was 3.2 m. At the critical wall height, a compound slip surface was fully developed, and plastic zones were spread out within the reinforced soil (figure 4.29). The first plastic zone within the reinforced soil occurred at wall height of 1.4 m (the same wall height as for case 2), and the first slip surface was internal and fully developed at a wall height $h=1.6$ m (table 4.6). The maximum forces in reinforcement were at the connections in the middle part of the wall and in the bottom layer (figure 4.42). Forces increased almost linearly with depth until the layer at elevation 1.4 m, reaching a maximum value of 4.23 kN at elevation 1.0 m, and then decreased in the bottom reinforcement layer (figure 4.43). Maximum horizontal displacement of 5.2 cm was observed at an elevation of 1 to 1.5 m (figure 4.40).

Comparing cases 2 and 8–2 (medium strength soil) showed that the lower reinforcement stiffness of case 8–2 allowed larger deformations within the reinforced soil and, as a consequence, failure mode changed from mixed (predominant compound mode) to compound, and the critical wall height decreased. First plastic zone occurred at the same wall height for both cases. The maximum reinforcement forces for case 2 were not at the connections, while the forces for case 8–2 were at the connections in the middle part of the wall and in the bottom layer. For case 2 (BR), the maximum reinforcement forces in the middle part of the wall were slightly smaller, compared to case 8–2. This can be explained by the fact that the middle part of the wall was internally stable, almost no plastic zones developed (figure 4.41-a).

4.1.4.3 Low Strength Soil

The effects of reinforcement stiffness on wall response in models with low strength soil and very stiff foundations were investigated by comparing case 3 ($s=0.2$ m, BR) and case 8–3 ($s=0.2$ m, DR). The most significant results are given in table 4.7.

For case 3, the compound mode of failure prevailed, and the critical wall height was 4.0 m. The plastic zone distribution for wall height $h=2.2$ m (the critical height of case 8–2) showed that few and scattered plastic zones developed behind the reinforced soil (figure 4.44-a). The first plastic zone occurred within the reinforced soil at a wall height of 1.2 m, and a compound slip surface developed at a wall height of 2.4 m (table 4.7). For wall height $h=2.2$ m, the maximum forces in reinforcement were not at the connections (figure 4.45-a). They increased almost linearly with

depth, reaching the maximum value of 2.26 kN at elevation 0.8 m, and then decreased in the lower reinforcement layers (figure 4.46-a). Maximum horizontal displacement of 0.8 cm was observed at an elevation of 1.0 to 1.5 m (figure 4.40).

For case 8–3, a compound mode of failure was identified, and the critical wall height was 2.2 m. At the critical wall height, a compound slip surface was fully developed, and plastic zones developed also within the reinforced soil (figure 4.44-b). The first plastic zone occurred within the reinforced soil at a wall height of 1.2 m (the same wall height as for case 2), and a compound slip surface developed at wall height of 1.2 m (table 4.7). The maximum forces in reinforcement were near the connections (figure 4.45-b). They increased almost linearly with depth until elevation 1.4 m, reaching the maximum value of 4.23 kN at elevation 1.0 m, and decreasing in the bottom layer (figure 4.46-b). Maximum horizontal displacement of 5.2 cm was observed at an elevation of 1 to 1.5 m (figure 4.40).

Comparing cases 3 and 8–3 (low strength soil) showed that the lower reinforcement stiffness of case 8–3 allowed for larger deformations within the reinforced soil and, as a consequence, failure mode changed from mixed (predominant compound mode) to purely compound, and the critical wall height decreased. The first plastic zone occurred at the same wall height for both cases. The maximum reinforcement forces for both cases were not located at the connections.

Based on the comparison between cases representing different soil strength and reinforcement stiffness, researchers drew the following conclusions:

- The reinforcement stiffness affected the failure mode and wall stability for all soil types.
- The DR allowed larger deformations to occur within the reinforced soil. Consequently, plastic zones developed in large parts of the reinforced soil, and a compound failure mode was observed for all soil types. Connection mode of failure was not observed. This could be a result of the effects of the very stiff foundation and the small reinforcement spacing.
- The critical wall height of all cases with DR was less than the critical wall height of the corresponding cases with BR. The difference between the critical wall height for cases with baseline and DR increases as soil strength decreases.
- The maximum forces in reinforcement for all cases with DR were identified either at the connections or near them.

- For all cases, the bottom reinforcement layers were less stressed, because of the effect of the very stiff foundation.
- The maximum horizontal displacements of the cases with DR were about 2.5 to 3 times larger than the maximum horizontal displacements of the corresponding cases with BR.
- Reinforcement stiffness was identified to affect the failure mode and wall stability of walls with small reinforcement spacing. The decrease of reinforcement stiffness affected the wall response similar to the increase of the reinforcement spacing (i.e., it increased the wall displacements and the possibility of internal instability).

4.1.5 Effects of Connection Strength on Failure Mechanisms as Function of Geosynthetic Spacing

Three types of connections were modeled to investigate the effects of connection strength on failure mechanisms: frictional connection with baseline strength, frictional connection with low strength, and structural connection. Interface properties that modeled these types of connections are given in table 3.7.

The effects of connection strength on failure mechanisms were investigated by comparatively analyzing the following two sets of cases that represented models with small and large reinforcement spacing:

- Cases with small reinforcement spacing, $s=0.2$ m: case 1 (FCon-B=frictional connection with baseline strength), case 9 (FCon-L=frictional connection with low strength), and case 12 (SC=structural connection).
- Cases with large reinforcement spacing, $s=0.6$ m: case 2 (FCon-B=frictional connection with baseline strength), and case 12 (SC=structural connection).

4.1.5.1 Cases with Small Reinforcement Spacing

Case 1 ($s=0.2$ m, FCon-B), case 9 ($s=0.2$ m, FCon-L), and case 12 ($s=0.2$ m, SC) represent models with high strength soil, very stiff foundations, and small reinforcement spacing ($s=0.2$ m). Interfaces at the facing of case 1 were modeled with angle of friction $\phi_{int}=30^\circ$ and zero cohesion to represent frictional connection between the reinforcement and the blocks. This type of connection was defined as a baseline type and was used in all models except the models of cases 9 and 12. The models of cases 9 and 12 were prepared by changing the interface properties of case 1. Interfaces at the facing of case 9 were modeled with angle of friction

$\phi_{int}=20^\circ$ and zero cohesion to represent frictional connection with lower strength. Interfaces at the facing of case 12 were modeled with angle of friction $\phi_{int}=30^\circ$ and cohesion $c_{int}=20$ kPa to represent structural connection. All interface properties are given in table 3.6. The most significant results for case 1 (FCon-B), case 9 (FCon-L), and case 12 (SC) are given in table 4.8.

Comparing the results for cases 1, 9, and 12 ($s=0.2$ m) indicates that connection strength had insignificant influence on wall behavior for cases with small reinforcement spacing. All models experienced external mode of failure and reached a critical state at wall height of 6.6 m (table 4.8). For case 9, the first plastic zones in the backfill soil occurred at lower wall height, and the connection and maximum forces were large compared with cases 1 and 12. This can be explained with the larger displacements developed in the model of case 9 facilitated by the lower connection strength. The connection force and the maximum force in reinforcement for cases 1, 9 and 12 ($s=0.2$ m) are given on figures 4.47 and 4.48, respectively. The horizontal displacements along section A (0.1 m behind the facing) are shown in figure 4.49.

The comparison between cases 1, 9, and 12 with small reinforcement spacing ($s=0.2$ m) and different connection strengths revealed that the connection strength did not affect the wall behavior significantly.

4.1.5.2 Cases with Large Reinforcement Spacing

Case 2 ($s=0.6$ m, FCon-B) and case 12 ($s=0.6$ m, SC) represented models with high strength soil, very stiff foundations, and large reinforcement spacing ($s=0.6$ m). Interfaces at the facing of case 2 were modeled with angle of friction $\phi_{int}=30^\circ$ and zero cohesion to represent frictional connection (frictional connection with baseline strength). The model of case 12 was prepared by changing the interface properties of case 2. Interfaces at the facing of case 12 were modeled with angle of friction $\phi_{int}=30^\circ$ and cohesion $c_{int}=20$ kPa to represent structural connection between the reinforcement and the blocks. All interface properties are given in table 3.7. The most significant results for the compared cases are given in table 4.9.

Comparing the results for cases 2 and 12 ($s=0.6$ m) indicates that connection strength had significant influence on wall behavior for cases with large reinforcement spacing. Due to the higher strength of the structural connection, the mode of failure changed from connection mode (case 2) to compound mode (case 12), and the critical wall height increased from 2.6 m (case 2) to 4.6 m (case 12). For case 2, the first plastic zone occurred at lower wall height, the maximum force was larger, and the connection forces were smaller compared to case 12 (table 4.9, figures 4.50

and 4.51). This can be explained with the larger displacements at the facing developed in the model of case 2, caused by the lower connection strength. The horizontal displacements along section A (0.1 m behind the facing) are shown in figure 4.52. The uneven distribution of the horizontal displacements along section A for case 2 indicated that the frictional connection allowed differential movements between the facing blocks.

The comparison between cases 2 and 12 with large reinforcement spacing ($s=0.6$ m) and different connection strengths revealed that the connection strength affected the wall behavior significantly. The connection strength increase led to a failure mode change, an increase of the critical wall height, and decrease of wall displacements.

The analysis of cases with high strength soil, very stiff foundations, and different connection strengths indicates that the effects of connection strength on wall behavior can be significant for large reinforcement spacing. For cases with small reinforcement spacing, connection strength effects were insignificant.

4.1.6 Effects of Foundation Stiffness on Failure Mechanisms as Function of Geosynthetic Spacing

Effects of foundation stiffness on failure mechanisms were investigated by changing the stiffness of foundation soil. Two major types of foundation were modeled: very stiff foundation and baseline foundation. In all numerical simulations, the elastic modulus of soil was updated after placing each soil layer and after equilibrium was attained using the hyperbolic stress-strain relationship given in Equation (3.2). Poisson's ratio was kept constant. The very stiff foundation soil was modeled with an artificially high cohesion ($c=1000$ kPa), and a hyperbolic model parameter $K=270200$ that was 1000 times larger than the value used to model the baseline soil stiffness ($K=270.2$, Ling et al. 2000). Soil properties that were used to model the soil stiffness are given in table 3.4.

Cases 1–6 and case 10 were designed to investigate the effects of foundation stiffness on failure mechanisms (tables 3.3, 3.4, and 3.8). Cases 1, 2, and 3 represent models with very stiff foundation soil, and soil strength of the reinforced and backfill soil that changed from high (case 1) to low (case 3). The models of cases 4, 5, and 6 were the same as those of cases 1, 2, and 3, respectively, but the foundation soil was modeled to be the same as the reinforced and backfill soil. For case 10, the soil stiffness was the same in all parts of the model, but the soil strength was different; the reinforced soil was of high strength, while the rest was of low strength.

The effects of foundation stiffness on wall behavior were identified by comparatively analyzing all cases with respect to failure mechanisms and wall stability. cases 1, 4, and 10 ($s=0.2$ m) were analyzed further, and the horizontal displacements along section A, stress distributions along section A, connection forces, and maximum forces in reinforcement were compared at wall height $h=3.2$ m.

The effects of foundation stiffness on wall stability were identified by the change of the critical wall height for cases with different foundation soil. The comparison of the critical wall height for case 1 (HS=high strength soil, VSt=very stiff foundation), case 4 (HS, BSt=foundation soil with baseline stiffness) and case 10 (H&LS=high strength reinforced soil, and low strength soil in foundation and backfill) is shown in figure 4.53-a. The comparison of the critical wall height for cases 2 (MS=medium strength soil, VSt), 5 (MS, BSt), and 10 (H&LS) is shown in figure 4.53-b. The comparison of the critical wall height for cases 3 (LS=low strength soil, VSt), 4 (LS, BSt), and 10 (H&LS) is shown in figure 4.53-c. All comparisons show that the lower stiffness or lower strength of foundation soil led to smaller critical wall height. It is important to note that the comparison of cases 3 and 10 ($s=0.4$ m) does not contradict this conclusion. The model of case 3 (LS, VSt, $s=0.4$ m) experienced compound mode of failure, and because the foundation soil was very stiff and strong, the wall stability was controlled by the low strength of the reinforced soil. The model of case 10 (H&LS, $s=0.4$ m) experienced deep-seated mode of failure, and since the reinforced soil was with high strength, the wall stability was controlled by the low strength of the foundation soil. This was also true for case 10 ($s=0.2$ m). The models of case 10 with reinforcement spacing $s=0.2$ and 0.4 m had the same critical wall height $h=3.2$ m and behaved identically. This indicates that, because of the small reinforcement spacing and high strength of the reinforced soil, the reinforced soil moved as a coherent block, and failure is controlled by the low strength of the foundation soil.

The effect of foundation stiffness on failure mechanisms was different for the cases with very stiff foundations and the cases with baseline stiff foundations. For the very stiff foundation (cases 1, 2, and 3), decrease of soil strength changed the mode of failure from external to compound mode, or from compound to connection mode (figure 4.1-a). A deep-seated mode of failure was not identified. For the baseline foundation (cases 4, 5, and 6), all four modes of failure were observed. For cases with large reinforcement spacing, decrease of foundation soil strength changed the mode of failure from external to connection mode. For cases with small reinforcement spacing, the decrease of foundation soil strength changed the mode of failure from external to deep-seated.

The foundation stiffness affected the wall behavior by changing the failure mechanisms. The artificially high stiffness and strength of foundation soil prevented

the development of deep-seated failure and increased wall stability. When the foundation soil was changed from baseline to very stiff soil, the cases with small reinforcement spacing that experienced deep-seated mode of failure exhibited compound failure mode. The current analysis implied that foundation effects should not be neglected in numerical analysis and design.

To express numerically the effects of foundation stiffness, the most significant results of cases 1, 4, and 10 ($s=0.2$ m) were analyzed (table 4.10). Horizontal displacements along section A, stress distributions along section A, connection forces, and maximum forces in reinforcement were compared at wall height $h=3.2$ m. The wall height of 3.2 m corresponded to the lowest critical height of all 3 cases.

The change of foundation stiffness from very stiff (case 1) to baseline soil (case 4) led to a decrease of the critical wall height from 6.6 (case 1) to 5.6 (case 4). The mode of failure for both cases was external, and distribution of plastic zones in the backfill soil was similar. For case 4 (baseline foundation), the plastic zones spread to the foundation soil under the toe, and the first zone in the reinforced and backfill soil occurred at lower wall height, compared to case 1. The very stiff foundation restrained the displacements at the bottom of the wall. The comparison between models of cases 1 and 4 with wall height $h=3.2$ m showed that the change of foundation soil from very stiff to baseline soil increased the horizontal displacements (figure 4.53-a) and maximum forces in reinforcement (figure 4.54). Forces in the reinforcement layers decreased at the bottom of the wall for both cases. Stress distributions along section A (0.15 m behind facing) showed a stress concentration at the bottom of the wall as a result of the toppling of the walls (figure 4.53-b).

The change of foundation strength from high strength (case 4) to low strength (case 10) led to a decrease of the critical wall height from 5.6 m (case 4) to 3.2 m (case 10), and to a change of failure mode from external to deep-seated. Plastic zones occurred predominantly in the backfill and foundation soil. For case 10 (low strength foundation soil), the first zone occurred at lower wall height compared to case 4 (high strength foundation soil) and were concentrated around the toe of the wall. The comparison between the models of cases 4 and 10 at wall height $h=3.2$ m showed that the change of foundation strength from high to low increased the horizontal displacements (figure 4.53-a) and the reinforcement forces (figure 4.53-b). Reinforcement forces of case 10 increased linearly with depth, and the maximum values were observed in the first layer. The reinforcement forces of case 4 increased linearly, reaching the maximum value at 0.6 m, and then decreased at the bottom of the wall. Stress distributions along section A (0.15 m behind facing) showed a stress concentration at the bottom of the wall due to the toppling (figure 4.53-c).

Foundation stiffness had significant effects on wall response. The decrease of foundation stiffness or strength decreased the critical wall height, changed the mode of failure, and increased the displacements and reinforcement forces. The current study confirmed that the modeling of foundation soil as very stiff significantly changed the wall response. The walls with large reinforcement spacing were more sensitive to the change of foundation properties than walls with small reinforcement spacing.

4.2 Effects of Reinforcement Length on Reinforcement Stresses and Wall Stability

The effects of reinforcement length on wall stability were identified by additional numerical analysis of case 1 ($s=0.2$ m, external mode), case 8–1 ($s=0.4$ m, compound mode), and case 10 ($s=0.2$ m, deep-seated mode). The wall height of these models was kept constant and equal to the critical height, while the reinforcement length was increased to predetermined values. The state corresponding to walls with height equal to the critical height and reinforcement length larger than 1.5 m (baseline length), is termed “stable state”. The effects of reinforcement length on reinforcement forces, stress distributions and horizontal displacements are presented graphically (figures 4.55–4.67).

The model of baseline case 1 ($s=0.2$ m, $l=1.5$ m, high strength soil, very stiff foundation) experienced external mode of failure and the critical state was identified at wall height $h=6.6$ m ($l/h=0.23$). Three stable states were investigated with the following reinforcement length: $l=2.0$ m ($l/h\approx0.3$); $l=2.6$ m ($l/h\approx0.4$); and $l=3.3$ m ($l/h=0.5$). The distributions of horizontal and vertical stresses along section A (0.15 m behind the facing) and section C (0.15 m behind the reinforced soil) are shown on figures 4.55 and 4.56. The movements of the wall at failure corresponded to wall toppling (figure 4.5–a). This led to a stress concentration along the bottom of section A and smaller stresses along section C. When the reinforcement length was increased, the stresses along section A decreased and the stresses along section C increased. This was an indication that rotation against the toe decreased and wall stability increased. The horizontal displacements along sections A and C also decreased as reinforcement length increased (figure 4.57). However, displacements were small and implied a movement of the reinforced soil as a composite block. The maximum axial forces in reinforcement decreased with the increase of the reinforcement length (figure 4.58). For a given state, the maximum reinforcement forces increased with depth almost linearly, reaching a maximum value at an elevation of 0.8 to 1.2 m, and then decreased in the bottom layers. The connection forces changed in the same way (figure 4.59).

The model of baseline case 8–1 ($s=0.4$ m, $l=1.5$ m, high strength soil, DR) experienced compound mode of failure, and the critical state was identified at wall

height $h=5.0$ m ($l/h=0.3$). Two stable states were investigated with the following reinforcement lengths: $l=2.0$ m ($l/h=0.4$); $l=2.5$ m ($l/h=0.5$). The distributions of horizontal and vertical stresses along section A (0.15 m behind the facing) and section C (0.15 m behind the reinforced soil) are shown in figures 4.60 and 4.61. The wall movements led to stress concentration along the bottom of section A and smaller stresses along section C. When the reinforcement length was increased, the stresses along section A decreased, and the stresses along section C increased. This indicated that rotation against the toe decreased, and wall stability increased. The horizontal displacements also decreased as reinforcement length increased (figure 4.62). The differences between the horizontal displacements along sections A and C increased as reinforcement length increased. The maximum difference was about 2 percent of the reinforcement length, indicating significant deformations within the reinforced soil. The maximum axial forces in reinforcement were at the connections and decreased as reinforcement length increased (figure 4.63). For a given state, the maximum reinforcement forces increased with depth almost linearly, reaching a maximum value at an elevation of 1.2 to 1.6 m, and then decreased in the bottom layers.

The model of baseline case 10 ($s=0.2$ m, $l=1.5$ m, high strength reinforced soil, low strength backfill and foundation soil) experienced deep-seated mode of failure, and the critical state was identified at wall height $h=3.2$ m ($l/h=0.47$). A stable state with reinforcement length $l=2.2$ m ($l/h=0.7$) was investigated. The distributions of horizontal and vertical stresses along section A (0.15 m behind the facing) and section C (0.15 m behind the reinforced soil) are shown in figures 4.64 and 4.65. When the reinforcement length was increased, the stresses along section A decreased, and the stresses along section C increased. This indicated that the wall stability increased. The differences between the horizontal displacements along sections A and C increased as reinforcement length increased. However, they were small and represented a movement of the reinforced soil as a composite block (figure 4.66). The maximum axial forces in reinforcement decreased as reinforcement length increased (figure 4.67). For a given state, the maximum reinforcement forces increased with depth almost linearly. The connection forces changed in the same way (figure 4.67).

The analysis of stable states of models representing external, compound, and deep-seated modes of failure indicates that increasing of reinforcement length improved wall stability and decreased wall displacements and reinforcement forces.

4.3 Effects of Secondary Reinforcement Layers on Connection Loads and Wall Stability

Effects of secondary reinforcement layers on wall behavior were investigated by comparing case 1 ($s=0.6$ m) and case 7 ($s=0.6/0.2$ m) (table 4.11, figure 3.12). The reinforcement layout of case 1 ($s=0.2$ m, medium strength soil, very

stiff foundation) was changed to create the model of case 7 (figures 3.12 and 4.68). The reinforcement layers that corresponded to the reinforcement layout of case 2 ($s=0.6$ m) were kept the same and were termed “primary reinforcement.” The other reinforcement layers were termed “secondary reinforcement.” The cable part of secondary layers was divided into two parts with different properties. The cable part next to the facing was 0.3 m long and had the same properties as the primary reinforcement. The other cable part was 1.2 m long and was modeled with very low stiffness and strength to avoid influencing the model response. The values of cable elastic modulus, cable tensile yield strength, grout shear stiffness, and grout cohesive strength were chosen to be 100 times smaller than the values used to model the primary reinforcement, i.e.:

- Cable elastic modulus: $E_c=10000$ kN/m²/m ($EA=20$ kN/m)
- Cable tensile yield strength: $T_y=2$ kN/m
- Grout shear stiffness: $kbond=230.77$ kPa
- Grout cohesive strength: $sbond=1$ kN/m
- Grout friction angle: $\phi_g=5^\circ$

The other properties of the cable were the same as the properties of the primary reinforcement (table 3.6).

The comparison between case 2 ($s=0.6$ m) and case 7 ($s=0.6/0.2$ m) shows that the intermediate reinforcement spacing changed the mode of failure from connection mode (case 2) to compound mode (case 7), and increased the critical wall height from 2.6 m (case 2) to 5.0 m (case 7). The comparison of plastic zones corresponding to wall height $h=2.6$ m demonstrates that secondary reinforcement increased internal stability of the reinforced soil, particularly at the facing (figures 4.28 and 4.69). The horizontal displacements along section A (0.1 m behind the facing) were larger for case 2 ($s=0.6$ m, $h=2.6$ m), particularly between the reinforcement layers (figure 4.70). The forces in the reinforcement were also larger for case 2 (figures 4.68 and 4.71).

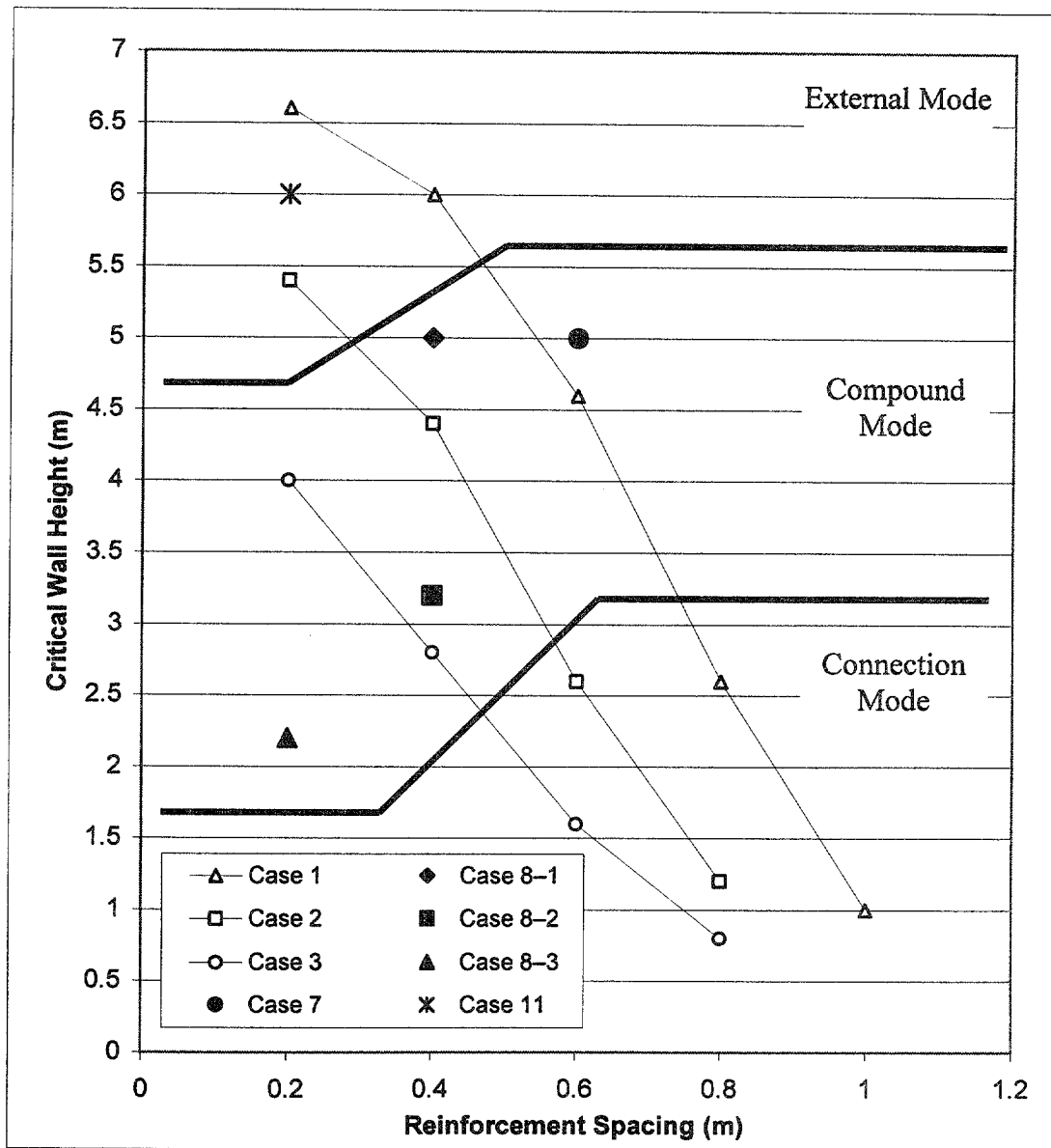
Introducing secondary reinforcement layers in a model with large reinforcement spacing changed the wall behavior significantly. The following effects were identified: mode of failure changed; global wall stability and local stability at the wall facing increased; and displacements and reinforcement forces decreased. The secondary reinforcement layers increased the stability of the wall by redistributing the stresses and connection forces at the facing.

4.4 Influence of Soil Dilatancy on Model Response

Influence of soil dilatancy on model response was investigated comparing the results of case 1 ($s=0.2$ m) and case 11. The model of case 11 was developed by setting dilation angle to zero for all soils in the model of case 1 ($s=0.2$ m). All other characteristics were the same in both models. The most significant results for the compared cases are given in table 4.12.

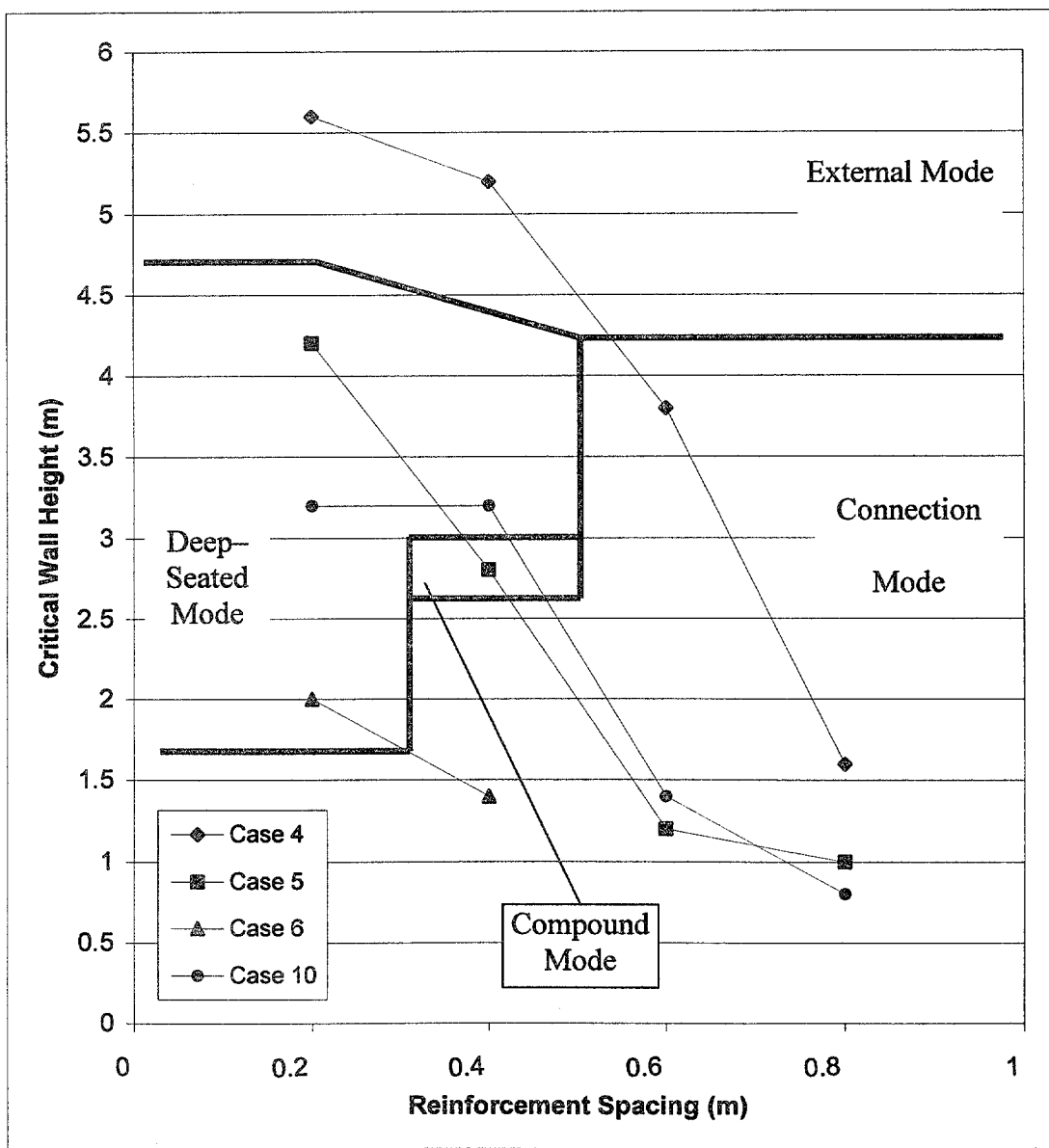
The comparison showed that soil dilatancy did not influence the observed mode of failure, but the model with zero dilation was less stable and experienced larger deformations and larger reinforcement forces compared to the model with non-zero dilation. External mode of failure was identified for both cases (figures 4.5 and 4.13). The critical height of case 11 ($h=6.0$ m, zero dilation) was smaller than the critical height of case 1 ($h=6.6$ m) (table 4.13). Failure zones that developed during wall construction showed that plastic zones for case 11 were located in narrower bands, compared to case 1. The first plastic zone in the model of case 11 evolved at a later stage of construction, compared to case 1. With respect to numerical stability, the model with zero dilation (case 11) required longer run time and more calculation steps than the model with nonzero dilation (case 1).

The current results showed that soil dilatancy influenced the model's response. Decreasing the dilation angle increased the displacements and reinforcement forces, and decrease the critical wall height. Decreasing the dilation angle did not change the mode of failure.



(a)

Figure 4.1 Critical Wall Height and Prevailing Mode of Failure: (a) Cases with Very Stiff Foundation; (b) Cases with Baseline Foundation.



(b)

Figure 4.1 Critical Wall Height and Prevailing Mode of Failure: (a) Cases with Very Stiff Foundation; (b) Cases with Baseline Foundation, Continued.

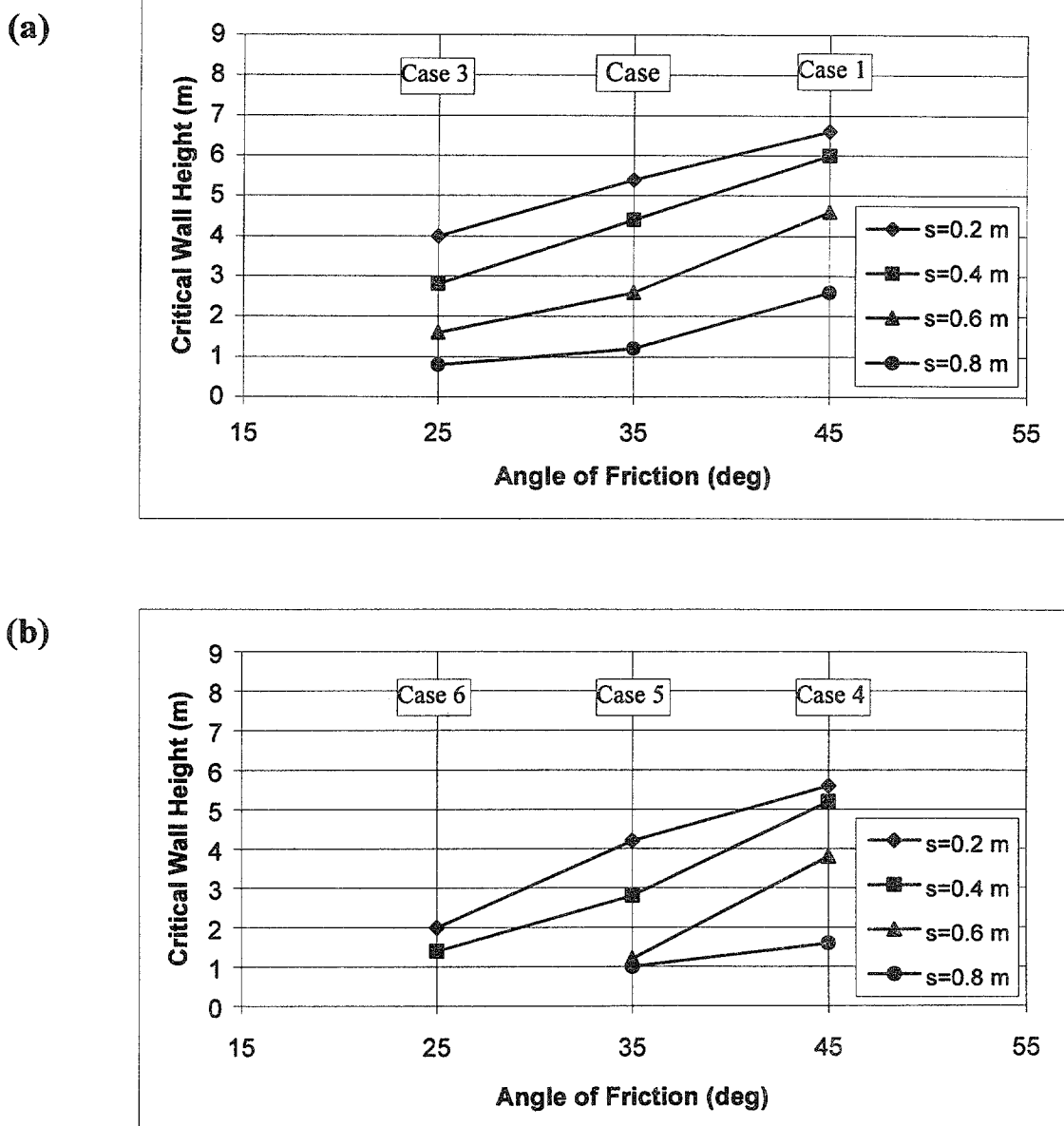


Figure 4.2 Change of Critical Wall Height with Respect to Soil Strength:
(a) Cases with Very Stiff Foundation; (b) Cases with Baseline Foundation.

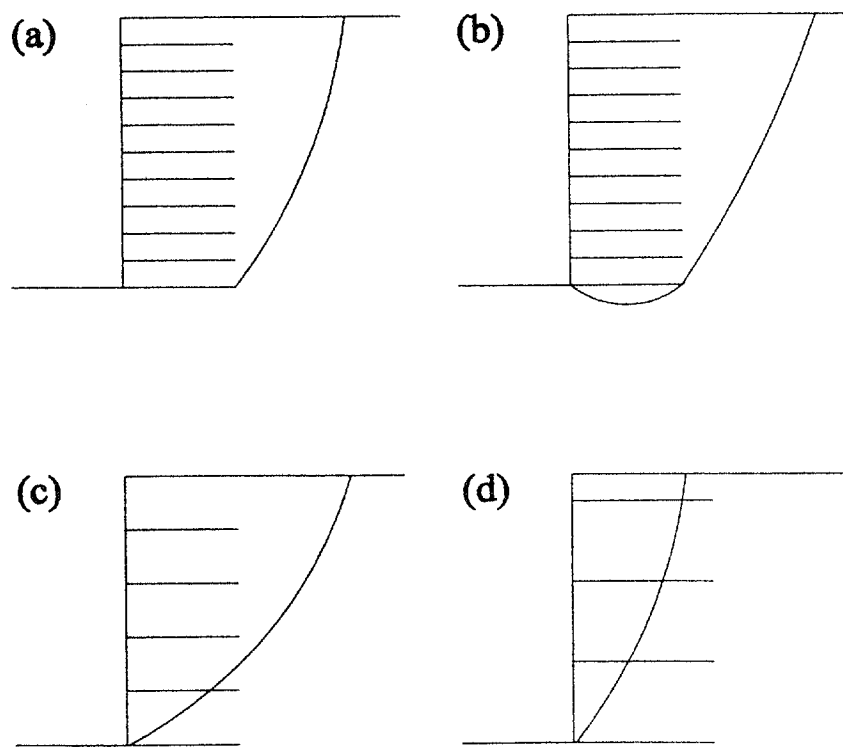


Figure 4.3 Slip Surface Types: (a) External Slip Surface; (b) Deep-Seated Slip Surface; (c) Compound Slip Surface; (d) Internal Slip Surface.

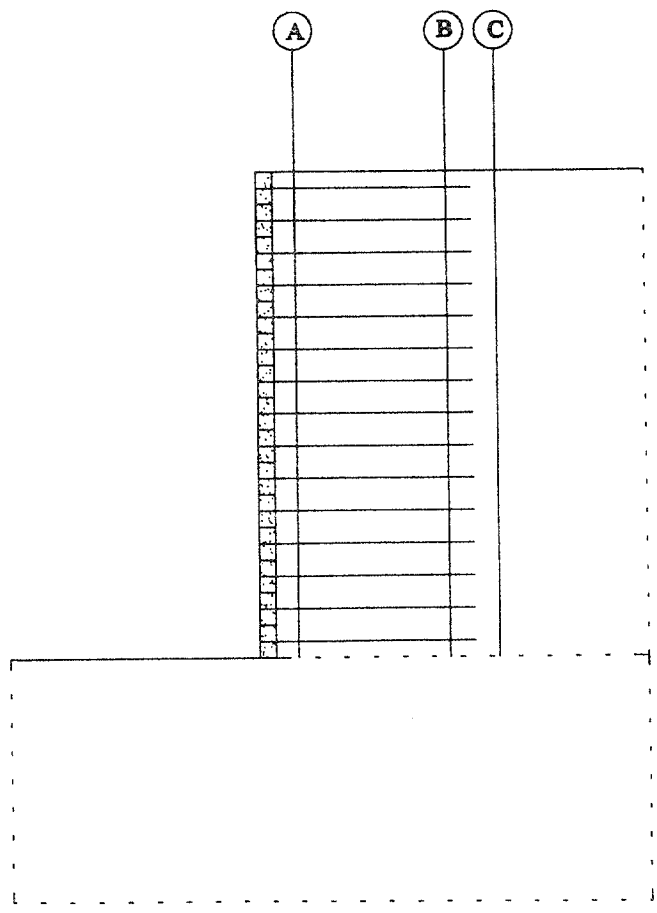
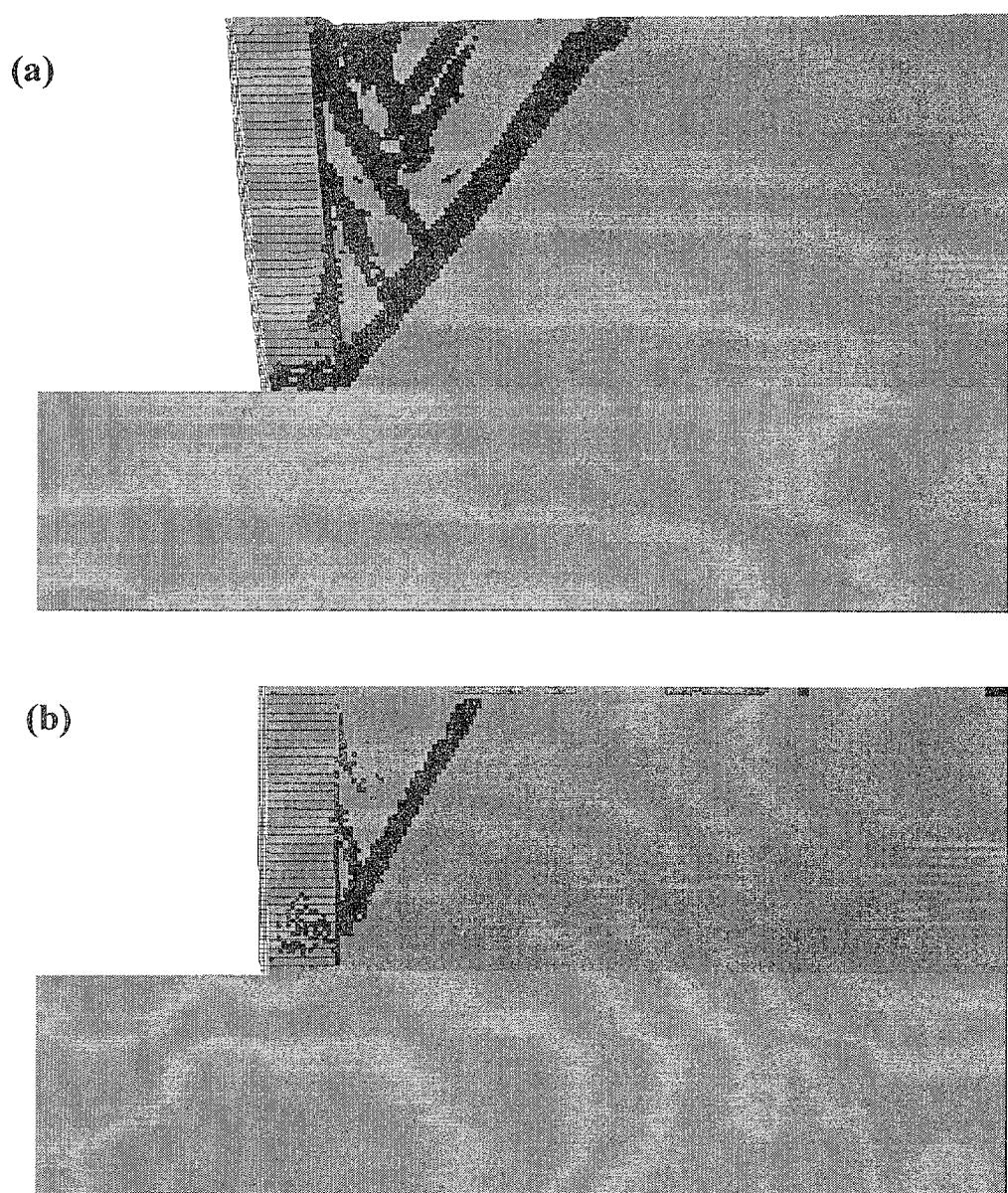


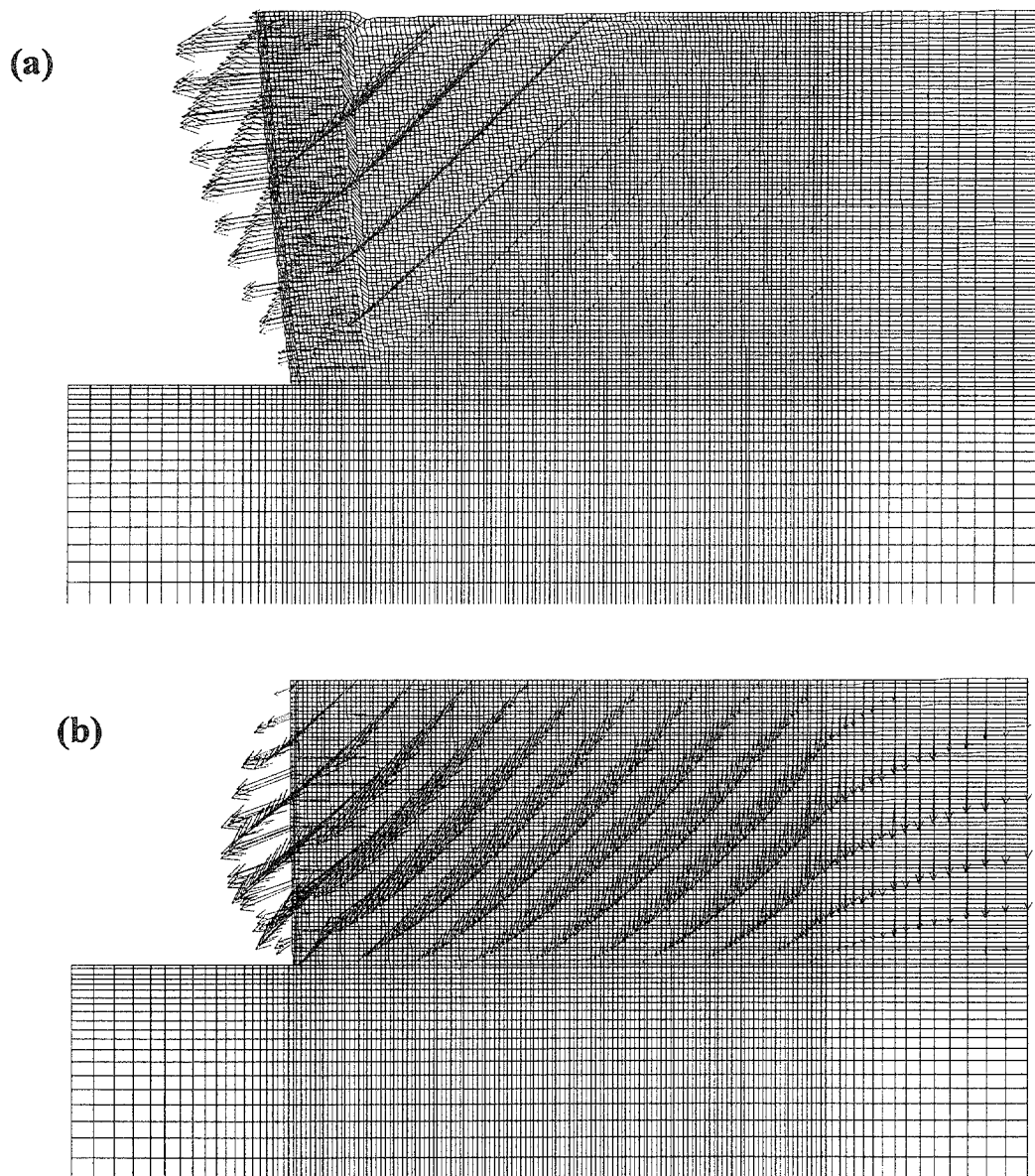
Figure 4.4 Definition of Vertical Sections A, B, and C along which Stress and Displacement Distributions Were Investigated.



LEGEND: State of Material

	Elastic		At Yield in Shear or Volume		Elastic, Yield in Past
--	---------	--	-----------------------------	--	------------------------

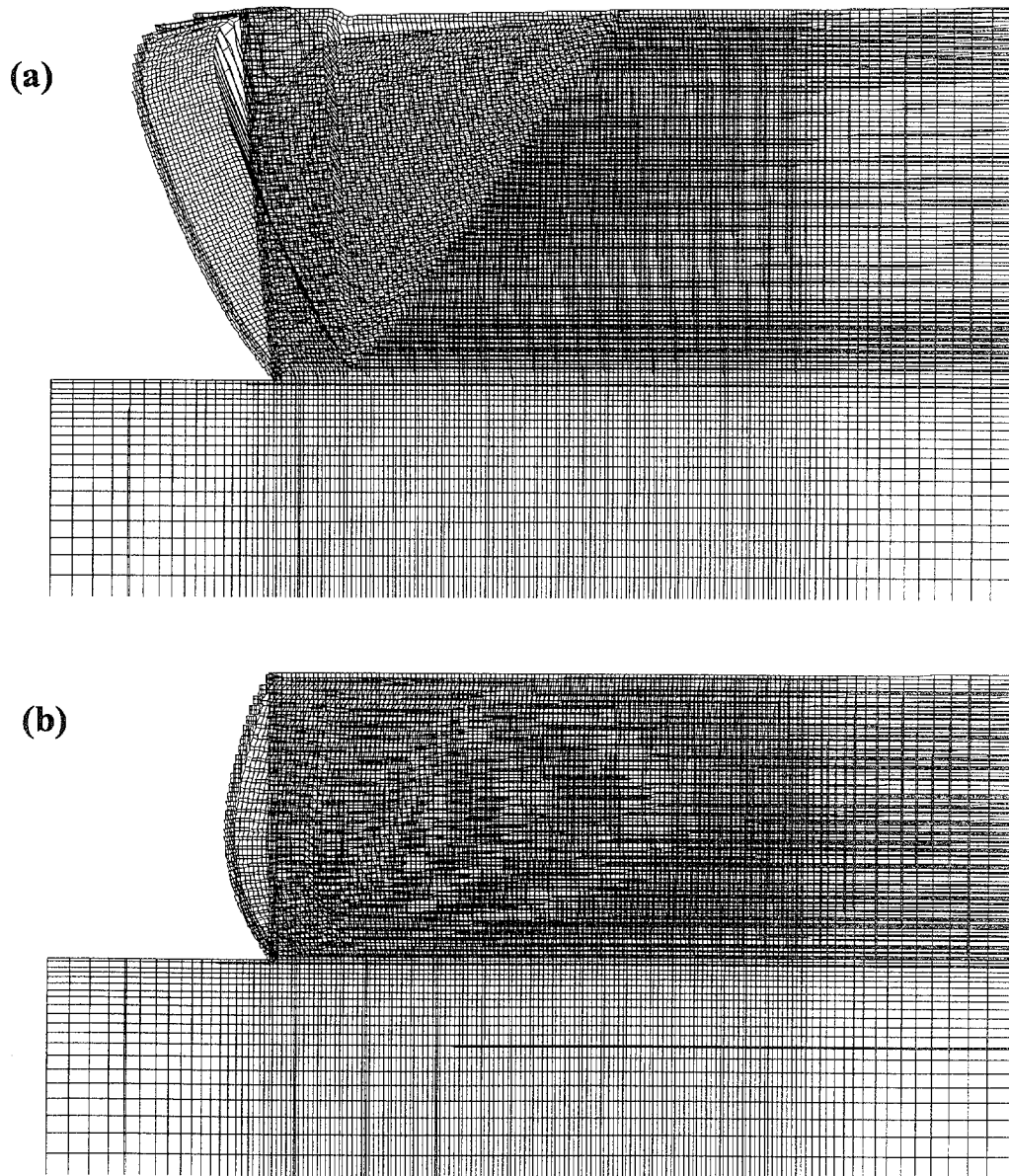
Figure 4.5 State of Soil for Case 1 ($s=0.2$ m, $t=1.5$ m): (a) Failure State ($h=8.6$ m, $l/h=0.17$); (b) Critical State ($h=6.6$ m, $l/h=0.23$).



LEGEND: Maximum Vector

- (a) 0.628 m
- (b) 0.043 m

Figure 4.6 Displacement Vectors for Case 1 ($s=0.2$ m, $l=1.5$ m): (a) Failure State ($h=8.6$ m, $l/h=0.17$); (b) Critical State ($h=6.6$ m, $l/h=0.23$).



LEGEND: Maximum Displacement

- (a) 0.640 m
- (b) 0.044 m

Figure 4.7 Distorted Grid for Case 1 ($s=0.2$ m, $l=1.5$ m): (a) Failure State ($h=8.6$ m, $l/h=0.17$); (b) Critical State ($h=6.6$ m, $l/h=0.23$).

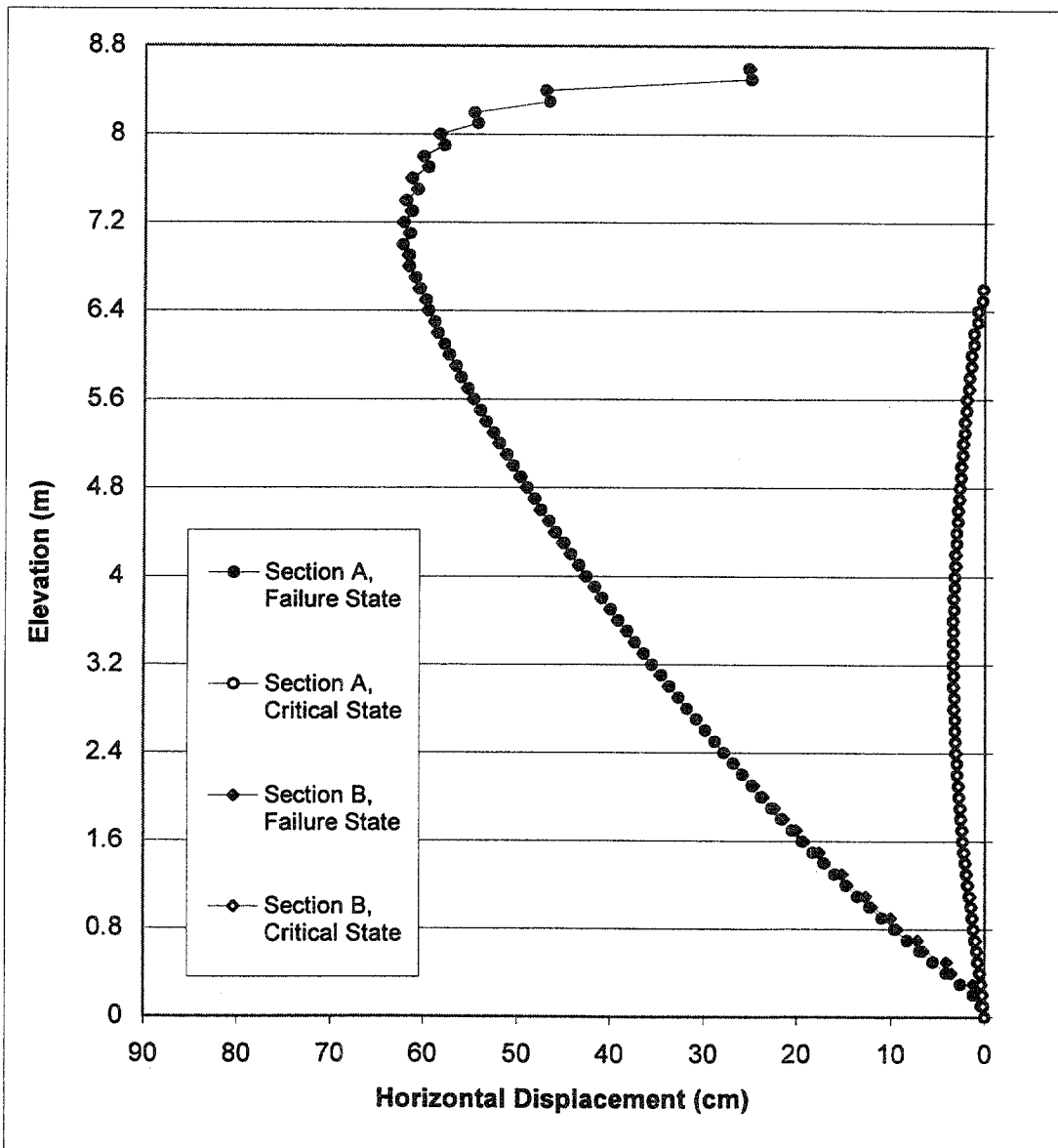


Figure 4.8 Cumulative Horizontal Displacements for Case 1 ($s=0.2$ m, $l=1.5$ m):
 (a) Failure State ($h=8.6$ m, $l/h=0.17$); (b) Critical State ($h=6.6$ m, $l/h=0.23$).

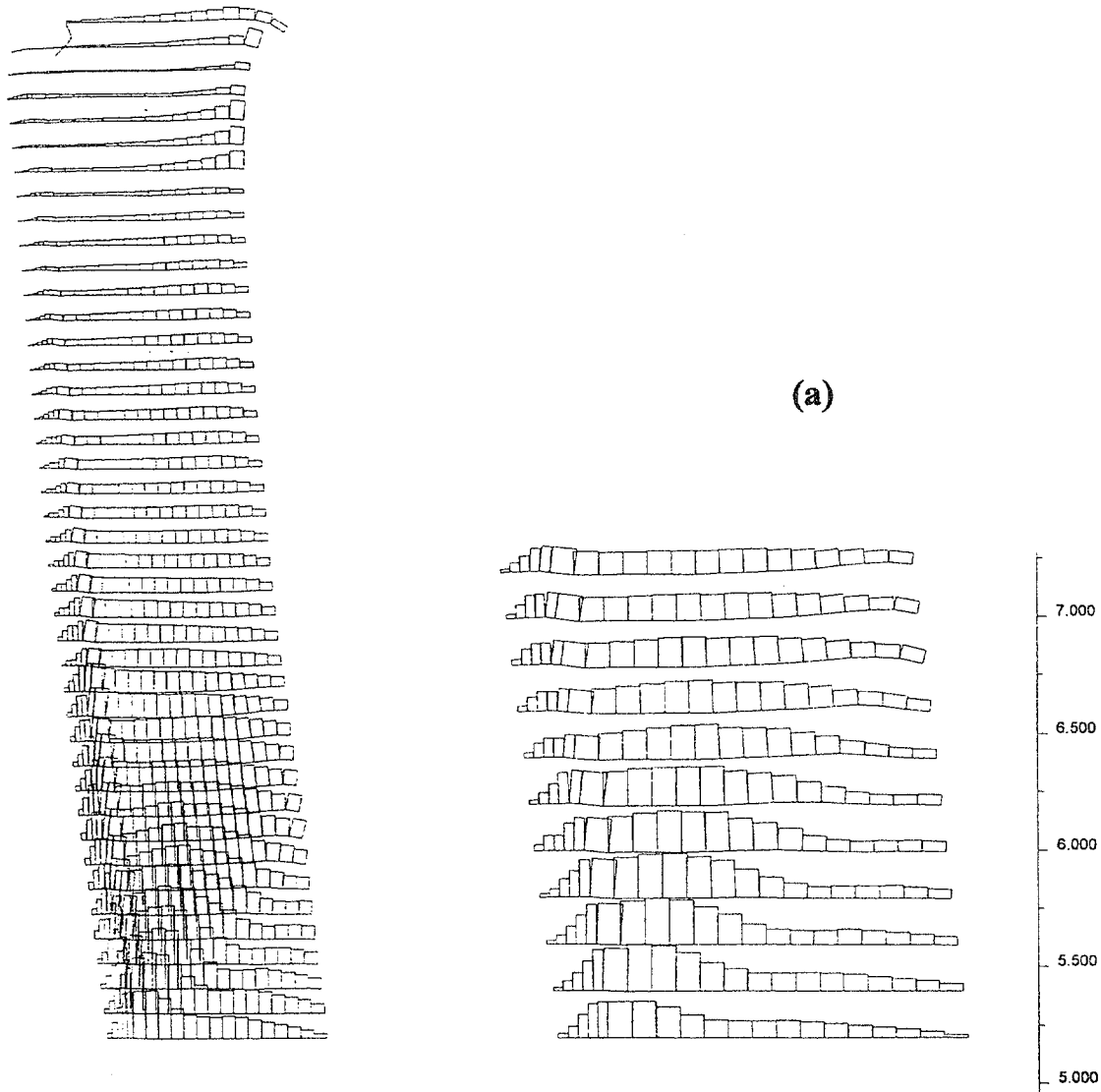


Figure 4.9 Axial Force Distribution in Reinforcement for Case 1 ($s=0.2$ m, $l=1.5$ m): (a) Failure State ($h=8.6$ m, $l/h=0.17$); (b) Critical State ($h=6.6$ m, $l/h=0.23$).

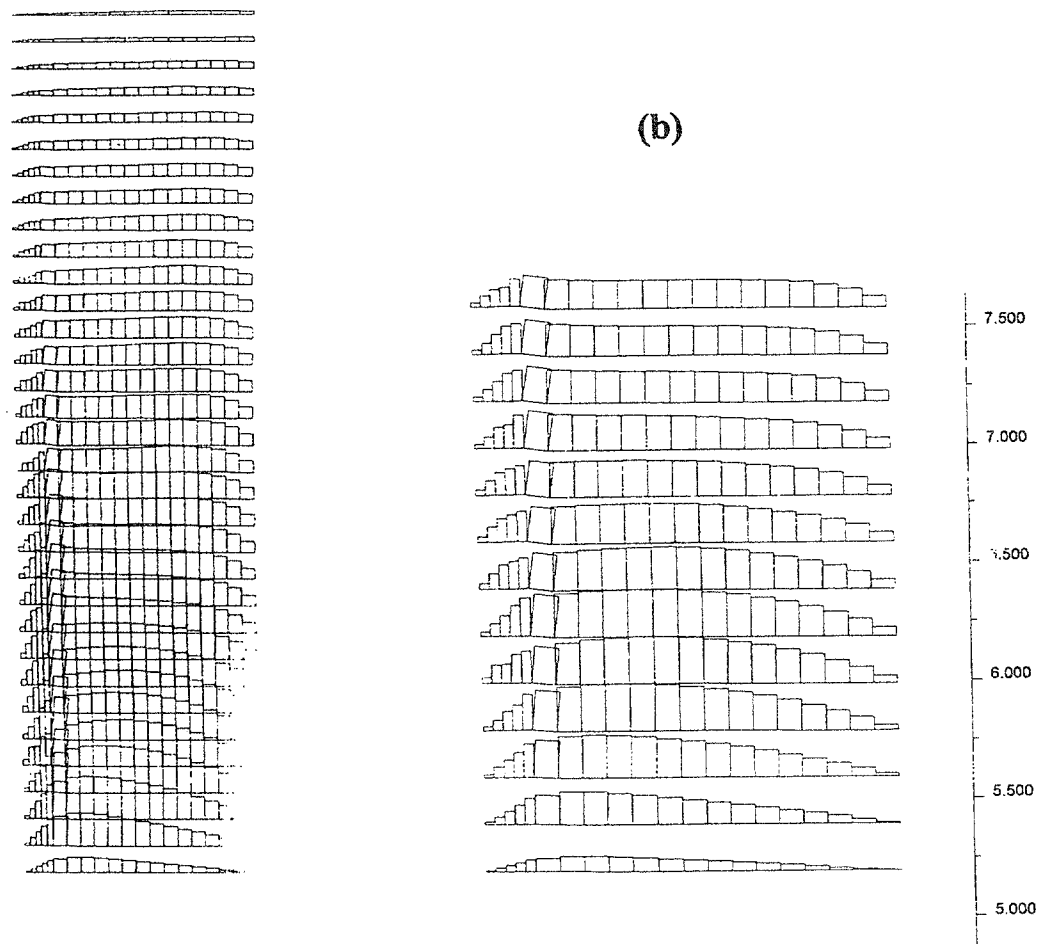
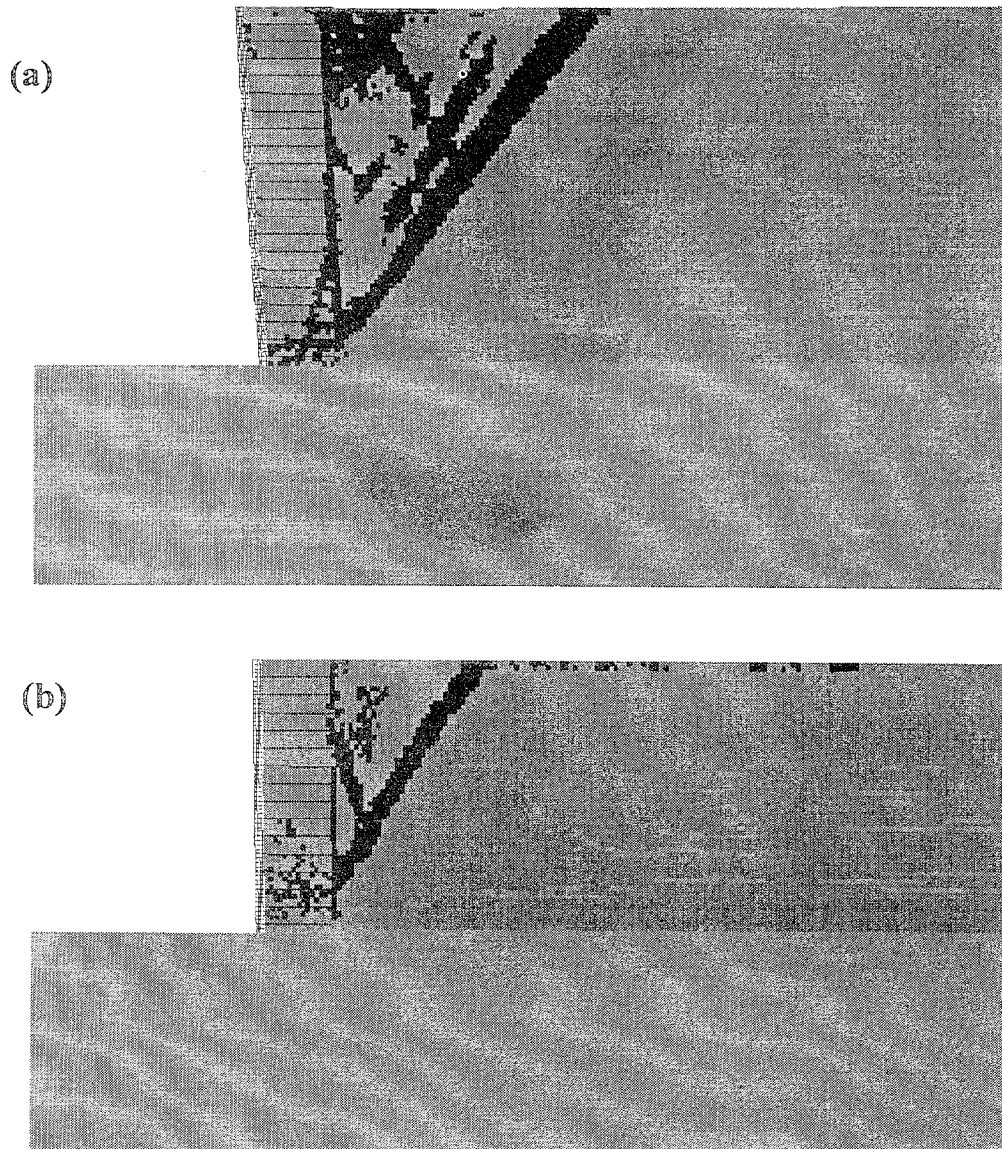


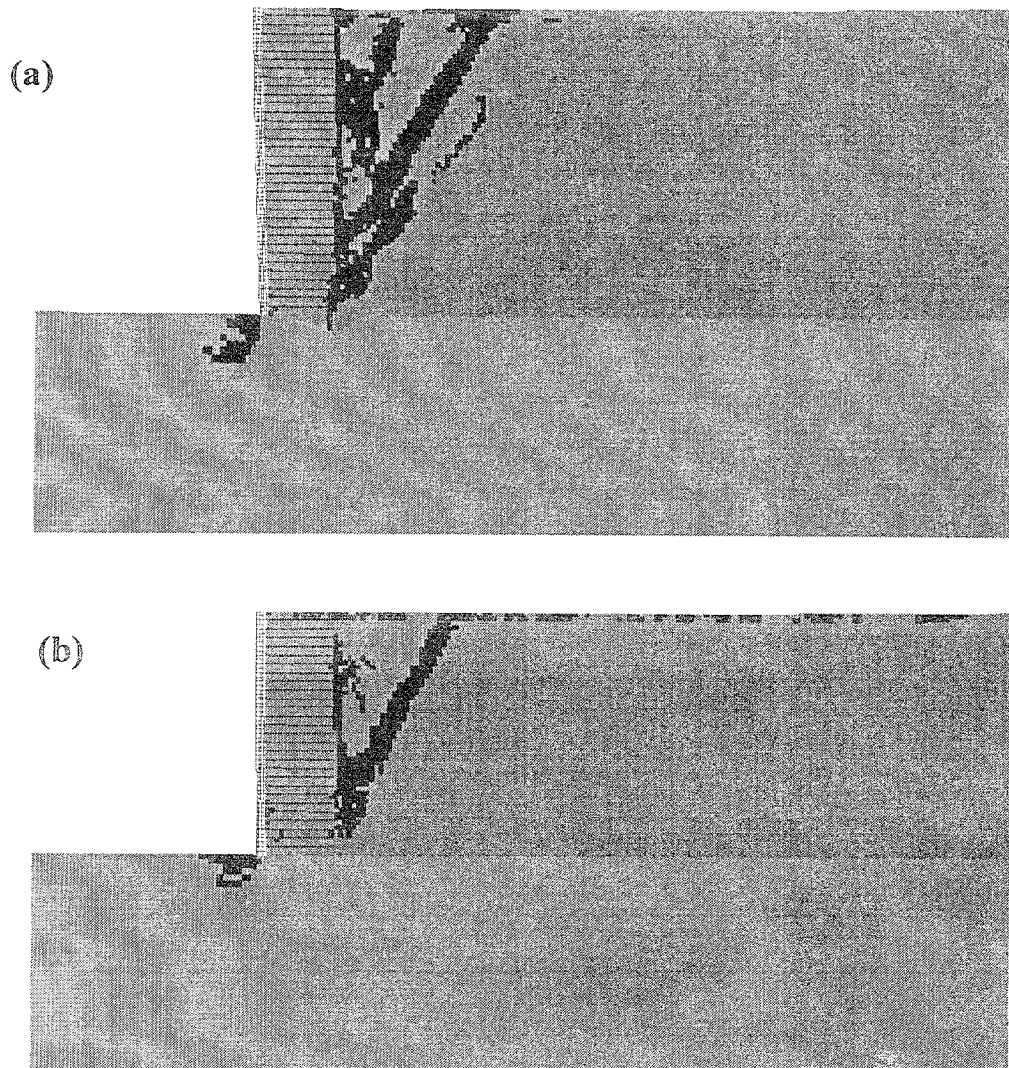
Figure 4.9 Axial Force Distribution in Reinforcement for Case 1 ($s=0.2$ m, $l=1.5$ m): (a) Failure State ($h=8.6$ m, $l/h=0.17$); (b) Critical State ($h=6.6$ m, $l/h=0.23$), Continued.



LEGEND: State of Material

	Elastic		At Yield in Shear or Volume		Elastic, Yield in Past
--	---------	--	-----------------------------	--	------------------------

Figure 4.10 State of Soil for Case 1 ($s=0.4$ m, $I=1.5$ m): (a) Failure State ($h=8.2$ m, $I/h=0.18$); (b) Critical State ($h=6.0$ m, $I/h=0.25$).



LEGEND: State of Material

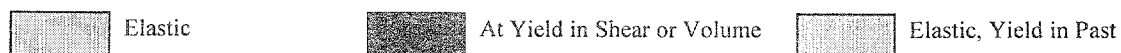
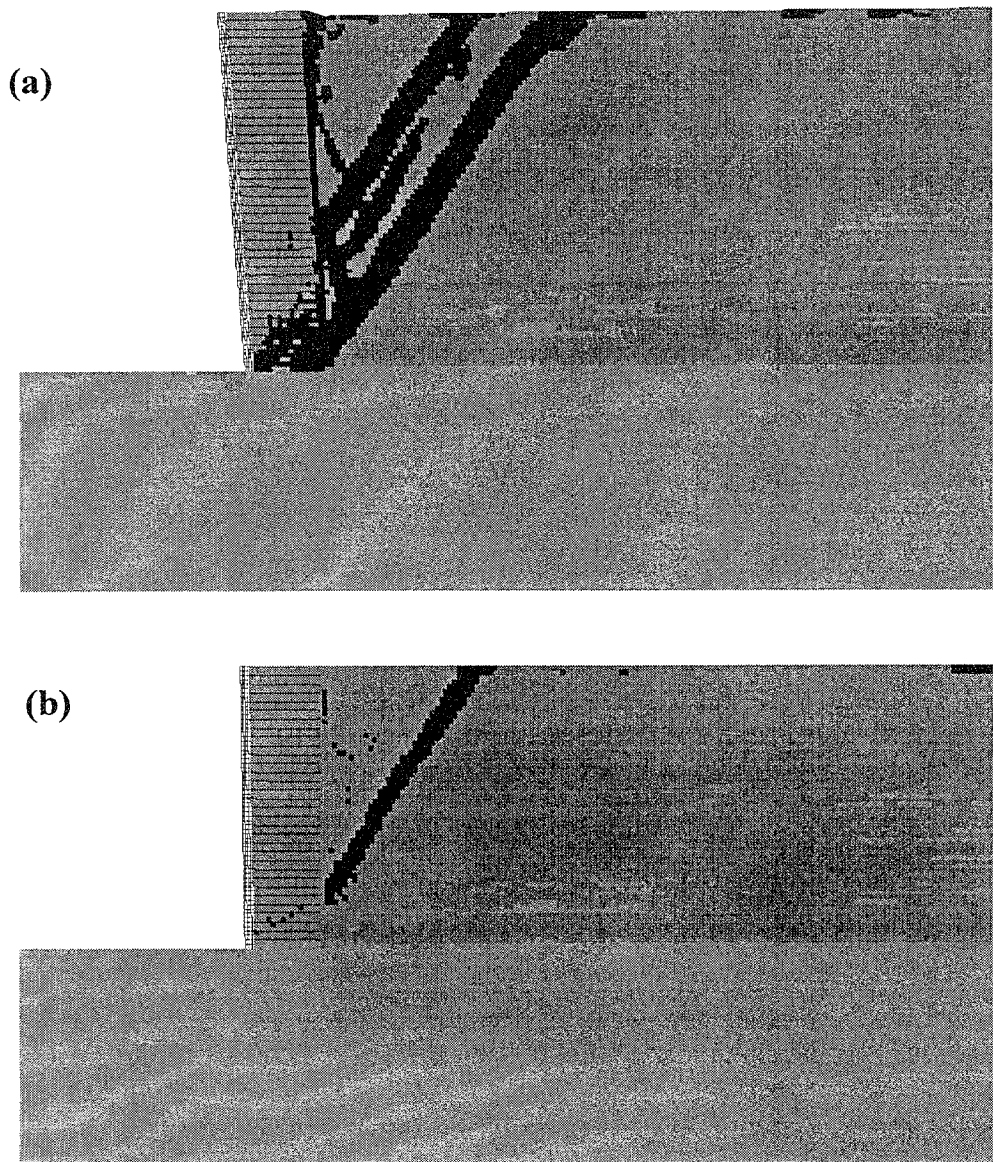


Figure 4.11 State of Soil for Case 4 ($s=0.2$ m, $l=1.5$ m): (a) Failure State ($h=7.0$ m, $l/h=0.21$); (b) Critical State ($h=5.6$ m, $l/h=0.27$).

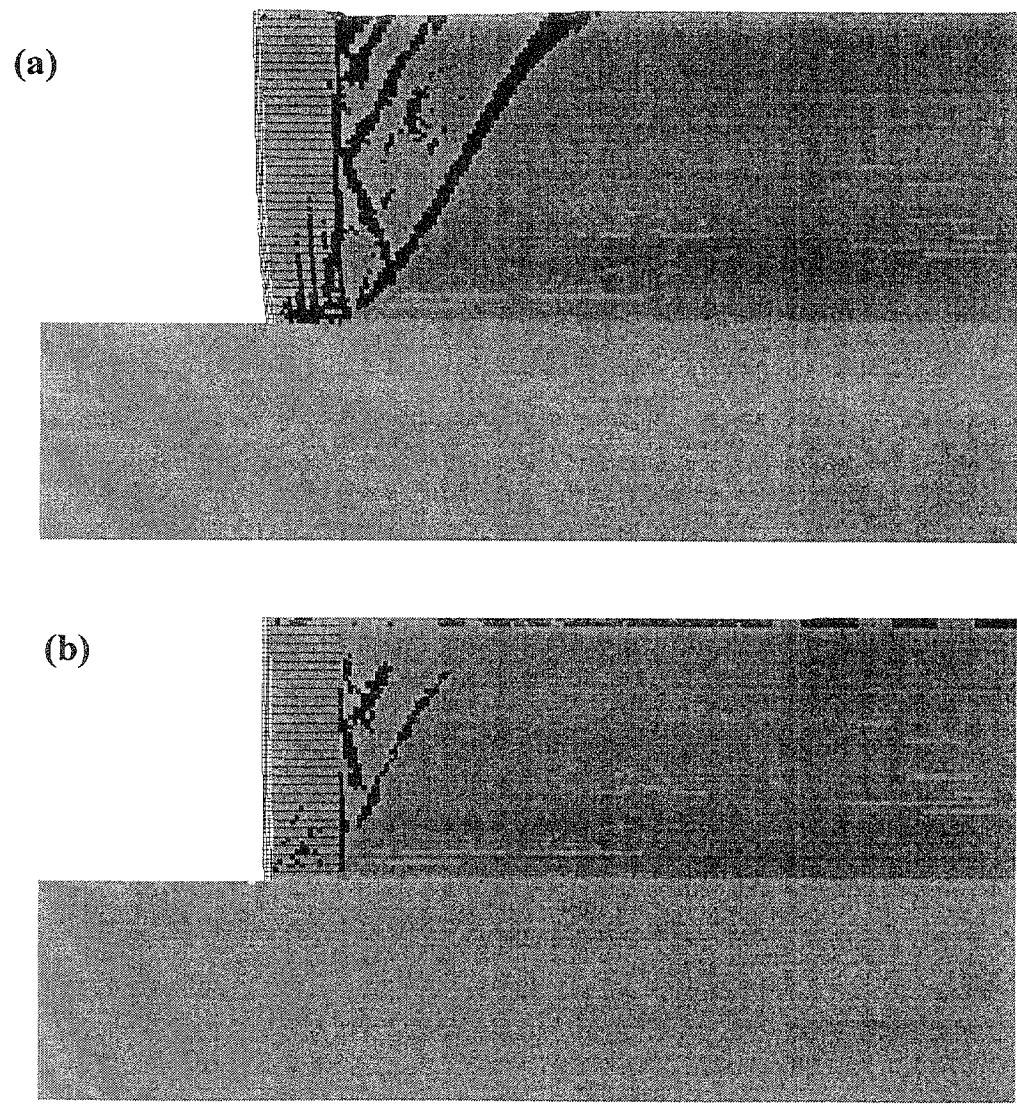


LEGEND: State of Material
 Elastic

At Yield in Shear or Volume

Elastic, Yield in Past

Figure 4.12 State of Soil for Case 9 ($s=0.2$ m, $l=1.5$ m): (a) Failure State ($h=8.2$ m, $l/h=0.18$); (b) Critical State ($h=6.6$ m, $l/h=0.23$).



LEGEND: State of Material
 Elastic At Yield in Shear or Volume Elastic, Yield in Past

Figure 4.13 State of Soil for Case 11 ($s=0.2$ m, $l=1.5$ m): (a) Failure State ($h=7.2$ m, $l/h=0.21$); (b) Critical State ($h=6.0$ m, $l/h=0.25$).

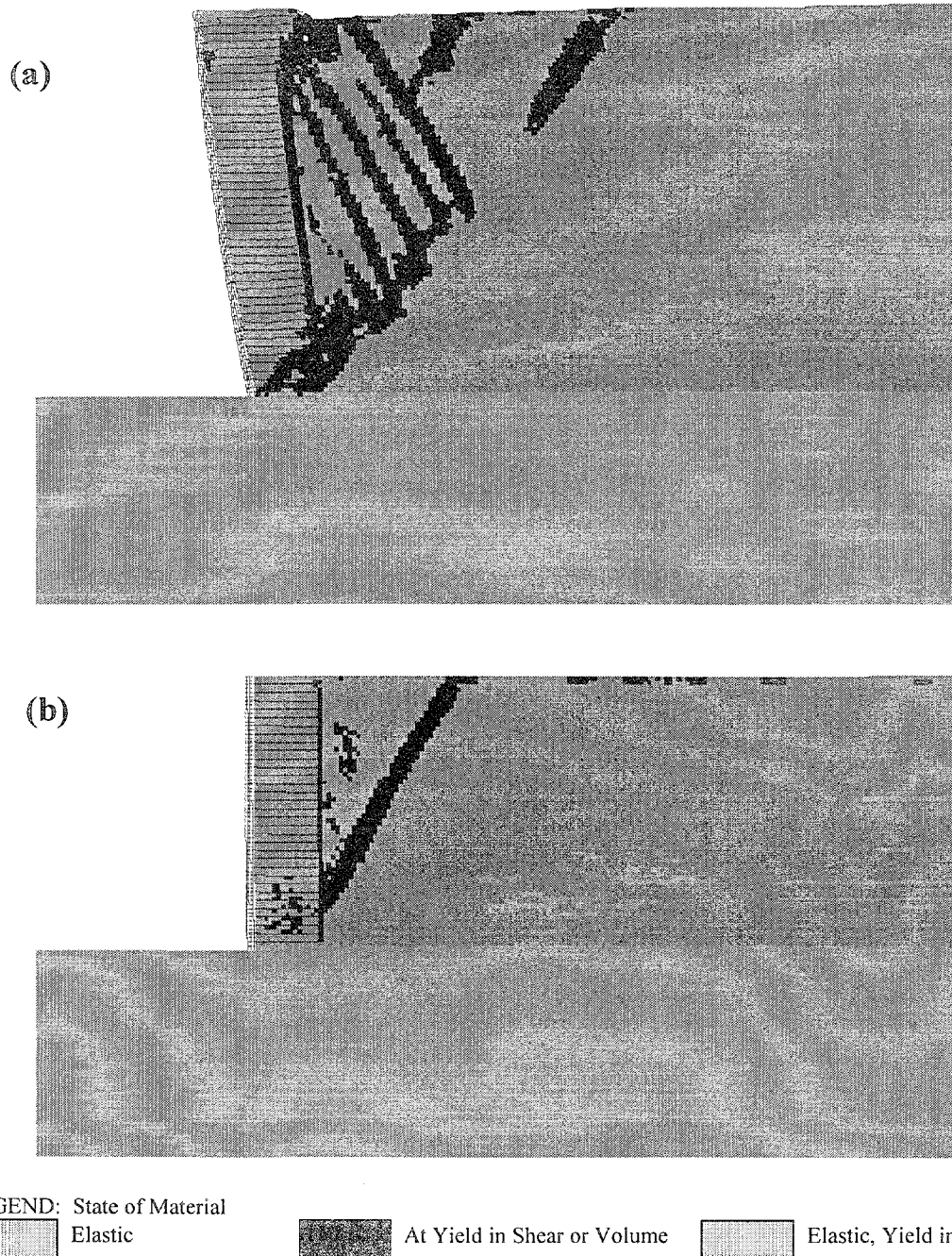
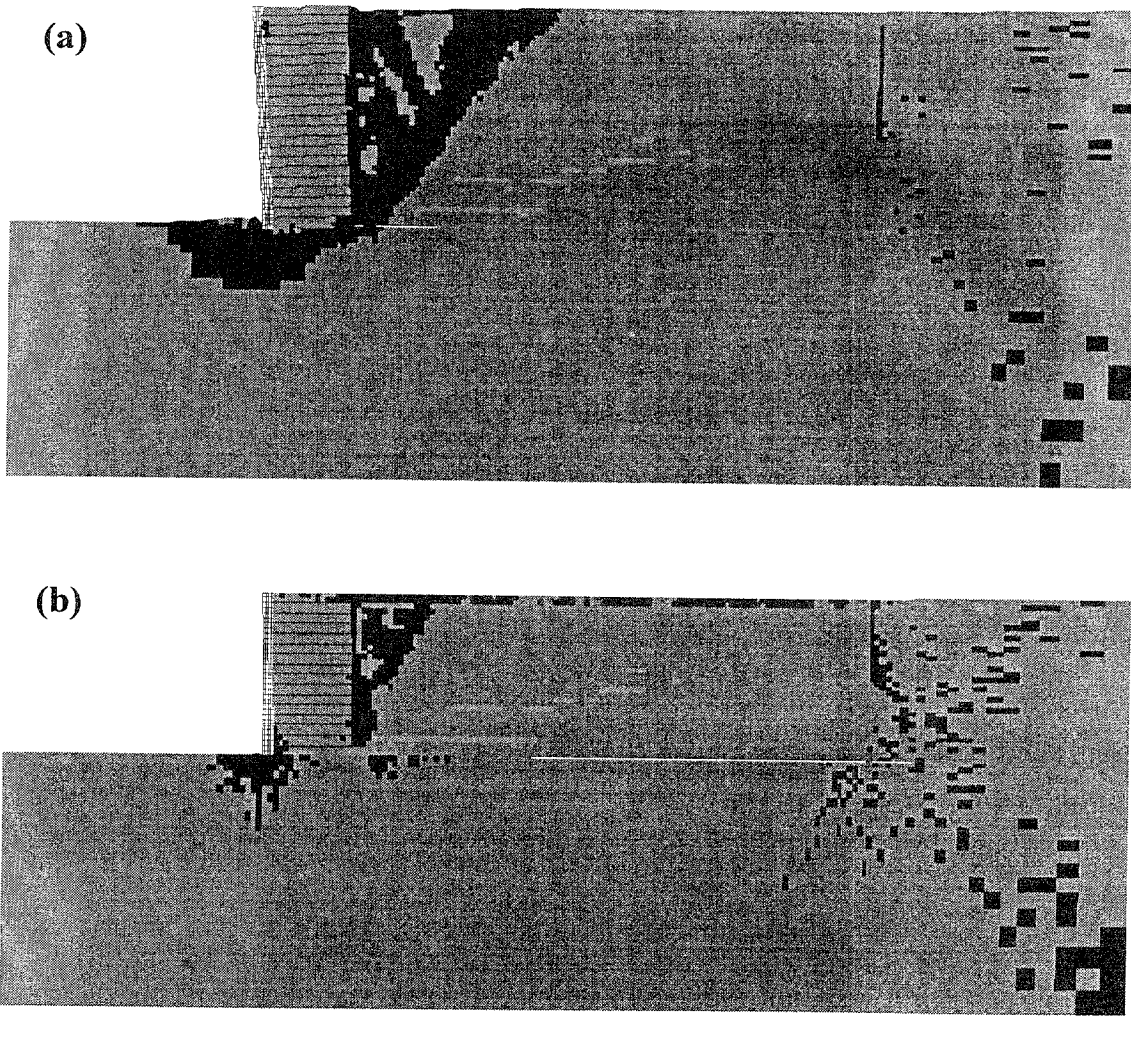


Figure 4.14 State of Soil for Case 12 ($s=0.2$ m, $l=1.5$ m): (a) Failure State ($h=9.4$ m, $l/h=0.16$); (b) Critical State ($h=6.6$ m, $l/h=0.23$).



LEGEND: State of Material



Elastic

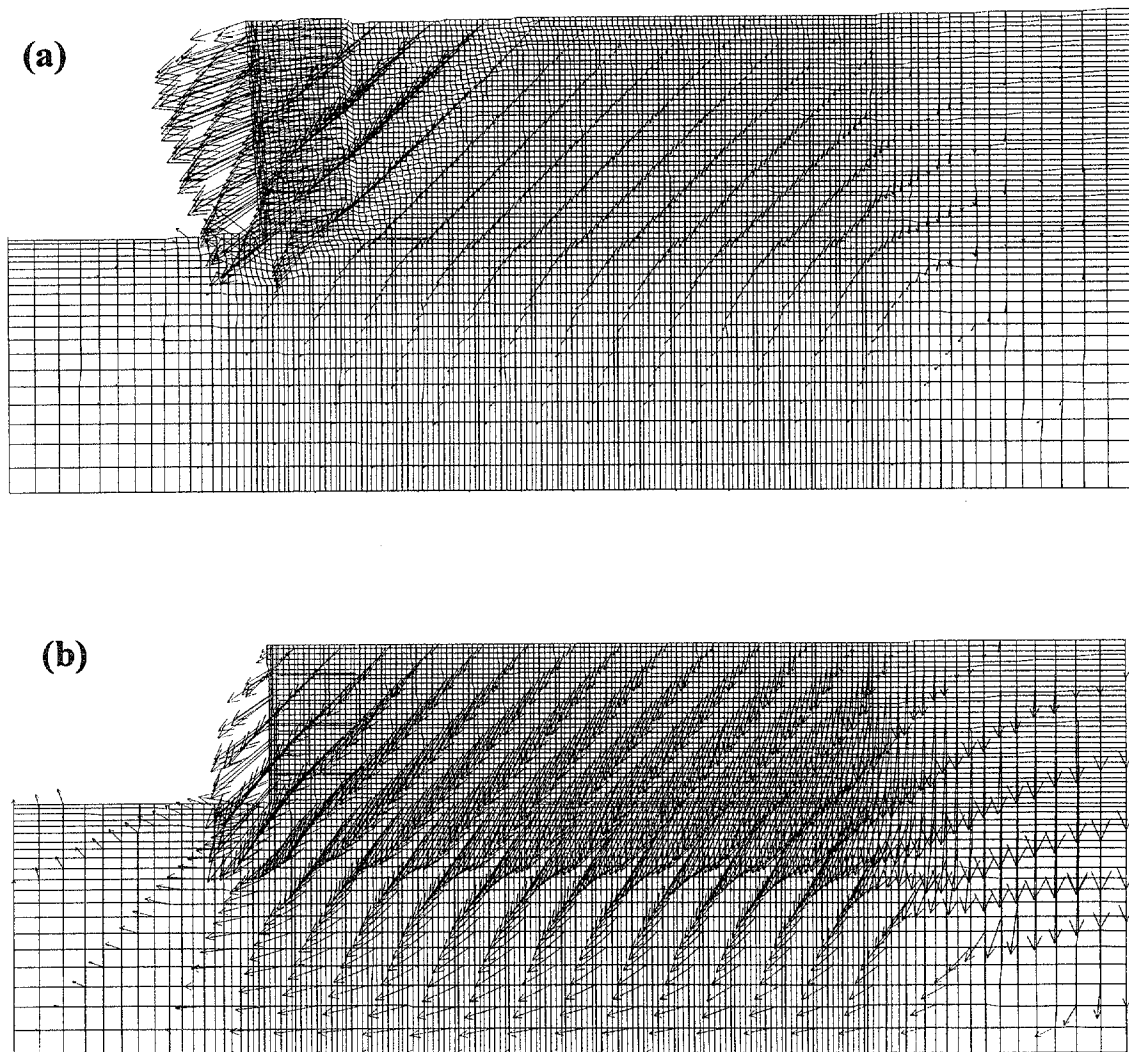


At Yield in Shear or Volume



Elastic, Yield in Past

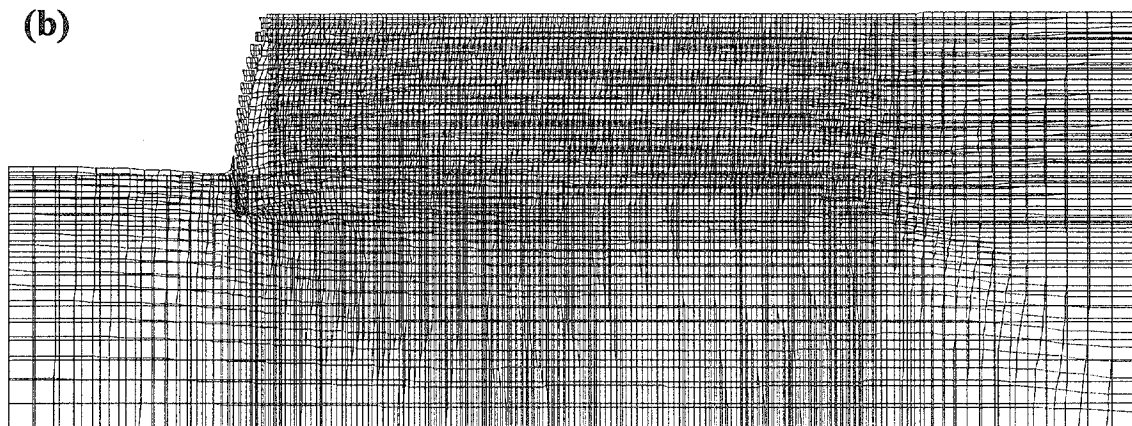
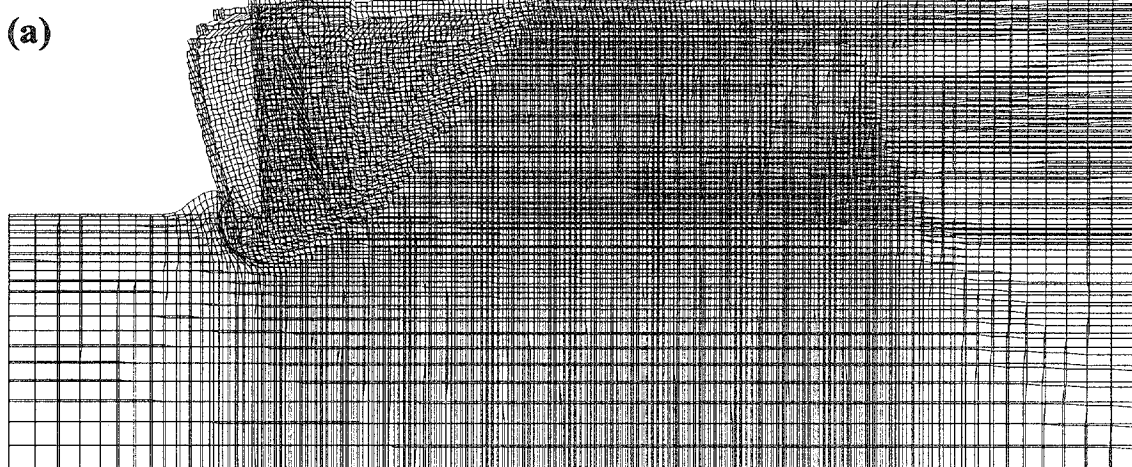
Figure 4.15 State of Soil for Case 10 ($s=0.2$ m, $l=1.5$ m): (a) Failure State ($h=4.4$ m, $I/h=0.34$); (b) Critical State ($h=3.2$ m, $I/h=0.47$).



LEGEND: Maximum Vector

- (a) 0.325 m
- (b) 0.036 m

Figure 4.16 Displacement Vectors for Case 10 ($s=0.2$ m, $l=1.5$ m): (a) Failure State ($h=4.4$ m, $l/h=0.34$); (b) Critical State ($h=3.2$ m, $l/h=0.47$).



LEGEND: Maximum Displacement

- (a) 0.325 m
- (b) 0.037 m

Figure 4.17 Distorted Grid for Case 10 ($s=0.2$ m, $l=1.5$ m): (a) Failure State ($h=4.4$ m, $l/h=0.34$); (b) Critical State ($h=3.2$ m, $l/h=0.47$).

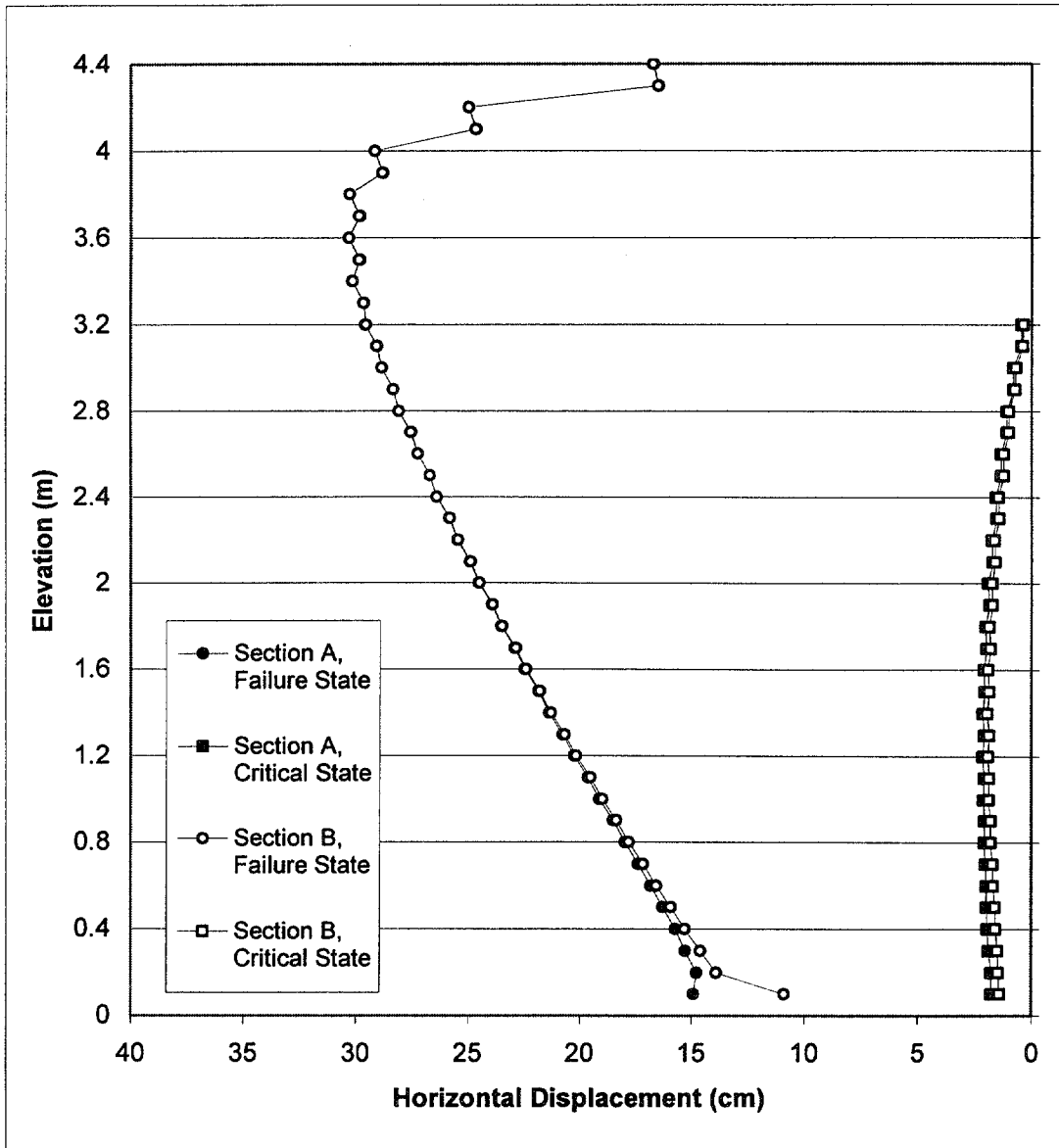


Figure 4.18. Horizontal Displacements for Case 10 ($s=0.2$ m, $l=1.5$ m) at Failure State ($h=4.4$ m, $l/h=0.34$) and Critical State ($h=3.2$ m, $l/h=0.47$).

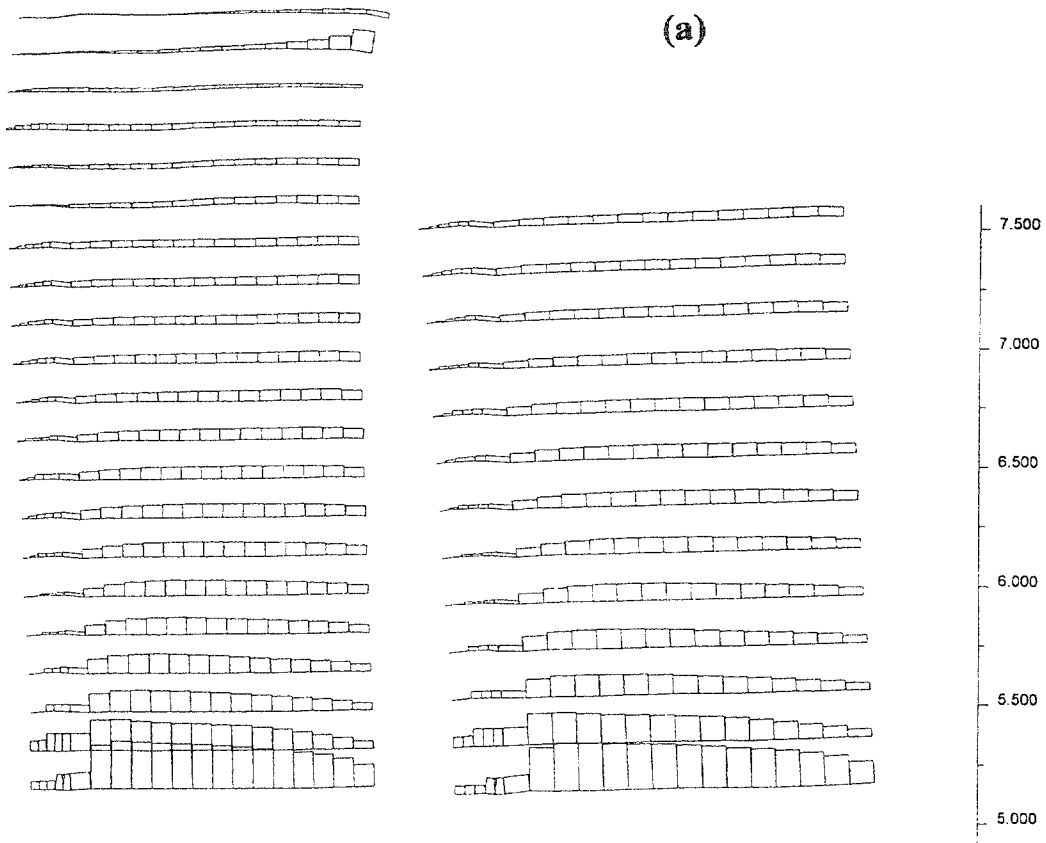


Figure 4.19 Axial Force Distribution in Reinforcement for Case 10 ($s=0.2$ m, $t=1.5$ m): (a) Failure State ($h=4.4$ m, $l/h=0.34$); (b) Critical State ($h=3.2$ m, $l/h=0.47$).

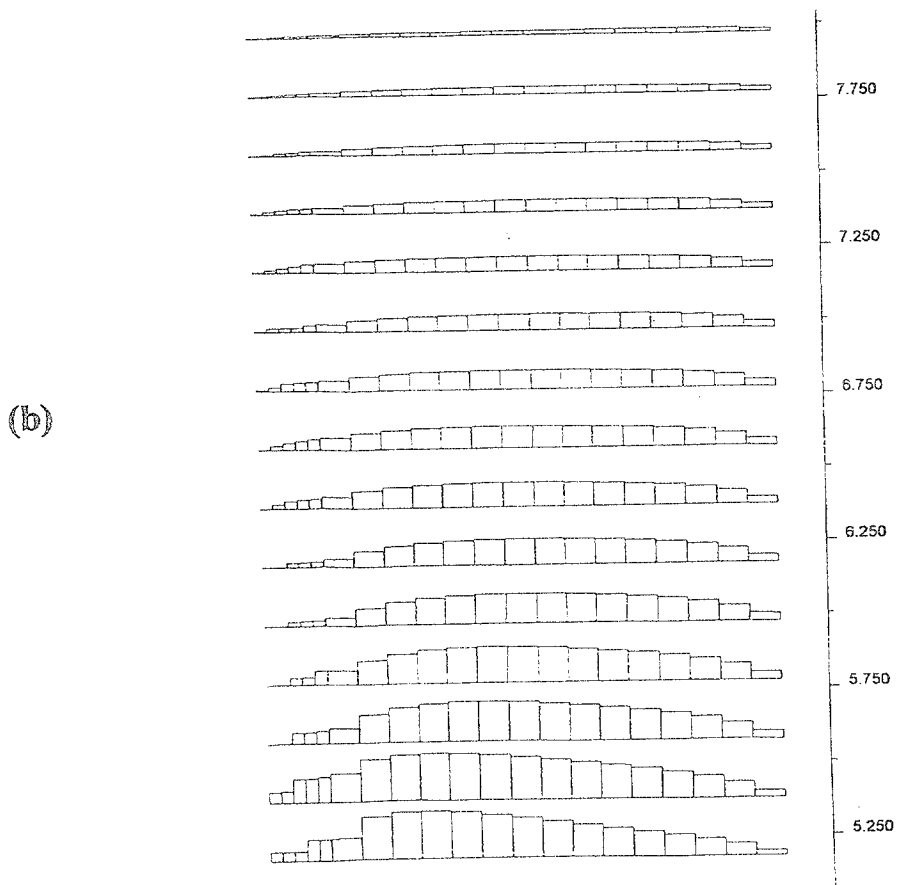
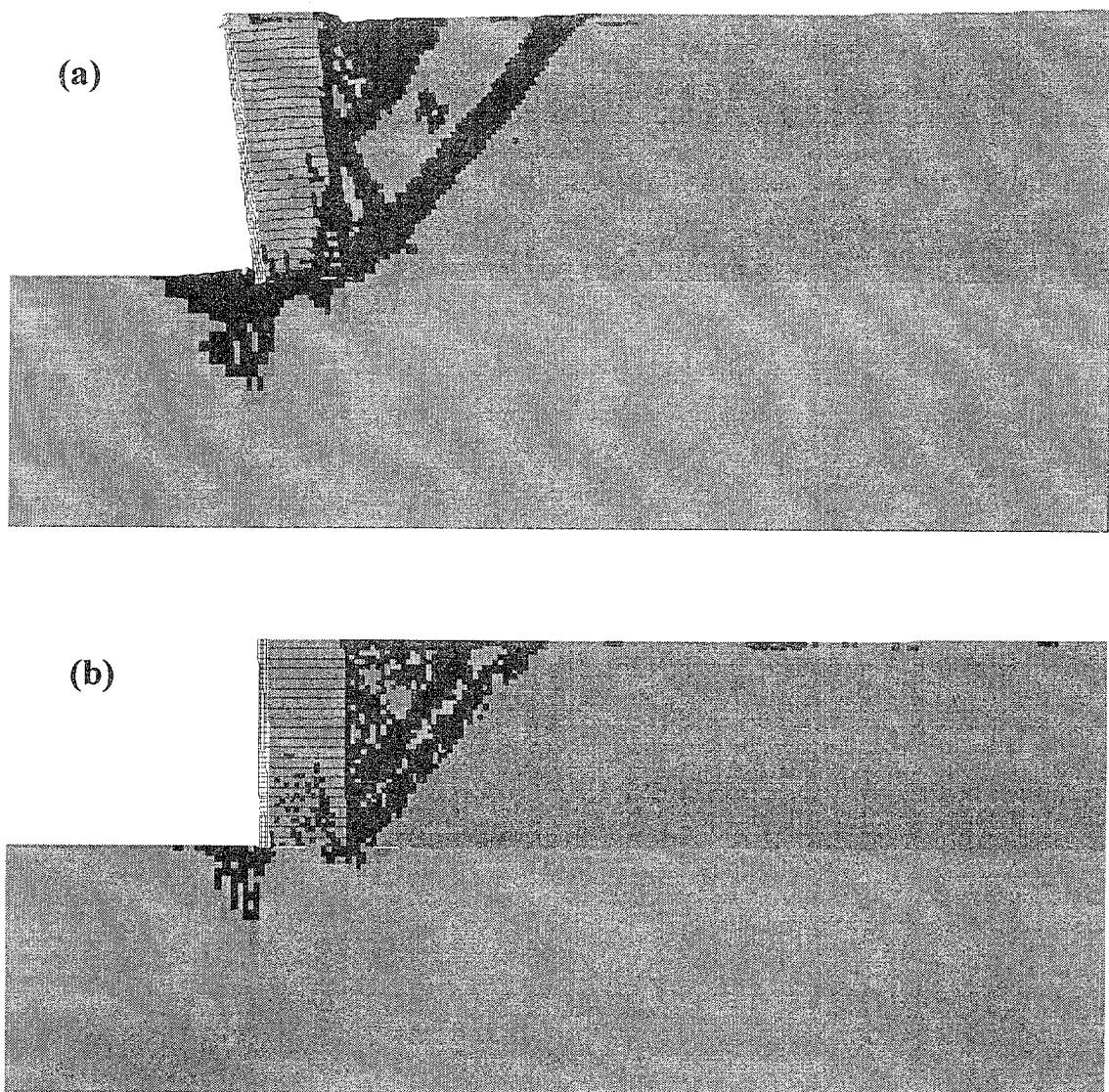


Figure 4.19 Axial Force Distribution in Reinforcement for Case 10 ($s=0.2$ m, $I=1.5$ m): (a) Failure State ($h=4.4$ m, $I/h=0.34$); (b) Critical State ($h=3.2$ m, $I/h=0.47$), Continued.



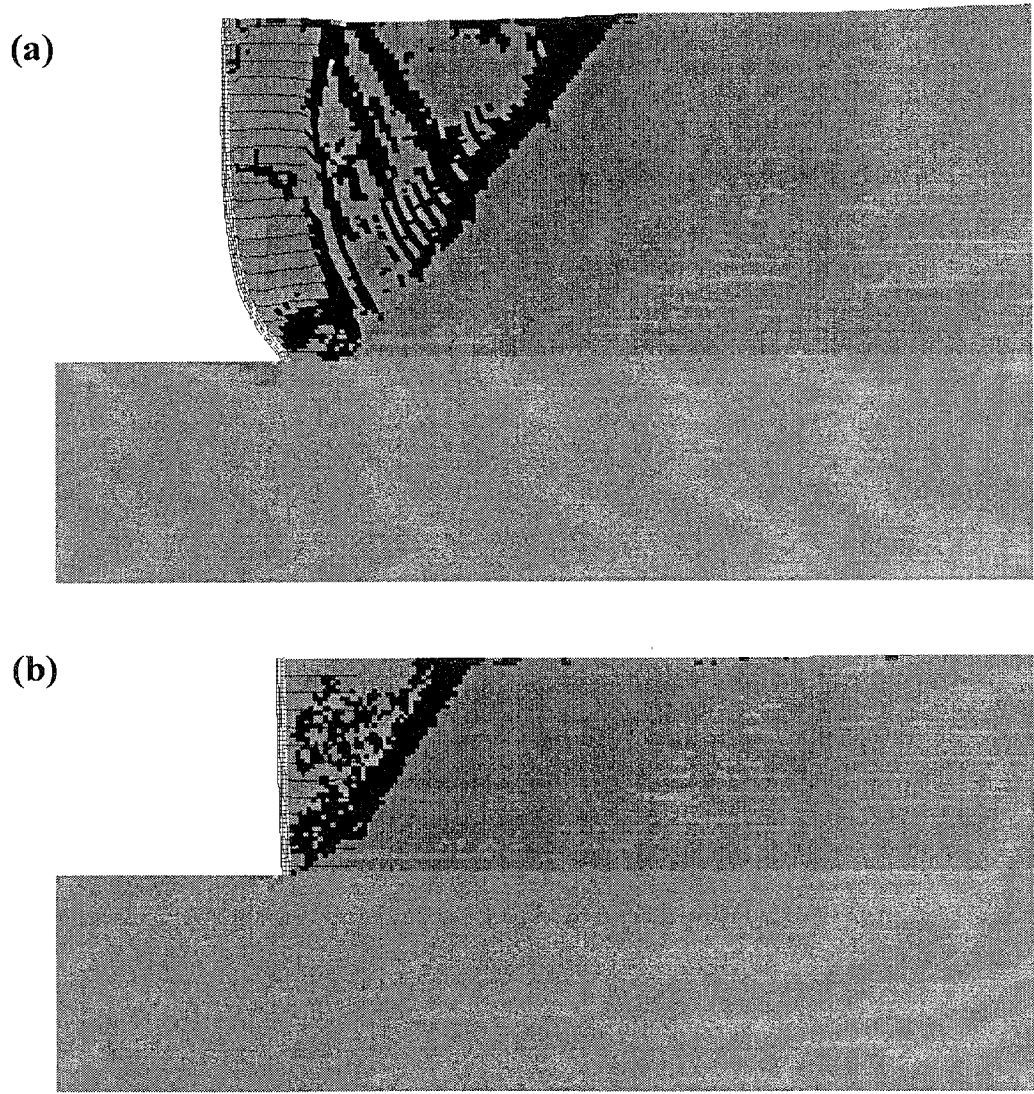
LEGEND: State of Material

Elastic

At Yield in Shear or Volume

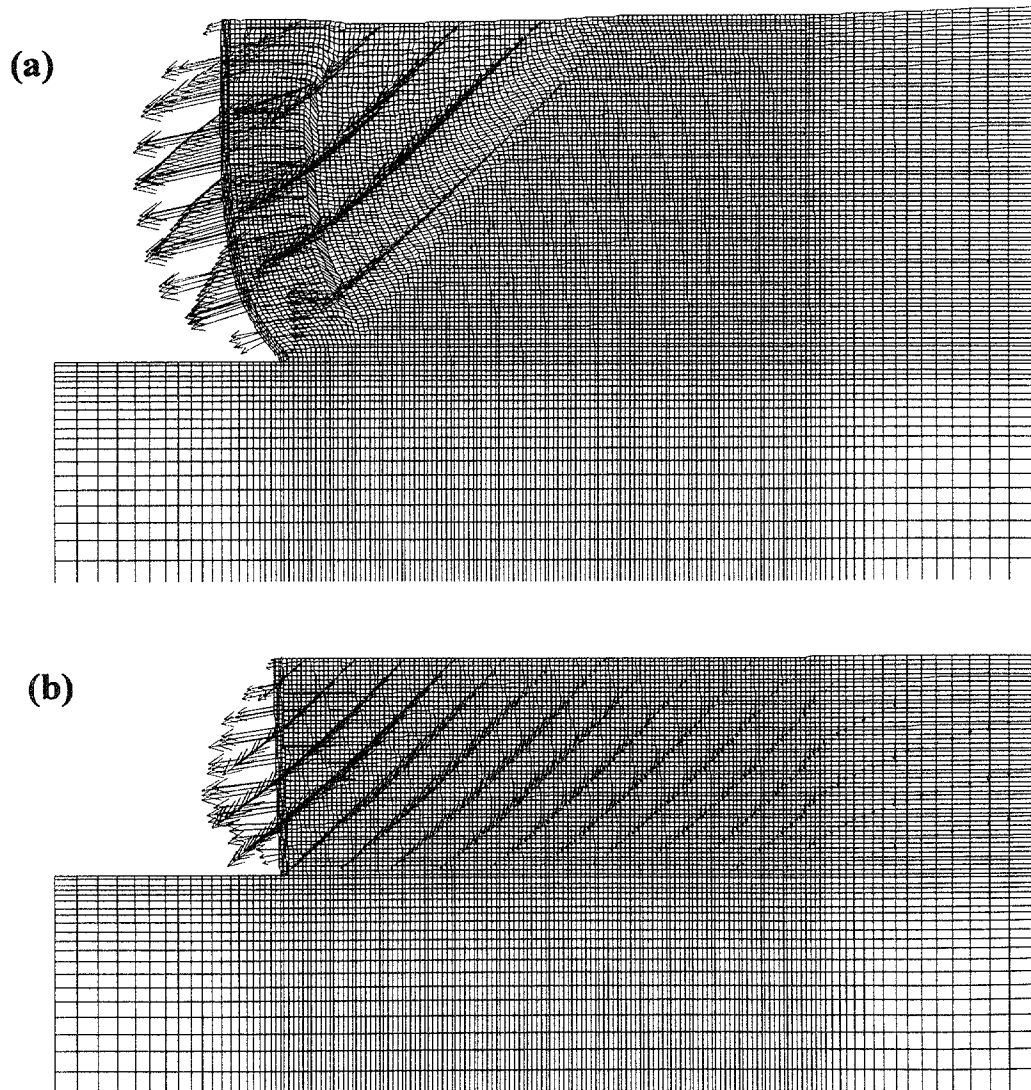
Elastic, Yield in Past

Figure 4.20 State of Soil for Case 5 ($s=0.2$ m, $l=1.5$ m): (a) Failure State ($h=5.4$ m, $l/h=0.28$); (b) Critical State ($h=4.2$ m, $l/h=0.36$).



LEGEND: State of Material
 Elastic At Yield in Shear or Volume Elastic, Yield in Past

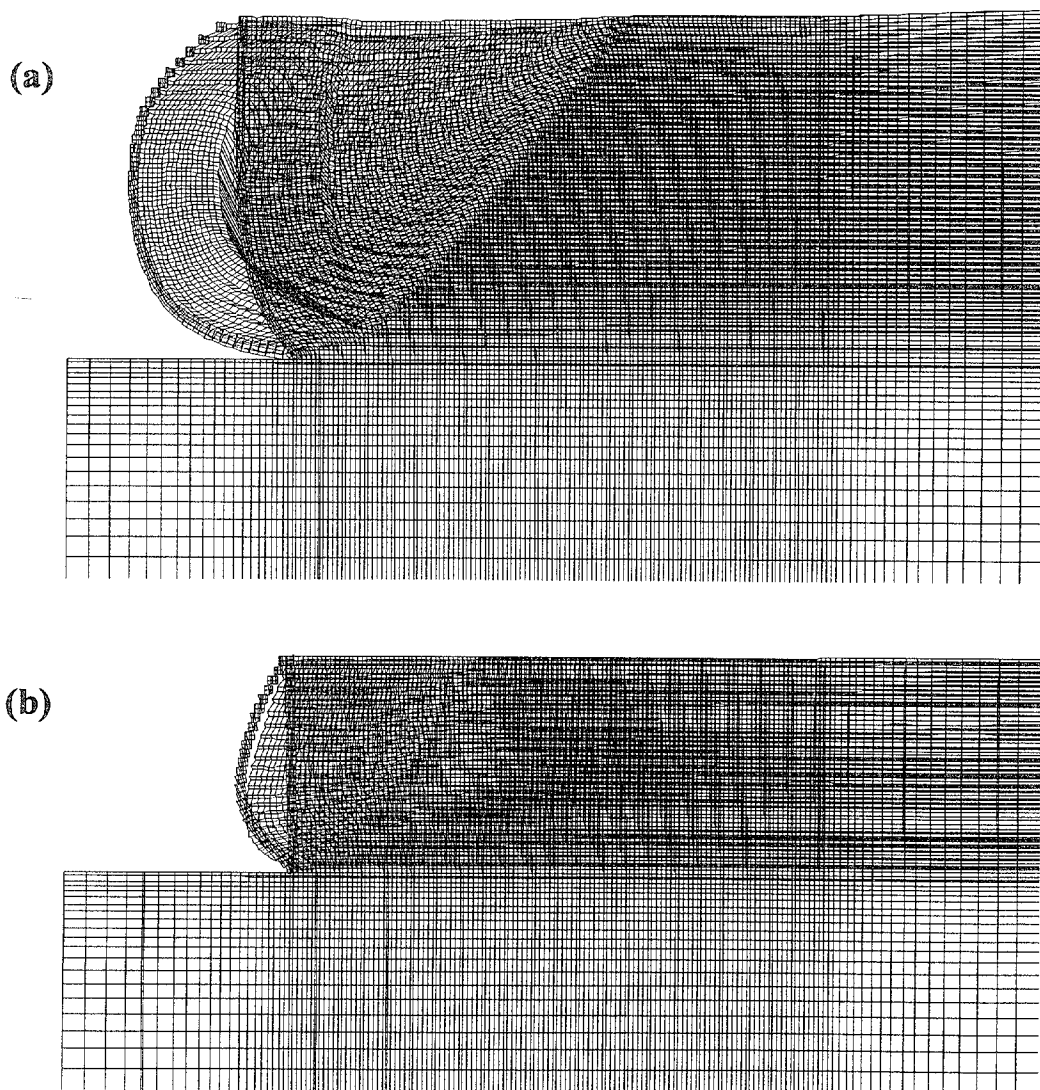
Figure 4.21 State of Soil for Case 8-1 ($s=0.4$ m, $l=1.5$ m): (a) Failure State ($h=8.0$ m, $l/h=0.19$); (b) Critical State ($h=5.0$ m, $l/h=0.3$).



LEGEND: Maximum Vector

- (a) 1.221 m
- (b) 0.0704 m

Figure 4.22 Displacement Vectors for Case 8-1 ($s=0.4$ m, $l=1.5$ m): (a) Failure State ($h=8.0$ m, $l/h=0.19$); (b) Critical State ($h=5.0$ m, $l/h=0.30$).



LEGEND: Maximum Displacement

- (a) 1.227 m
- (b) 0.073 m

Figure 4.23 Distorted Grid for Case 8-1 ($s=0.4$ m, $l=1.5$ m): (a) Failure State ($h=8.0$ m, $l/h=0.19$); (b) Critical State ($h=5.0$ m, $l/h=0.30$).

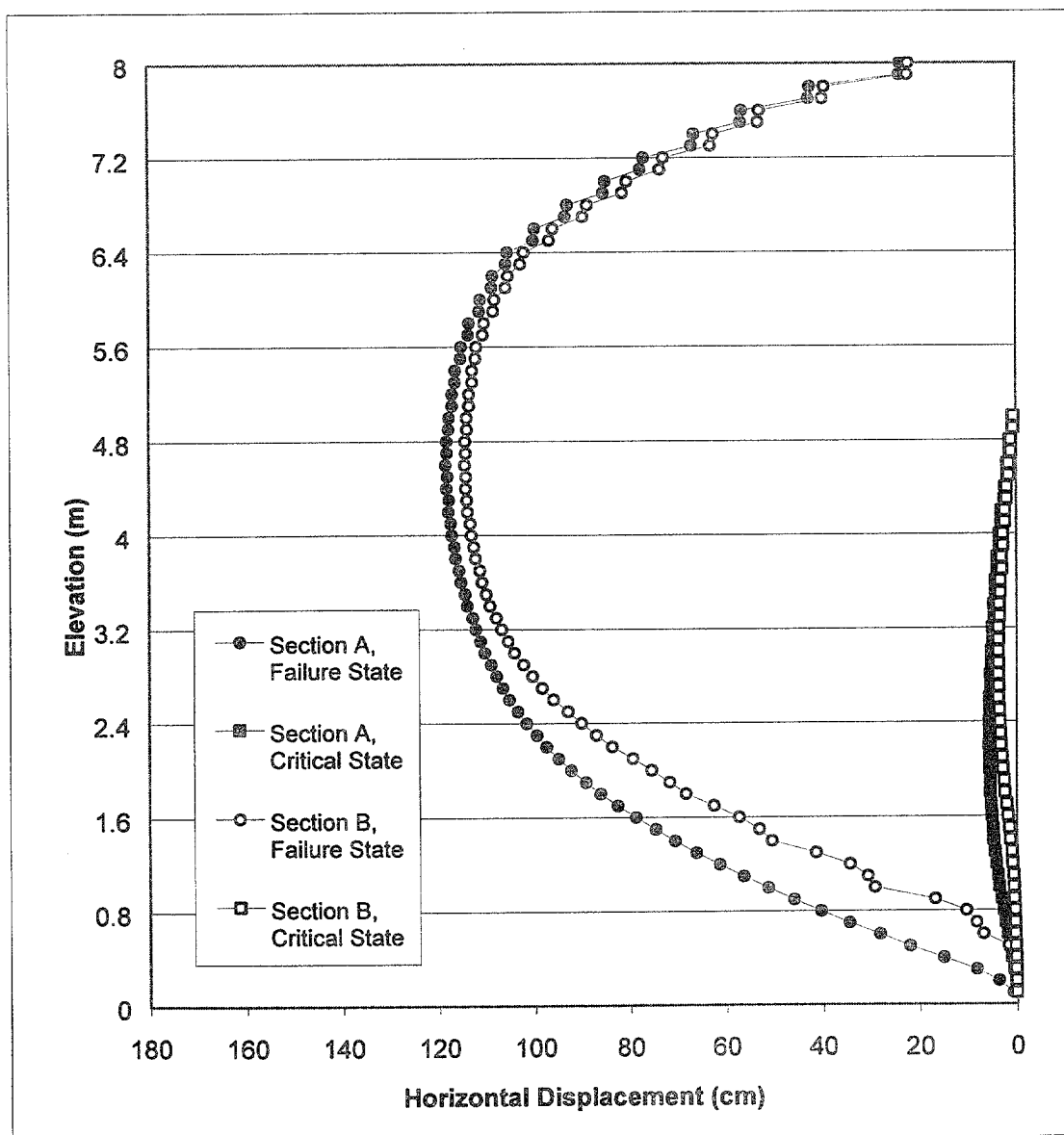


Figure 4.24 Horizontal Displacements for Case 8-1 ($s=0.4$ m, $l=1.5$ m) at Failure ($h=8.0$ m, $l/h=0.19$) and Critical State ($h=5.0$ m, $l/h=0.30$).

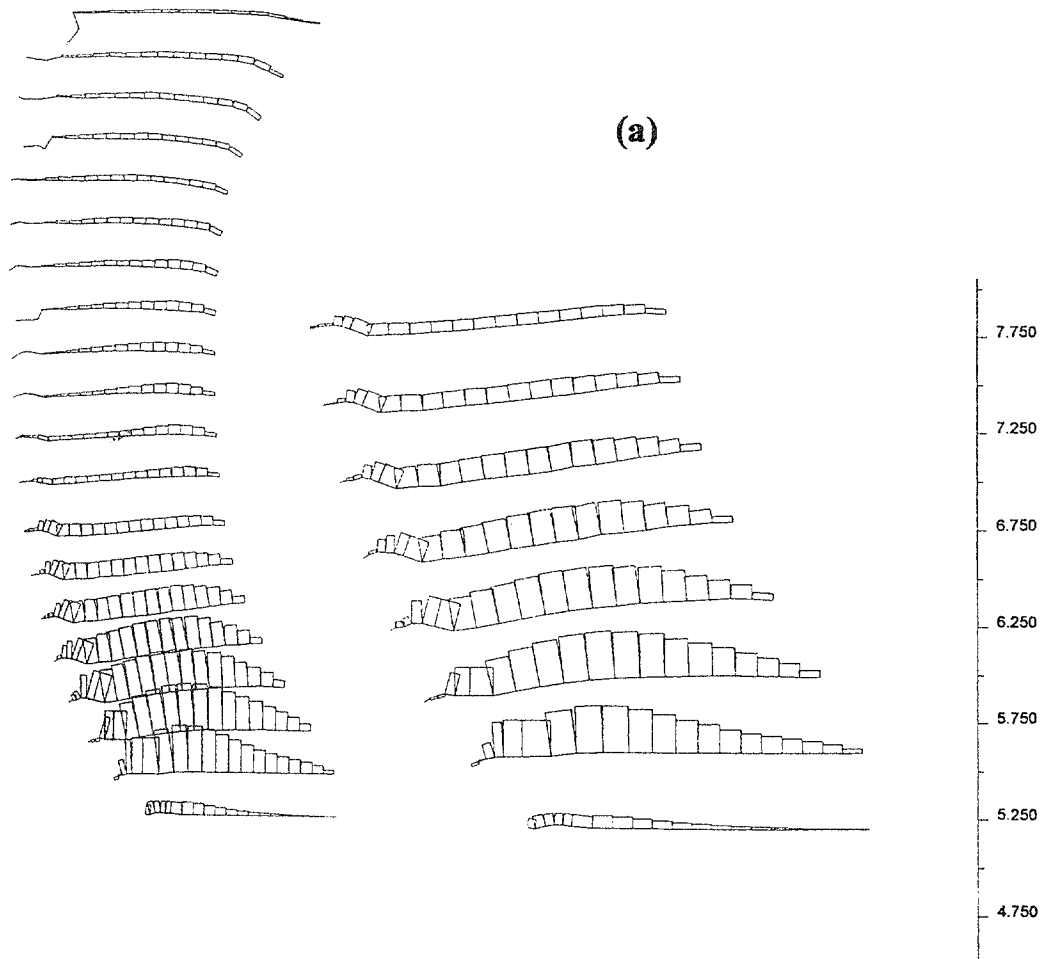


Figure 4.25 Axial Force Distribution in Reinforcement for Case 8-1 ($s=0.4$ m, $t=1.5$ m): (a) Failure State ($h=8.0$ m, $I/h=0.19$); (b) Critical State ($h=5.0$ m, $I/h=0.30$).

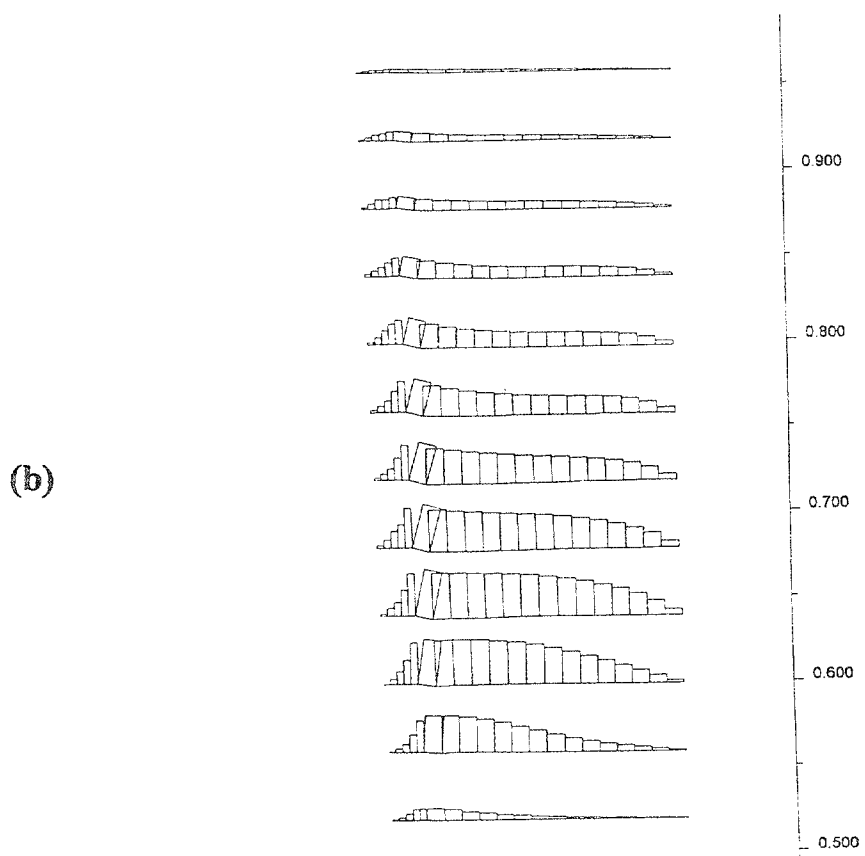
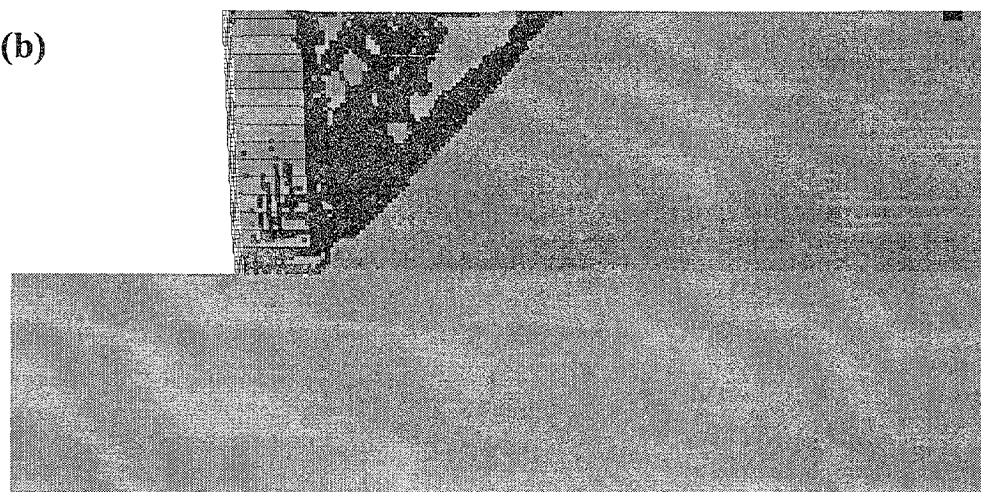
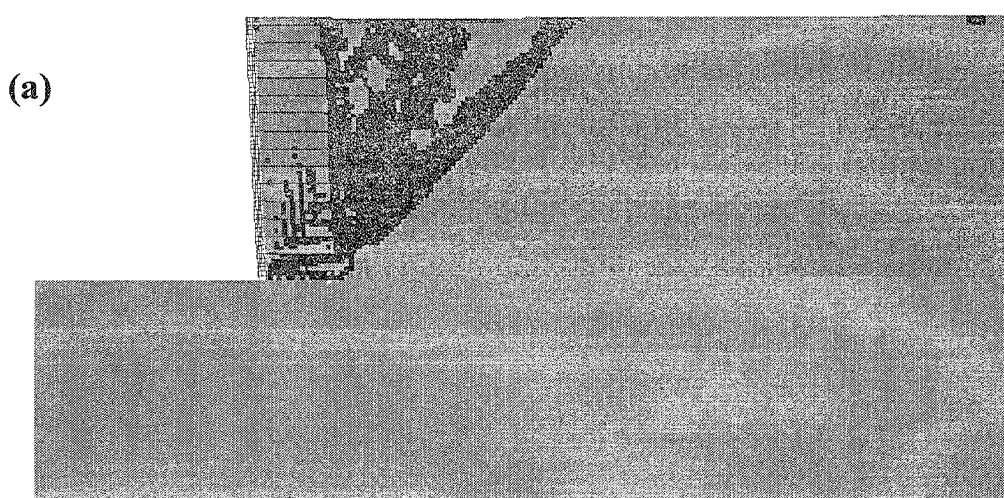


Figure 4.25 Axial Force Distribution in Reinforcement for Case 8-1 ($s=0.4$ m, $t=1.5$ m): (a) Failure State ($h=8.0$ m, $l/h=0.19$); (b) Critical State ($h=5.0$ m, $l/h=0.30$), Continued.



LEGEND: State of Material



Elastic

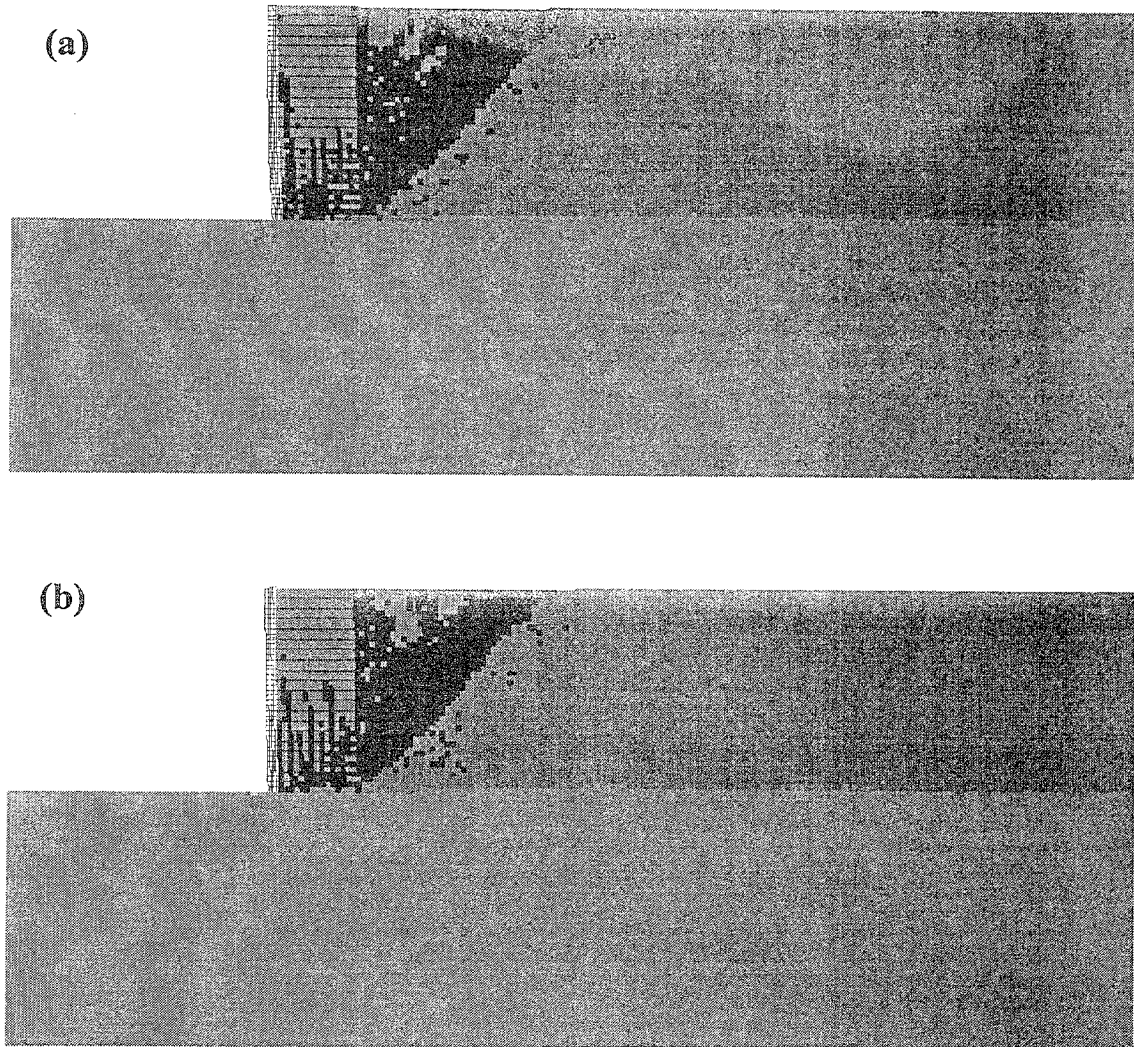


At Yield in Shear or Volume



Elastic, Yield in Past

Figure 4.26 State of Soil for Case 2 ($s=0.4$ m, $l=1.5$ m): (a) Failure State ($h=6.0$ m, $l/h=0.25$); (b) Critical State ($h=4.4$ m, $l/h=0.34$).



LEGEND: State of Material



At Yield in Shear or Volume



Elastic, Yield in Past

Figure 4.27 State of Soil for Case 3 ($s=0.2$ m, $I=1.5$ m): (a) Failure State ($h=4.2$ m, $I/h=0.36$); (b) Critical State ($h=4.0$ m, $I/h=0.38$).

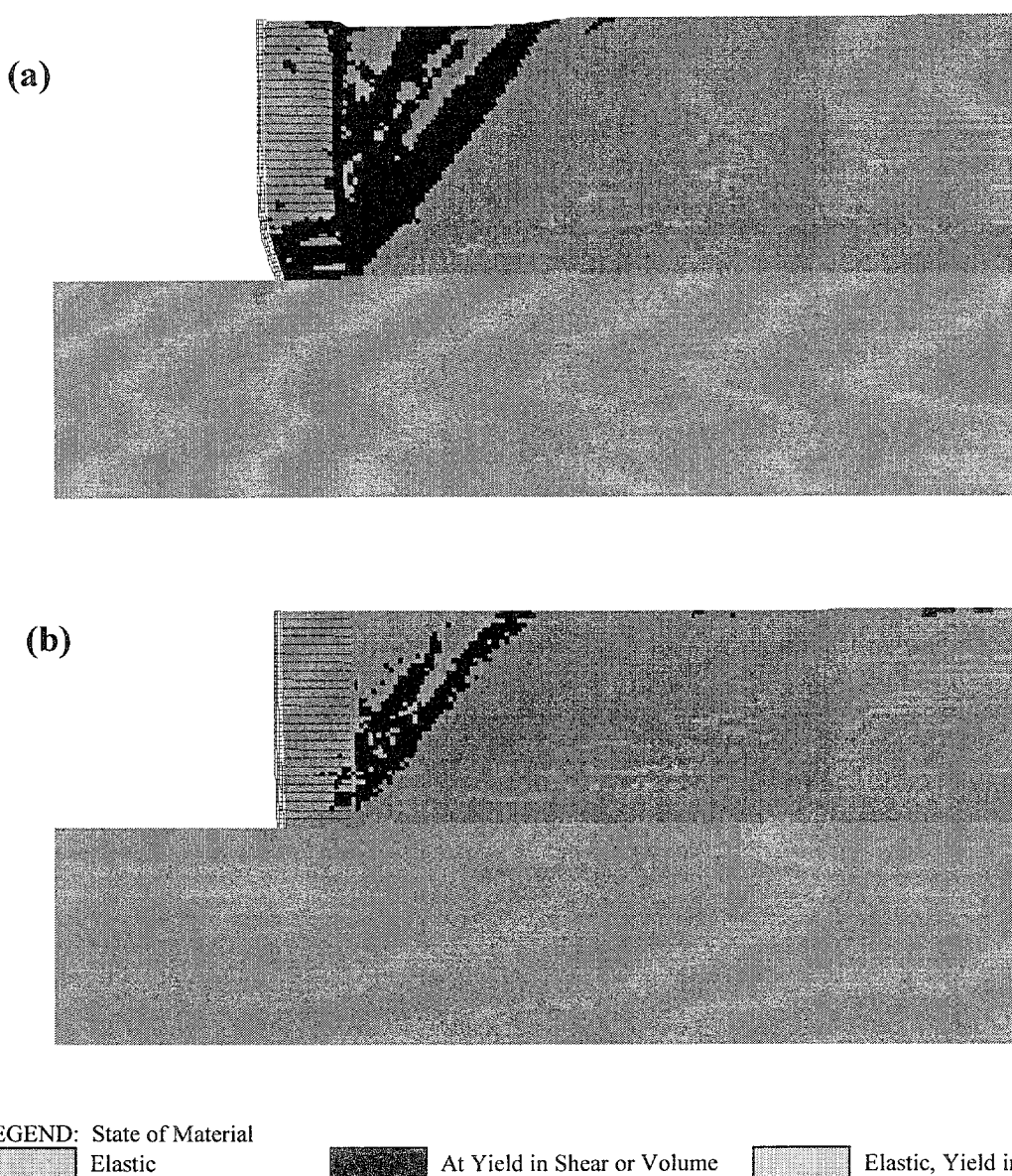
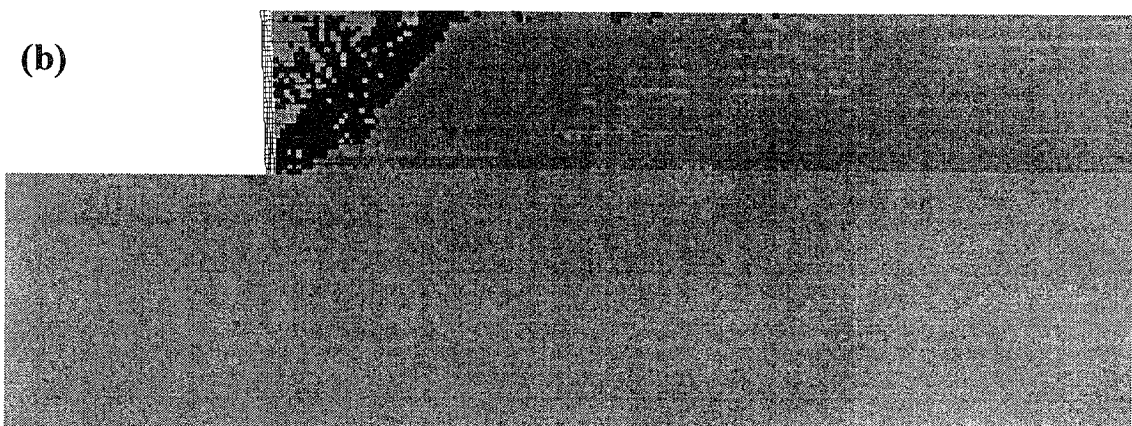
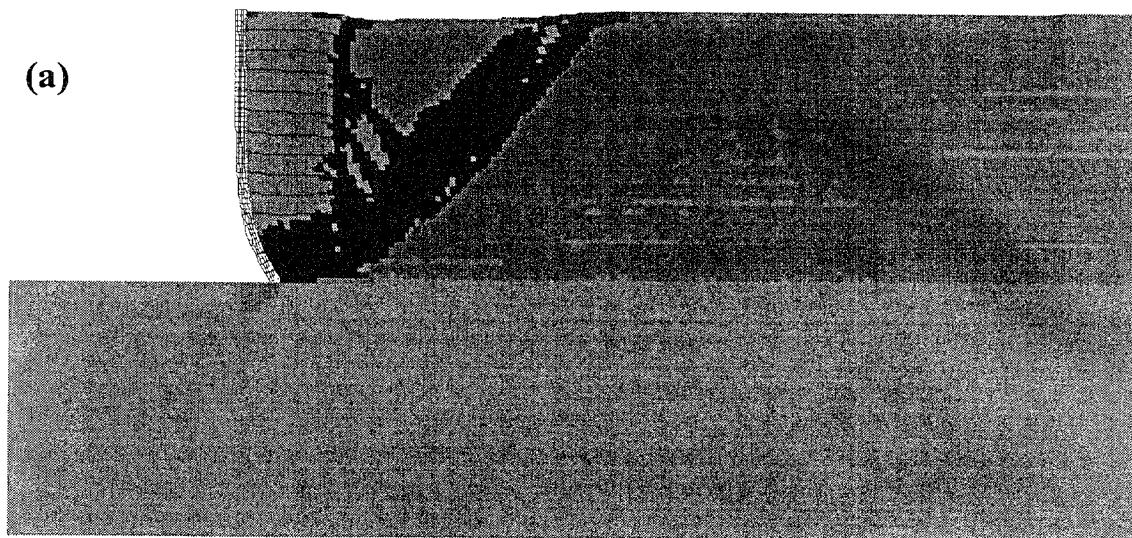


Figure 4.28 State of Soil for Case 7 ($s=0.6/0.2$ m, $l=1.5$ m): (a) Failure State ($h=6.0$ m, $l/h=0.25$); (b) Critical State ($h=5.0$ m, $l/h=0.30$).



LEGEND: State of Material



Elastic



At Yield in Shear or Volume



Elastic, Yield in Past

Figure 4.29 State of Soil for Case 8-2 ($s=0.4$ m, $l=1.5$ m): (a) Failure State ($h=5.4$ m, $l/h=0.28$); (b) Critical State ($h=3.2$ m, $l/h=0.47$).

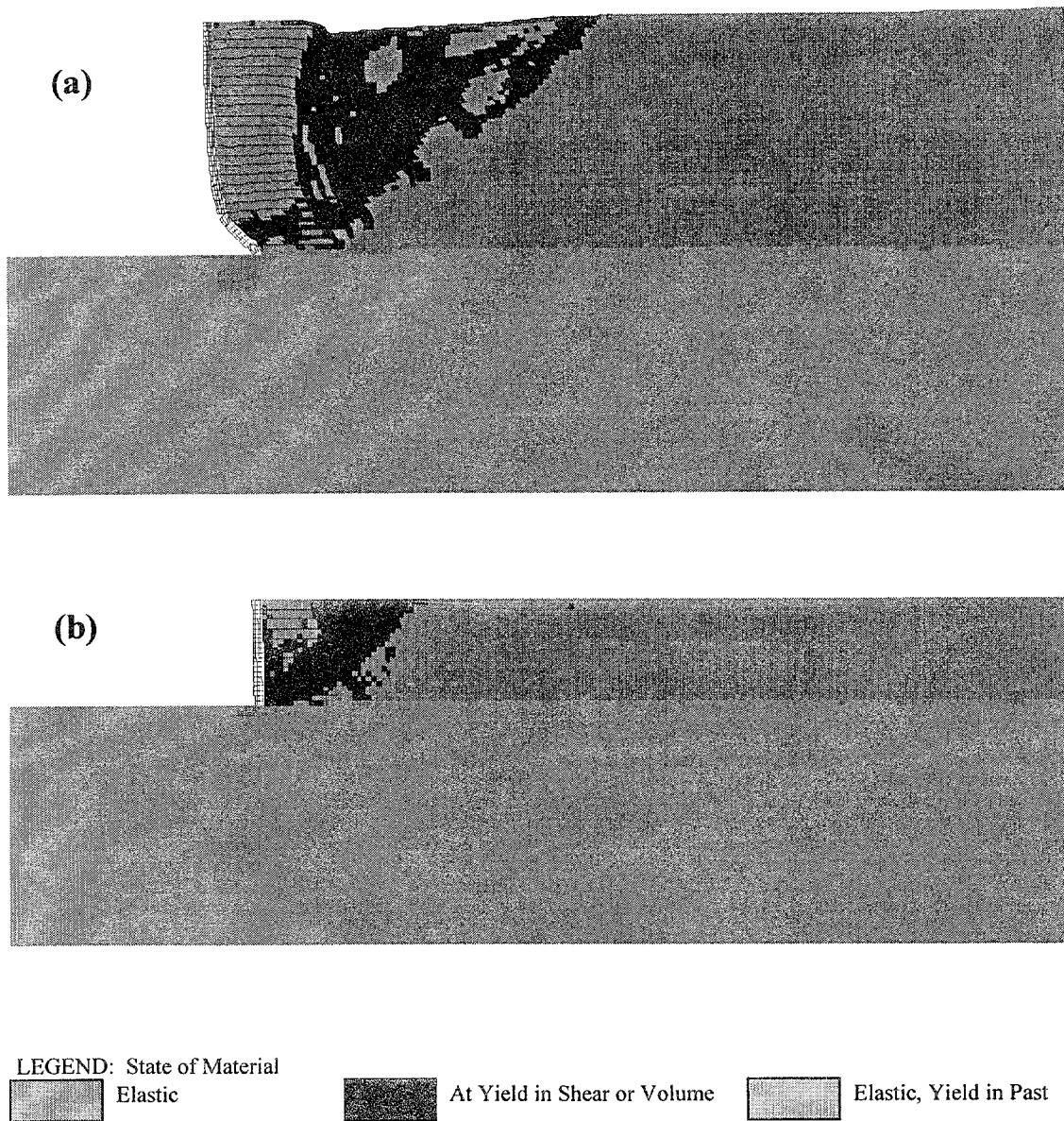
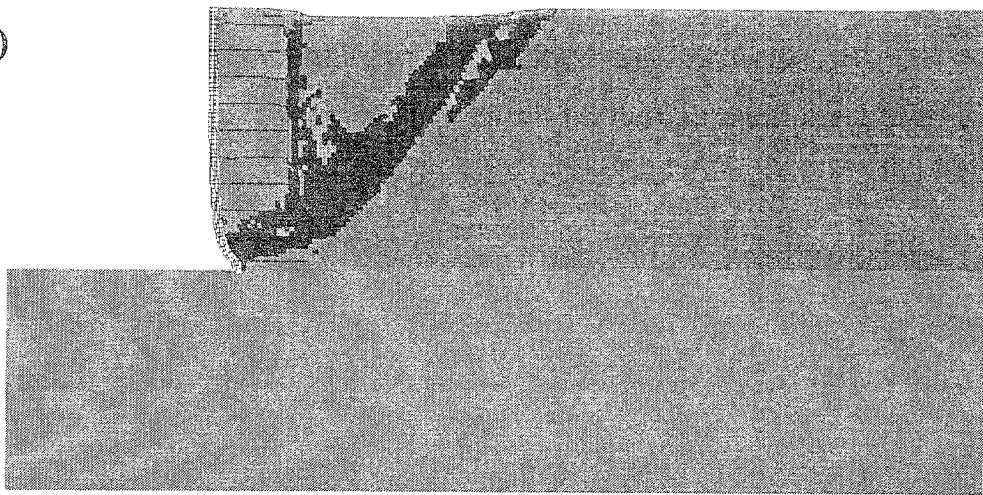
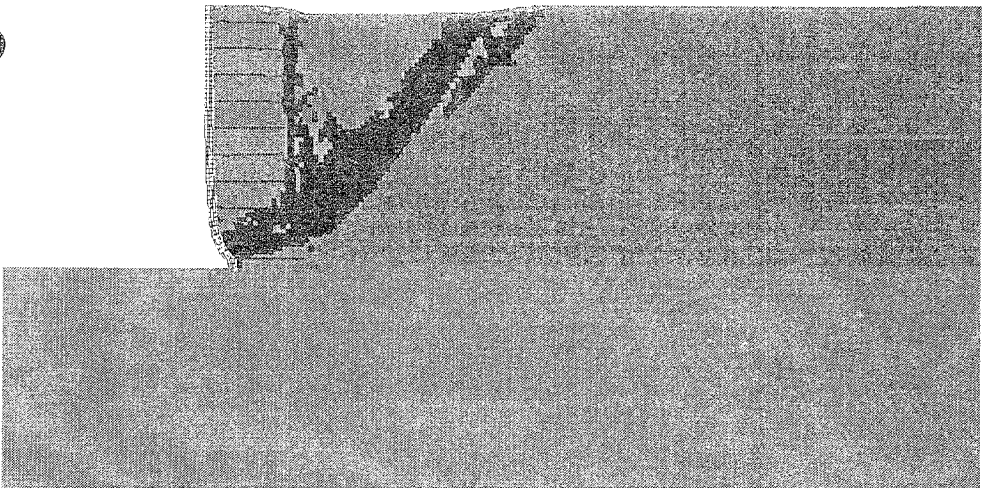


Figure 4.30 State of Soil for Case 8-3 ($s=0.2$ m, $l=1.5$ m): (a) Failure State ($h=5.0$ m, $l/h=0.30$); (b) Critical State ($h=2.2$ m, $l/h=0.68$).

(a)



(b)



LEGEND: State of Material



Elastic



At Yield in Shear or Volume



Elastic, Yield in Past

Figure 4.31 State of Soil for Case 12 ($s=0.6$ m, $J=1.5$ m): (a) Failure State ($h=6.0$ m, $J/h=0.25$); (b) Critical State ($h=4.6$ m, $J/h=0.33$).

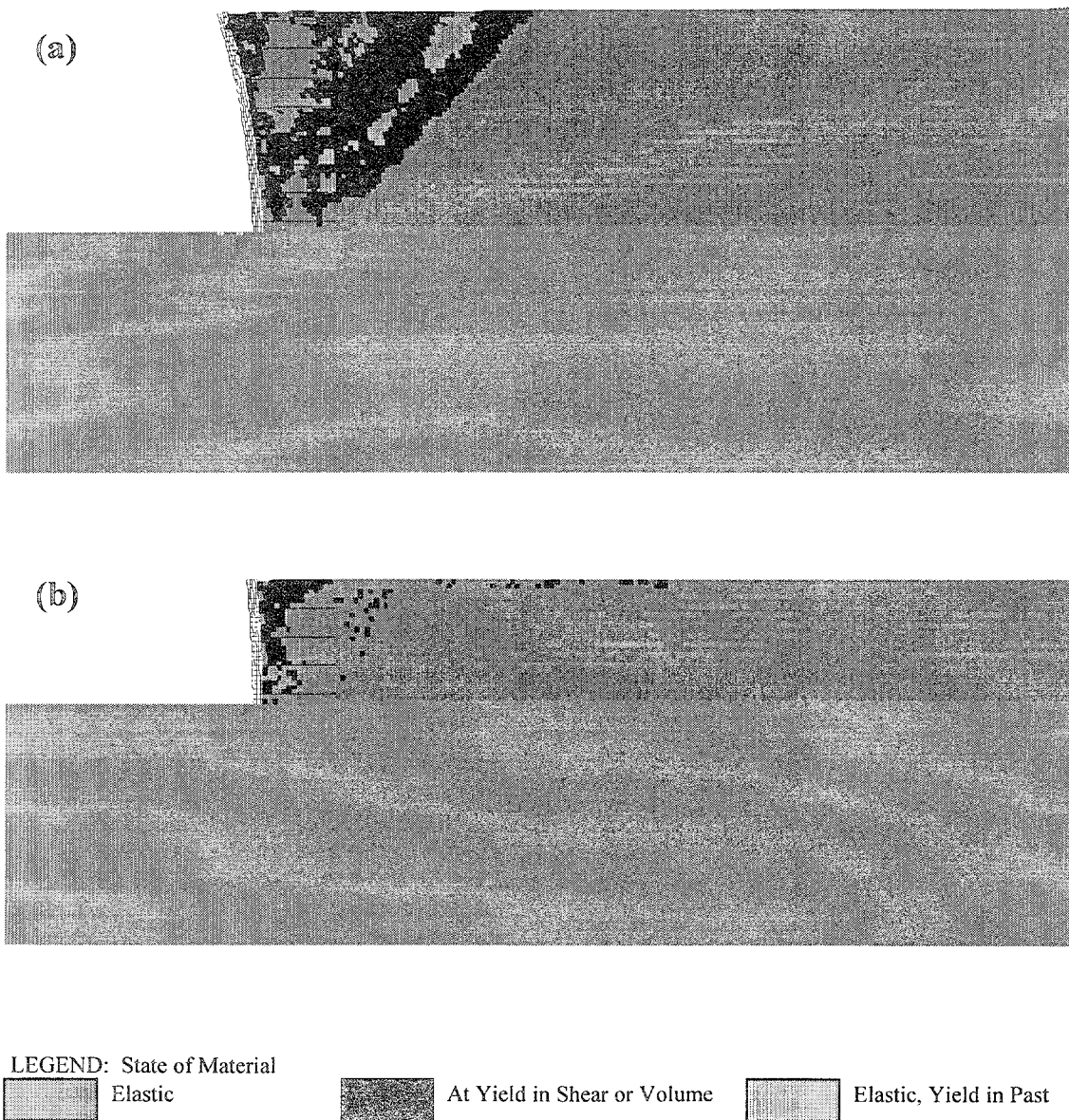
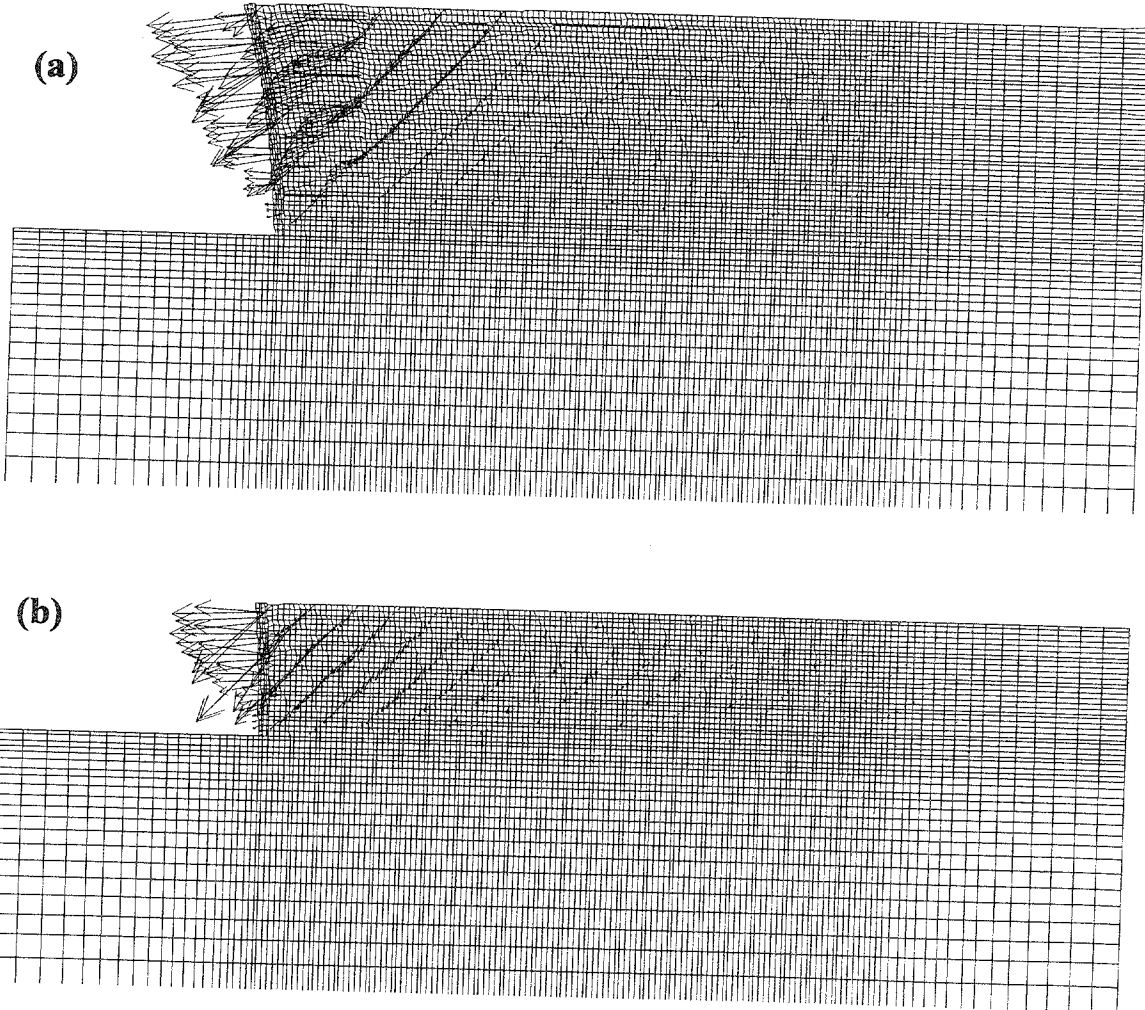


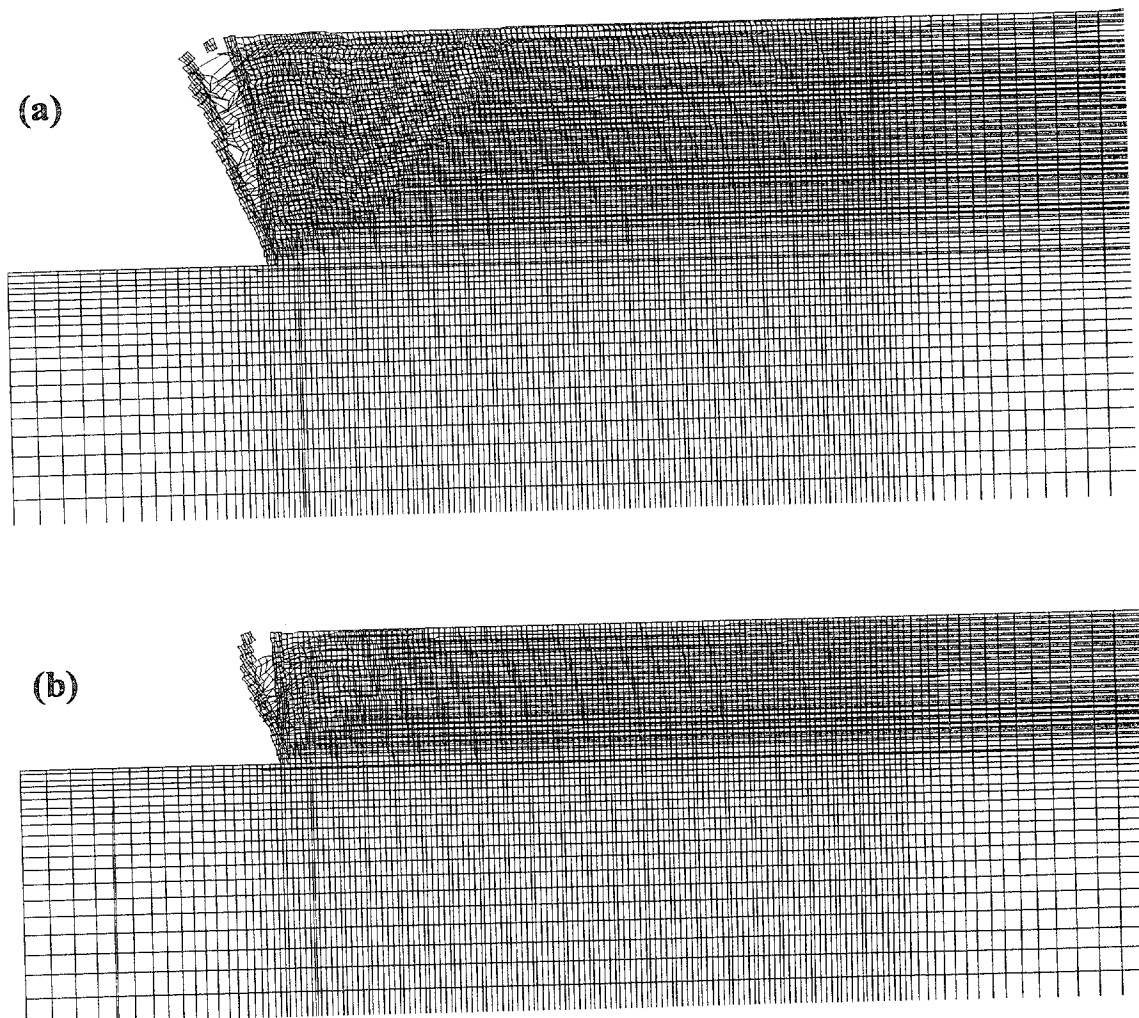
Figure 4.32 State of Soil for Case 2 ($s=0.6$ m, $l=1.5$ m): (a) Failure State ($h=4.6$ m, $l/h=0.33$); (b) Critical State ($h=2.6$ m, $l/h=0.58$).



LEGEND: Maximum Vector

- (a) 0.239 m
- (b) 0.544 m

Figure 4.33 Displacement Vectors for Case 2 ($s=0.6$ m, $t=1.5$ m): (a) Failure State ($h=4.6$ m, $t/h=0.33$); (b) Critical State ($h=2.6$ m, $t/h=0.58$).



LEGEND: Maximum Displacement

- (a) 0.240 m
- (b) 0.071 m

Figure 4.34 Distorted Grid for Case 2 ($s=0.6$ m, $l=1.5$ m): (a) Failure State ($h=4.6$ m, $l/h=0.33$); (b) Critical State ($h=2.6$ m, $l/h=0.58$).

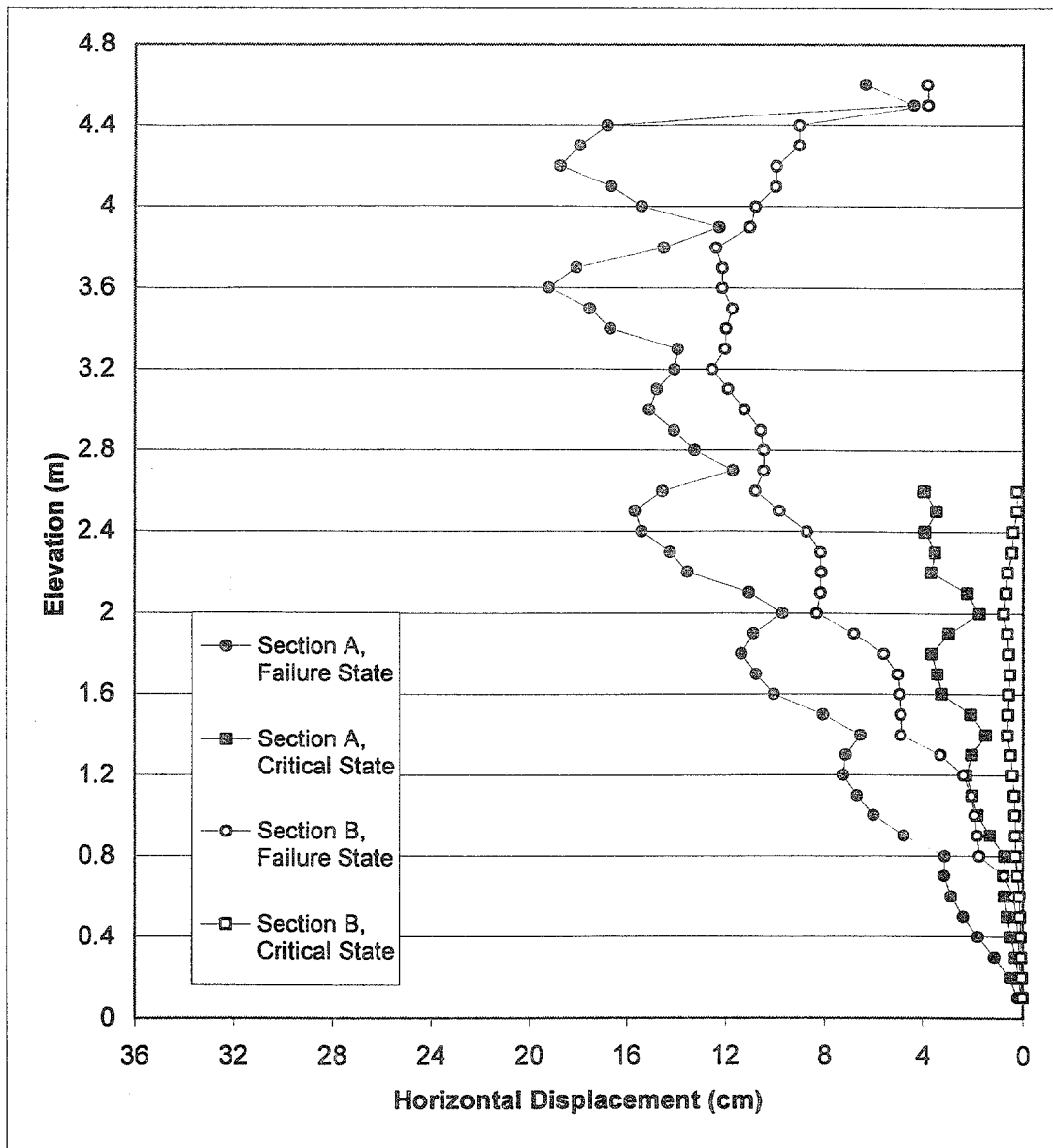


Figure 4.35 Horizontal Displacements for Case 2 ($s=0.6$ m, $l=1.5$ m) at Failure State ($h=4.6$ m, $l/h=0.33$) and Critical State ($h=2.6$ m, $l/h=0.58$).

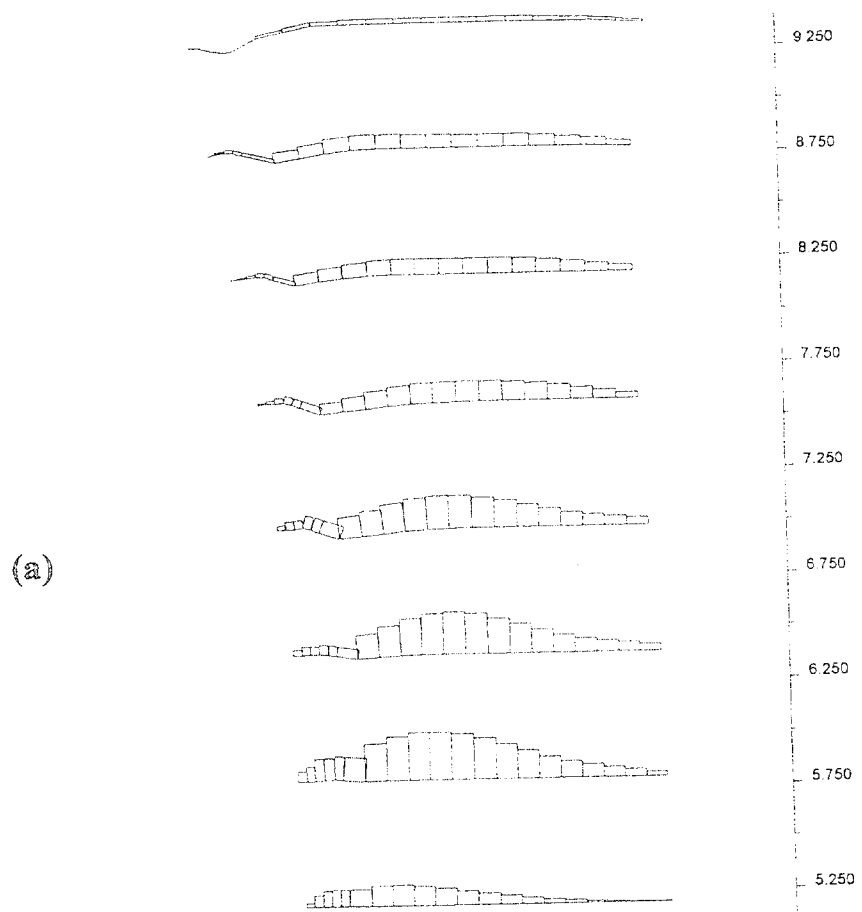


Figure 4.36 Axial Force Distribution in Reinforcement for Case 2 ($s=0.6$ m, $l=1.5$ m): (a) Failure State ($h=4.6$ m, $l/h=0.33$); (b) Critical State ($h=2.6$ m, $l/h=0.58$).

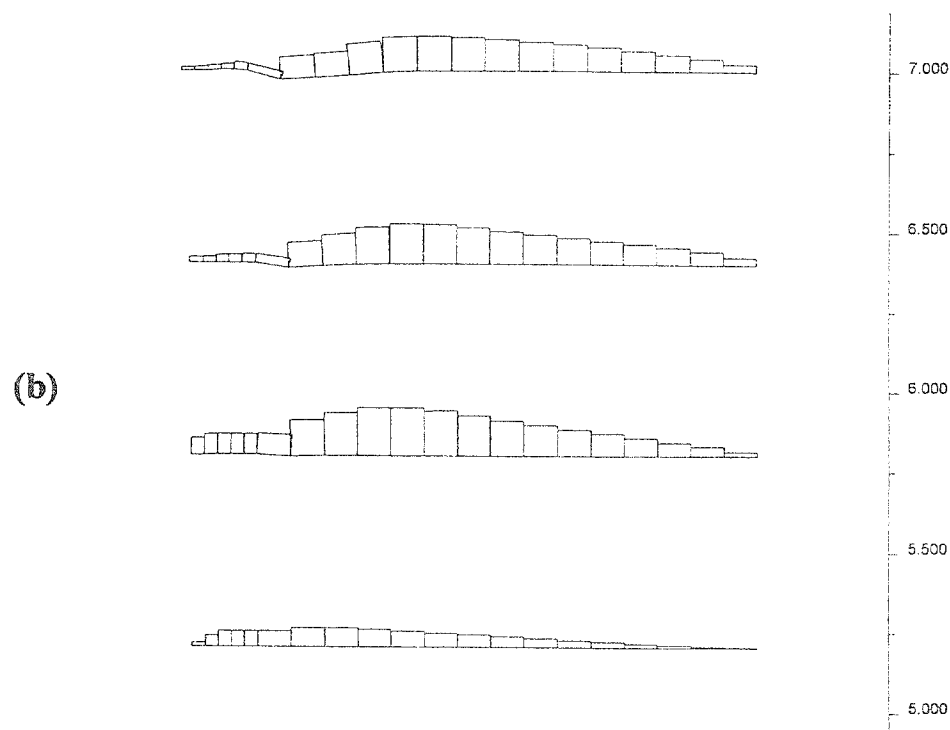
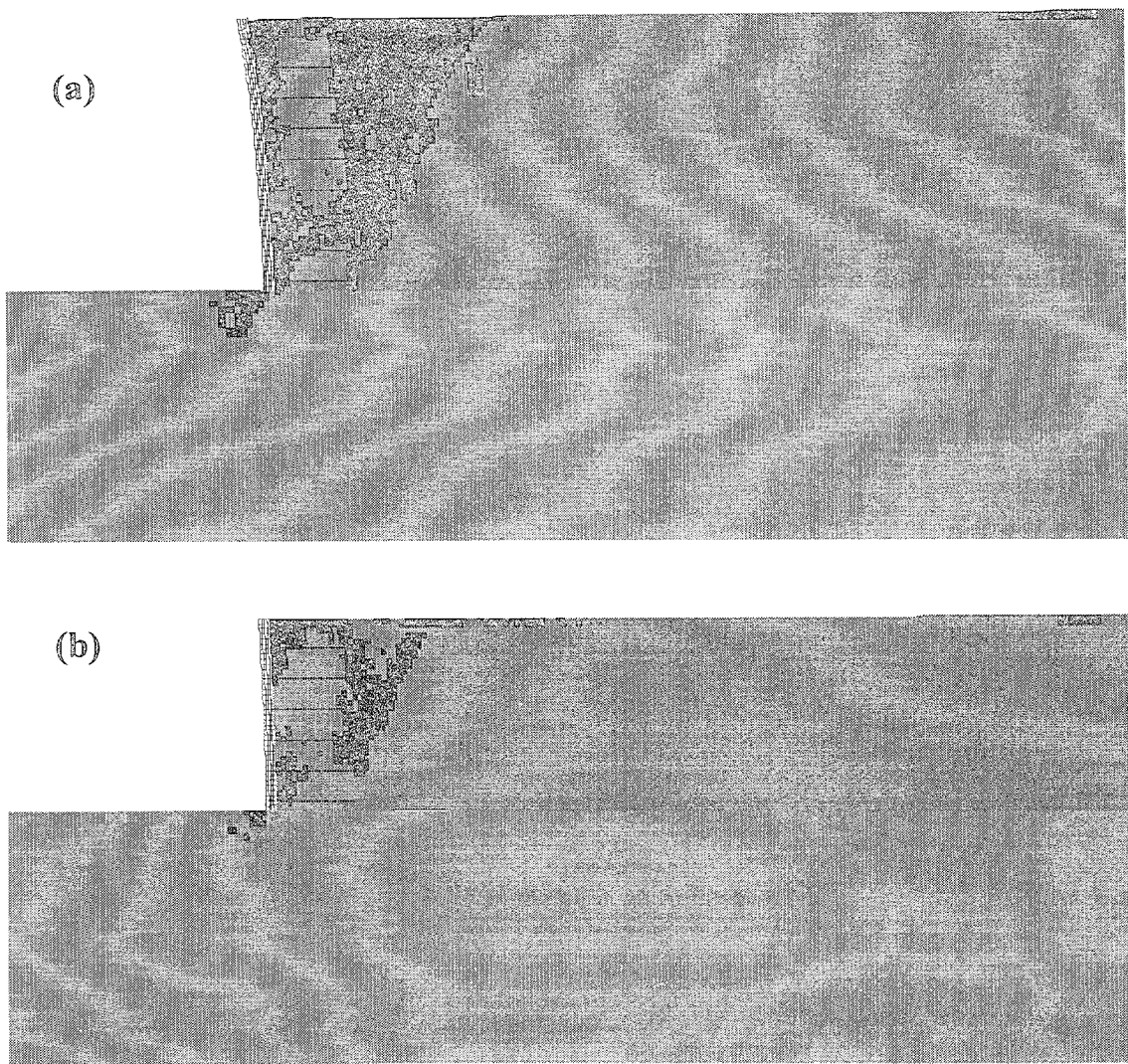


Figure 4.36 Axial Force Distribution in Reinforcement for Case 2 ($s=0.6$ m, $l=1.5$ m): (a) Failure State ($h=4.6$ m, $l/h=0.33$); (b) Critical State ($h=2.6$ m, $l/h=0.58$), Continued.



LEGEND: State of Material
 Elastic At Yield in Shear or Volume Elastic, Yield in Past

Figure 4.37 State of Soil for Case 4 ($s=0.6$ m, $I=1.5$ m): (a) Failure State ($h=5.4$ m, $I/h=0.28$); (b) Critical State ($h=3.8$ m, $I/h=0.39$).

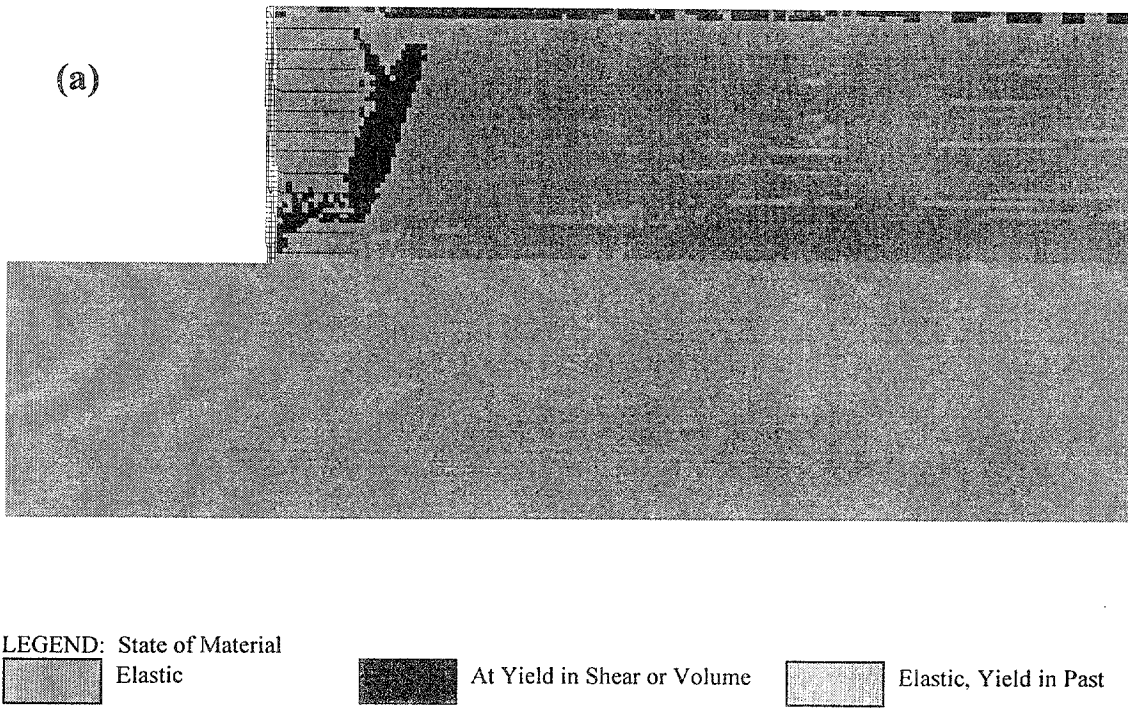


Figure 4.38 Case 1 ($s=0.4$ m, $l=1.5$ m, $h=5.0$ m): (a) State of Soil; (b) Axial Force Distribution in Reinforcement.

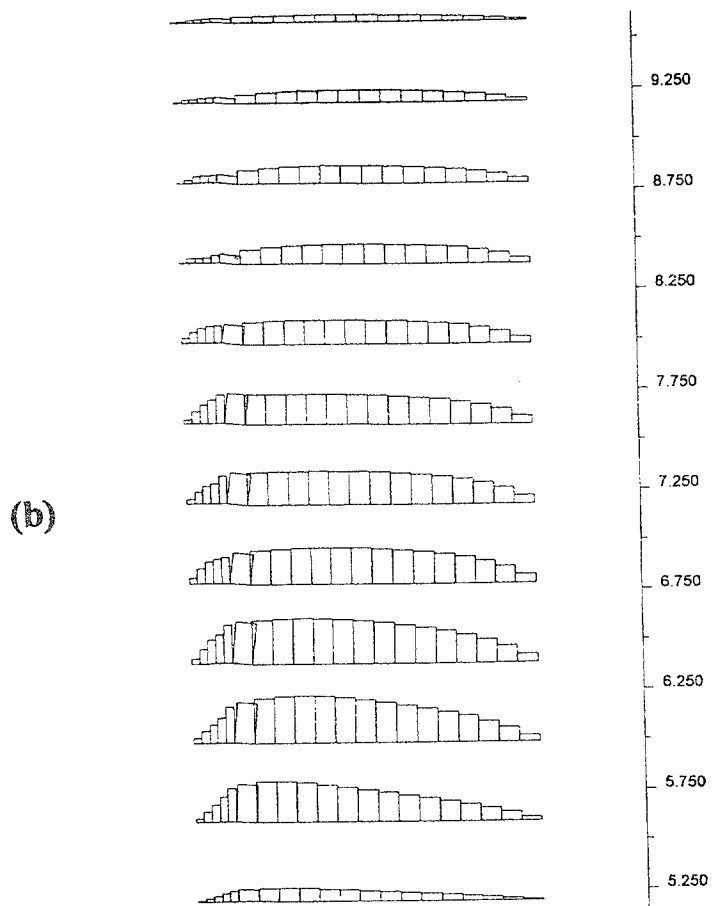


Figure 4.38 Case 1 ($s=0.4$ m, $t=1.5$ m, $h=5.0$ m): (a) State of Soil; (b) Axial Force Distribution in Reinforcement, Continued.

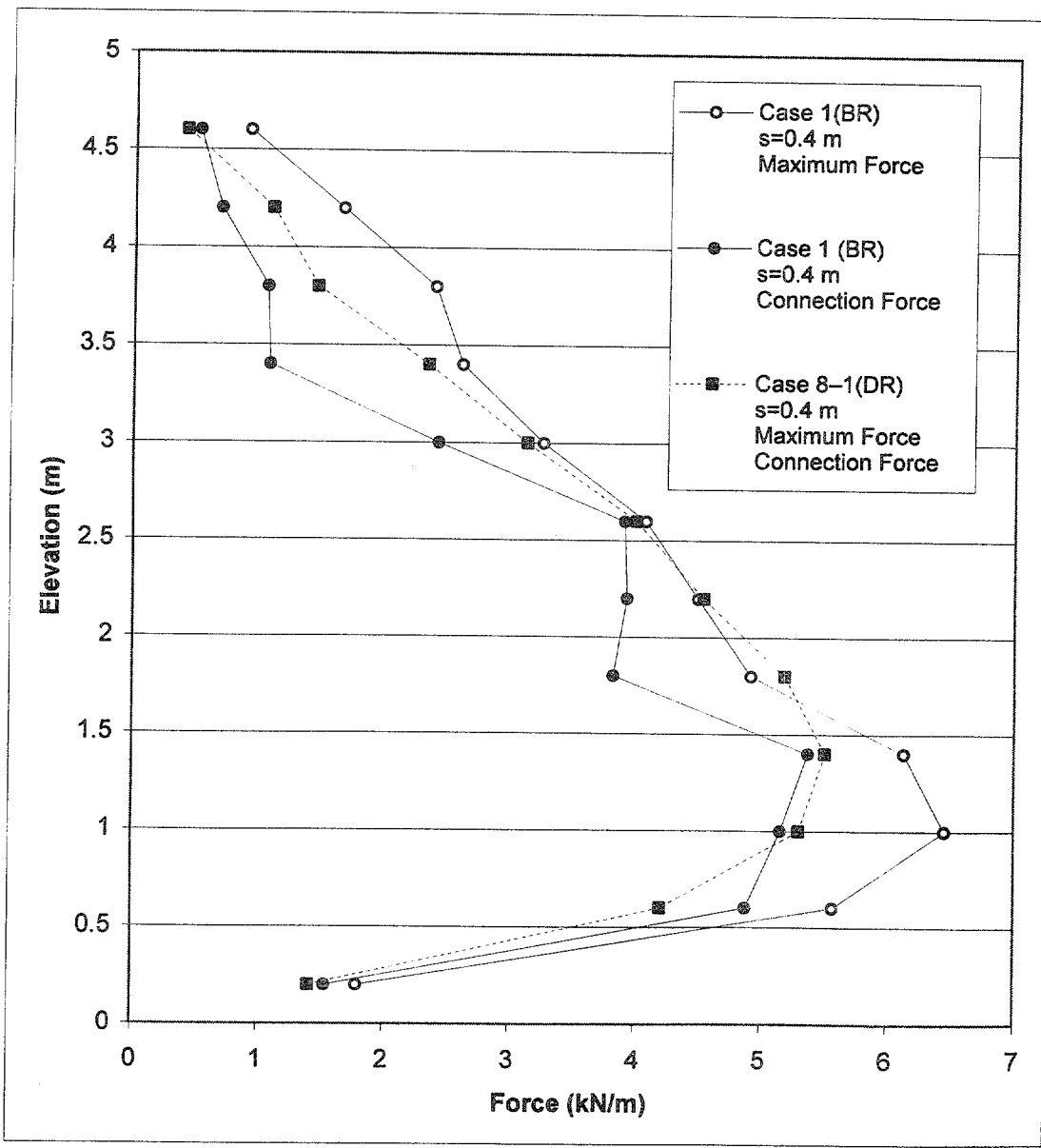


Figure 4.39 Connection Force and Maximum Force in Reinforcement for Case 1 ($s=0.4 \text{ m}$, $h=5.0 \text{ m}$, BR) and Case 8-1 ($s=0.4 \text{ m}$, $h=5.0 \text{ m}$, DR): Effects of Reinforcement Stiffness.

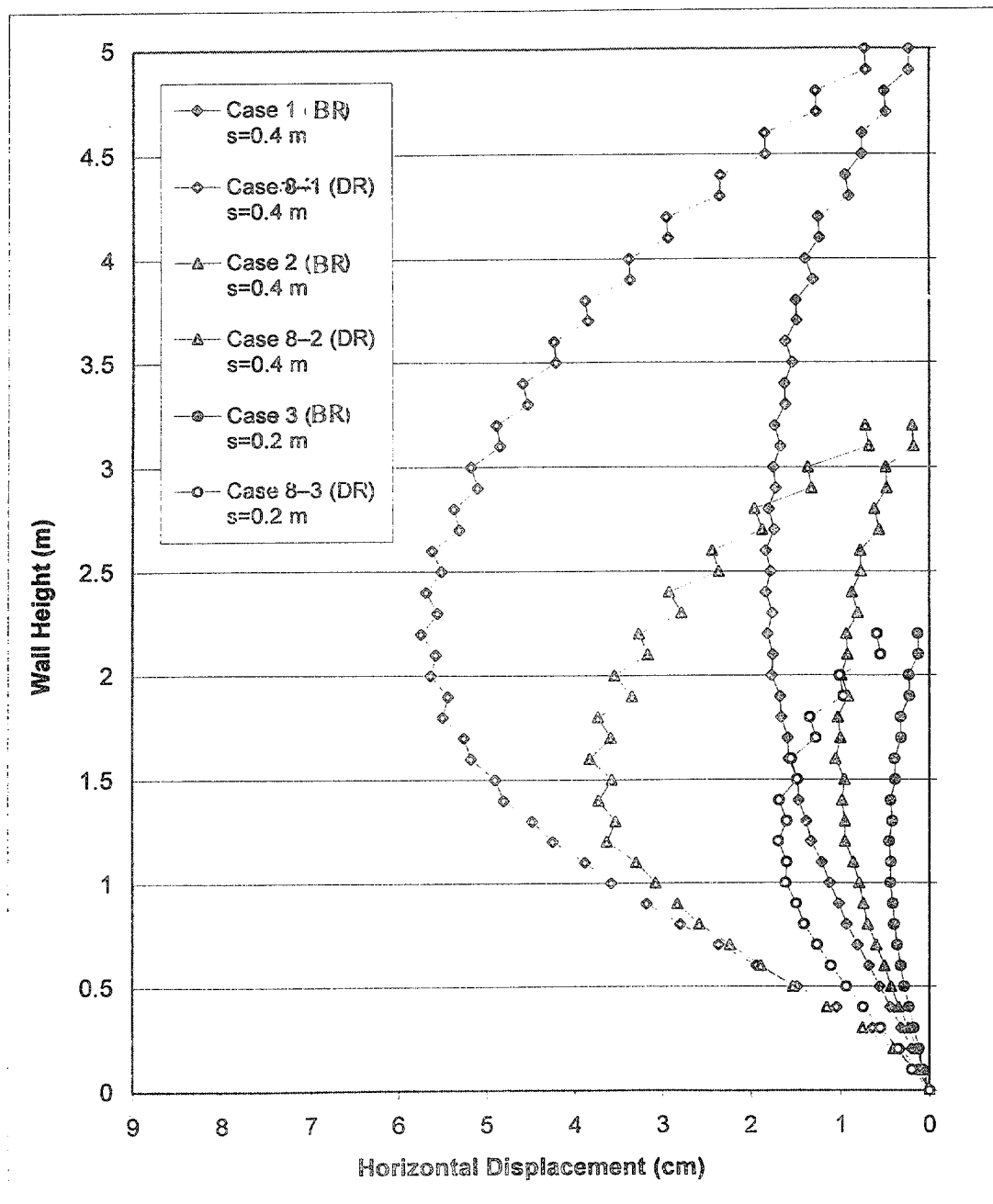
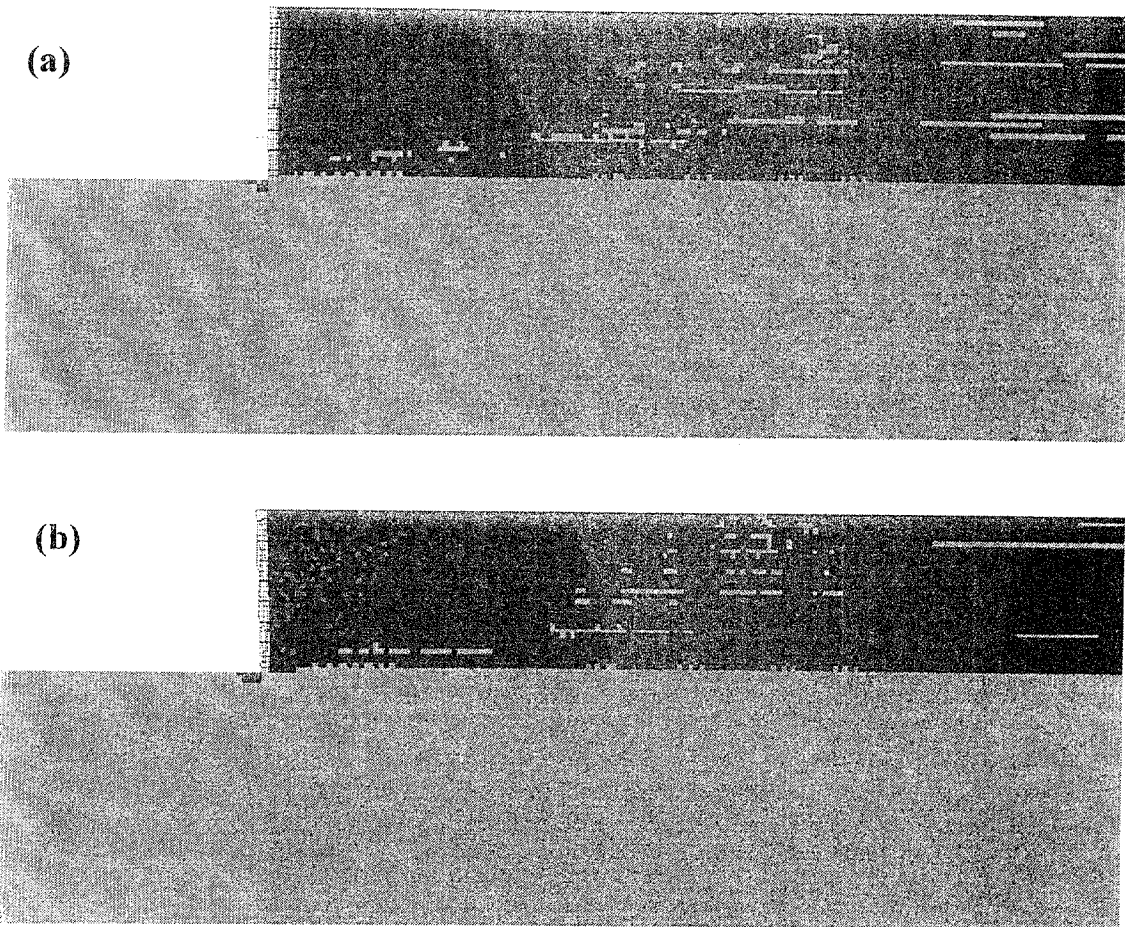


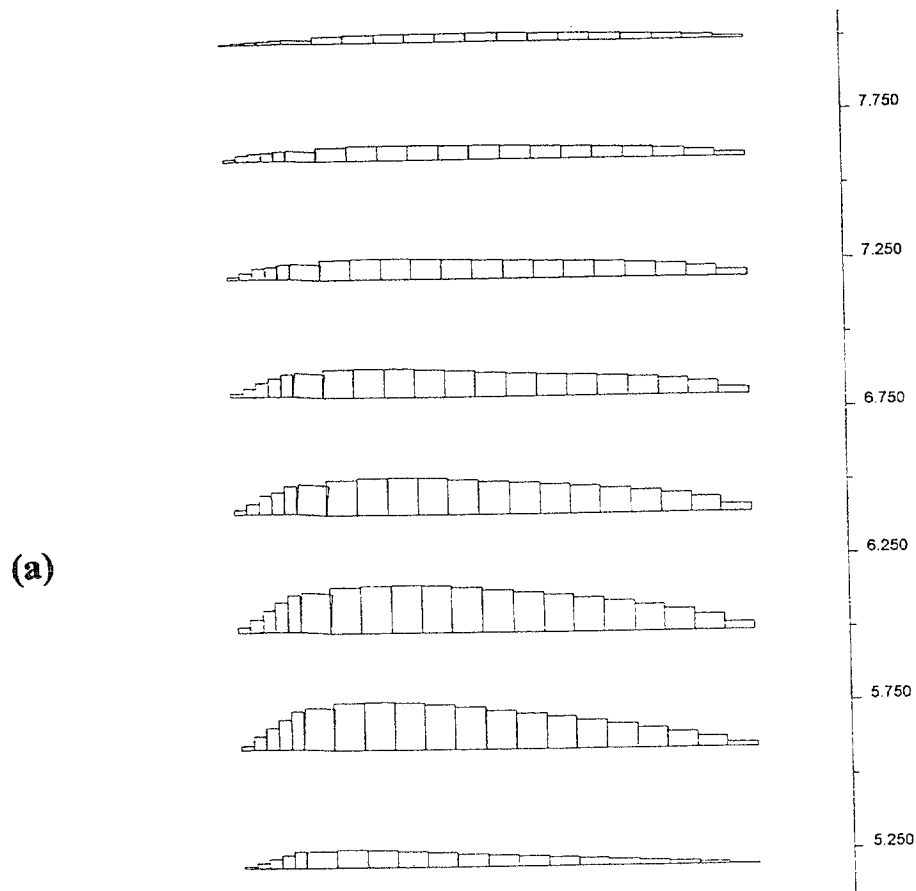
Figure 4.40 Horizontal Displacements along Section A: Comparison with Respect to Reinforcement Stiffness.



LEGEND: State of Material

	Elastic		At Yield in Shear or Volume		Elastic, Yield in Past
--	---------	--	-----------------------------	--	------------------------

Figure 4.41 State of Soil for Cases 2 and 8-2 ($s=0.4$ m, $h=3.2$ m, $t=1.5$ m): (a) Case 2 (BR); (b) Case 8-2 (DR).



(a)

Figure 4.42 Axial Force Distributions in Reinforcement for Cases 2 and 8–2
($s=0.4$ m, $h=3.2$ m, $l=1.5$ m): (a) Case 2 (BR); (b) Case 8–2 (DR).

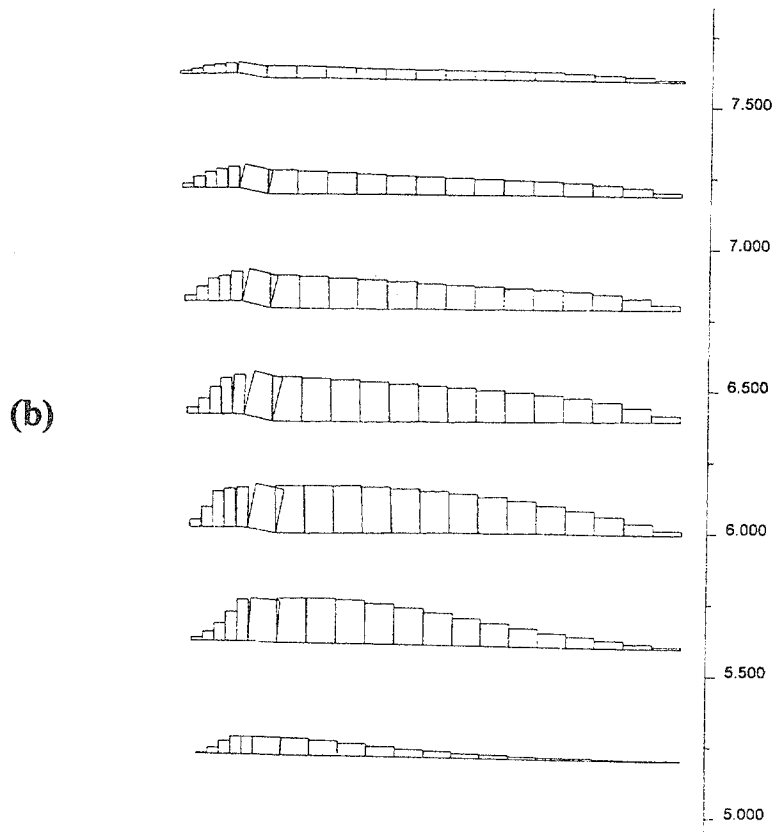


Figure 4.42 Axial Force Distributions in Reinforcement for Cases 2 and 8-2 ($s=0.4$ m, $h=3.2$ m, $l=1.5$ m): (a) Case 2 (BR); (b) Case 8-2 (DR), Continued.

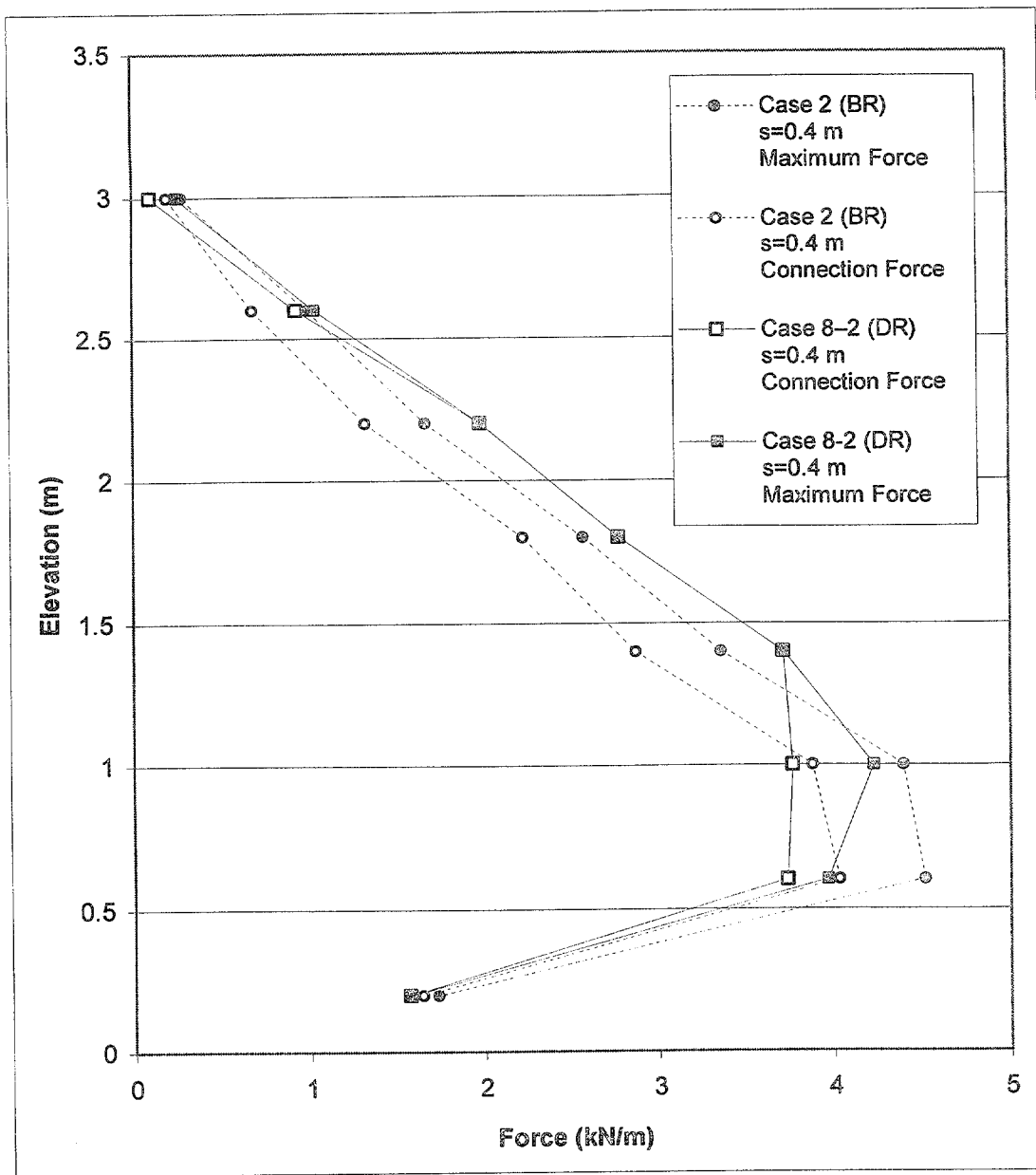
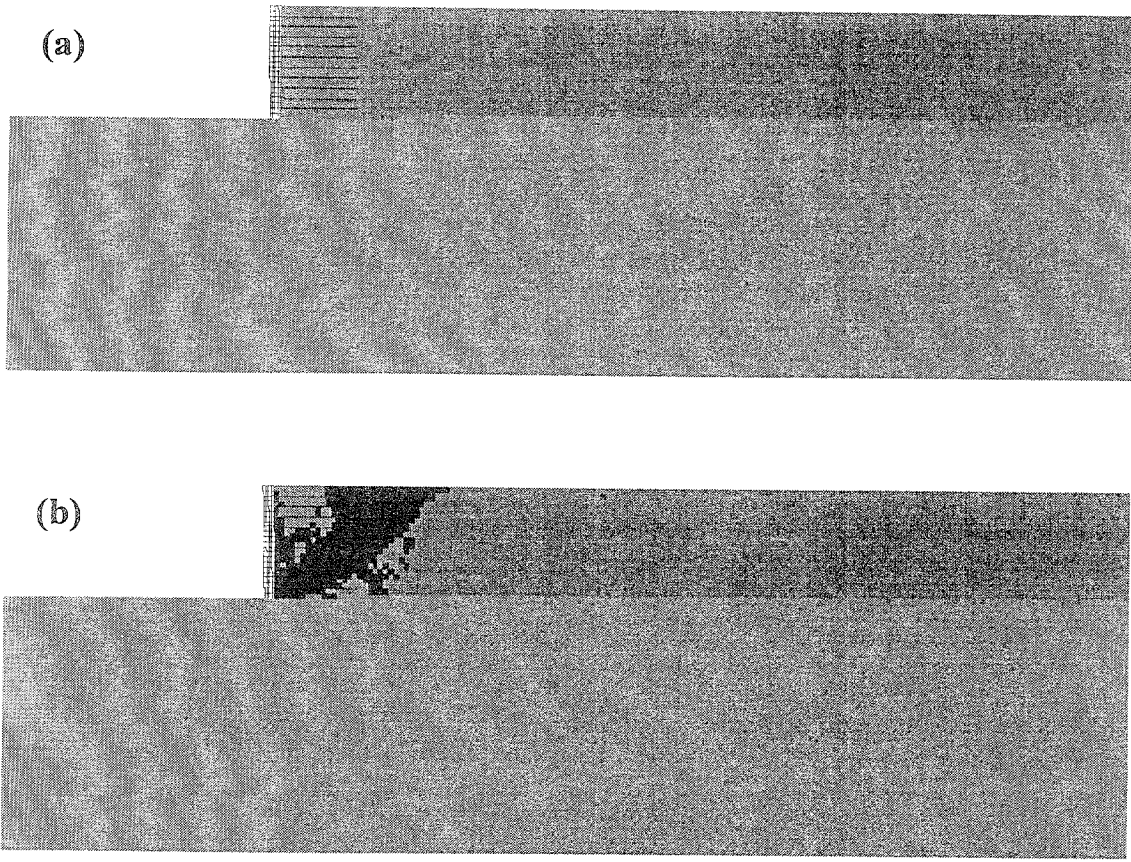


Figure 4.43 Connection Force and Maximum Force in Reinforcement for Case 2 ($s=0.4$ m, $h=3.2$ m, BR) and Case 8-2 ($s=0.4$ m, $h=3.2$ m, DR): Effects of Reinforcement Stiffness.



LEGEND: State of Material
 Elastic  At Yield in Shear or Volume  Elastic, Yield in Past

**Figure 4.44 State of Soil for Cases 3 and 8-3 ($s=0.2$ m, $h=2.2$ m, $l=1.5$ m):
 (a) Case 3 (BR); (b) Case 8-3 (DR).**

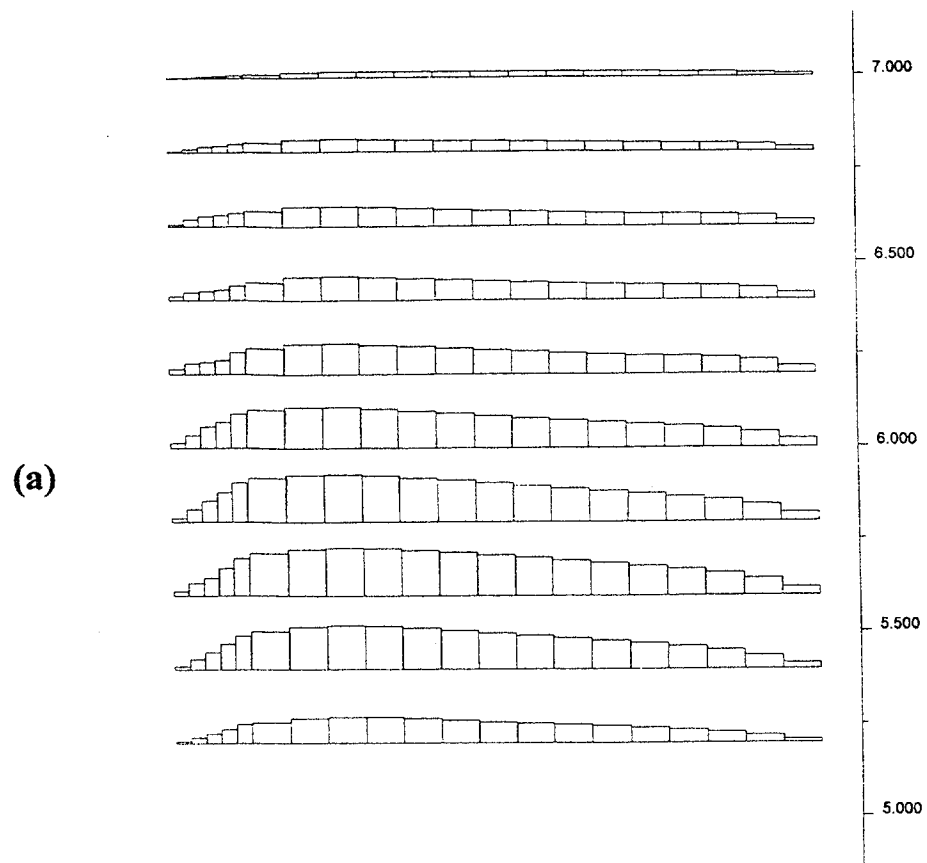


Figure 4.45 Axial Force Distributions in Reinforcement for Cases 3 and 8–3
 $(s=0.2 \text{ m}, h=2.2 \text{ m}, l=1.5 \text{ m})$: (a) Case 3 (BR); (b) Case 8–3 (DR).

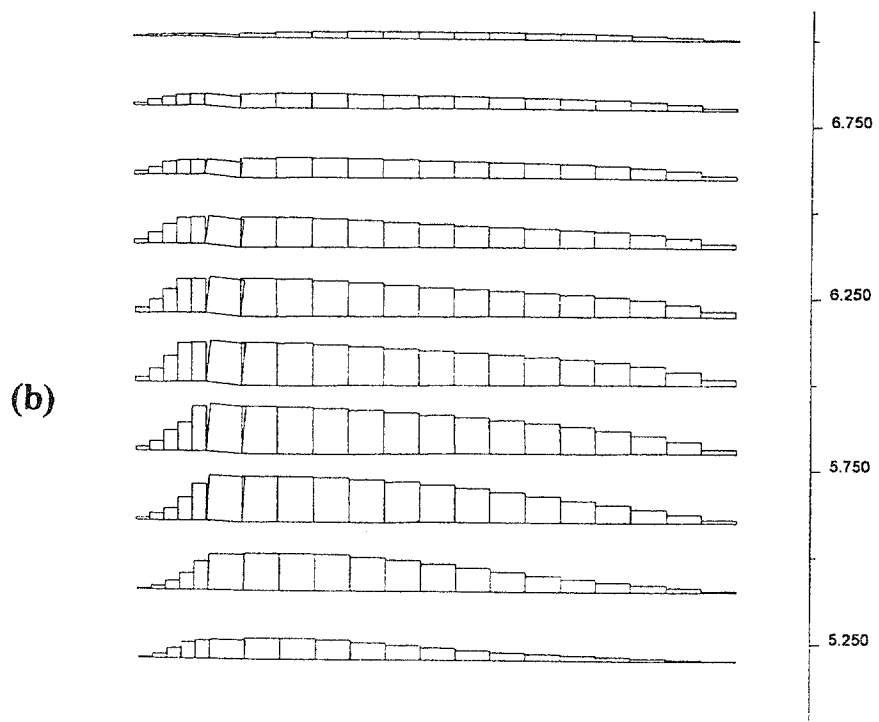


Figure 4.45 Axial Force Distributions in Reinforcement for Cases 3 and 8-3
($s=0.2$ m, $h=2.2$ m, $l=1.5$ m): (a) Case 3 (BR); (b) Case 8-3 (DR), Continued.

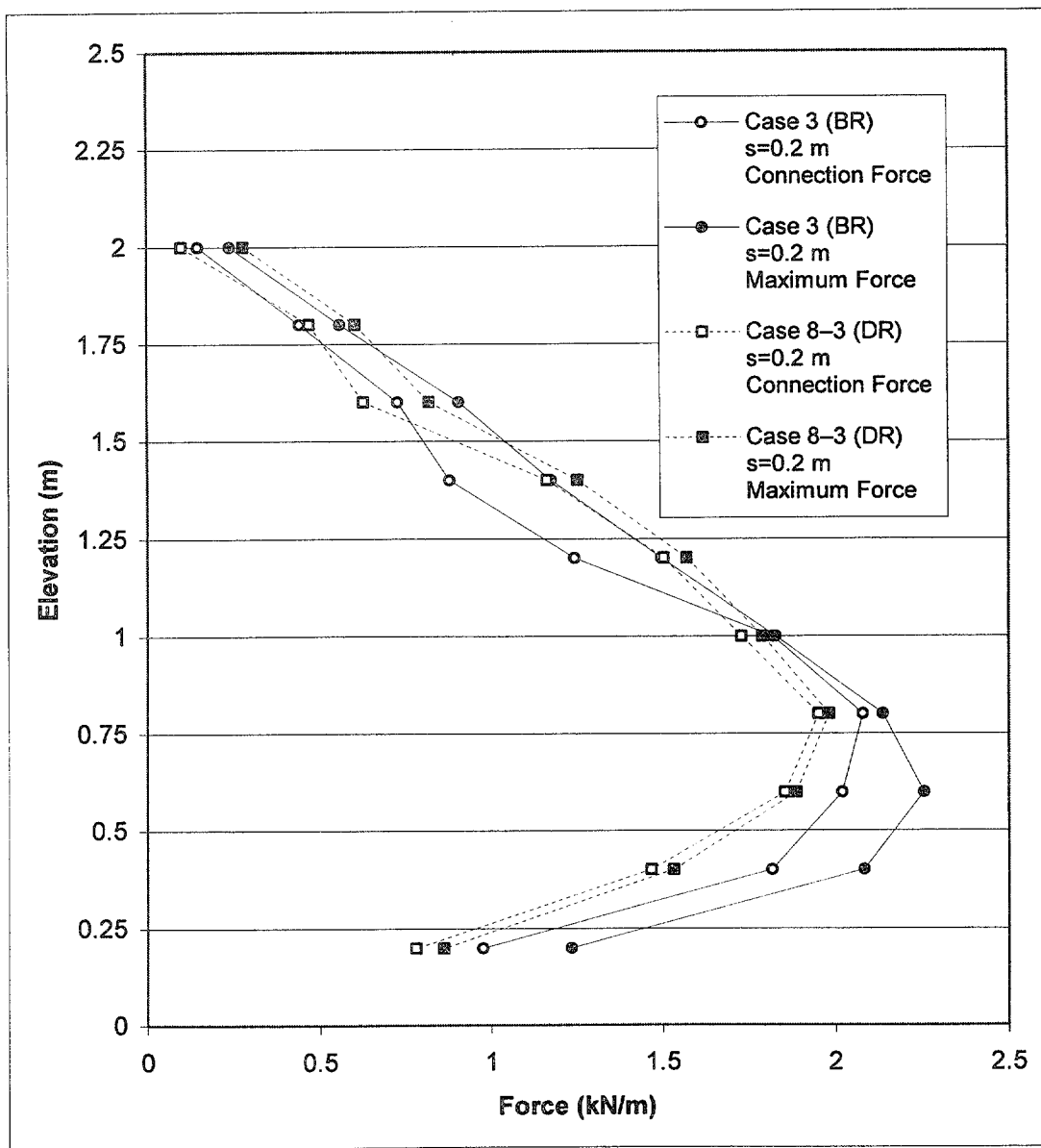


Figure 4.46 Connection Force and Maximum Force in Reinforcement for Case 3 ($s=0.2$ m, $h=2.2$ m, BR) and Case 8-3 ($s=0.2$ m, $h=2.2$ m, DR): Effects of Reinforcement Stiffness.

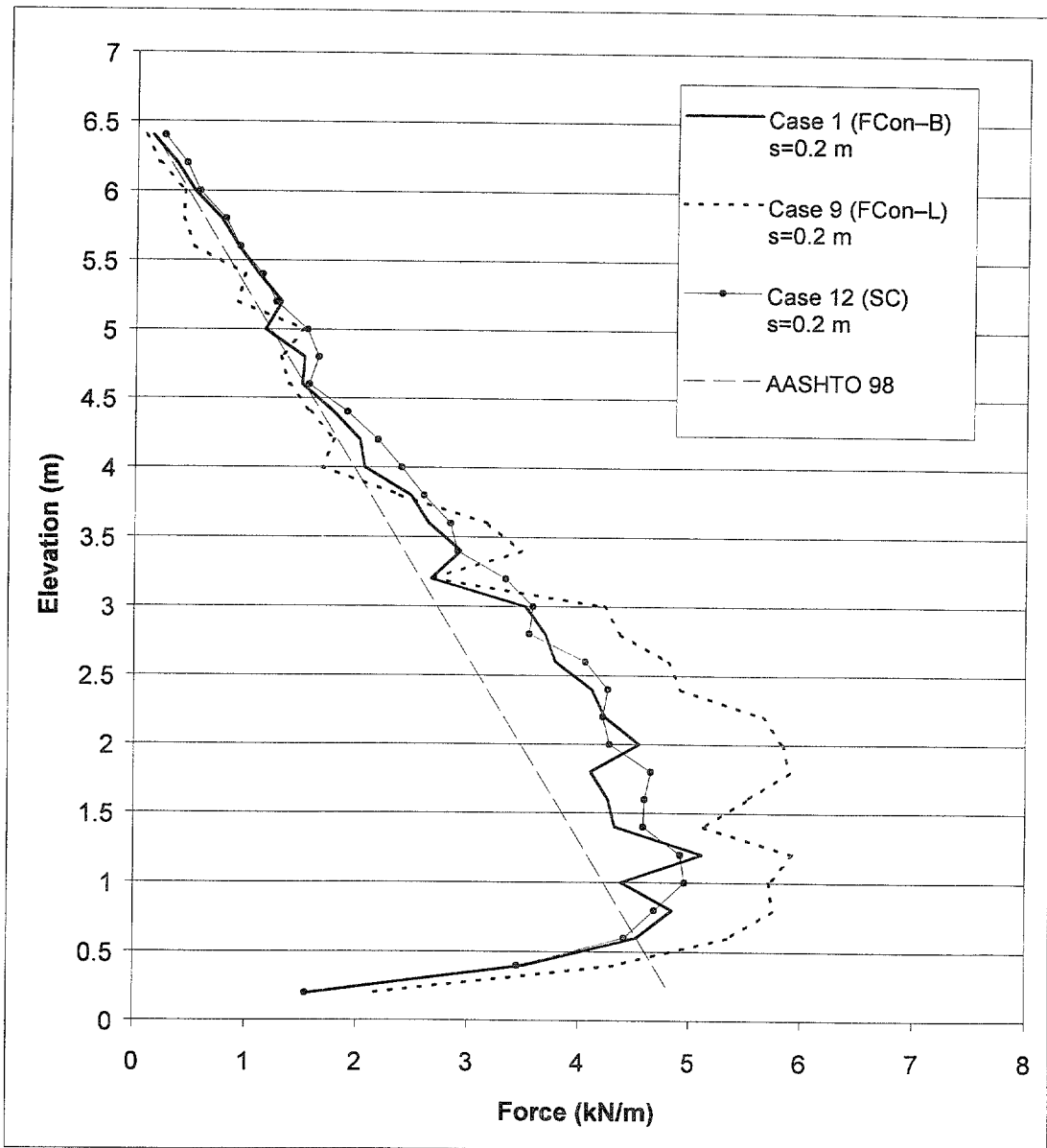


Figure 4.47 Effects of Connection Strength on Connection Force for Cases with Small Reinforcement Spacing ($s=0.2$ m).

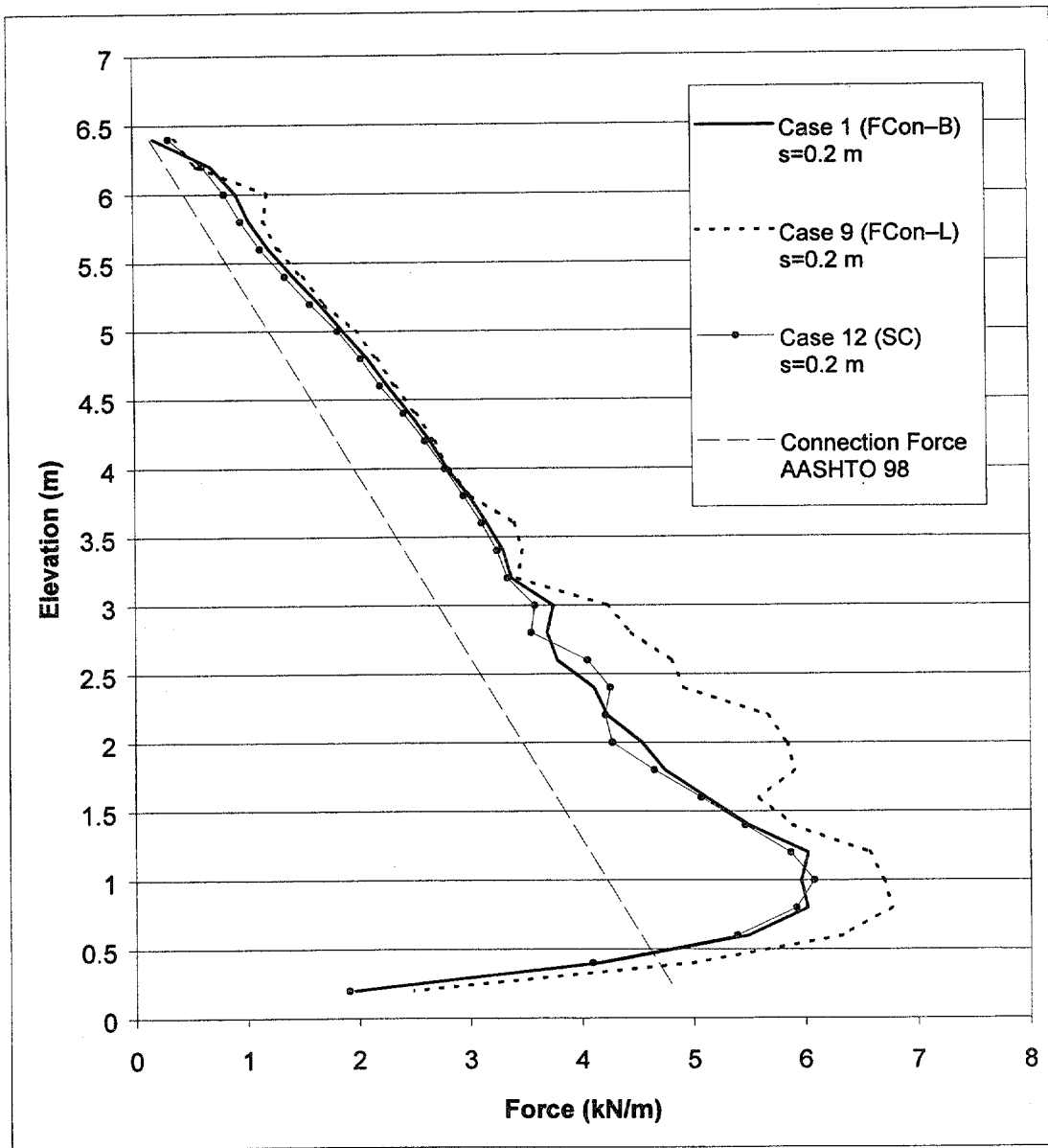


Figure 4.48 Effects of Connection Strength on Maximum Force in Reinforcement for Cases with Small Reinforcement Spacing ($s=0.2\text{ m}$).

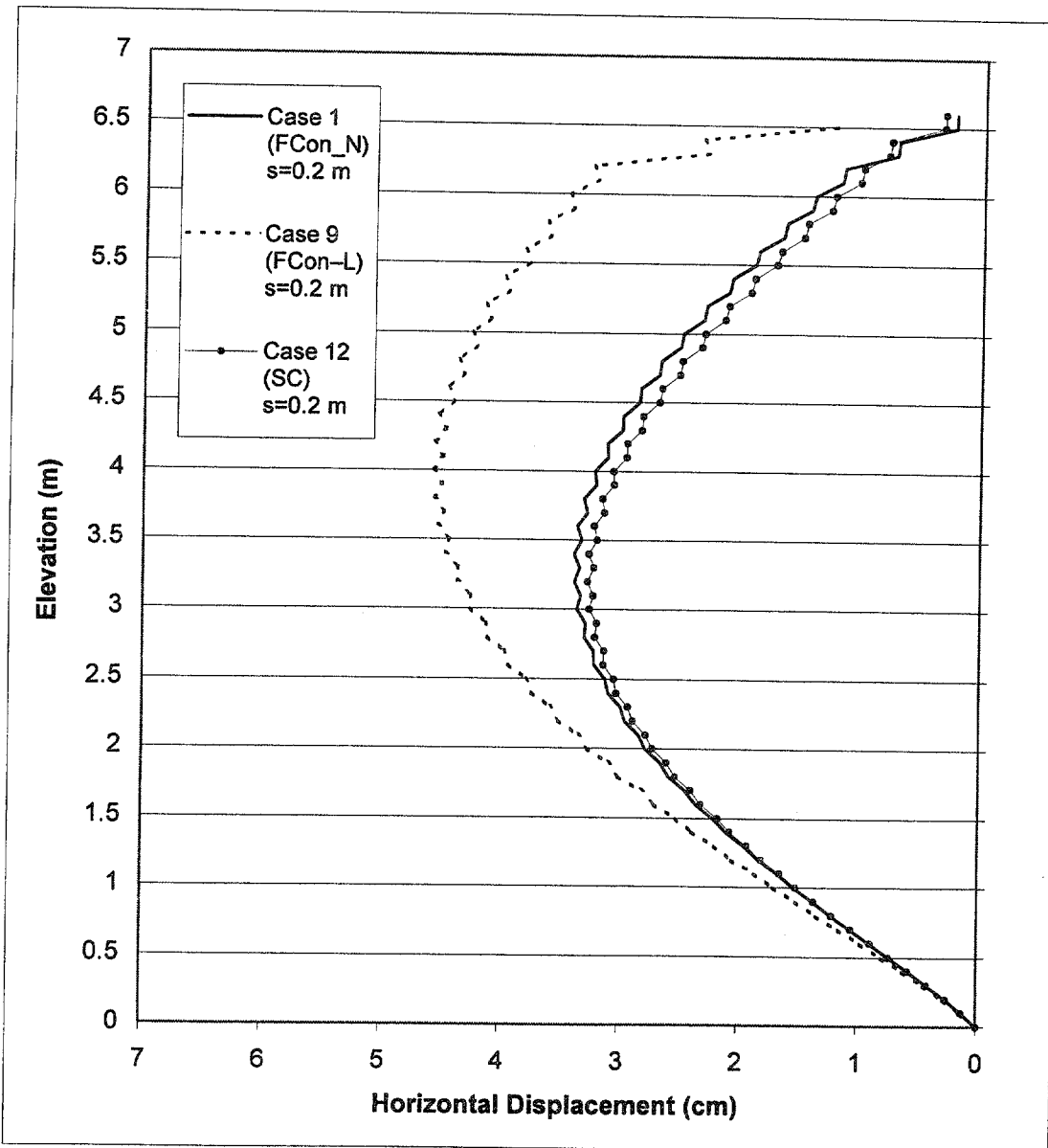


Figure 4.49 Effects of Connection Strength on Horizontal Displacements along Section A for Cases with Small Reinforcement Spacing ($s=0.2$ m).

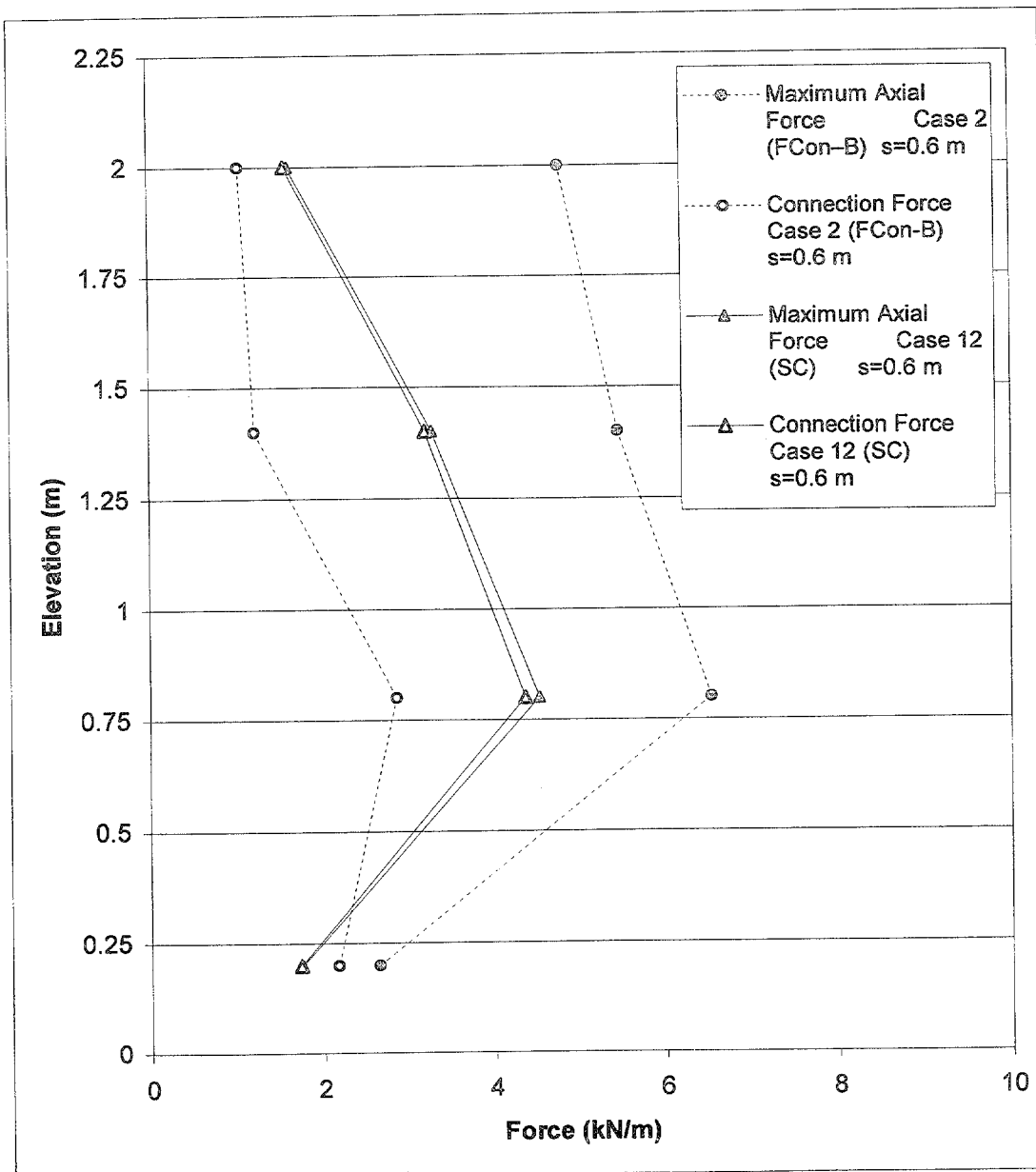


Figure 4.50 Effects of Connection Strength on Connection Force and Maximum Force in Reinforcement for Cases with Large Reinforcement Spacing ($s=0.6 \text{ m}$).

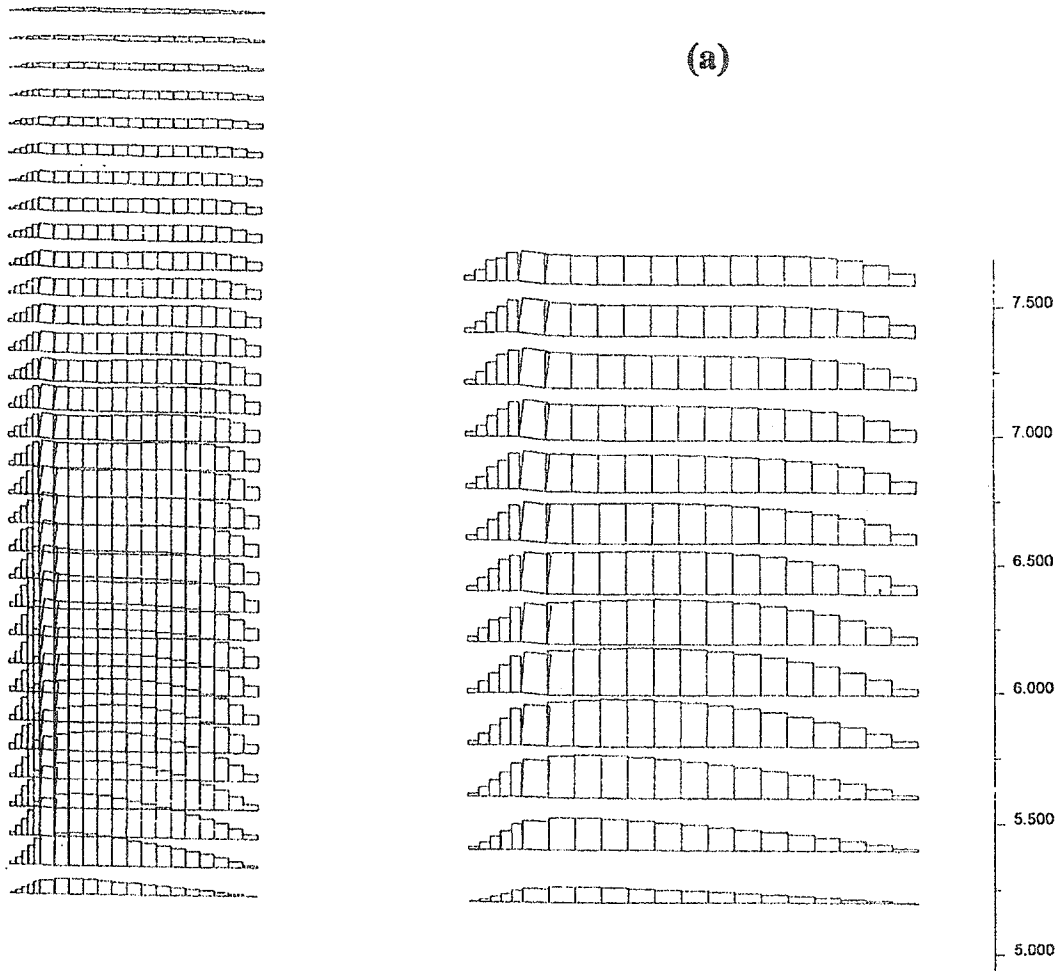


Figure 4.51 Axial Force Distribution in Reinforcement for Case 12 ($l=1.5$ m):
(a) $s=0.2$ m, $h=6.6$ m; (b) $s=0.6$ m, $h=2.6$ m.

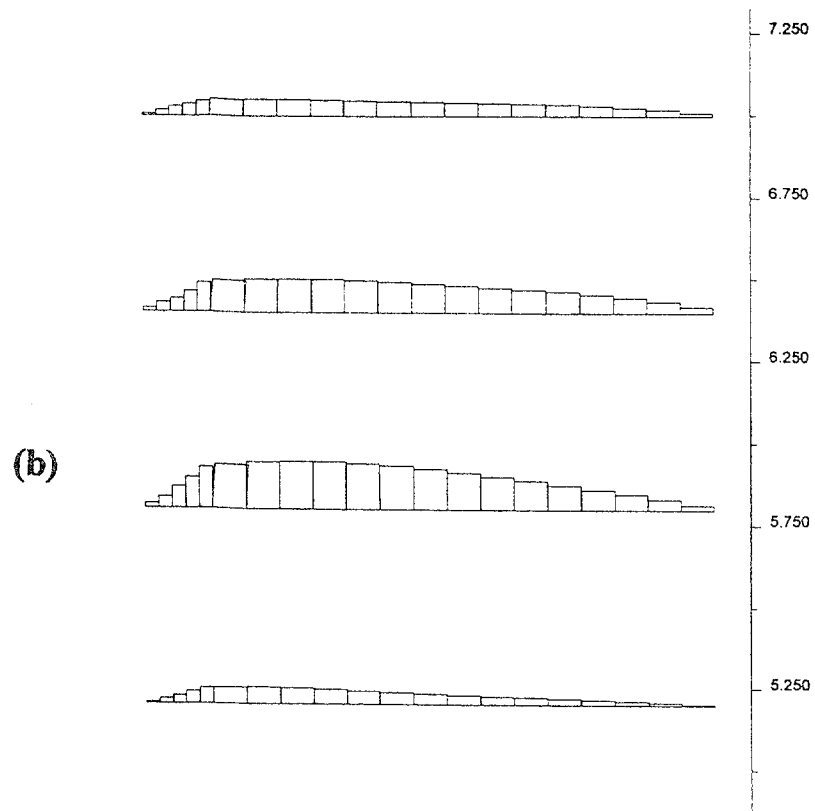


Figure 4.51 Axial Force Distribution in Reinforcement for Case 12 ($l=1.5$ m):
(a) $s=0.2$ m, $h=6.6$ m; (b) $s=0.6$ m, $h=2.6$ m, Continued.

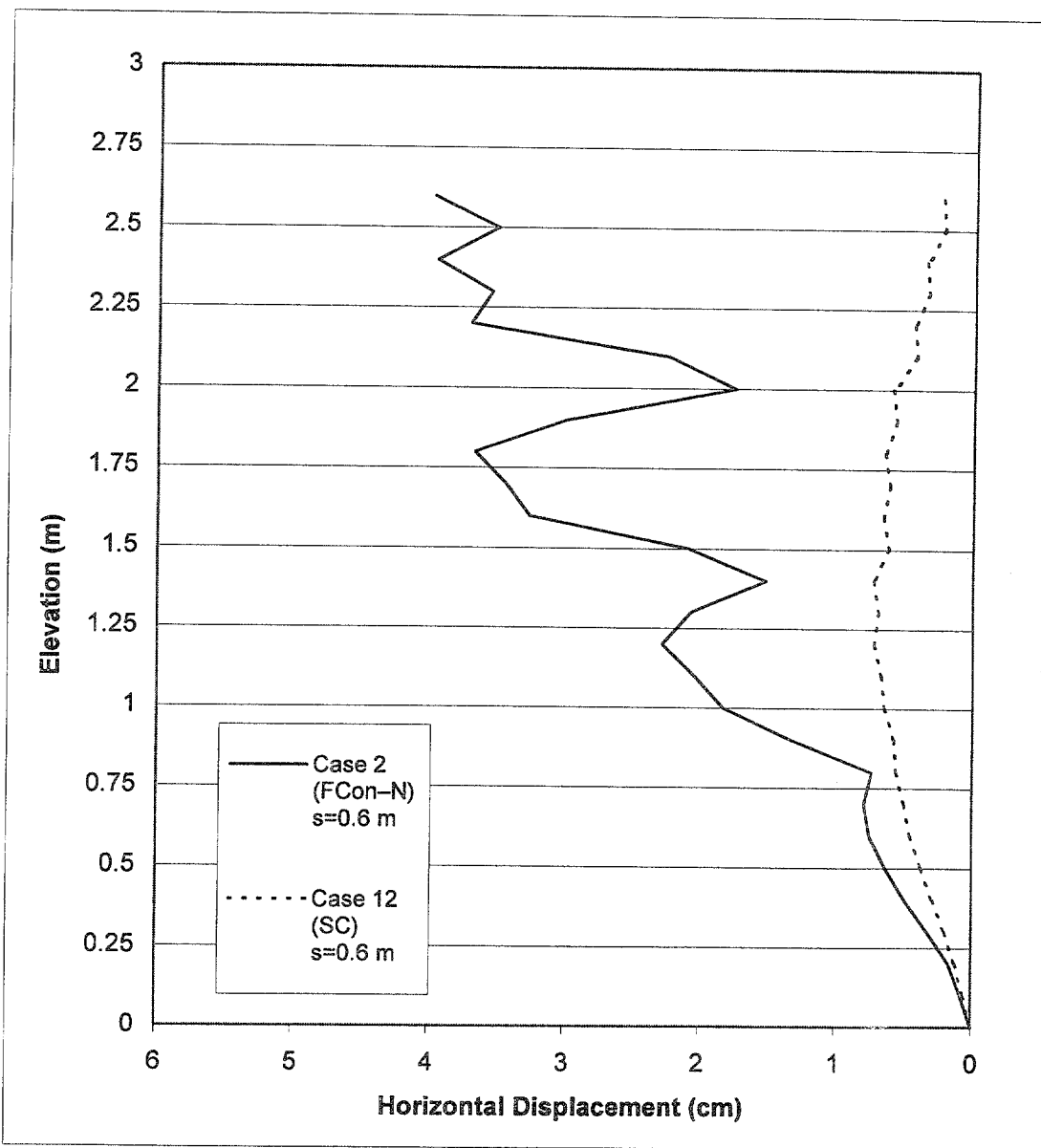


Figure 4.52 Effects of Connection Strength on Horizontal Displacements along Section A for Cases with Large Reinforcement Spacing ($s=0.6$ m).

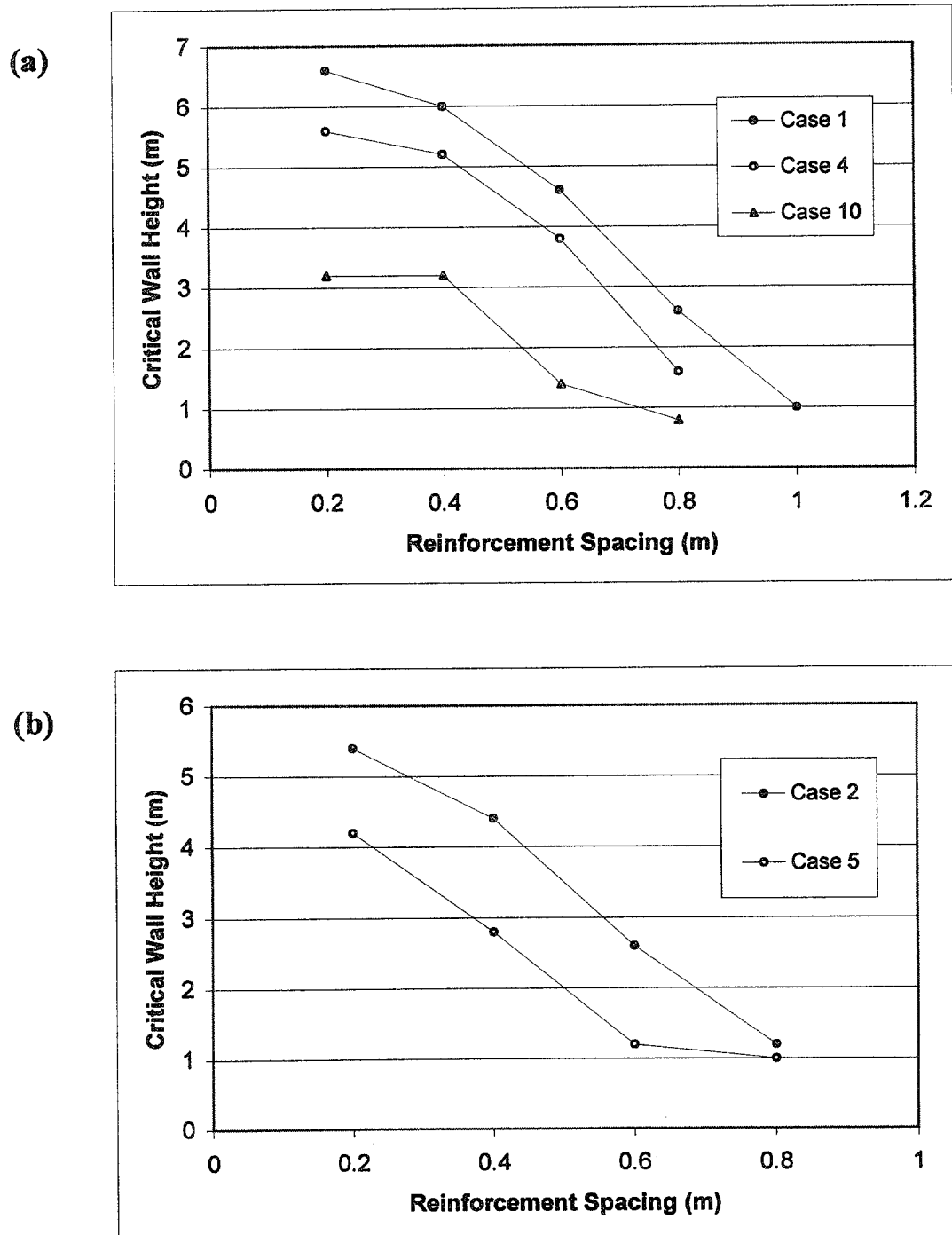


Figure 4.53 Effects of Foundation Strength on Critical Wall Height.

(c)

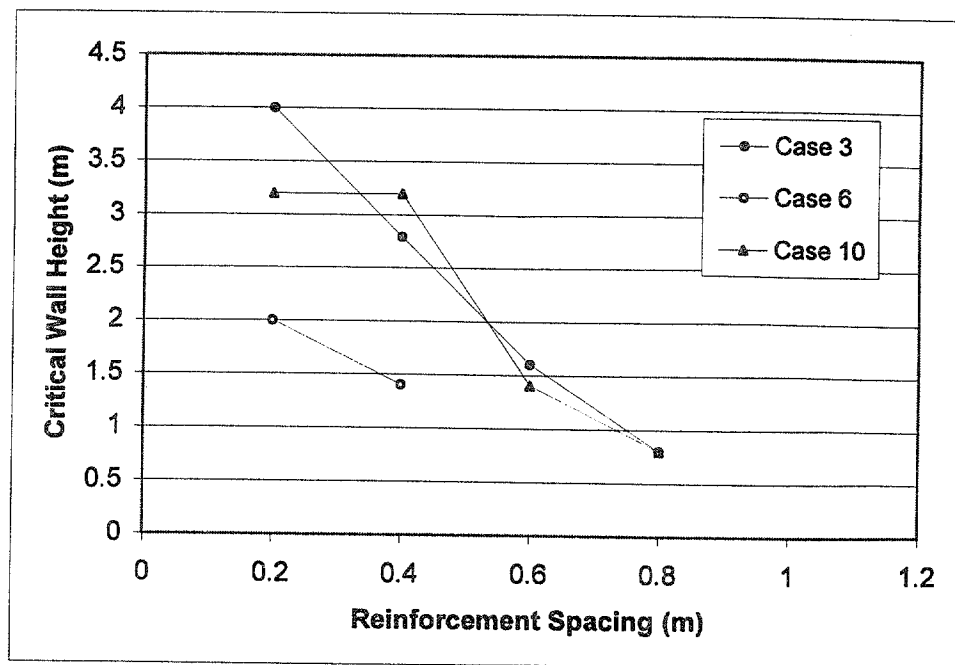
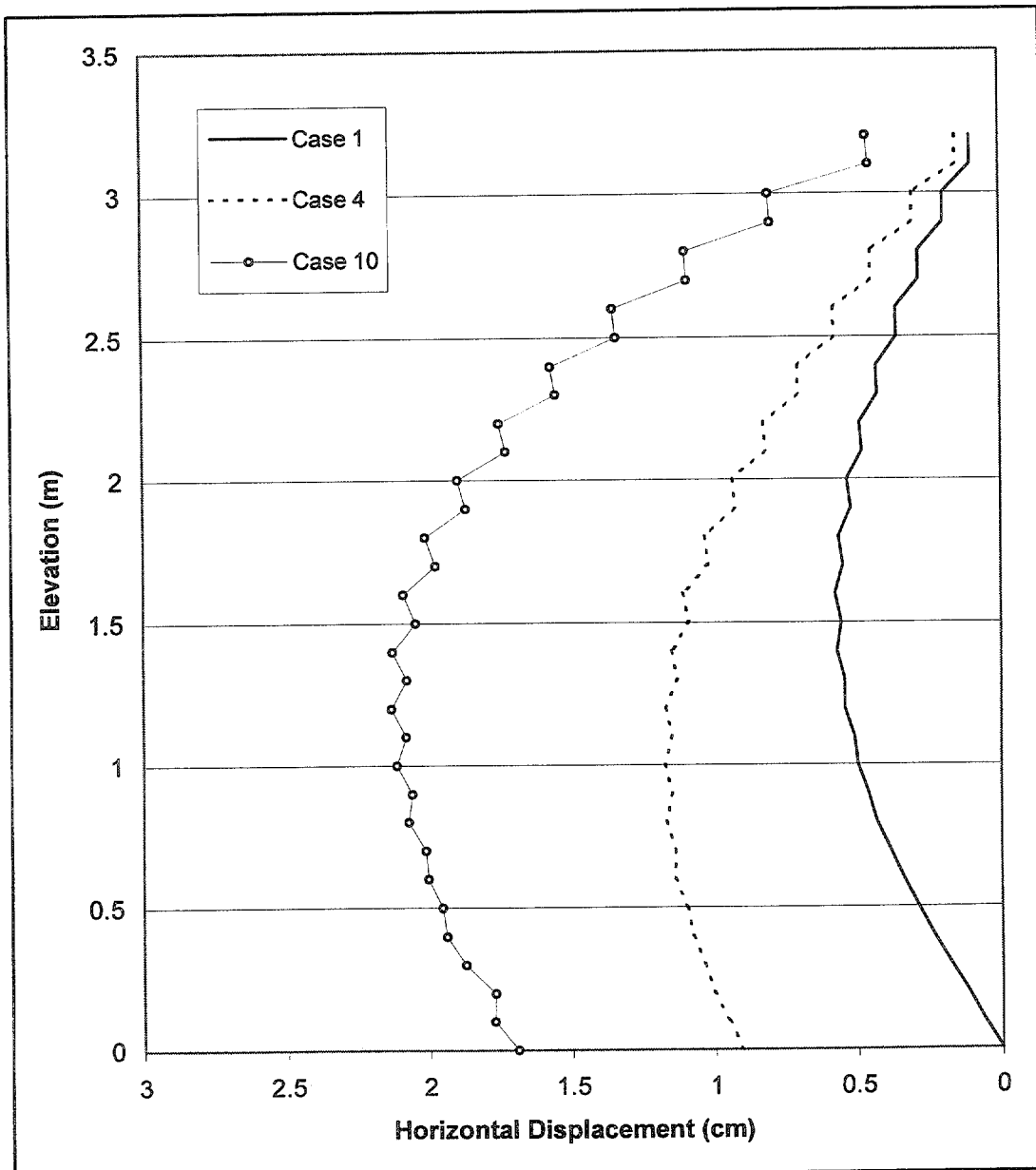
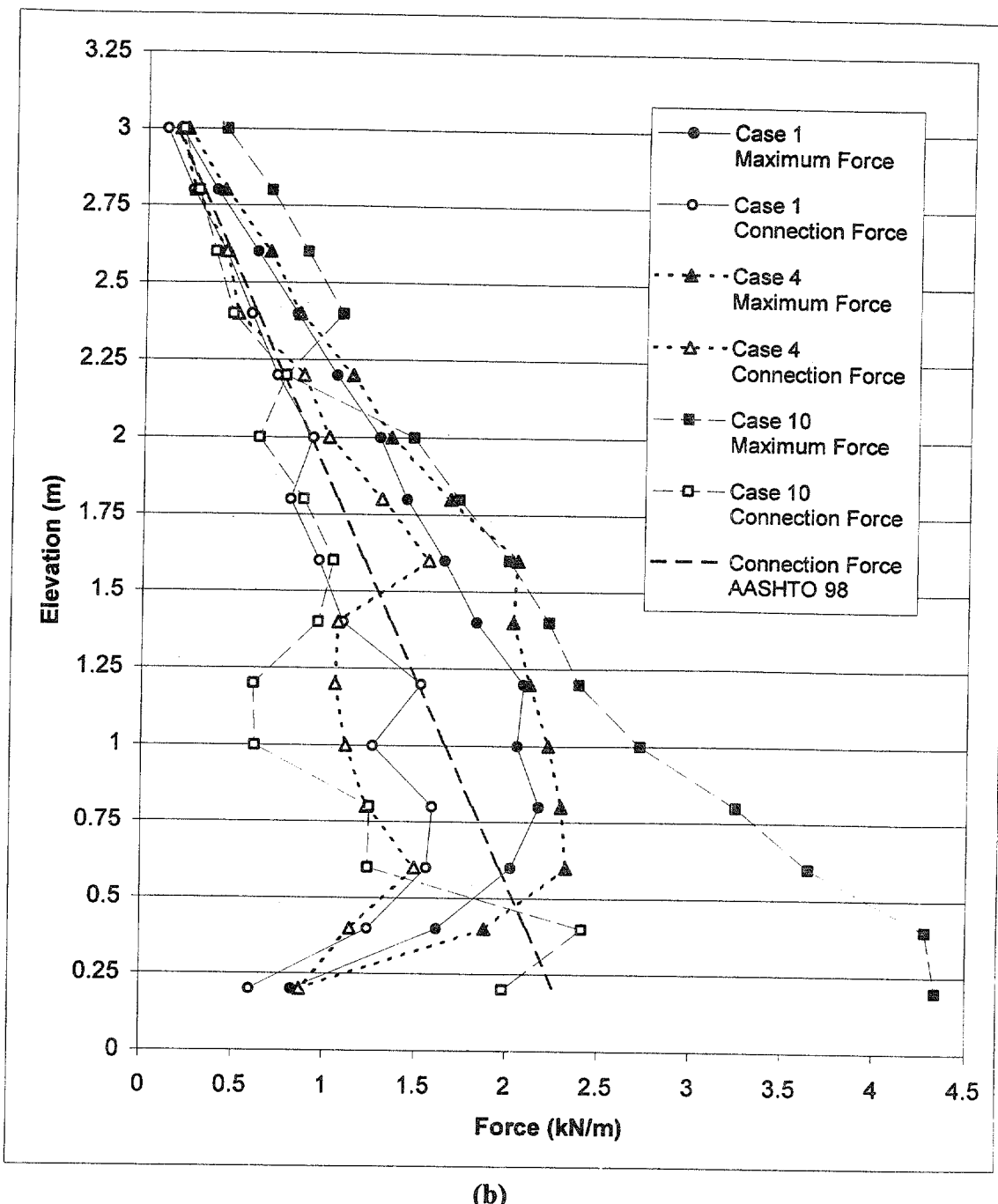


Figure 4.53 Effects of Foundation Strength on Critical Wall Height, Continued.



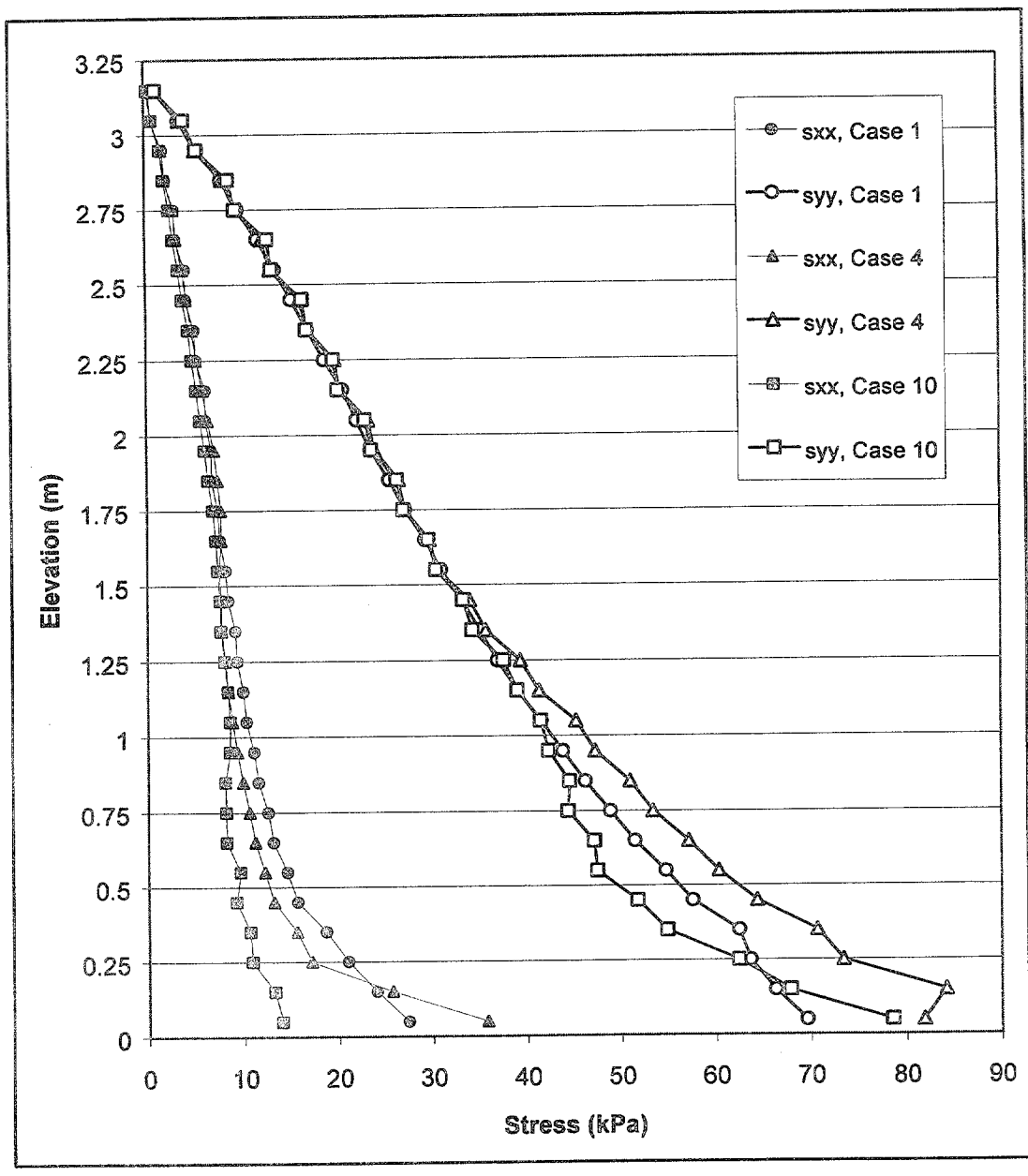
(a)

Figure 4.54 Effects of Foundation Strength for Cases 1, 4, and 10 ($s=0.2$ m, $l=1.5$ m $h=3.2$ m) on: (a) Horizontal Displacements along Section A; (b) Connection Force and Maximum Axial Force in Reinforcement; (c) Stresses along Section A.



(b)

Figure 4.54 Effects of Foundation Strength for Cases 1, 4, and 10 ($s=0.2$ m, $l=1.5$ m $h=3.2$ m) on: (a) Horizontal Displacements along Section A; (b) Connection Force and Maximum Axial Force in Reinforcement; (c) Stresses along Section A, Continued.



(c)

Figure 4.54 Effects of Foundation Strength for Cases 1, 4, and 10 ($s=0.2$ m, $t=1.5$ m $h=3.2$ m) on: (a) Horizontal Displacements along Section A; (b) Connection Force and Maximum Axial Force in Reinforcement; (c) Stresses along Section A, Continued.

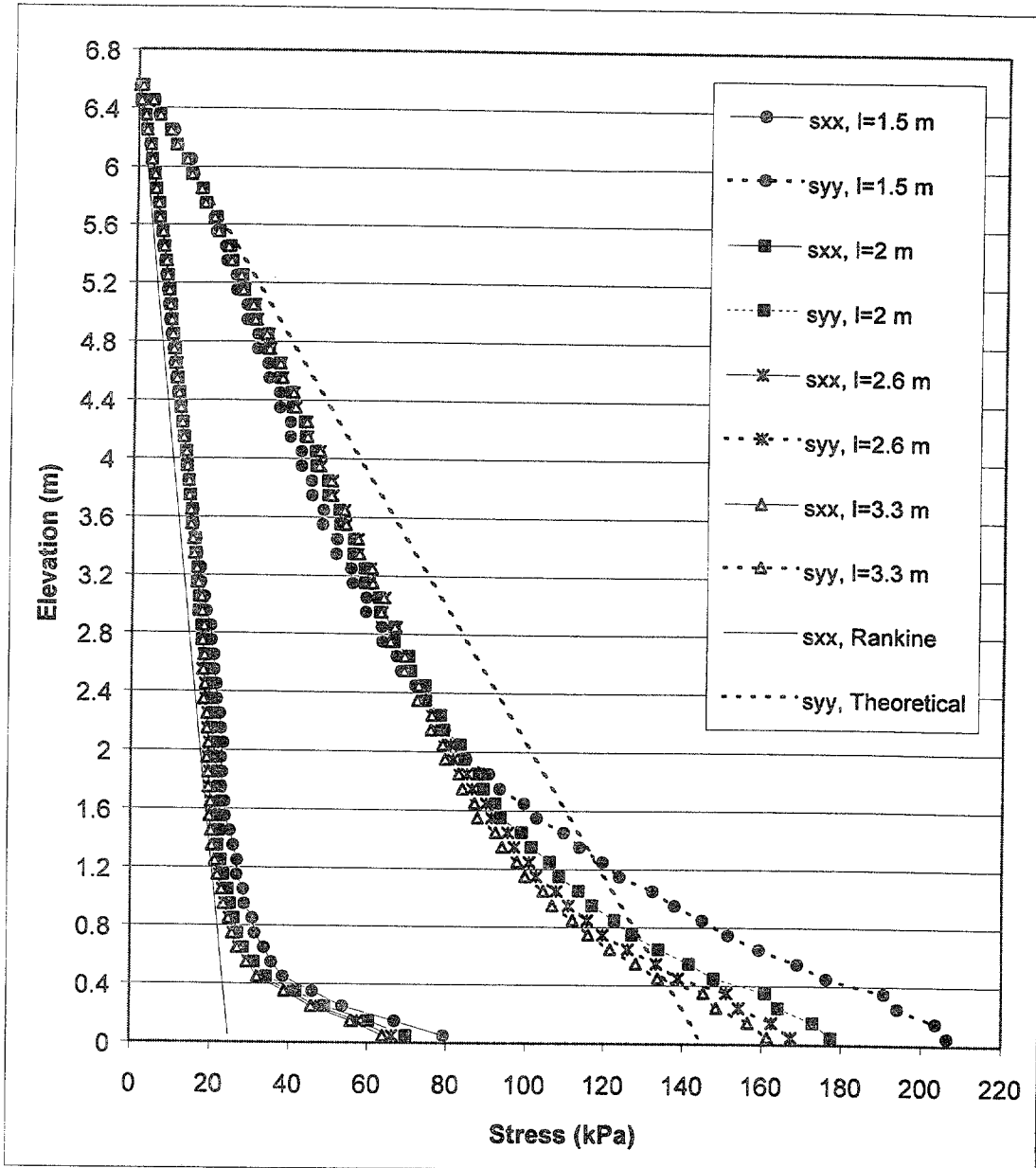


Figure 4.55 Stress Distributions along Section A for Critical and Stable States of Case 1 ($s=0.2 \text{ m}$, $h=6.6 \text{ m}$, $l/h=0.23-0.5$).

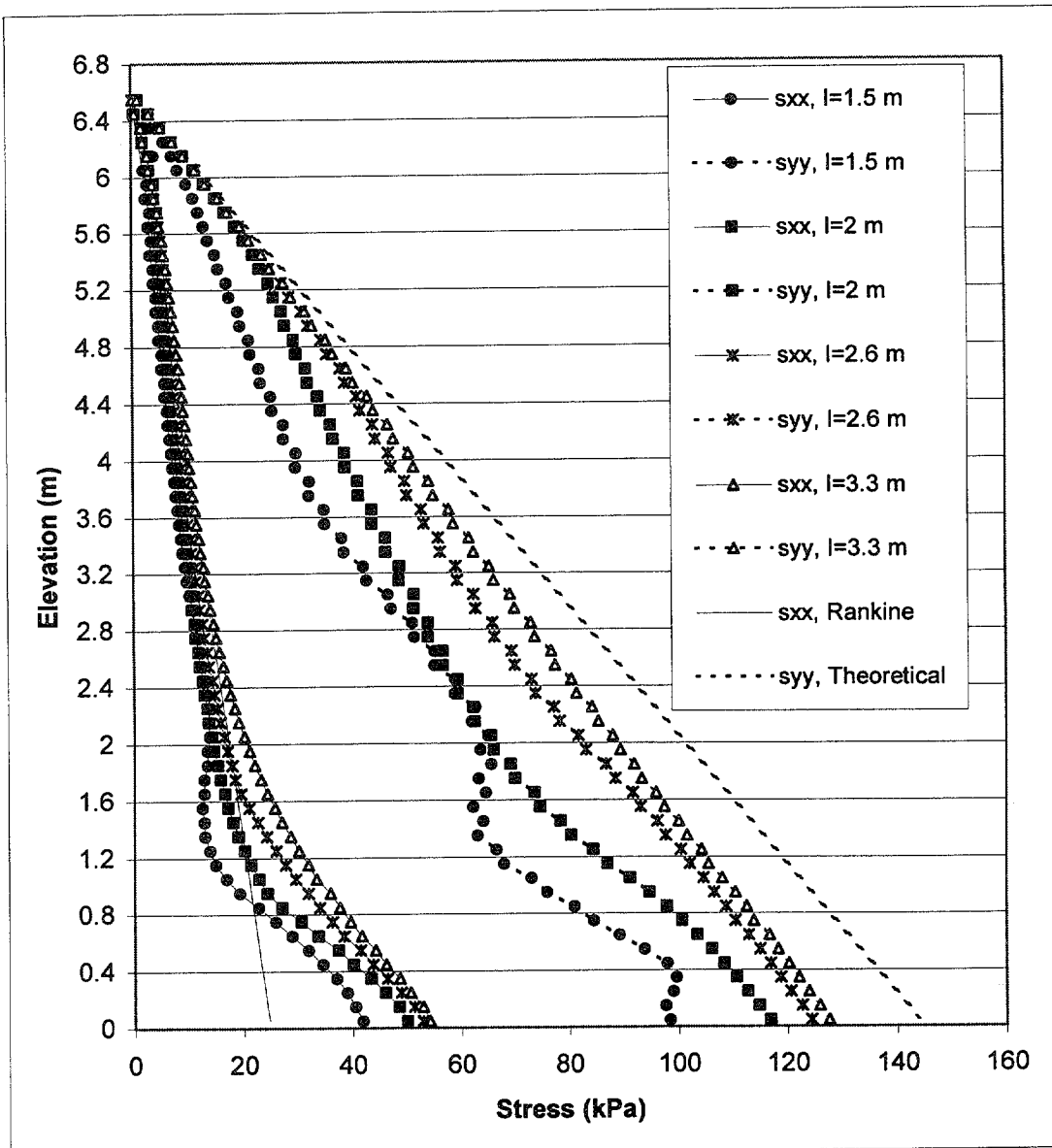


Figure 4.56 Stress Distributions along Section C for Critical and Stable States of Case 1 ($s=0.2$ m, $h=6.6$ m, $l/h=0.23-0.5$).

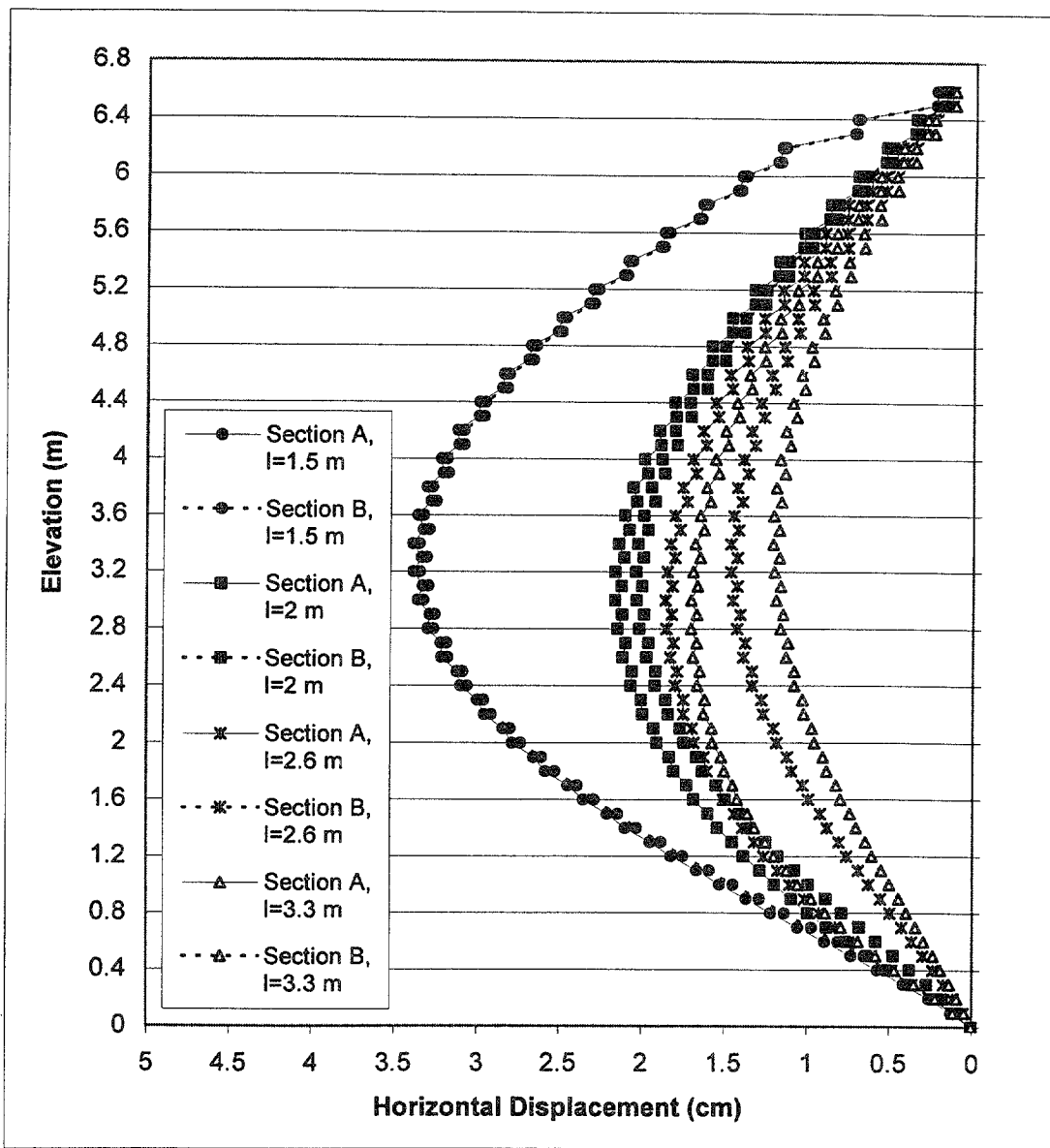


Figure 4.57 Horizontal Displacements along Sections A and B for Critical and Stable States of Case 1 ($s=0.2$ m, $h=6.6$ m, $l/h=0.23-0.5$).

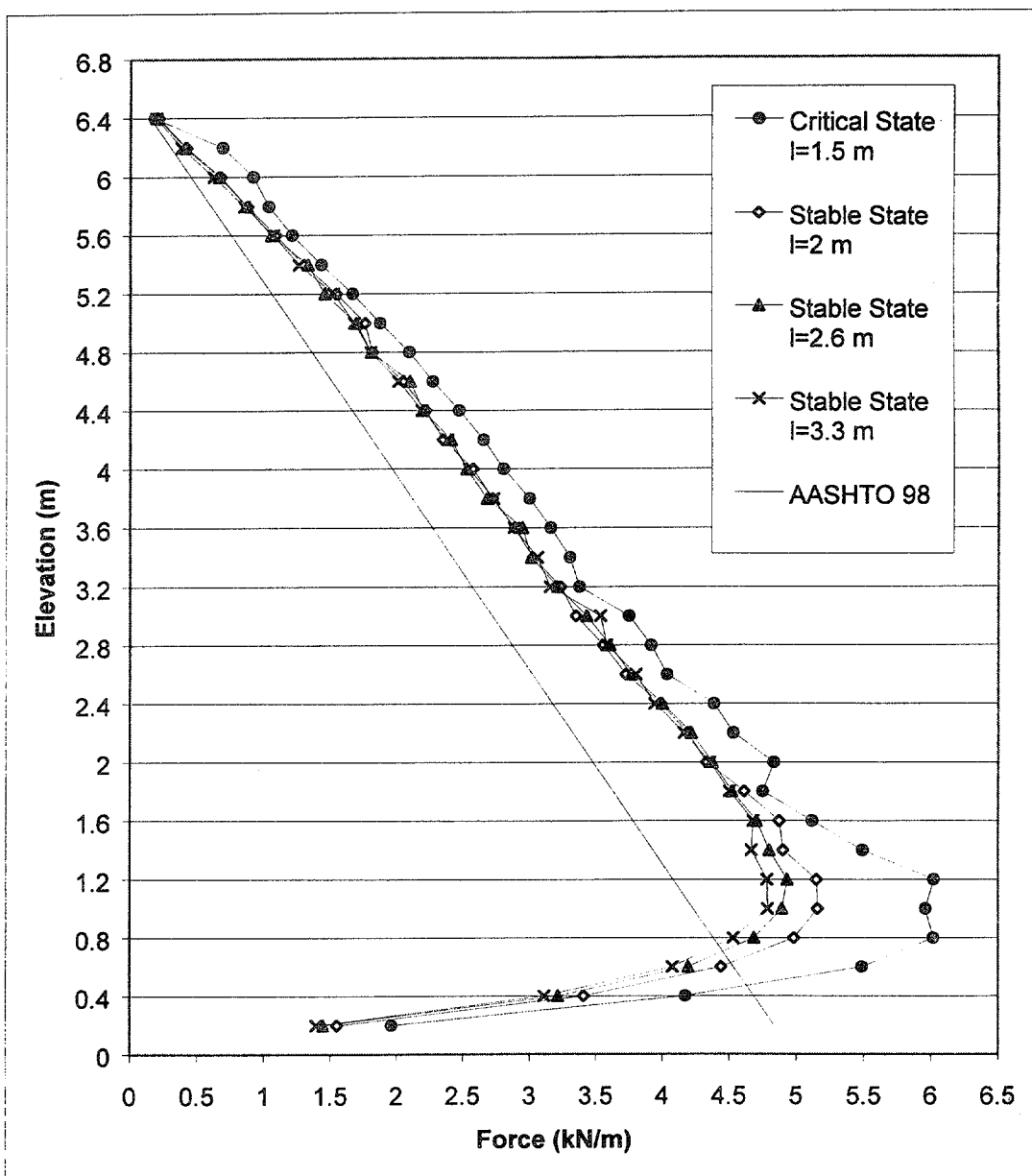


Figure 4.58 Maximum Axial Force in Reinforcement for Critical and Stable States of Case 1 ($s=0.2$ m, $h=6.6$ m, $l/h=0.23-0.5$).

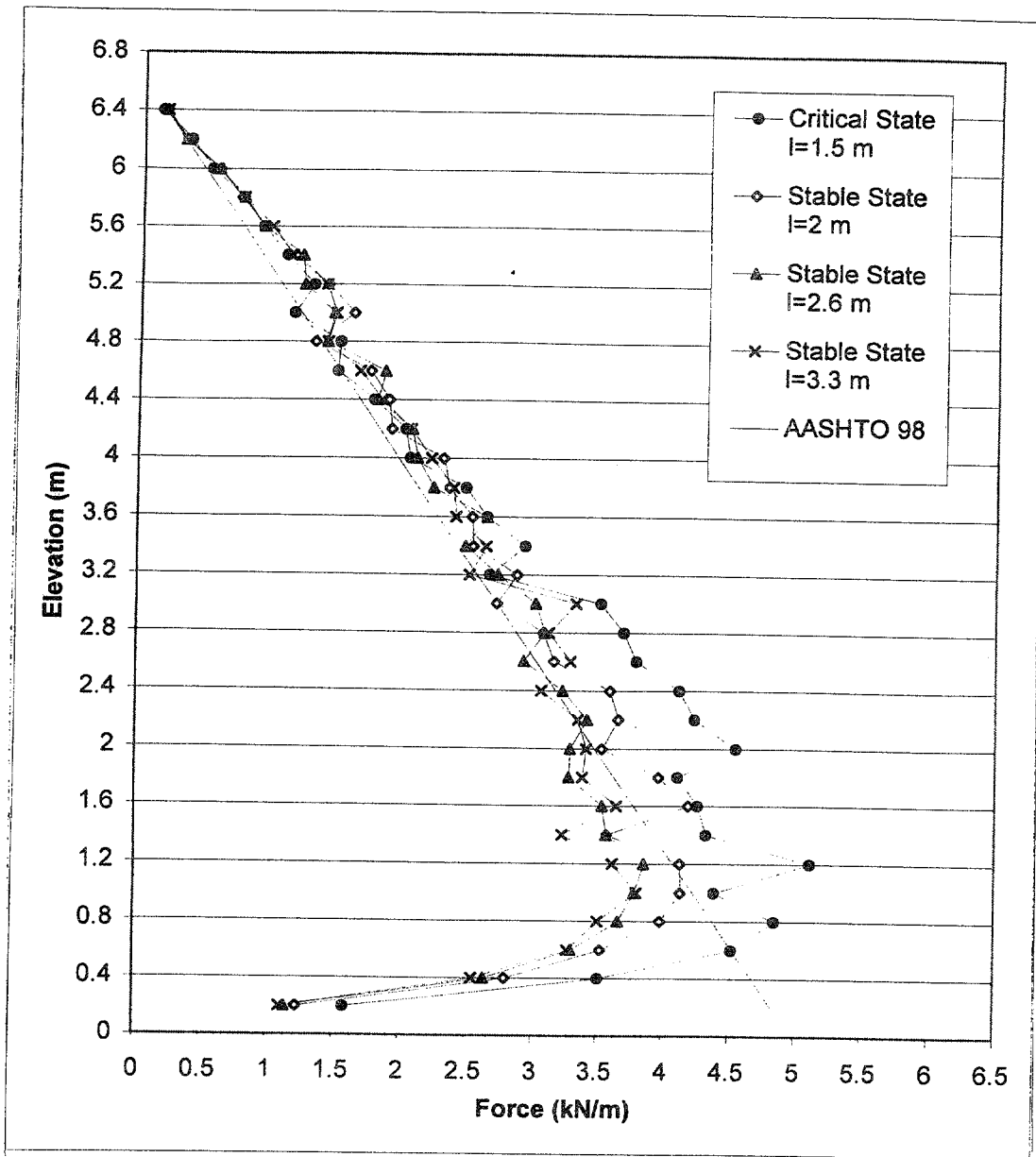


Figure 4.59 Connection Force for Critical and Stable States of Case 1 ($s=0.2$ m, $h=6.6$ m, $I/h=0.23-0.5$).

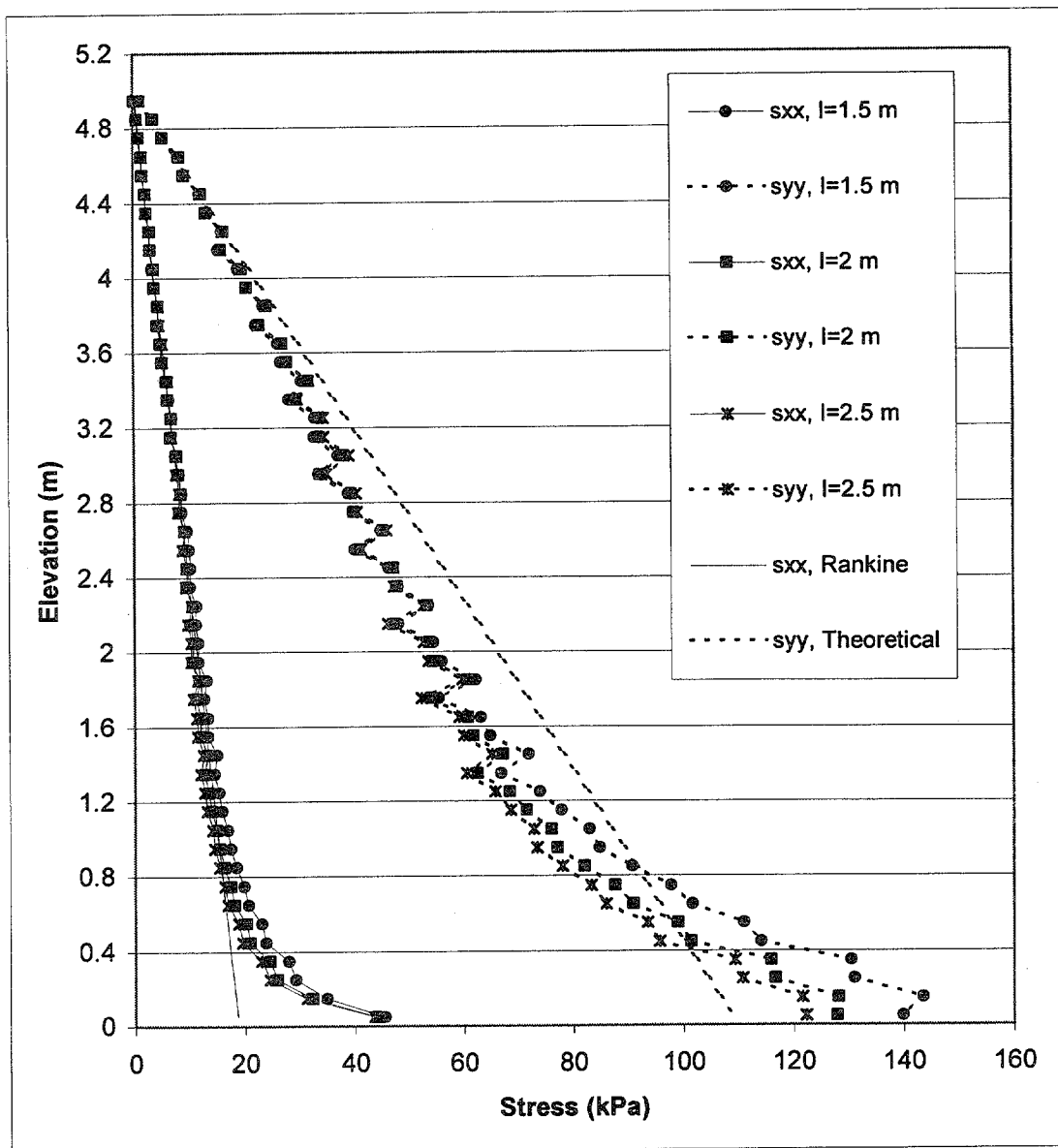


Figure 4.60 Stress Distributions along Section A for Critical and Stable States of Case 8-1 ($s=0.4$ m, $h=5.0$ m, $l/h=0.3-0.5$).

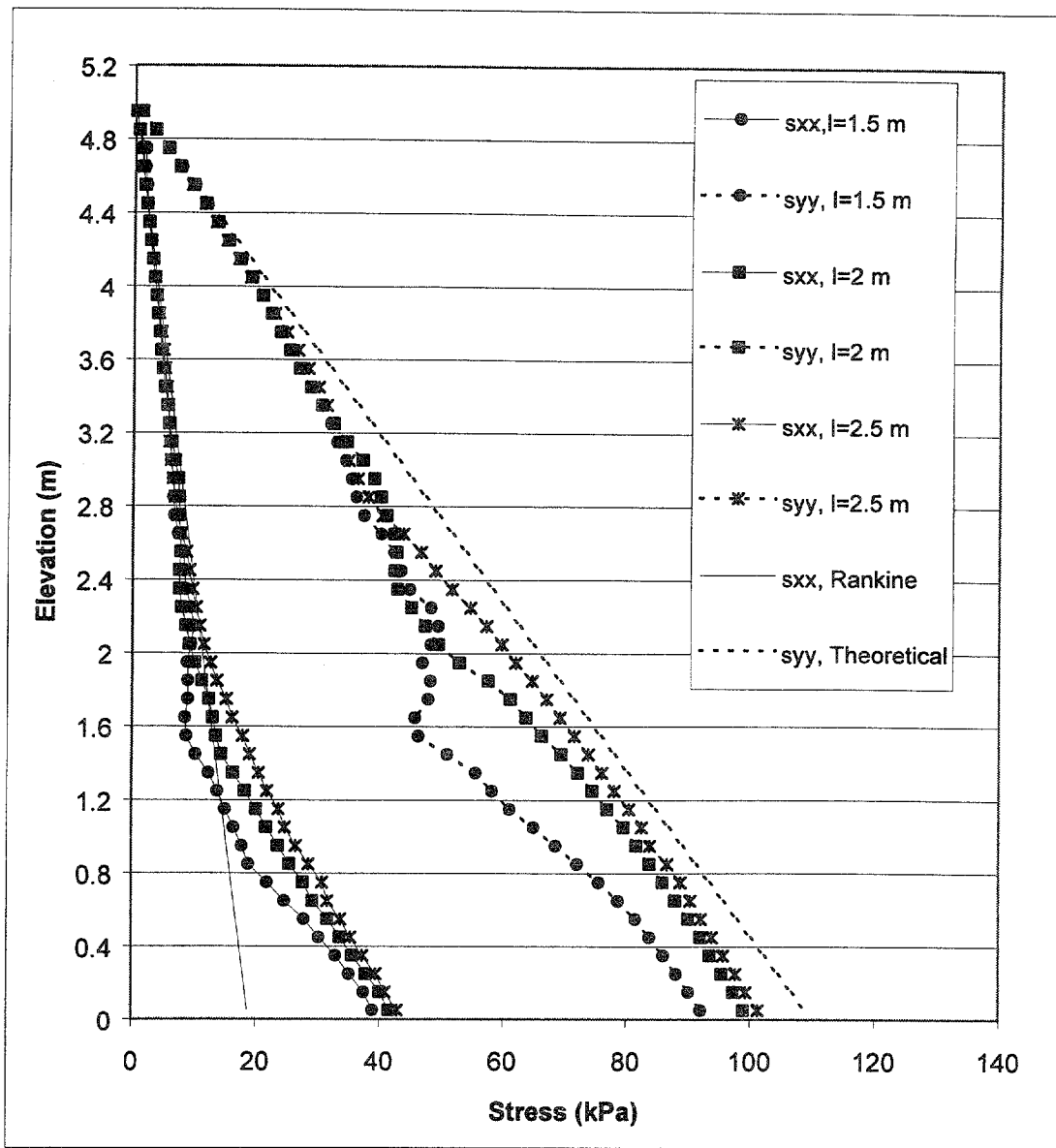


Figure 4.61 Stress Distributions along Section C for Critical and Stable States of Case 8-1 ($s=0.4\text{ m}$, $h=5.0\text{ m}$, $l/h=0.3-0.5$).

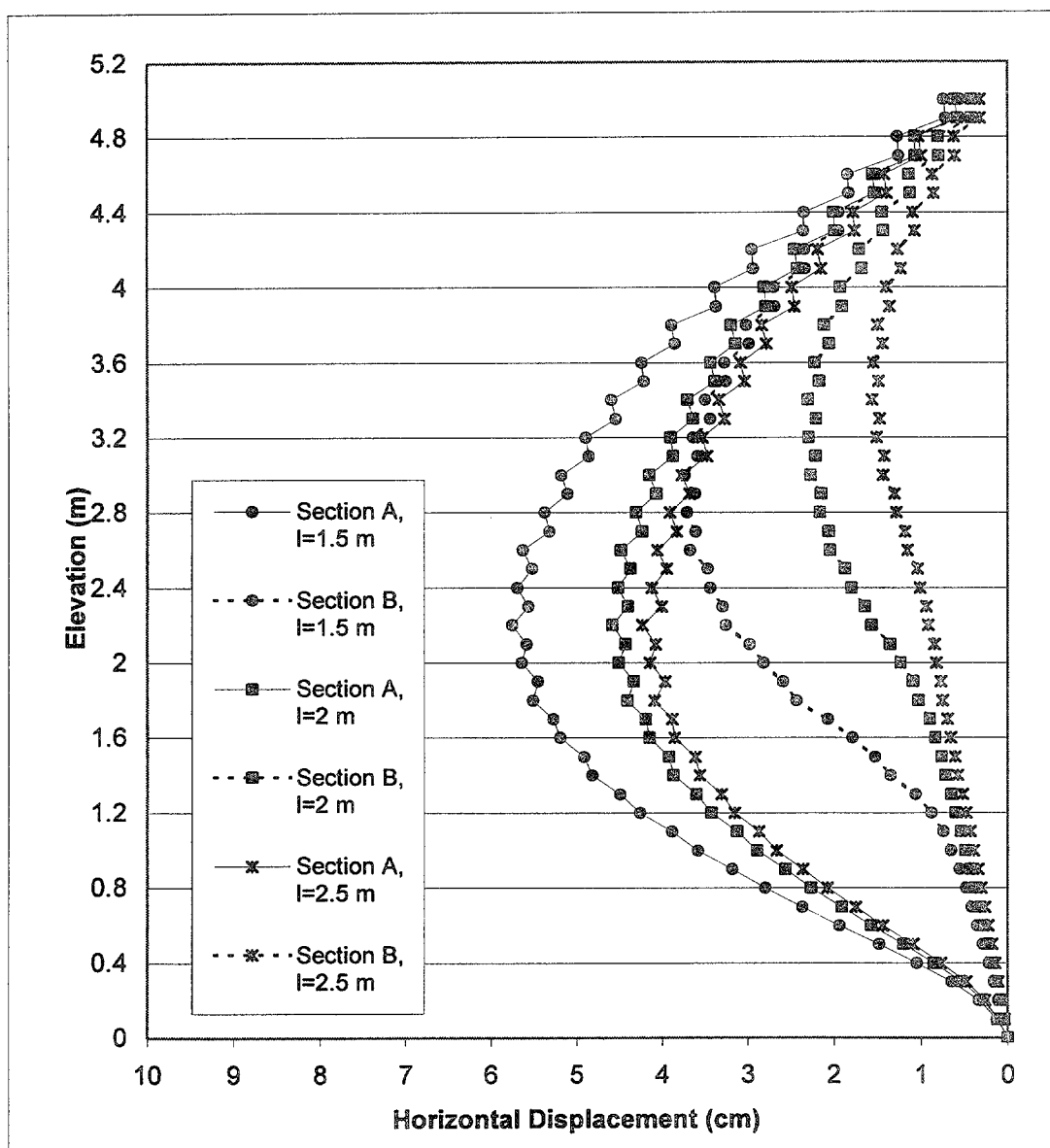


Figure 4.62 Horizontal Displacements along Sections A and B for Critical and Stable States of Case 8–1 ($s=0.4\text{ m}$, $h=5.0\text{ m}$, $I/h=0.3\text{--}0.5$).

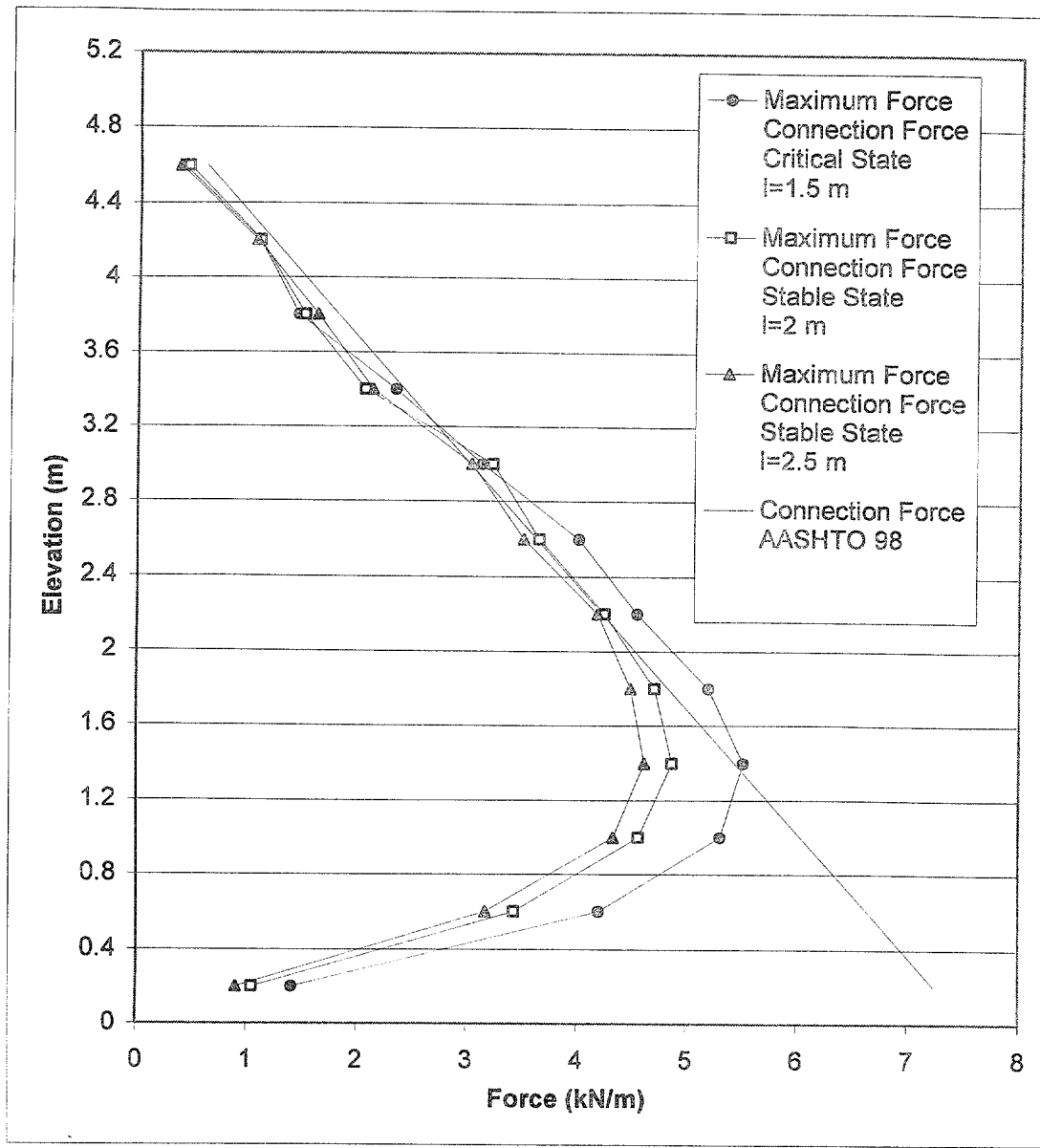


Figure 4.63 Connection Force and Maximum Axial Force in Reinforcement for Critical and Stable States of Case 8-1 ($s=0.4\text{ m}$, $h=5.0\text{ m}$, $l/h=0.3-0.5$).

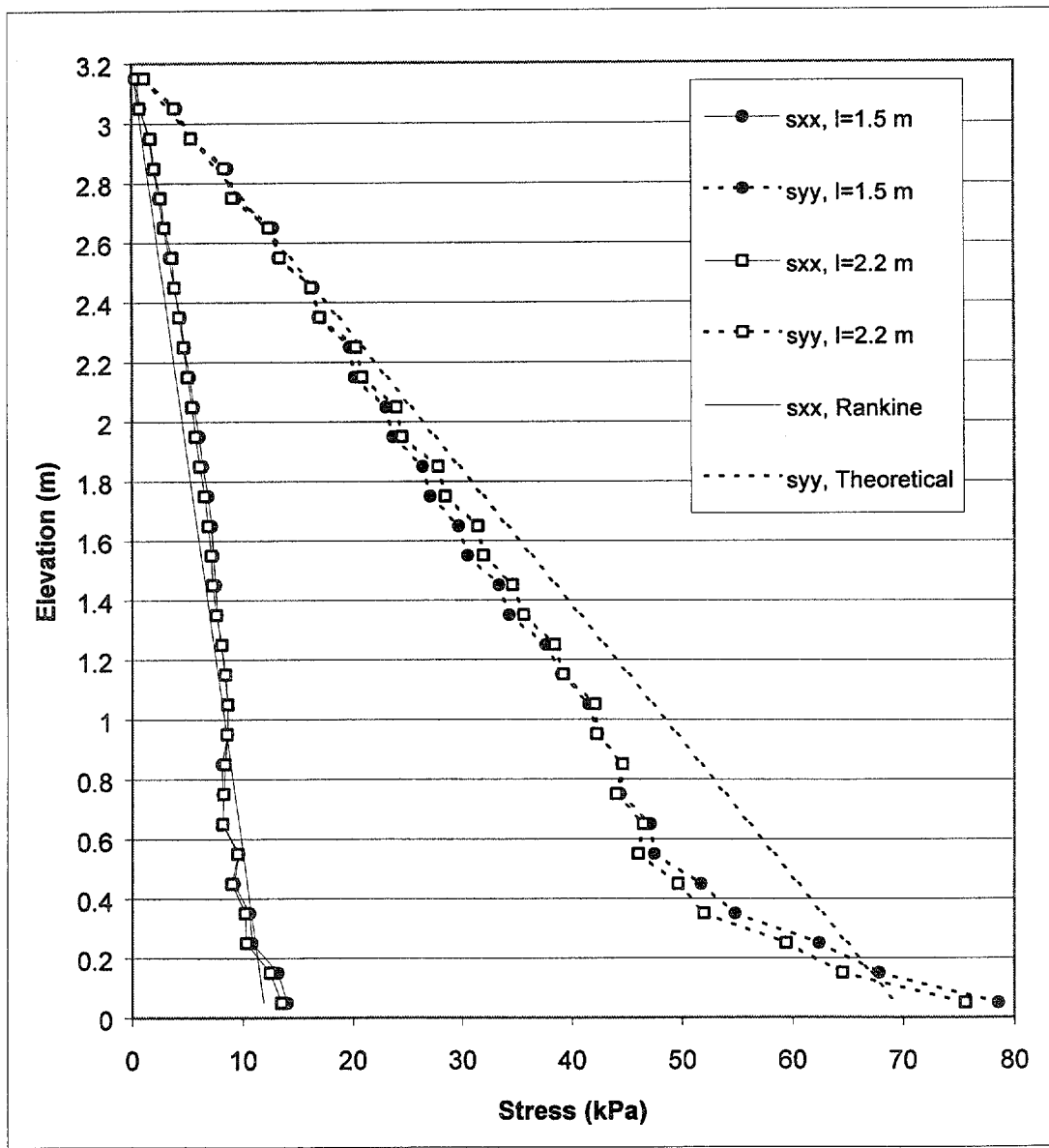


Figure 4.64 Stress Distributions along Section A for Critical and Stable States of Case 10 ($s=0.2\text{ m}$, $h=3.2\text{ m}$, $l/h=0.47-0.7$).

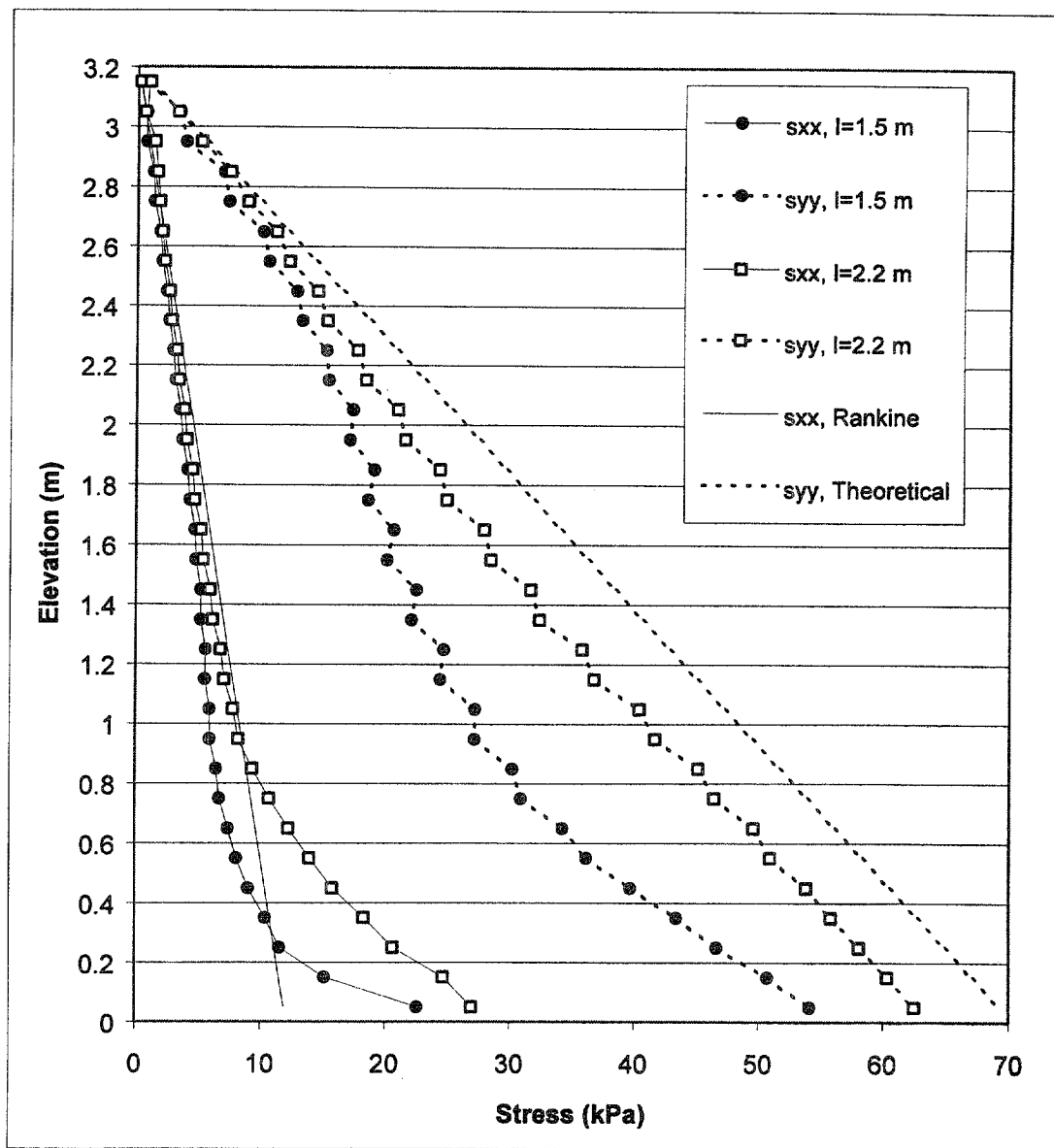


Figure 4.65 Stress Distributions along Section C for Critical and Stable States of Case 10 ($s=0.2$ m, $h=3.2$ m, $l/h=0.47-0.7$).

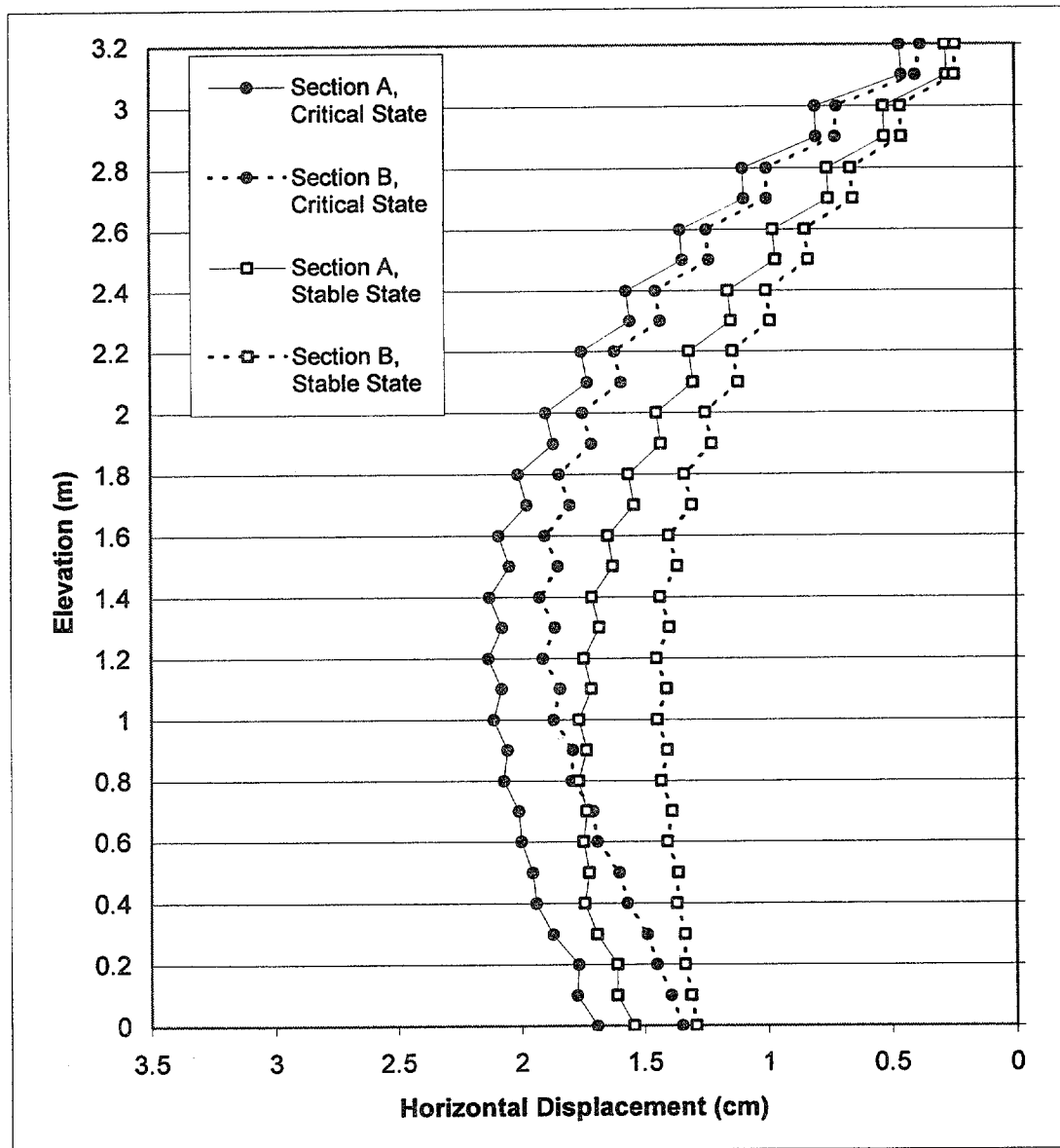


Figure 4.66 Horizontal Displacements along Sections A and B for Critical and Stable States of Case 10 ($s=0.2$ m, $h=3.2$ m, $l/h=0.47-0.7$).

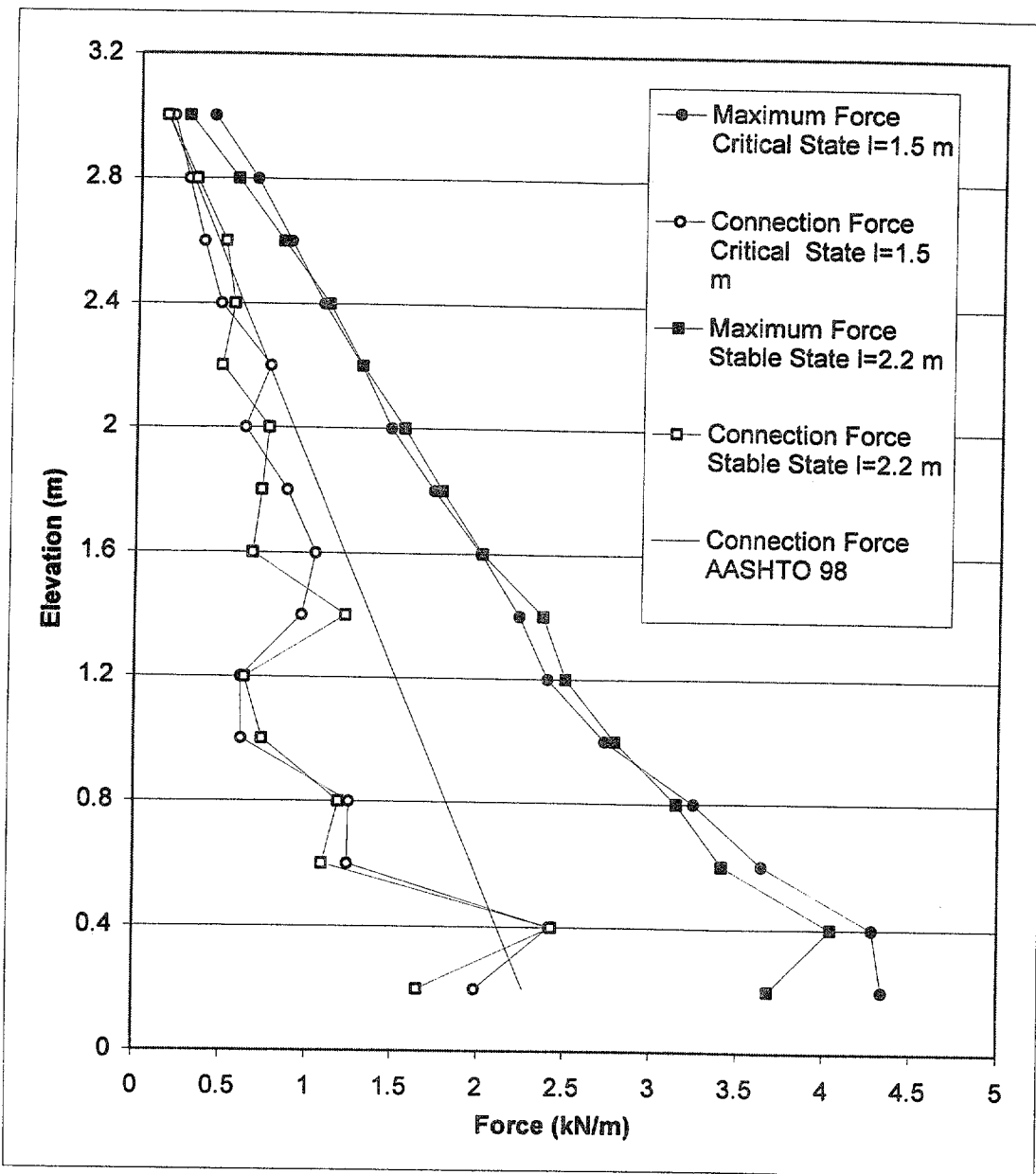


Figure 4.67 Connection Force and Maximum Axial Force in Reinforcement for Critical and Stable States of Case 10 ($s=0.2$ m, $h=3.2$ m, $l/h=0.47-0.7$).

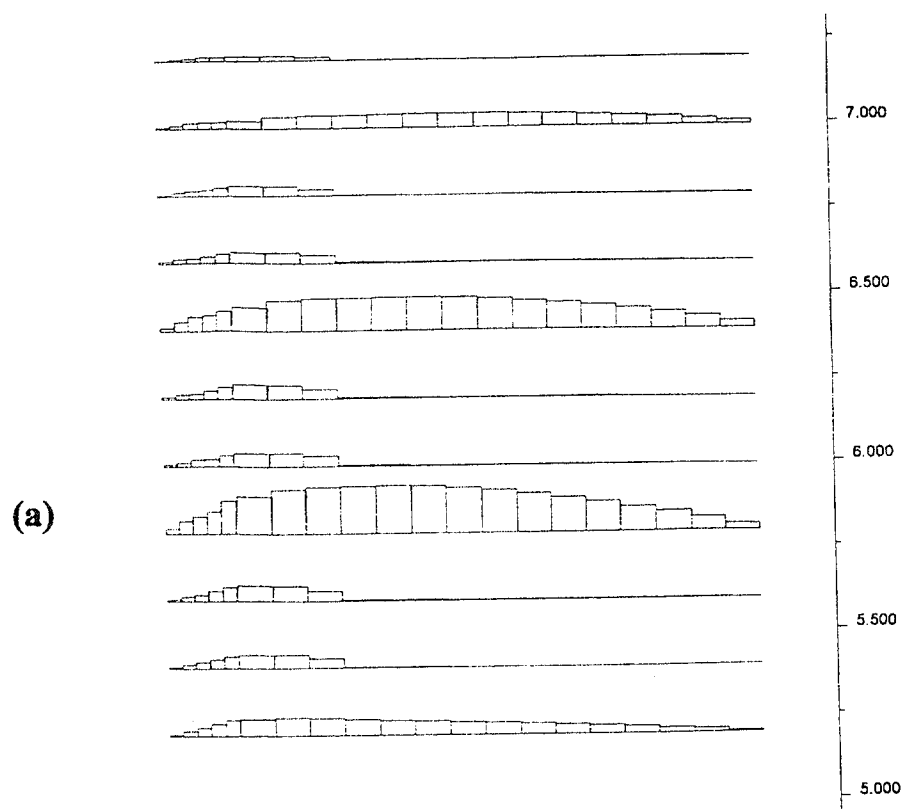


Figure 4.68 Effects of Secondary Reinforcement: Axial Force Distribution in Reinforcement for Case 7 ($s=0.6/0.2$ m), (a) $h=2.6$ m; (b) $h=5.0$ m.

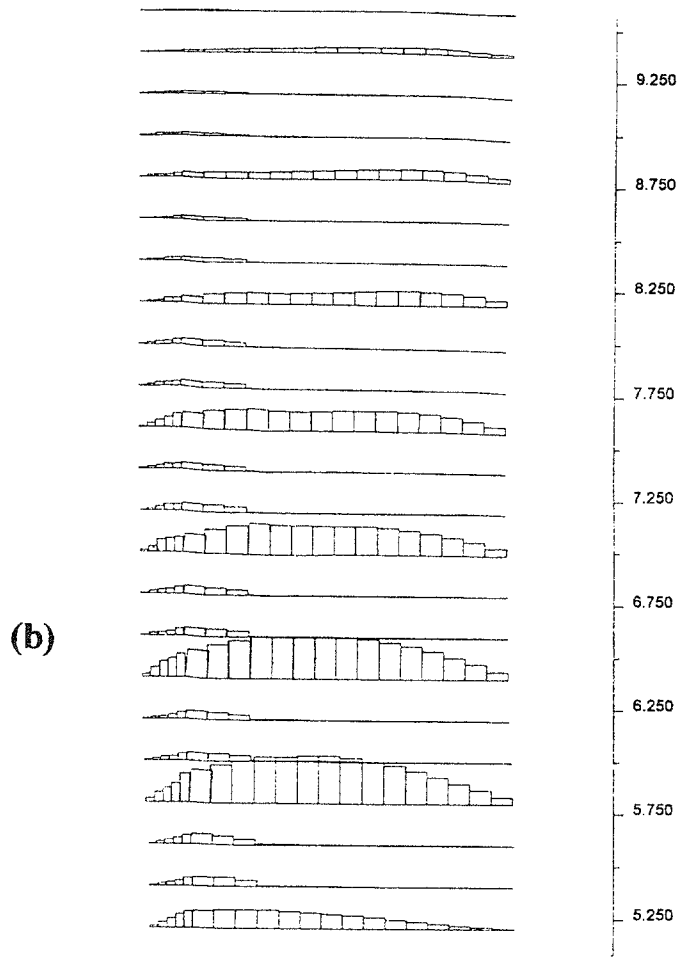


Figure 4.68 Effects of Secondary Reinforcement: Axial Force Distribution in Reinforcement for Case 7 ($s=0.6/0.2$ m), (a) $h=2.6$ m; (b) $h=5.0$ m, Continued.

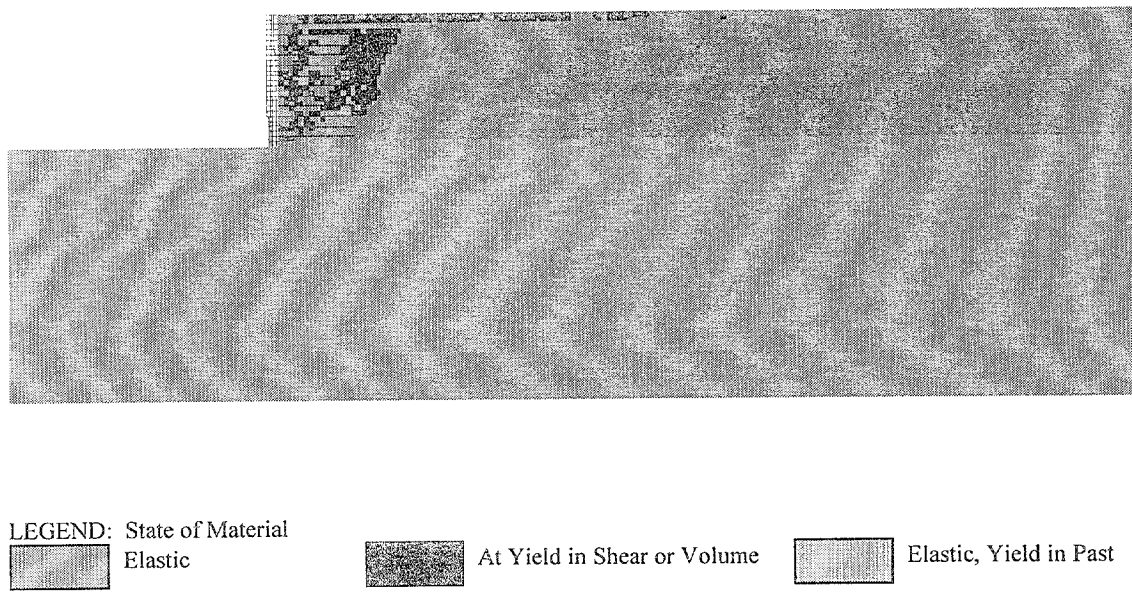


Figure 4.69 Effects of Secondary Reinforcement: State of Soil for Case 7
 $(h=2.6 \text{ m}, s=0.6/0.2 \text{ m})$.

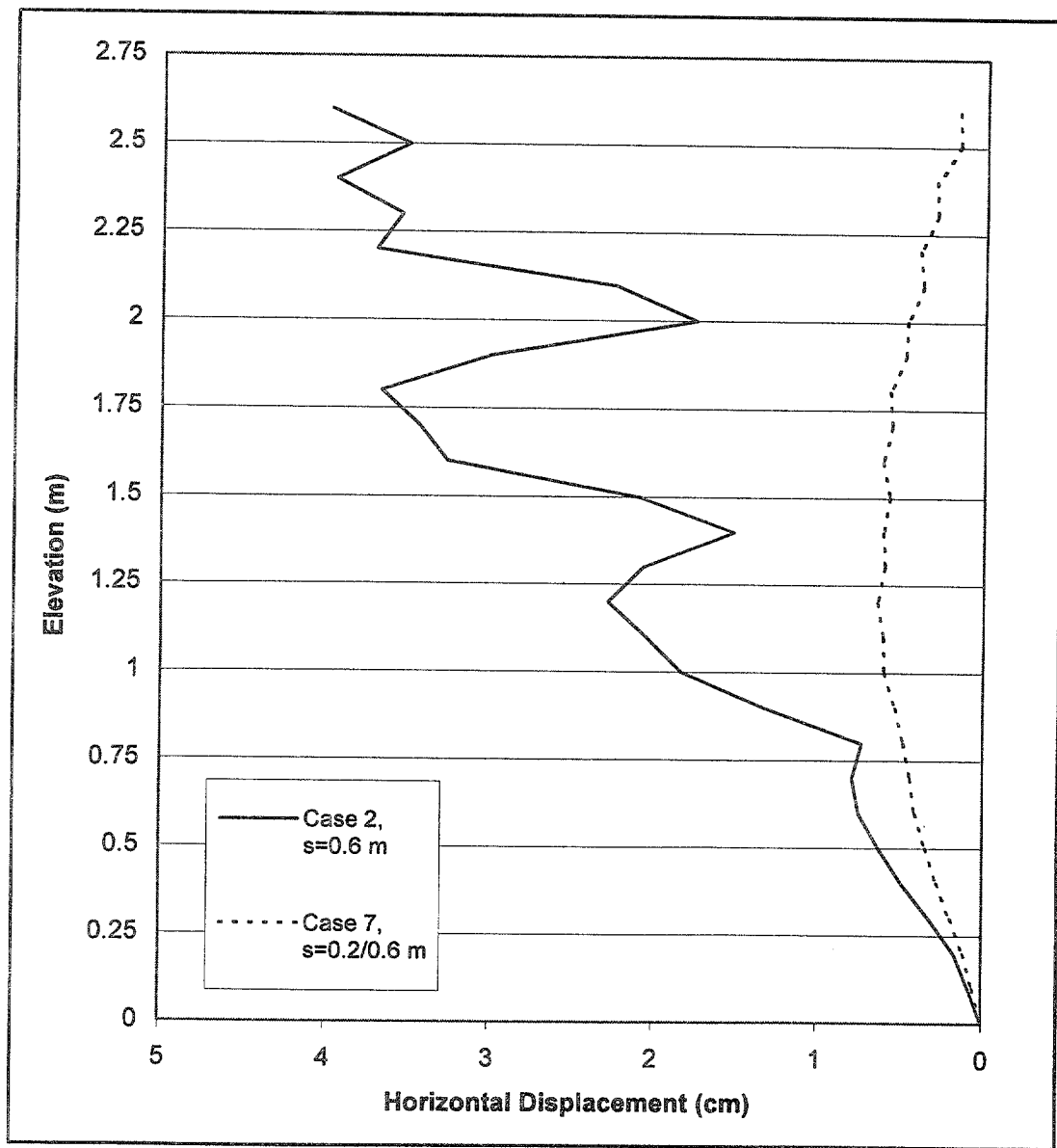


Figure 4.70 Effects of Secondary Reinforcement: Horizontal Displacements along Section A for Cases 2 and 7 ($h=2.6\text{ m}$).

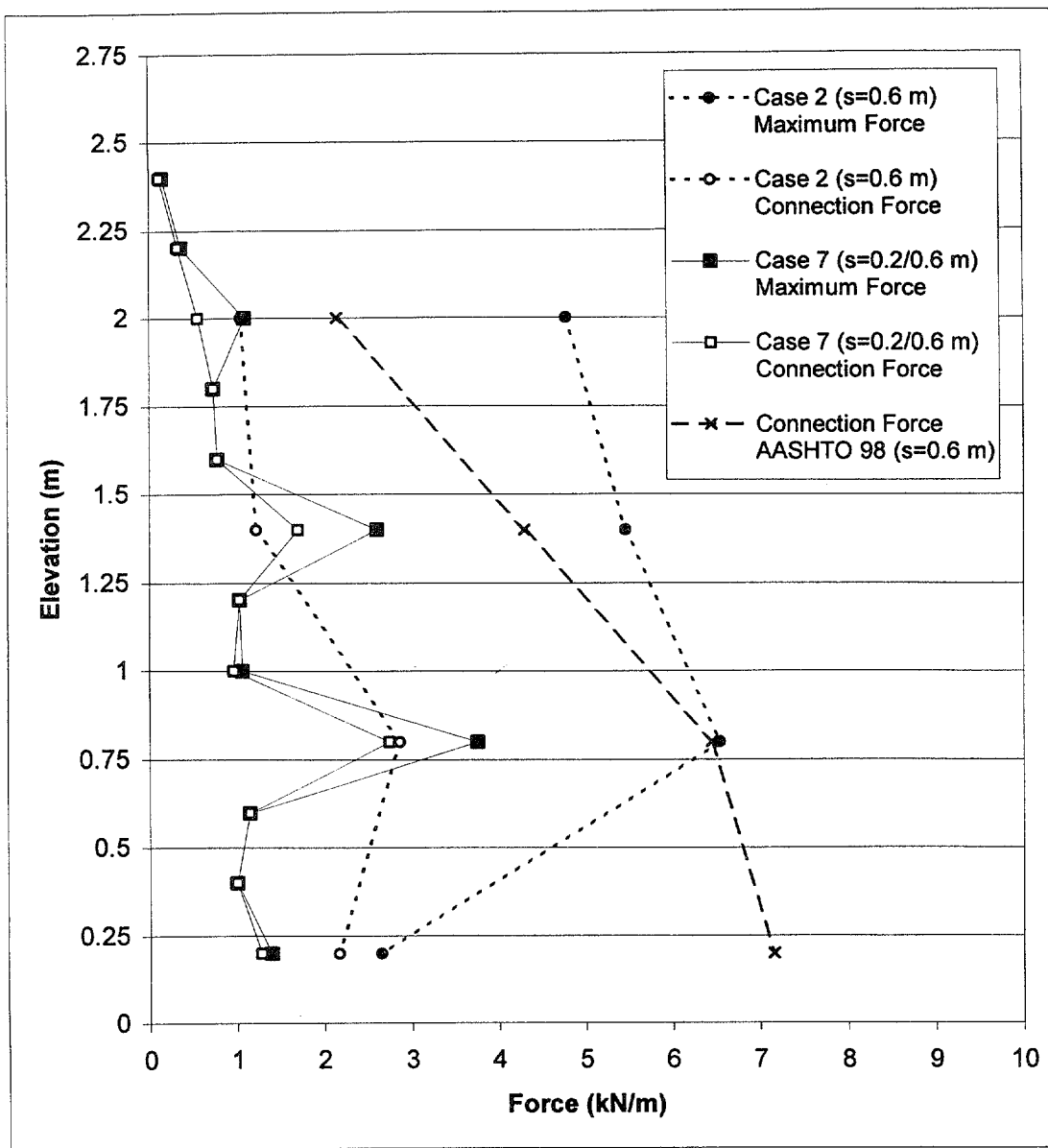


Figure 4.71 Effects of Secondary Reinforcement: Connection Force and Maximum Axial Force in Reinforcement for Cases 2 and 7 ($h=2.6$ m).

Table 4.1 Summary of Results Identifying Failure Modes.

Case	Spacing (m)	First Slip Surface Fully Developed		Wall Height at Which Plastic Zones Occur for the First Time in:			Mode of Failure
		at Wall Height (m)	Type	Foundation Soil	Reinforced Soil	Backfill Soil	
1	0.2	6.6	External	—	6.0	3.8	External mode
	0.4	5.8	External	—	4.0	3.2	Mixed mode: external mode is prevailing over compound mode
	0.6	4.4	Compound	—	1.4	2.6	Mixed mode: compound mode is prevailing over connection mode
	0.8	1.8	Internal	—	1.0	2.2	Connection mode
	1.0	1.0	Internal	—	1.0	1.4	Connection mode
2	0.2	3.4	Compound	—	3.0	2.4	Mixed mode: external mode is prevailing over compound mode
	0.4	2.8	Compound	—	1.4	2.0	Mixed mode: compound mode is prevailing over external mode
	0.6	1.4	Internal	—	1.0	1.4	Mixed mode: connection mode is prevailing over compound mode
	0.8	1.0	Internal	—	0.8	—	Connection mode

Table 4.1 Summary of Results Identifying Failure Modes, Continued.

Case	Spacing (m)	First Slip Surface Fully Developed		Wall Height at Which Plastic Zones Occur for the First Time in:			Mode of Failure
		at Wall Height (m)	Type	Foundation Soil	Reinforced Soil	Backfill Soil	
3	0.2	2.4	Compound	—	1.2	1.2	Mixed mode: compound mode is prevailing over external mode
	0.4	1.6	Compound	—	1.0	1.0	Compound mode
	0.6	1.4	Compound	—	1.0	1.0	Connection mode
	0.8	1.0	Internal	—	1.0	1.0	Connection mode
4	0.2	5.4	External	1.8	5.6	3.4	External mode
	0.4	5.2	External	1.6	1.6	2.4	Mixed mode: external mode is prevailing over compound mode
	0.6	1.4	Internal	1.6	1.0	2.2	Mixed mode: connection mode is prevailing over compound mode
	0.8	1.0	Internal	1.4	1.0	—	Connection mode
5	0.2	2.8	External	0.6	0.8	1.4	Deep-seated mode
	0.4	2.4	Compound	0.6	0.8	1.4	Compound mode
	0.6	1.4	Internal	0.4	0.6	1.4	Connection mode
	0.8	1.0	Internal	0.4	0.4	1.2	Connection mode
6	0.2	1.2	External	0.4	0.4	0.8	Deep-seated mode

Table 4.1 Summary of Results Identifying Failure Modes, Continued.

Case	Spacing (m)	First Slip Surface Fully Developed		Wall Height at Which Plastic Zones Occur for the First Time in:			Mode of Failure
		at Wall Height (m)	Type	Foundation Soil	Reinforced Soil	Backfill Soil	
6	0.4	1.2	Internal	0.4	0.4	1.2	Mixed mode: connection mode is prevailing over deep-seated mode
7	0.6/0.2	2.6	Compound	—	1.2	2.2	Compound mode
8-1	0.4	1.8	Internal	—	1.6	3.0	Compound mode
8-2	0.4	1.6	Internal	—	1.4	2.0	Compound mode
8-3	0.2	1.2	Compound	—	1.2	1.2	Compound mode
9	0.2	6.4	External	—	6.0	3.2	External mode
10	0.2	3.0	External	0.4	0.4	2.2	Deep-seated mode
	0.4	3.0	External	0.4	0.4	1.8	Deep-seated mode
	0.6	1.4	Internal	0.4	0.4	1.8	Mixed mode: connection mode is prevailing over deep-seated mode
	0.8	0.8	Internal	0.4	0.4	—	Connection mode
11	0.2	5.4	External	—	5.4	3.6	External mode
12	0.2	6.6	External	—	6	3.8	External mode
	0.6	2.6	Compound	—	1.2	1.8	Compound mode

Table 4.2 Critical Wall Height and Prevailing Mode of Failure.

Case	Reinforcement Spacing (m)				
	0.2	0.4	0.6	0.8	1.0
1	6.6	6.0	4.6	2.6	1.0
2	5.4	4.4	2.6	1.2	—
3	4.0	2.8	1.6	0.8	—
4	5.6	5.2	3.8	1.6	—
5	4.2	2.8	1.2	1.0	—
6	2.0	1.4	—	—	—
7	—	—	5.0	—	—
8-1	—	5.0	—	—	—
8-2	—	3.2	—	—	—
8-3	2.2	—	—	—	—
9	6.6	—	—	—	—
10	3.2	3.2	1.4	0.8	—
11	6.0	—	—	—	—
12	6.6	—	4.6	—	—

LEGEND:

Prevailing Mode of Failure:

External Mode (Direct Sliding/Toppling)

Deep-Seated Mode

Compound Mode

Connection Mode

Table 4.3 Maximum Axial Force in Reinforcement.

Case	Spacings (m)	Maximum Axial Force					
		Failure State			Critical State		
		Value (kN/m)	Elevation (m)	Wall Height (m)	Value (kN/m)	Elevation (m)	Wall Height (m)
1	0.2	20.5	0.4	8.6	6.0	1.2	6.6
	0.4	27.7	0.6	8.2	9.6	1.0	6.0
	0.6	15.8	0.8	6.2	8.1	0.8	4.6
	0.8	10.6	1.0	4.0	4.6	1.0	2.6
	1.0	7.9	1.2	2.0	0.5	0.2	1.0
2	0.2	22.5	0.6	6.6	8.1	0.8	5.4
	0.4	27.2	0.6	6.0	9.5	1.0	4.4
	0.6	25.4	0.8	4.6	6.5	0.8	2.6
	0.8	7.8	1.0	1.8	1.4	0.2	1.2
3	0.2	10.8	0.4	4.2	9.3	0.4	4.0
	0.4	17.2	0.2	3.8	8.7	0.6	2.8
	0.6	8.2	0.8	2.0	4.6	0.8	1.6
	0.8	2.6	0.2	1.0	0.7	0.2	0.8
4	0.2	8.8	0.6	7.0	4.8	0.6	5.6
	0.4	10.9	0.6	6.0	7.6	1.0	5.2
	0.6	15.8	1.4	5.4	7.2	0.8	3.8
	0.8	6.0	1.0	1.8	2.5	1.0	1.6

Table 4.3 Maximum Axial Force in Reinforcement, Continued.

Case	Spacings (cm)	Maximum Axial Force					
		Failure State			Critical State		
		Value (kN/m)	Elevation (m)	Wall Height (m)	Value (kN/m)	Elevation (m)	Wall Height (m)
5	0.2	21.3	0.2	5.4	7.8	0.2	4.2
	0.4	11.1	0.2	3.8	5.6	0.2	2.8
	0.6	8.7	0.8	2.4	2.0	0.2	1.2
	0.8	4.2	0.2	1.2	3.3	0.2	1.0
6	0.2	7.8	0.2	2.4	4.8	0.2	2.0
	0.4	15.1	0.2	2.6	4.8	0.2	1.4
7	0.6/0.2	40.2	1.2	6.0	17.8	1.2	5.0
8-1	0.4	40.6	1.0	8.0	5.5	1.4	5.0
8-2	0.4	24.9	0.6	5.4	4.2	1.0	3.2
8-3	0.2	18.2	0.6	5.0	2.0	0.8	2.2
9	0.2	16.1	0.4	8.2	6.8	0.8	6.6
10	0.2	11.4	0.2	4.4	4.3	0.2	3.2
	0.4	15.0	0.2	4.4	6.1	0.2	3.2
	0.6	8.2	0.2	2.8	3.3	0.8	1.4
	0.8	4.4	0.2	1.0	1.1	0.2	0.8
11	0.2	15.3	0.4	7.2	6.1	0.8	6.0
12	0.2	23.1	0.4	8.8	6.1	1.0	6.6
	0.6	47.0	0.8	6.0	16.1	0.8	4.6

Table 4.4 Maximum Connection Force.

Case	Spacings (m)	Maximum Connection Force					
		Failure State			Critical State		
		Value (kN/m)	Elevation (m)	Wall Height (m)	Value (kN/m)	Elevation (m)	Wall Height (m)
1	0.2	17.9	0.4	8.6	5.1	1.2	6.6
	0.4	23.5	0.6	8.2	7.4	1.0	6.0
	0.6	13.1	0.8	6.2	6.8	0.8	4.6
	0.8	6.7	1.0	4.0	2.8	1.0	2.6
	1.0	1.4	0.2	2.0	0.4	0.2	1.0
2	0.2	20.7	0.4	6.6	6.0	0.6	5.4
	0.4	22.4	0.6	6.0	7.4	0.6	4.4
	0.6	12.4	0.8	4.6	2.9	0.8	2.6
	0.8	0.4	0.2	1.8	1.2	0.2	1.2
3	0.2	9.3	0.4	4.2	7.1	0.4	4.0
	0.4	13.5	0.6	3.8	5.0	0.6	2.8
	0.6	2.7	0.8	2.0	1.9	0.2	1.6
	0.8	0.9	0.2	1.0	0.6	0.2	0.8
4	0.2	5.9	0.6	7.0	3.0	0.6	5.6
	0.4	6.6	1.0	6.0	4.6	0.6	5.2
	0.6	6.9	2.0	5.4	3.0	0.2	3.8
	0.8	1.2	0.2	1.8	1.2	0.2	1.6

Table 4.4 Maximum Connection Force, Continued.

Case	Spacings (cm)	Maximum Connection Force					
		Failure State			Critical State		
		Value (kN/m)	Elevation (m)	Wall Height (m)	Value (kN/m)	Elevation (m)	Wall Height (m)
5	0.2	6.4	0.6	5.4	4.4	0.2	4.2
	0.4	7.6	0.2	3.8	4.1	0.2	2.8
	0.6	3.8	0.2	2.4	1.3	0.2	1.2
	0.8	1.8	0.2	1.2	1.5	0.2	1.0
6	0.2	2.9	0.4	2.4	1.5	0.4	2.0
	0.4	4.6	0.6	2.6	1.9	0.2	1.4
7	0.6/0.2	2.9	0.2	6.0	10.6	0.8	5.0
8-1	0.4	30.9	0.6	8.0	5.5	1.4	5.0
8-2	0.4	23.4	0.6	5.4	3.8	1.0	3.2
8-3	0.2	15.7	0.2	5.0	2.0	0.8	2.2
9	0.2	14.0	0.4	8.2	5.9	1.2	6.6
10	0.2	4.2	0.4	4.4	2.4	0.4	3.2
	0.4	5.2	0.6	4.4	2.2	0.6	3.2
	0.6	3.9	0.2	2.8	1.9	0.2	1.4
	0.8	1.4	0.2	1.0	0.8	0.2	0.8
11	0.2	13.9	0.4	7.2	4.5	0.8	6.0
12	0.2	22.0	0.4	8.8	5.0	1.0	6.6
	0.6	34.3	0.8	6.0	12.5	0.8	4.6

**Table 4.5 Effects of Reinforcement Stiffness on Model Response:
Comparison of Case 1 ($s=0.4$ m) and Case 8–1 ($s=0.4$ m).**

Parameter	Case 1 ($s=0.4$ m)	Case 8–1 ($s=0.4$ m)	
Reinforcement type (table 3.5)	Baseline	Ductile	
Mode of failure (table 4.1)	External mode	Compound mode	
Critical wall height (m) (table 4.5, figure 4.1–a)	6.0	5.0	
Plastic zones distribution	Figure 4.5	Figure 4.31	
Wall height at which plastic zones occur for first time in (table 4.1):	Foundation soil Reinforced soil Backfill soil	— 4.0 3.2	— 1.6 3.0
Slip surface developed for the first time	At wall height (m) Type (figure 4.3)	5.8 External	1.8 Internal
Slip surface at critical state (table 4.2)	Slope (deg) Type (figure 4.3)	58 External	53 Compound
Wall height $h=5.0$ m	Maximum force in reinforcement Maximum connection force Maximum displacement (cm) Number of steps	6.46 kN at elevation 1.0 m 5.38 kN at elevation 1.4 m 2.9 278508 (Grid 159×321)	5.51 kN at elevation 1.4 m 5.51 kN at elevation 1.4 m 7.3 485049 (Grid 159×221)

Table 4.6 Effects of Reinforcement Stiffness of Model Response: Comparison of Case 2 ($s=0.4$ m) and Case 8–2 ($s=0.4$ m).

Parameter	Case 2 ($s=0.4$ m)	Case 8–2 ($s=0.4$ m)
Reinforcement type (table 3.5)	Baseline	Ductile
Mode of failure (table 4.1)	Compound mode	Compound mode
Critical wall height (m) (table 4.5, figure 4.1-a)	4.4	3.2
Plastic zones distribution	Figure 4.58	Figure 4.75
Wall height at which plastic zones occur for first time in (table 4.1):	Foundation soil	—
	Reinforced soil	1.4
	Backfill soil	2.0
Slip surface developed for the first time	At wall height (m)	2.8
	Type (figure 4.3)	Compound
Slip surface at critical state (table 4.2)	Slope (deg)	50
	Type (figure 4.3)	External
Wall height $h=3.2$ m	Maximum force in reinforcement	4.51 kN at elevation 0.6 m
	Maximum connection force	4.03 kN at elevation 0.6 m
	Maximum displacement (cm)	1.7
	Number of steps	126614 (grid 159×321)
		4.23 kN at elevation 1.0 m
		3.76 kN at elevation 1.0 m
		5.2
		173555 (grid 159×181)

Table 4.7 Effects of Reinforcement Stiffness on Model Response: Comparison of Case 3 ($s=0.2$ m) and Case 8-3 ($s=0.2$ m).

Parameter	Case 3 ($s=0.2$ m)	Case 8-3 ($s=0.2$ m)
Reinforcement type (table 3.5)	Baseline	Ductile
Mode of failure (table 4.1)	Compound mode	Compound mode
Critical wall height (m) (table 4.5, figure 4.1-a)	4.0	2.2
Plastic zones distribution	Figure 4.60	Figure 4.76
Wall height at which plastic zones occur for first time in (table 4.1):	Foundation soil	—
	Reinforced soil	1.2
	Backfill soil	1.2
Slip surface developed for the first time	At wall height (m)	2.4
	Type (figure 4.3)	Compound
Slip surface at critical state (table 4.2)	Slope (deg)	45
	Type (figure 4.3)	Compound
Wall height $h=2.2$ m	Maximum force in reinforcement	2.26 kN at elevation 0.6 m
	Maximum connection force	2.08 kN at elevation 0.8 m
	Maximum displacement (cm)	0.8
	Number of steps	51792 (grid 159×321)
		1.98 kN at elevation 0.8 m
		1.95 kN at elevation 0.8 m
		2.4
		90776 (grid 159×181)

Table 4.8 Effects of Connection Strength on Model Response: Cases with Small Reinforcement Spacing ($s=0.2$ m).

Parameter	Case 1	Case 9	Case 12	
Connection type (table 3.6)	FCon-B	FCon-L	SC	
Mode of failure (table 4.1)	External	External	External	
Critical wall height (m) (table 4.5, figure 4.1-a)	6.6	6.6	6.6	
Plastic zones distribution	Figure 4.5	Figure 4.77	Figure 4.82	
Wall height at which plastic zones occur for first time in (table 4.1):	Foundation soil Reinforced soil Backfill soil	— 6.0 3.8	— 6.0 3.2	— 6.0 3.8
Slip surface developed for the first time	At wall height (m) Type (figure 4.3)	6.6 External	6.4 External	6.6 External
Slip surface at critical state (table 4.2)	Slope (deg) Type (figure 4.3)	54 External	52 External	56 External
Wall height $h=6.6$ m	Maximum force in reinforcement Maximum connection force Maximum displacement (cm) Number of steps	6.02 kN at elevation 1.2 m 5.12 kN at elevation 1.2 m 4.4 419538 (grid 159×321)	6.77 kN at elevation 0.8 m 5.93 kN at elevation 1.2 m 5.6 375455 (grid 159×201)	6.08 kN at elevation 1.0 m 4.96 kN at elevation 1.2 m 4.2 573000 (grid 159×321)

Table 4.9 Effects of Connection Strength on Model Response: Cases with Large Reinforcement Spacing ($s=0.6$ m).

Parameter	Case 2 ($s=0.6$ m)	Case 12 ($s=0.6$ m)
Connection type (table 3.6)	FCon-B	SC
Mode of failure (table 4.1)	Connection	Compound
Critical wall height (m) (table 4.5, figure 4.1-a)	2.6	4.6
Plastic zones distribution	Figure 4.44	Figure 4.83
Wall height at which plastic zones Occur for first time in (table 4.1)	Foundation soil	—
	Reinforced soil	1.0
	Backfill soil	1.4
Slip surface developed for the first time	At wall height (m)	1.4
	Type (figure 4.3)	Internal
Slip surface at critical state (table 4.2)	Slope (deg)	65
	Type (figure 4.3)	Internal
Wall height $h=2.6$ m	Maximum force in reinforcement	6.53 kN at elevation 0.8 m
	Maximum connection force	2.85 kN at elevation 0.8 m
	Maximum displacement (cm)	7.1
	Number of steps	248497 (grid 159×321)
NOTE: FCon-B=Frictional Connection with Baseline Strength; FCon-L=Frictional Connection with Low Strength; SC=Structural Connection.		

Table 4.10 Effects of Foundation Stiffness on Model Response: Comparison of Cases 1, 4, and 10 ($s=0.2$ m).

Parameter	Case 1	Case 4	Case 10
Foundation soil type (table 3.3)	Very stiff soil	Baseline stiffness high strength	Baseline stiffness low strength
Strength of reinforced soil	High	High	High
Strength of backfill soil	High	High	Low
Mode of failure (table 4.1)	External	External	Deep-seated
Critical wall height (m), (table 4.5)	6.6	5.6	3.2
Plastic zones distribution	Figure 4.5	Figure 4.64	Figure 4.18
Wall height at which plastic zones occur for first time in (table 4.1):	Foundation soil	—	1.8
	Reinforced soil	6.0	5.6
	Backfill soil	3.8	3.4
Slip surface developed for the first time	At wall height (m)	6.6	5.4
	Type (figure 4.3)	External	External
Slip surface at critical state (table 4.2)	Slope (deg)	54	60
	Type (figure 4.3)	External	External
Wall height $h=3.2$ m	Maximum force in reinforcement	2.18 kN at elevation 0.8 m	2.33 kN at elevation 0.6 m
	Maximum connection force	1.59 kN at elevation 0.8 m	1.50 kN at elevation 0.6 m
	Maximum displacement (cm)	1.1	3.0
			3.7

Table 4.11 Effects of Secondary Reinforcement on Model Response.

Parameter	Case 2 (s=0.6 m)	Case 7 (s=0.6/0.2 m)	
Mode of failure (table 4.1)	Connection	Compound	
Critical wall height (m) (table 4.5, figure 4.1-a)	2.6	5.0	
Plastic zones distribution	Figure 4.44	Figure 4.74	
Wall height at which plastic zones occur for first time in (table 4.1):	Foundation soil Reinforced soil Backfill soil	— 1.0 1.4	— 1.2 2.2
Slip surface developed for the first time	At wall height (m) Type (figure 4.3)	1.4 Internal	2.6 Compound
Slip surface at critical State (table 4.2)	Slope (deg) Type (figure 4.3)	65 Internal	46 Compound
Wall height h=2.6 m	Maximum force in reinforcement Maximum connection force Maximum displacement (cm) Number of steps	6.53 kN at elevation 0.8 m 2.85 kN at elevation 0.8 m 7.1 248497 (grid 159×321)	3.75 kN at elevation 1.2 m 2.55 kN at elevation 0.8 m 1.0 79737 (grid 159×181)

Table 4.12 Effects of Soil Dilatancy on Model Response: Comparison of Case 1 ($s=0.2$ m) and Case 11 ($s=0.2$ m).

Parameter	Case 1 ($s=0.2$ m)	Case 11 ($s=0.2$ m)
Soil dilation (deg)	15	0
Mode of failure (table 4.1)	External mode	External mode
Critical wall height (m) (table 4.5, figure 4.1-a)	6.6	6.0
Plastic zones distribution	Figure 4.5	Figure 4.81
Wall height at which plastic zones occur for first time in (table 4.1):	Foundation soil — Reinforced soil 4.0 Backfill soil 3.2	— 5.4 3.6
Slip surface developed for the First Time	At wall height (m) 6.6 Type (figure 4.3) External	5.4 External
Slip surface at critical state (table 4.2)	Slope (deg) 54 Type (figure 4.3) External	57 External
Wall height $h=6.0$ m	Maximum force in reinforcement 4.903 kN at elevation 1.2 m Maximum connection force 3.89 kN at elevation 1.2 m Maximum displacement (cm) 3.24 Number of steps (grid 159×321) 303203	6.06 kN at elevation 0.8 m 4.52 kN at elevation 0.8 m 5.20 455957

CHAPTER 5. COMPARISON WITH EXISTING DESIGN PRACTICE

This chapter compares FLAC predictions with calculations done in accordance with AASHTO, Section 5.8, 1998 (AASHTO 1998). The details of AASHTO design are given in “Demonstration Project No. 82: Mechanically Stabilized Earth Walls and Reinforced Soil Slopes, Design and Construction Guidelines,” (FHWA, 1997).

First, the program MSEW 1.1 (ADAMA Engineering 1998) was used to analyze four baseline cases that represent all four failure mechanisms identified by FLAC. Second, the slopes’ slip planes of all cases at the critical and failure states were measured from FLAC plots, and are presented together with the values resulting from the Rankine’s and Coulomb’s earth pressure theories. Third, stress distributions from FLAC analysis were compared with the AASHTO values.

5.1 Analysis of Baseline Cases using AASHTO

Four model walls at the critical state were analyzed according to AASHTO design method using the program MSEW 1.1 (ADAMA Engineering 1998). The purpose was to compare FLAC predictions with an existing design method. The following four cases were selected to represent different failure modes identified with FLAC:

- Case 1 ($s=0.4$ m)—external mode (direct sliding/overturning).
- Case 2 ($s=0.6$ m)—connection mode.
- Case 8–1 ($s=0.4$ m)—compound mode.
- Case 10 ($s=0.2$ m)—deep-seated mode.

The input data used in the AASHTO 98 analysis with the MSEW 1.1 program are given in table 5.1. The analysis mode of the program was used for simple wall geometry, modular block facing, and geotextile reinforcement. No water table, surcharge loads, or seismicity were introduced in the analysis. The wall geometry and reinforcement layout were the same as those used in the FLAC models (figure 3.1). The ultimate strength of reinforcement was specified to correspond to the maximum axial force in reinforcement calculated by FLAC. Since up to five different reinforcement types can be specified in MSEW 1.1, only the maximum axial forces of the bottom five layers were used. All reduction and correction factors in the MSEW 1.1 analysis were specified to be equal to 1.0. Major results from the MSEW 1.1 analysis are given in table 5.2. The factors of safety for sliding and overturning are calculated for the wall-foundation interface and represent their minimum values. The excessive factors of safety against bearing capacity for cases 1, 2, and 8–1 were a

result of the artificially high cohesion used in FLAC models to represent very stiff foundation soil.

The results for case 1 show that, according to analysis, the wall was at the verge of failure due to toppling ($F_s=1.09$). The factors of safety against sliding and bearing capacity showed that the wall was stable with respect to direct sliding ($F_s=2.914$) and bearing capacity failure ($F_s=86.4$). The ultimate strength of geotextile exceeded the maximum reinforcement force from internal stability analysis (T_{max}), except for the fifth layer, which indicated that, internally, the wall was stable. AASHTO results for case 1 ($s=0.4$ m) confirmed that at height $h=6.0$ m, the wall was at the verge of failure, which coincided with the definition of a critical state in FLAC analysis. The predicted FLAC external mode of failure comprised the overturning mode of failure identified by MSEW 1.1 calculations. The maximum forces in reinforcements provided by FLAC and MSEW 1.1 calculations are given in figure 5.1.

The results for case 2 implied that according to AASHTO the wall was stable externally and unstable internally. All external stability factors of safety were greater than one and exceed the values used in design. The wall was stable with respect to direct sliding ($F_s=2.981$), overturning ($F_s=3.68$), and bearing capacity failure ($F_s=594.9$). However, the maximum reinforcement force from internal stability analysis (T_{max}) significantly exceeded the ultimate strength of geotextile, which indicated that the wall was internally unstable. AASHTO results for case 2 ($s=0.6$ m) confirmed that at height $h=2.6$ m, the wall was internally unstable. The connection mode of failure predicted by FLAC matched the internal instability identified by MSEW 1.1 calculations. The maximum forces in reinforcements provided by FLAC and MSEW 1.1 calculations are given in figure 5.1.

The results for case 8–1 implied that, according to AASHTO, the wall was stable externally and unstable internally. All external stability factors of safety were greater than one and exceeded the values used in design. The wall was stable with respect to direct sliding ($F_s=3.497$), overturning ($F_s=1.57$), and bearing capacity failure ($F_s=449.1$). However, the maximum reinforcement force from internal stability analysis (T_{max}) significantly exceeded the ultimate strength of geotextile in the

reinforcement layers at the bottom of the wall. The MSEW 1.1 results for case 8–1 ($s=0.4$ m) indicated that at height $h=5.0$ m, the bottom part of the wall was internally unstable. A compound stability analysis using the L–method¹ (a modification of Demo 82 approach proposed by Leshchinsky (ADAMA Engineering 1998, Leshchinsky 1999) was conducted for further investigation. The compound mode of failure predicted by FLAC was identified by the MSEW 1.1 calculations using the L–method. The calculated factor of safety was 1.005, which confirmed that the wall was at the verge of failure with respect to compound failure. The other two methods implemented in MSEW 1.1 gave conservative results: the factor of safety calculated by using the Demo 82 method was 0.76, and the factor of safety calculated by using the comprehensive Bishop’s method was 0.63. The maximum forces in reinforcements given by FLAC and MSEW 1.1 calculations are given in figure 5.2. The critical slip surface from the compound stability analysis and the failure zones distribution given by FLAC are shown in figure 5.3.

The results for case 10 showed that, according to AASHTO, the wall failed because of bearing capacity failure ($F_s=0.38$). The factors of safety against direct sliding ($F_s=1.08$), overturning ($F_s=1.62$), and eccentricity ($e=0.46$ m) also indicated instability. The ultimate strength of geotextile exceeded the maximum reinforcement force from internal stability analysis (T_{max}), which indicated that the wall was internally stable. The MSEW 1.1 results for case 10 ($s=0.4$ m) indicated that at height $h=3.2$ m (which corresponded to the critical state predicted by FLAC) the wall had failed earlier as a result of bearing capacity failure. Further deep-seated stability analysis indicated that, for the critical state predicted by FLAC, the wall was at the verge of deep-seated failure ($F_s=1.047$). The deep-seated mode of failure predicted by FLAC was also identified by MSEW 1.1 calculations. The maximum forces in reinforcement calculated by FLAC and MSEW 1.1 are given in figure 5.2. The critical slip surface corresponding to deep-seated stability analysis and the failure zones distribution given by FLAC are shown in figure 5.4.

The comparison between the MSEW 1.1 calculations and FLAC predictions for the specified cases showed good agreement between the results. The existing design method was able to distinguish the modes of failure identified by FLAC analysis, especially those due to external instability.

¹ In the L–method, the factor of safety is directly related to the reinforcement strength, based on the premise that the soil shear strength is mobilized fully, and stability is entirely dependent on reinforcement strength (Leshchinsky 1999). The peak shear strength of soil is reduced, accounting for possible large deformations and progressive failure. For further details, see the help menu of program MSEW 1.1.

5.2 Slope of Slip Planes

The slope of slip surfaces that developed at the critical and failure states of all models were measured from FLAC plots of failure zones distributions (see the schematic in figure 4.44–b). The slip surfaces were approximated as planes starting from the top of the backfill. The planar approximation was accurate for models that experienced external or connection modes of failure. The slip surfaces of models that experienced compound or deep-seated modes of failure were nonplanar, and can better be approximated more accurately by circular arcs, as done in the slope stability analysis. In most cases, the slip surfaces became nonplanar in the zone near or within the reinforced soil.

The slip surface slopes measured on FLAC plots were lower than the values given by the Rankine's and Coulomb's earth pressure theories at both critical and failure states (table 5.3). The slopes of surfaces calculated by using Coulomb's equation were closer to FLAC results than to those calculated by using Rankine's equation.

5.3 Stresses

According to AASHTO, the horizontal stresses are calculated using the Rankine's earth pressure coefficient. Therefore, researchers compared Rankine's earth pressure theory and the stresses produced by FLAC along section A (0.15 m behind the facing) and section C (0.15 m behind the end of reinforcement) at the critical and failure states. Horizontal and vertical stresses for case 1 ($s=0.2$ m, external failure mode), case 2 ($s=0.6$ m, connection failure mode), case 8–1 ($s=0.4$ m, compound failure mode) and case 10 ($s=0.2$ m, deep-seated failure mode) are presented in figures 5.5–5.12.

The model of case 1 ($s=0.2$ m, high strength soil, very stiff foundation) experienced external mode of failure. Stress distributions at the critical and failure states are shown in figures 5.5 and 5.6. At the failure state, toppling of the wall led to stress concentration at the toe of the wall (section A), while horizontal and vertical stresses along section C were almost the same. At the critical state, the stress concentration at the toe was smaller; however, the stress distributions also indicated the identified mode of failure. The stresses produced by FLAC differed from the stresses used in AASHTO design. The horizontal stresses behind the facing (section A) were larger than those calculated by using AASHTO for both critical and failure states. The horizontal stresses behind the reinforced soil (section C) were smaller than those calculated by using AASHTO for both critical and failure states, except the stresses at the bottom of the wall which were larger.

The model of case 2 ($s=0.6$ m, medium strength soil, very stiff foundation) experienced connection mode of failure. Stress distributions at the critical and failure states are shown in figures 5.7 and 5.8. Deformations of the reinforced soil and at the facing led to uneven distribution of stresses. At the critical state, the stress distribution indicated internal instability at the upper part of the wall's facing. Horizontal stresses produced by FLAC oscillated around the stresses used in AASHTO design in the upper part of the wall. The horizontal stresses were larger than those calculated by AASHTO at the bottom of the wall.

The model of case 8–1 ($s=0.4$ m, high strength soil, very stiff foundation, DR) experienced compound mode of failure. Stress distributions at the critical and failure states are shown in figures 5.9 and 5.10. The horizontal stresses produced by FLAC oscillated around the stresses used in AASHTO design, except at the bottom of the wall where they were much larger.

The model of case 10 ($s=0.2$ m, high strength reinforced soil, low strength foundation and backfill soil) experienced deep-seated mode of failure. Stress distributions at the critical and failure states are shown in figures 5.11 and 5.12. The stresses produced by FLAC differed from the stresses used in AASHTO design. The FLAC horizontal stresses along sections A and C were closer to the AASHTO horizontal stresses corresponding to section A (high strength soil). The horizontal stresses behind the reinforced soil (section C) were smaller than AASHTO horizontal stresses corresponding to section C (low strength soil).

The horizontal stresses calculated by FLAC differed from the horizontal stresses used in AASHTO design. At the critical states, FLAC stresses behind the facing were approximately 25 percent larger than AASHTO stresses. This difference was much larger at the bottom part of all models in which stress concentration was observed, and for the case that experienced connection mode of failure.

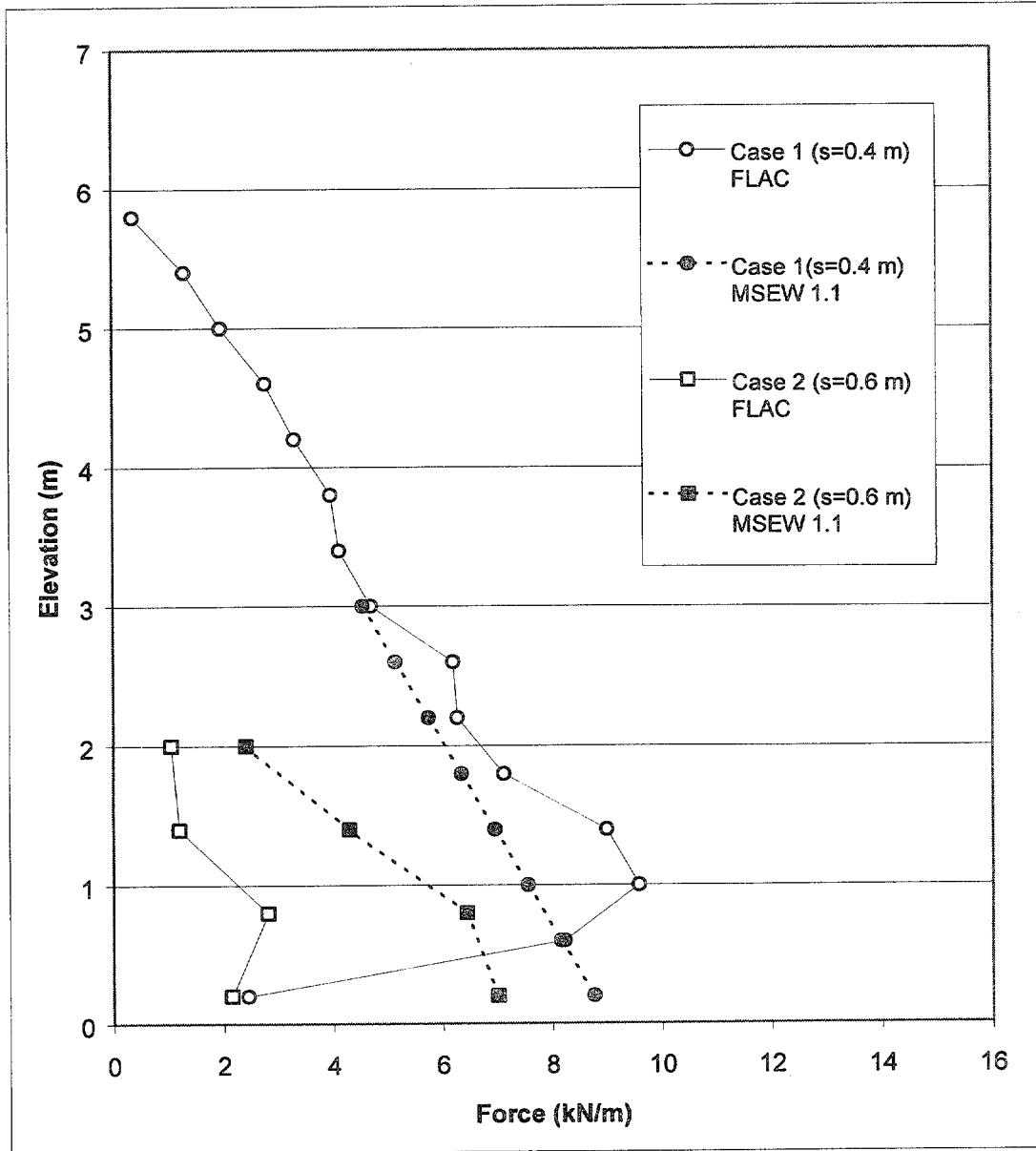


Figure 5.1 Maximum Force in Reinforcement: Comparison of FLAC and AASHTO Results for Case 1 ($s=0.4$ m) and Case 2 ($s=0.6$ m).

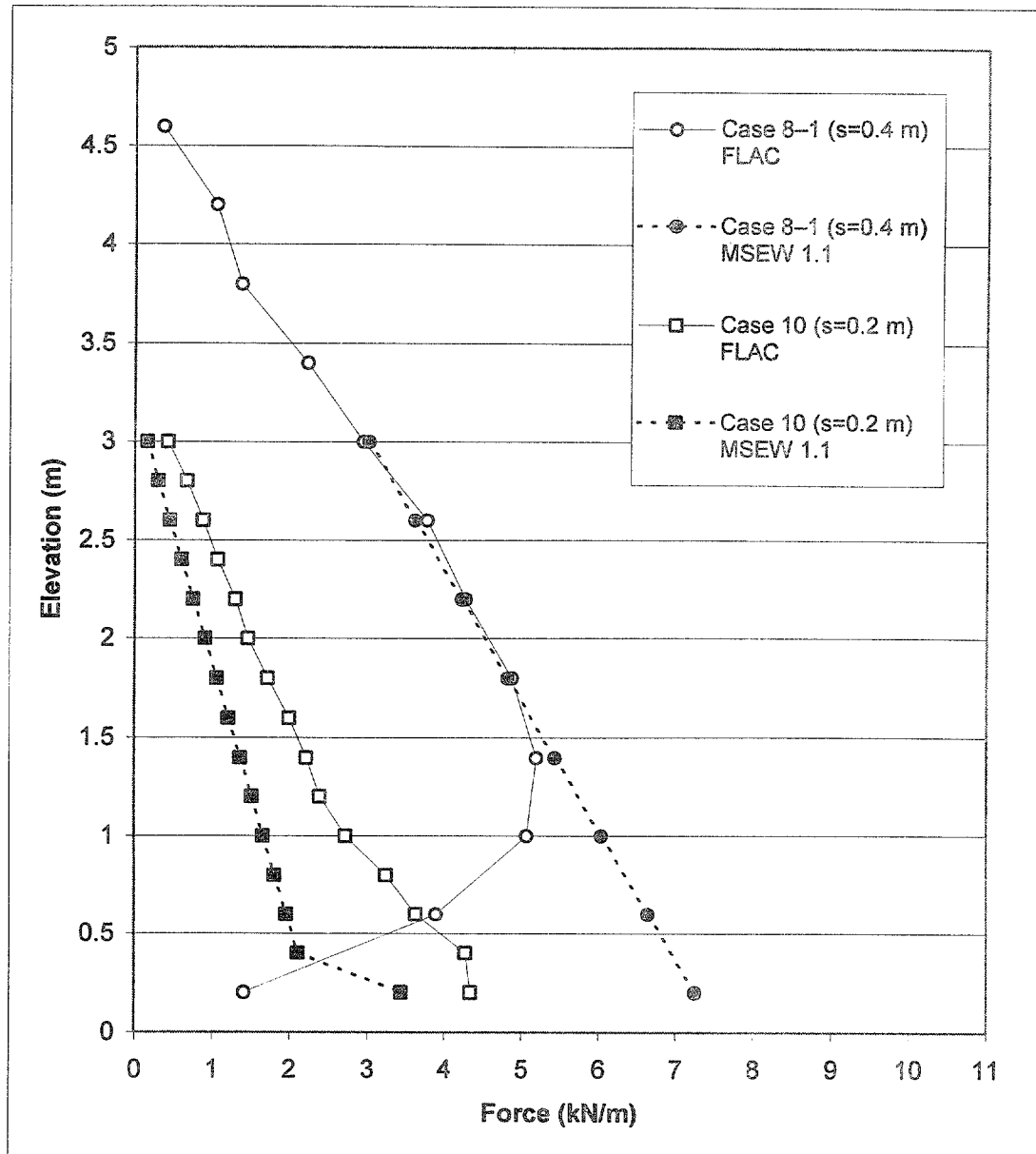
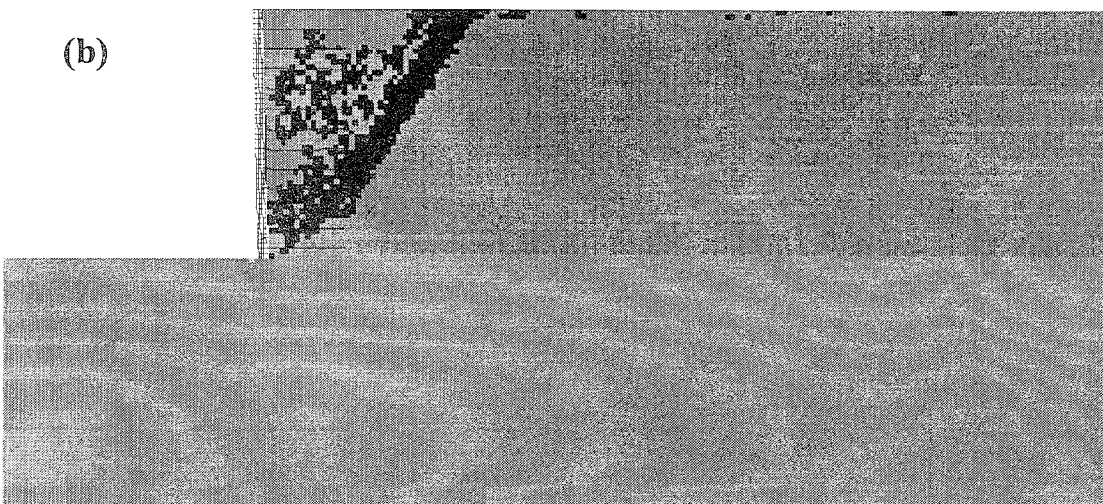
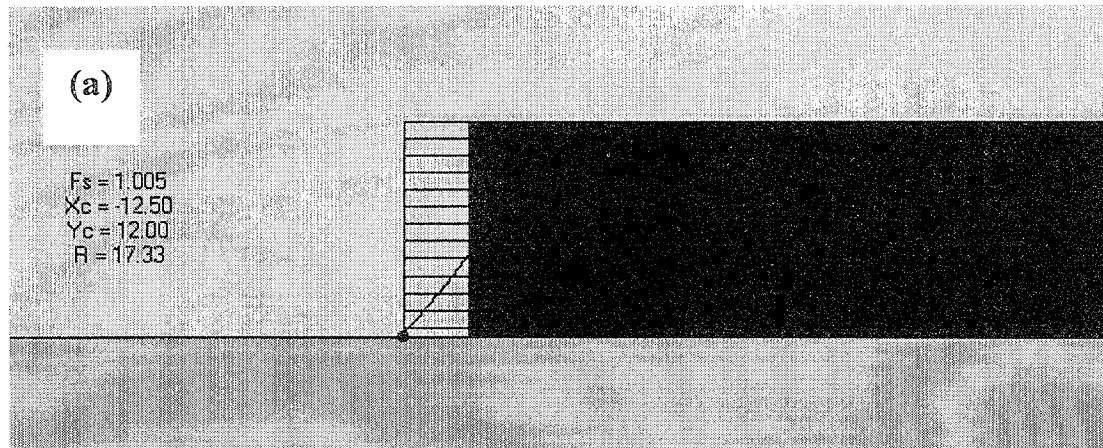


Figure 5.2 Maximum Force in Reinforcement: Comparison of FLAC and AASHTO Results for Case 8-1 ($s=0.4$ m) and Case 10 ($s=0.2$ m).



LEGEND: State of Material

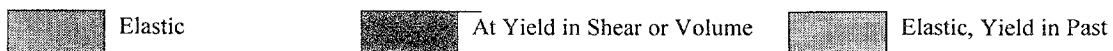
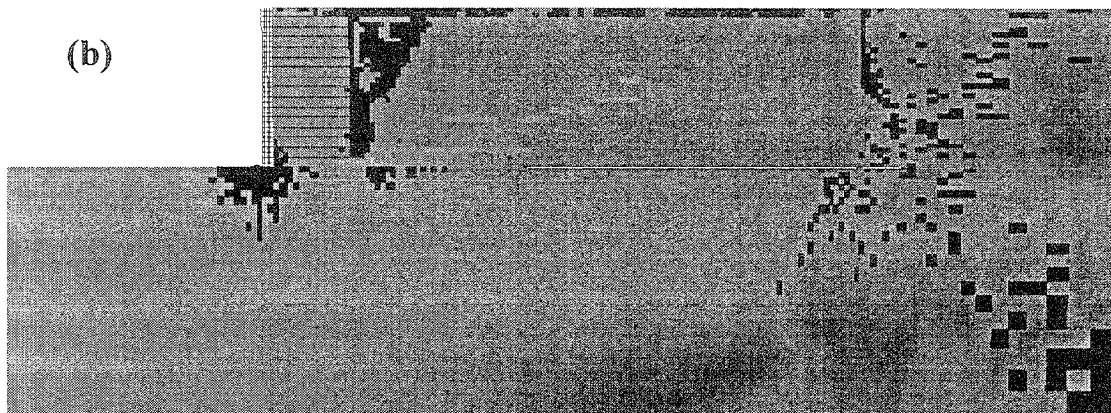
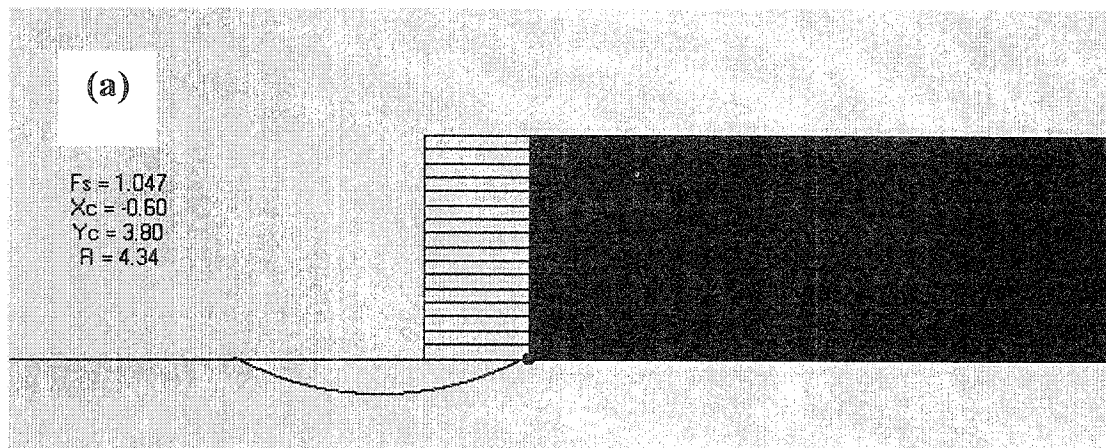


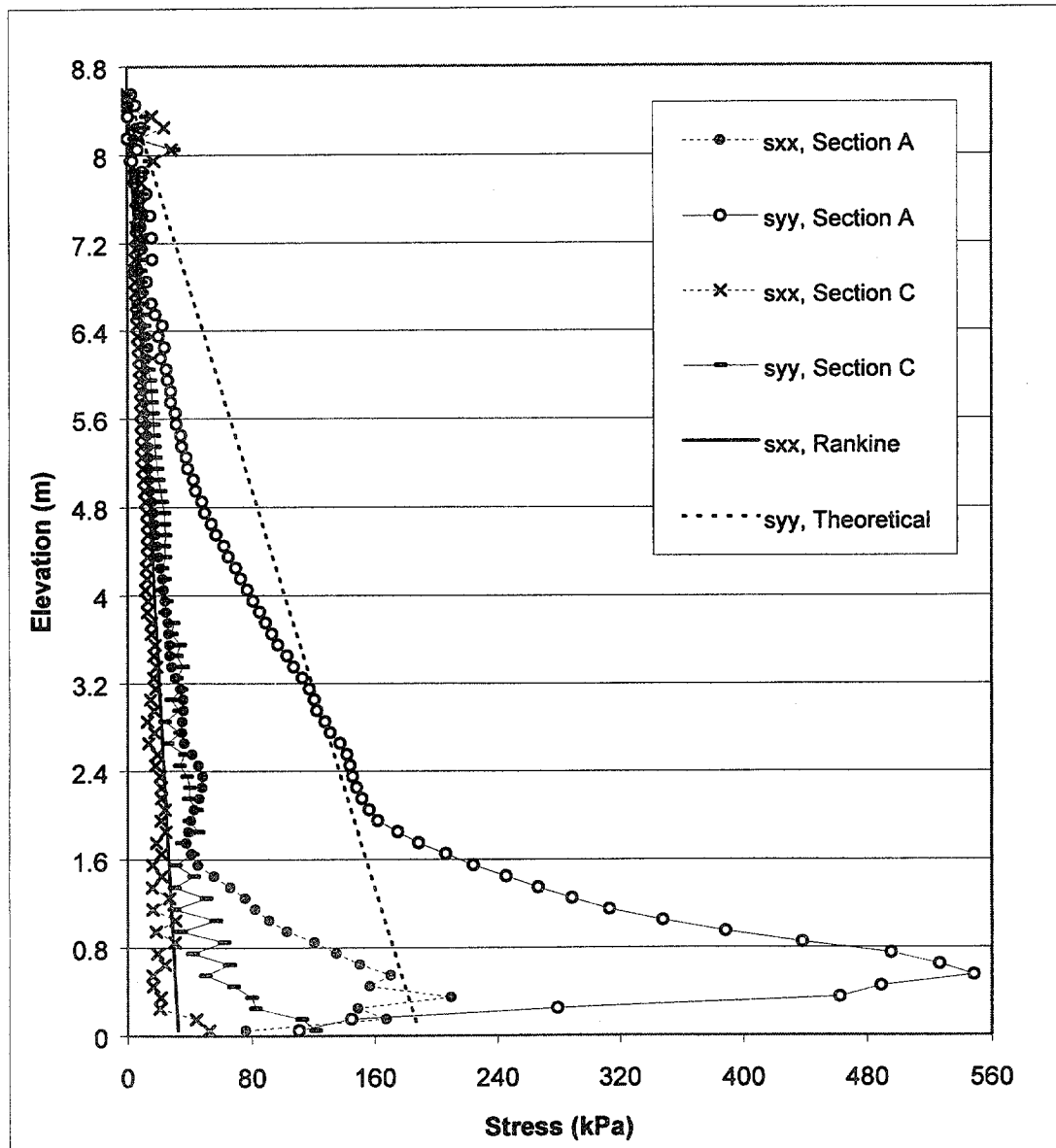
Figure 5.3 Comparison of FLAC and AASHTO Results for Case 8-1 ($s=0.4$ m, $h=5.0$ m, $t=1.5$ m): (a) MSEW 1.1 Analysis: Critical Slip Surface from Compound Stability Analysis; (b) FLAC Analysis: Failure Zones Distribution at the Critical State.



LEGEND: State of Material

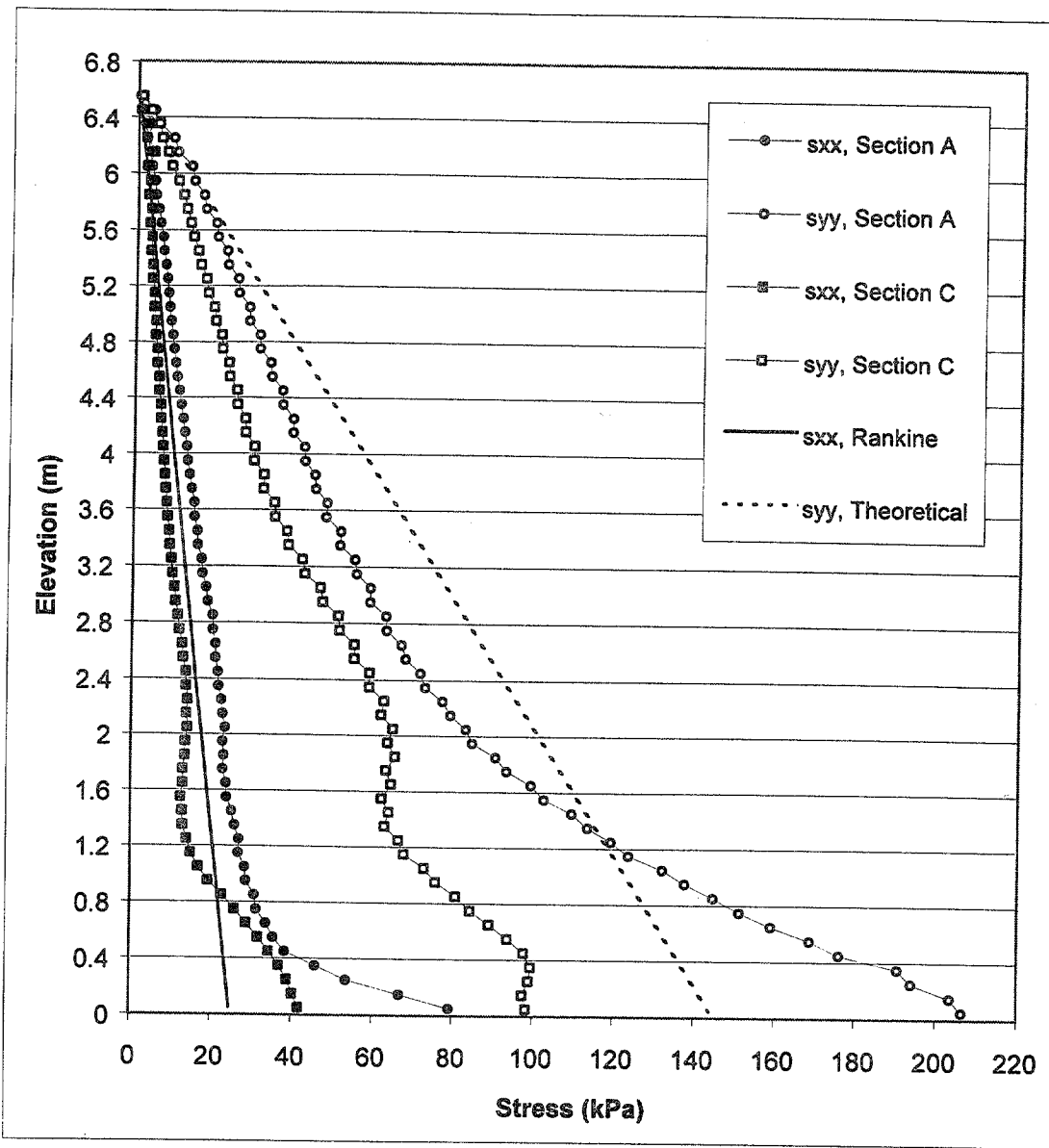
	Elastic		At Yield in Shear or Volume		Elastic, Yield in Past
--	---------	--	-----------------------------	--	------------------------

Figure 5.4 Comparison of FLAC and AASHTO Results for Case 10 ($s=0.2$ m, $h=3.2$ m, $t=1.5$ m): (a) MSEW 1.1 Analysis: Critical Slip Surface from Deep-Seated Stability Analysis; (b) FLAC Analysis: Failure Zones Distribution at the Critical State.



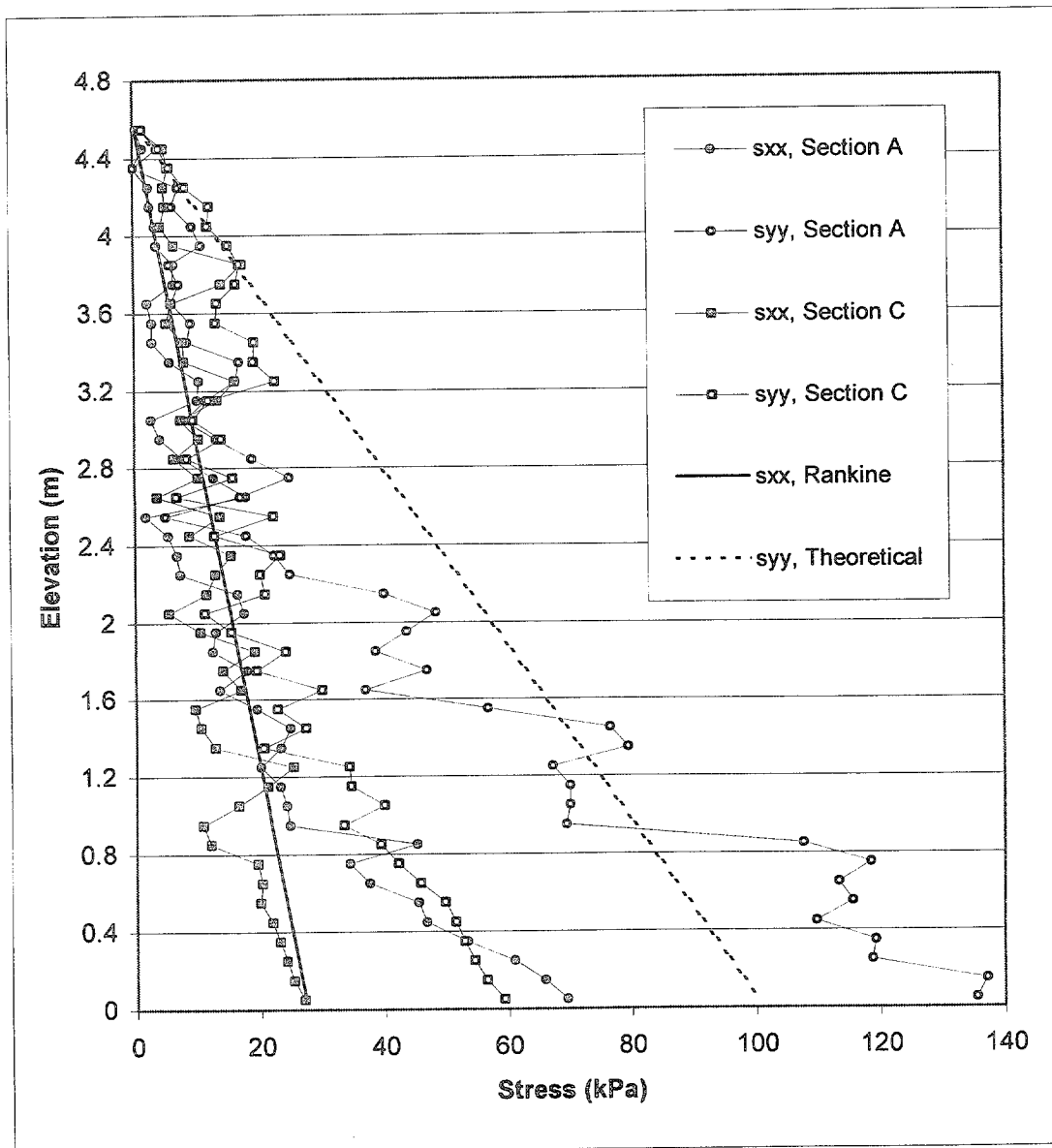
NOTE: Line A is located 0.15 m behind the facing. Section C is located 0.15 m behind the end of reinforcement.

Figure 5.5 Stress Distributions along Sections A and C for Failure State of Case 1 ($s=0.2$ m, $h=8.6$ m, $l/h=0.17$).



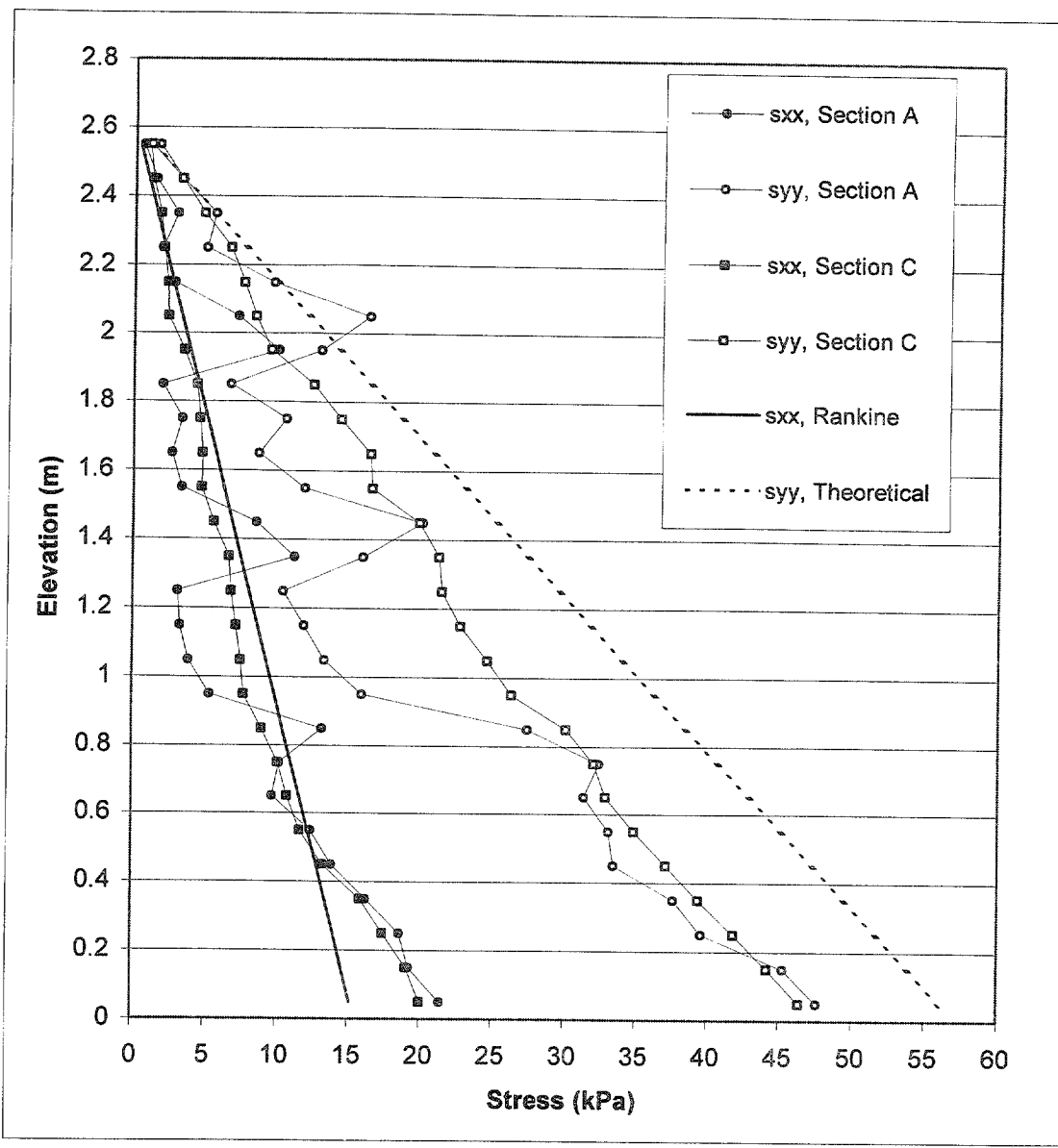
NOTE: Section A is located 0.15 m behind the facing. Section C is located 0.15 m behind the end of reinforcement.

Figure 5.6 Stress Distributions along Sections A and C for Critical State of Case 1 ($s=0.2$ m, $h=8.6$ m, $l/h=0.17$).



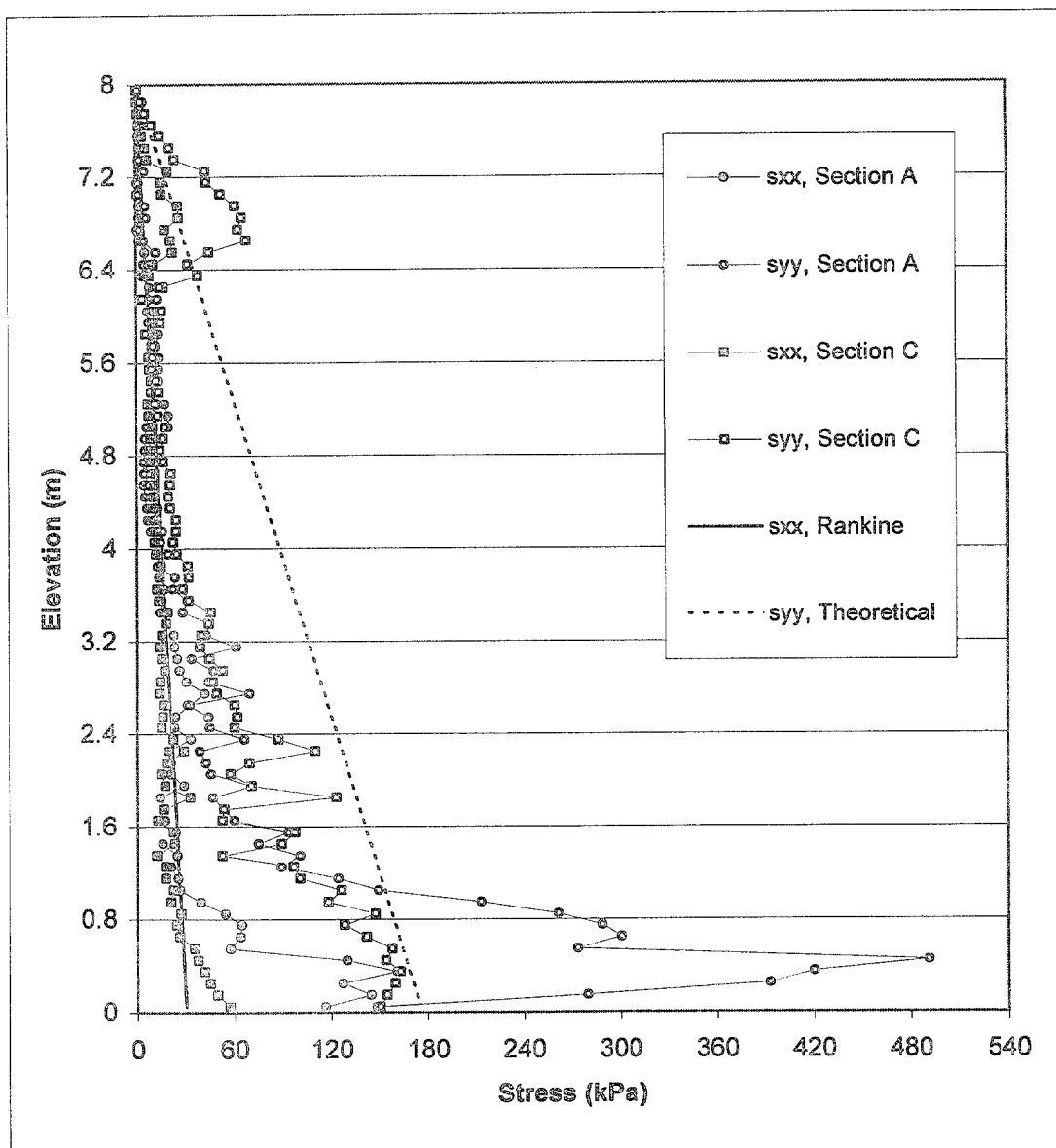
NOTE: Section A is located 0.15 m behind the facing. Section C is located 0.15 m behind the end of reinforcement.

Figure 5.7 Stress Distributions along Sections A and C for Failure State of Case 2 ($s=0.6$ m, $h=4.6$ m, $l/h=0.33$).



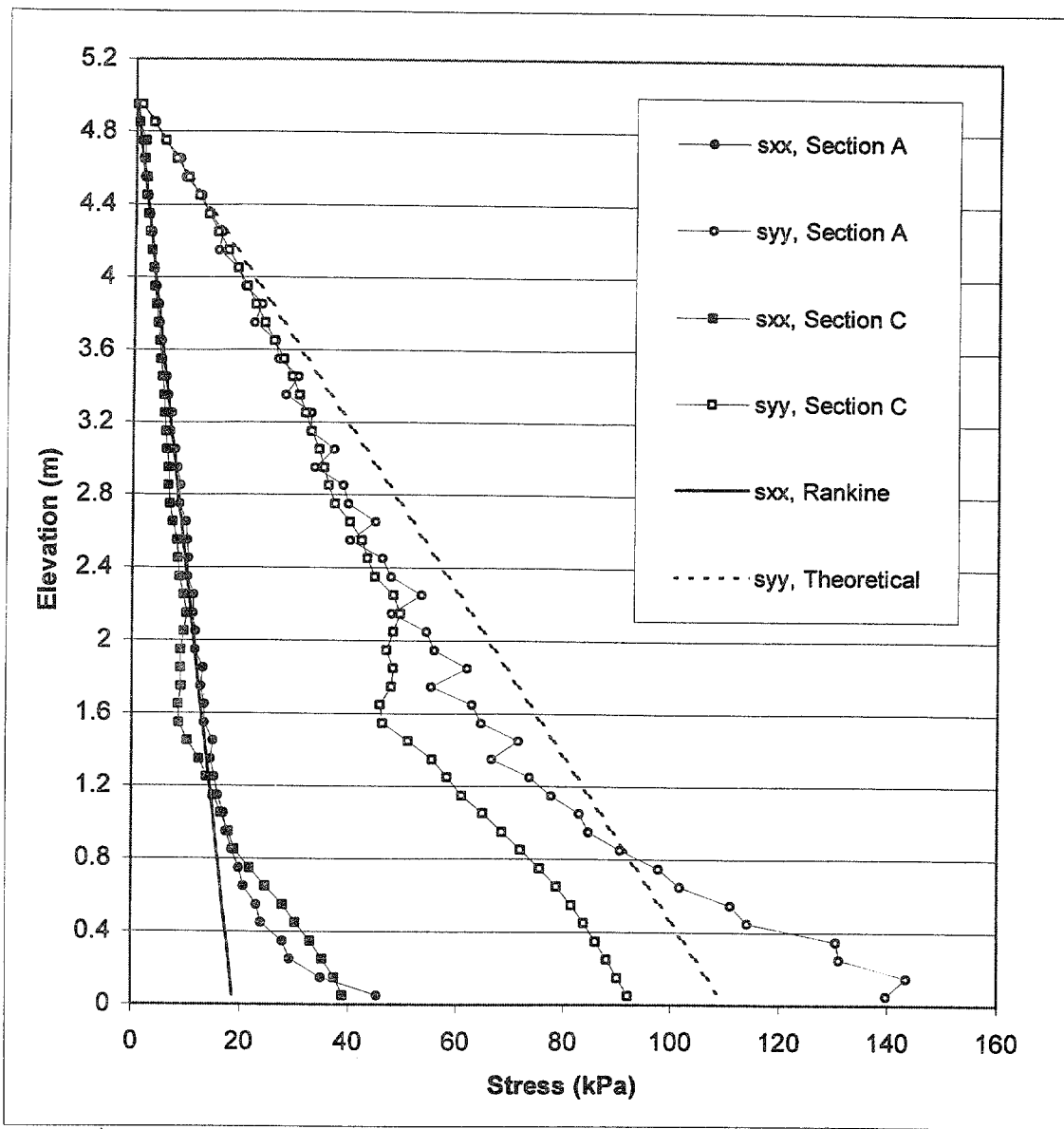
NOTE: Section A is located 0.15 m behind the facing. Section C is located 0.15 m behind the end of reinforcement.

Figure 5.8 Stress Distributions along Sections A and C for Critical State of Case 2 ($s=0.6$ m, $h=4.6$ m, $l/h=0.33$).



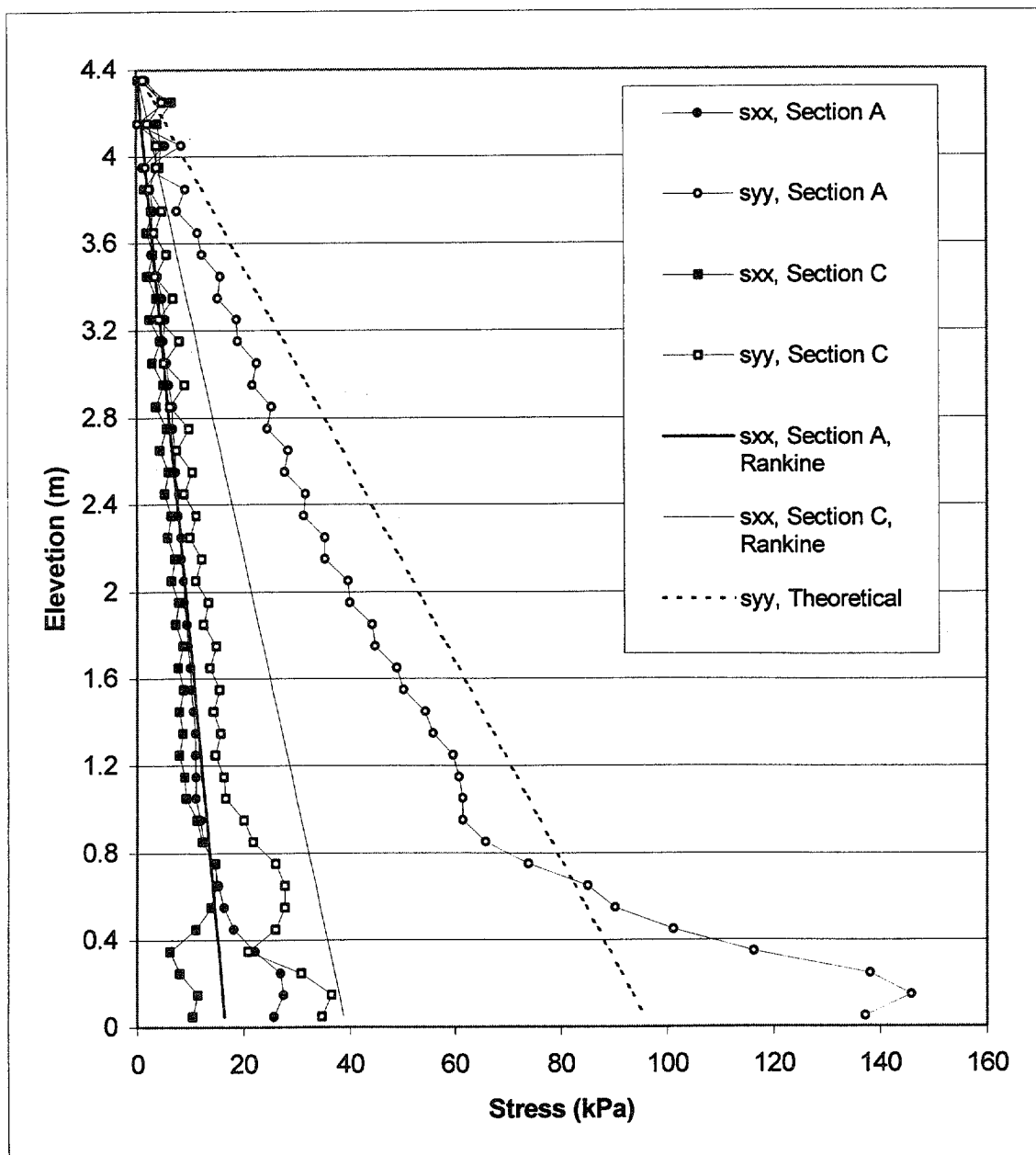
NOTE: Section A is located 0.15 m behind the facing. Section C is located 0.15 m behind the end of reinforcement.

Figure 5.9 Stress Distributions along Sections A and C for Failure State of Case 8-1 ($s=0.4$ m, $h=8.0$ m, $l/h=0.19$).



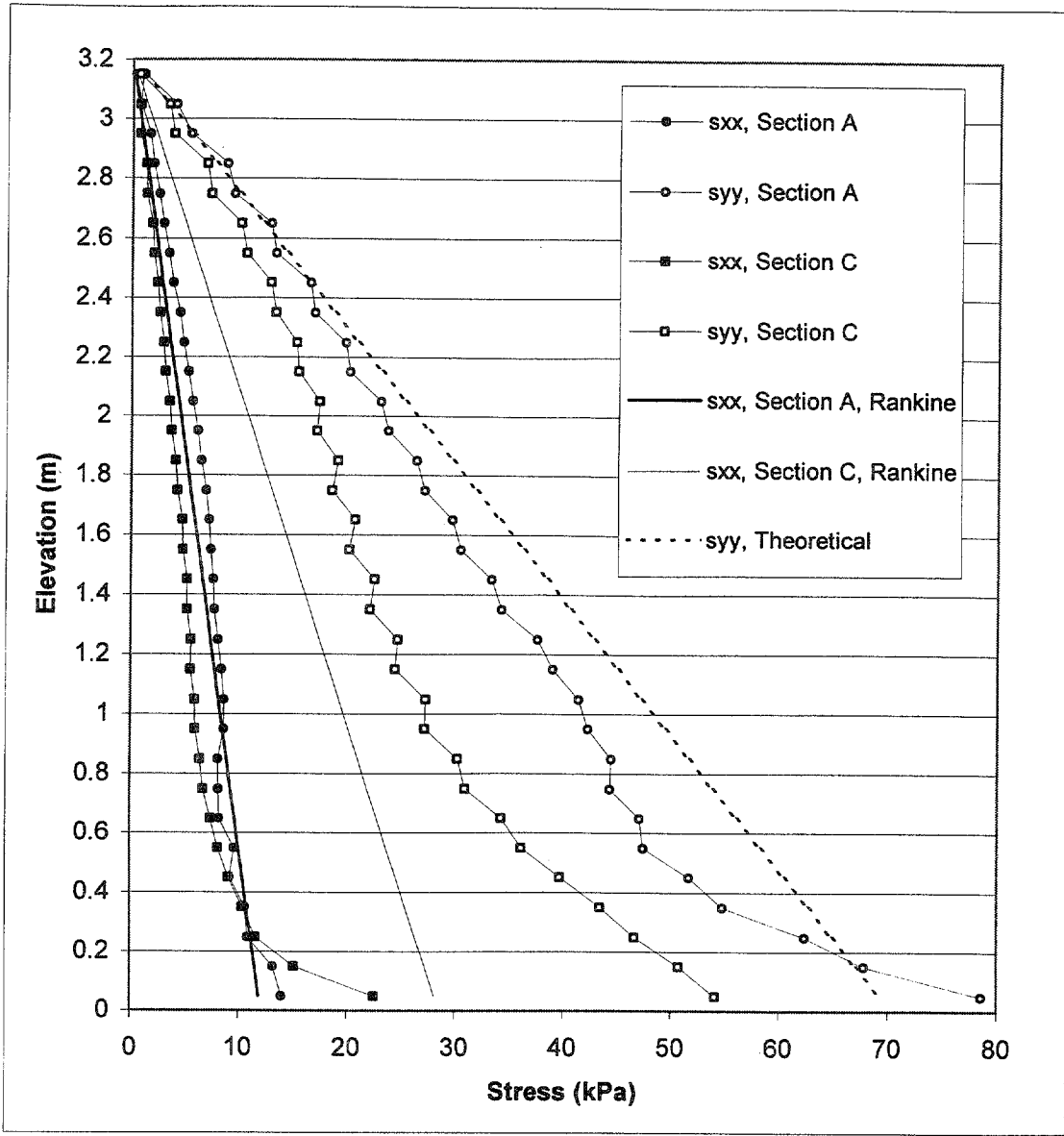
NOTE: Section A is located 0.15 m behind the facing. Section C is located 0.15 m behind the end of reinforcement.

Figure 5.10 Stress Distributions along Sections A and C for Critical State of Case 8-1 ($s=0.4$ m, $h=8.0$ m, $l/h=0.19$).



NOTE: Section A is located 0.15 m behind the facing. Section C is located 0.15 m behind the end of reinforcement.

Figure 5.11 Stress Distributions along Sections A and C for Failure State of Case 10 ($s=0.2$ m, $h=4.4$ m, $I/h=0.34$).



NOTE: Section A is located 0.15 m behind the facing. Section C is located 0.15 m behind the end of reinforcement.

Figure 5.12 Stress Distributions along Sections A and C for Critical State of Case 10 ($s=0.2$ m, $h=4.4$ m, $l/h=0.34$).

Table 5.1 Input Data for AASHTO Analysis Using MSEW 1.1 Program.

Input Data		Case 1 (s=0.4 m)	Case 2 (s=0.6 m)	Case 8-1 (s=0.4 m)	Case 10 (s=0.2 m)
Wall height (m)		6.0	2.6	5.0	3.2
Reinforcement spacing (m)		0.4	0.6	0.4	0.2
Reinforcement length (m)		1.5	1.5	1.5	1.5
Embedded depth (m)		0	0	0	0
Reinforced soil	Unit weight (kN/m ³)	22	22	22	22
	Angle of friction (deg)	45	35	45	45
Retained soil	Unit weight (kN/m ³)	22	22	22	22
	Angle of friction (deg)	45	35	45	25
Foundation soil	Unit weight (kN/m ³)	22	22	22	22
	Angle of friction (deg)	45	35	45	25
	Cohesion (kPa)	1000	1000	1000	0
Ultimate strength of geotextile reinforcement kN/m) in layer	1	2.4	2.2	1.4	4.3
	2	8.2	2.8	3.9	4.3
	3	9.6	1.2	5.1	3.6
	4	9.0	1.0	5.2	3.2
	5	7.1	—	4.9	2.7
Soil-geotextile angle of friction (deg)		35	35	35	35

NOTE: The following cases were selected to represent different failure modes identified with FLAC:

- Case 1 (s=0.4 m)—external mode (direct sliding/overturning).
- Case 2 (s=0.6 m)—connection mode.
- Case 8-1 (s=0.4 m)—compound mode.
- Case 10 (s=0.2 m)—deep-seated mode.

Table 5.2 Results from AASHTO Analysis Using MSEW 1.1 Program

Output Data	Case 1 (s=0.4 m)	Case 2 (s=0.6 m)	Case 8-1 (s=0.4 m)	Case 10 (s=0.2 m)
Factor of safety against direct sliding	2.914	2.981	3.497	1.08
Factor of safety against overturning	1.09 (1.0)	3.68	1.57	1.62
Factor of safety against compound failure	—	—	1.005 (1.0)	—
Factor of safety against deep-seated failure	—	—	—	1.047 (1.0)
Eccentricity (m)	0.69	0.20	0.48	0.46
Factor of safety against bearing capacity	86.40	594.90	449.10	0.38
Meyerhof stress (kPa)	1553.95	78.51	301.80	183.20
Ultimate bearing capacity (kPa)	134254.9	46701.0	135508.6	69.0
Number of layers taken into account in internal stability analysis	9	4	9	15
T_{max} reinforcement force from internal stability analysis (kN/m) in layer	1	8.8 (2.4)	7.0 (2.2)	7.2 (1.4)
	2	8.2 (8.2)	6.4 (2.8)	6.6 (3.9)
	3	7.5 (9.6)	4.3 (1.2)	6.0 (5.1)
	4	6.9 (9.0)	2.4 (1.0)	5.4 (5.2)
	5	6.3 (7.1)	—	4.8 (4.9)
NOTE: Values in brackets correspond to FLAC calculations.				

Table 5.3 Slope of Slip Planes.

Case	Spacings (m)	Slip Surface Slope (deg)					
		Theoretical Value		Failure State		Critical State	
		Rankine	Coulomb	FLAC Value	Slip Surface Type	FLAC Value	Slip Surface Type
1	0.2	67.5	63.4	50	External	54	External
	0.4	67.5	63.4	48	External	58	External
	0.6	67.5	63.4	50	Compound	65	Compound
	0.8	67.5	64.8	43	Internal	62	Internal
	1.0	67.5	64.8	62	Internal	62	Internal
2	0.2	62.5	57.4	43	External	45	External
	0.4	62.5	57.4	42	External	50	External
	0.6	62.5	58.1 (57.4)	42	External	65	Internal
	0.8	62.5	58.1	51	Internal	63	Internal
3	0.2	57.7	57.3	43	Compound	45	Compound
	0.4	57.7	51.3	45	Compound	34	Compound
	0.6	57.7	51.3 (50.3)	43	Compound	Not Clear	Internal
	0.8	57.7	50.3	39	Internal	Not Clear	Internal
4	0.2	67.5	63.4	58	External	60	External
	0.4	67.5	63.4	53	External	59	External
	0.6	67.5	64.8	60	External	60	External
	0.8	67.5	64.8	59	Internal	58	Internal

Table 5.3. Slope of Slip Planes, Continued.

Case	Spacings (m)	Slip Surface Slope (deg)					
		Theoretical Value		Failure State		Critical State	
		Rankine	Coulomb	FLAC Value	Slip Surface Type	FLAC Value	Slip Surface Type
5	0.2	62.5	57.4	46	External	47	External
	0.4	62.5	57.4	48	External	57	External
	0.6	62.5	57.4 (58.1)	52	External	Not Clear	Internal
	0.8	62.5	58.1	68	Internal	49	Internal
6	0.2	57.5	51.3	36	External	44	External
	0.4	57.5	50.3	37	External	Not Clear	Not Clear
7	0.6/0.2	62.5	58.1	48	External	46	External
8-1	0.4	67.5	51.3 (64.8)	46	Compound	53	Compound
8-2	0.4	62.5	57.4	45	Compound	45	Compound
8-3	0.2	57.2	51.3	42	Compound	41	Compound
9	0.2	67.5	63.4	51	External	52	External
10	0.2	57.2	51.3	51	External	62	External
	0.4	57.2	51.3	48	External	54	External
	0.6	57.2/67.5	64.8	51	External	57	Internal
	0.8	67.5	64.8	44	Internal	63	Internal
11	0.2	67.5	63.4	53	External	57	External
12	0.2	67.5	63.4	51	External	56	External
	0.6	62.5	57.4	49	Compound	50	Compound

@Seismicisolation

CHAPTER 6. IMPLICATIONS TO DESIGN

The existing design methodology of MSEWs is based on internal and external stability analysis using limit state methods. Internal stability calculations are based on the assumption that the most critical slip surface will develop through the reinforced soil. This can happen only when the reinforcement spacing is relatively large, and the reinforced soil does not behave as a solid coherent block. However, the relation between the reinforcement spacing and the failure mode is not considered in current design.

With respect to existing design methods for MSEW with modular block facing and geosynthetic reinforcement, the numerical results imply the following:

- MSEW design should use the design methodology of reinforced steep slopes. The identified MSEW failure modes numerically corresponded to the failure mechanisms considered in stability analysis of reinforced steep slopes using limit equilibrium methods: two-part wedge mechanism considered in direct sliding analysis; rotational mechanism considered in deep-seated stability analysis and in compound stability analysis; and log-spiral failure mechanism considered in internal stability analysis (tieback analysis). A comparison between FLAC predictions and MSEW 1.1 calculations according to AASHTO design method showed good agreement between the results. The existing design method was capable to distinguish the modes of failure identified by FLAC analysis especially these due to external instability.
- The critical slip surface always develops behind the reinforced soil when the reinforcement spacing is less than 0.4 m, and the reinforcement stiffness and soil strength are not very low. The reinforced soil behaved as a composite block and no slip surfaces developed within the reinforced soil for models based on typical design values for the reinforcement stiffness and soil strength..
- The length-to-height ratio is lower than 0.7 (the value used in current static design) for walls with small reinforcement spacing on competent foundation. In the analysis, the length-to-height ratio was identified in the range of 0.23-0.34 at the critical state for cases with competent foundation and small reinforcement spacing. The critical length-to-height ratio was larger than 0.4 only for cases with reinforcement spacing larger than 0.6 m and medium or low soil strength. Values close to or larger than 0.7 were identified only for cases that experienced connection mode of failure. However, in these cases, the wall stability is

controlled by other factors and not by the reinforcement length (or length-to-height ratio, respectively).

- The performance of walls with large reinforcement spacing can be improved significantly by increasing the strength of connections (e.g., by using structural connections instead of frictional connections).
- The performance of walls with large reinforcement spacing can be improved significantly by using secondary reinforcement layers at each connection between the primary reinforcement layers. The secondary reinforcement layers have the same effect on wall behavior as the increase of connection strength.
- When the foundation is not competent, the wall stability can be improved by either increasing reinforcement length or decreasing reinforcement spacing.
- The slope of the critical slip surface identified numerically was less than the values calculated by Rankine's and Coulomb's earth pressure theories. For all cases, slip surface slope was closer to the value given by Coulomb's theory, and decreased with failure progression.
- Small reinforcement spacing in MSEW with modular block facing should be considered in cases of incompetent foundation, space constraints, low strength, or frictional connection between modular blocks, and lateral movement limitations.

It must be noted that the design implications mentioned above are based on the numerical results of current study. Further parametric studies that implement experimental data from laboratory and large-scale testing must be conducted to quantify the effects of connection strength, reinforcement stiffness and soil properties on the behavior of MSEWs.

CHAPTER 7. CONCLUSIONS AND RECOMMENDATIONS

The results of numerical analysis of MSEWs with modular block facing and geosynthetic reinforcement using program FLAC have been presented. The emphasis was to identify the effects of reinforcement spacing on wall behavior, considering the effects of soil strength, reinforcement stiffness, connection strength, secondary reinforcement layers, foundation stiffness, and reinforcement length. Parametric studies were conducted on numerical models constructed, layer by layer, up to failure under gravity loading with reinforcement spacing in the range of 0.2–1.0 m, 3 soil types with different soil strength, 2 different foundation conditions with respect to soil stiffness, 3 different connection conditions, and 2 reinforcement stiffness values. The material properties were based on literature data representing typical values used in design practice. The reinforcement length was kept constant, equal to 1.5 m in models investigating the wall response with respect to failure. It was increased to correspond to length-to-height ratio in the range of 0.3–0.5 in models investigating the effects of reinforcement length on wall stability. The most important conclusions are summarized below:

- Four MSEW failure modes were identified numerically: external, deep-seated, compound, and connection mode. They correspond to the following failure mechanisms considered in stability analysis of reinforced steep slopes using limit equilibrium methods: two-part wedge mechanism considered in direct sliding analysis; rotational mechanism considered in deep-seated stability analysis and in compound stability analysis; and log-spiral failure mechanism considered in internal stability analysis (tieback analysis).
- The reinforcement spacing was a major factor in controlling the behavior of MSEWs. Either increasing reinforcement spacing from 0.2 to 1.0 m or decreasing soil strength decreased the wall stability and changed the failure mode from external or deep-seated to compound and connection mode. Two types of spacing were considered: small (less than or equal to 0.4 m) and large (larger than 0.4 m). The failure of walls with large reinforcement spacing was always accompanied by some degree of instability within the reinforced mass. The critical wall height (defined as a general characteristic of wall stability) always increased when the reinforcement spacing decreased. The only exception was observed when the failure was controlled by the strength of foundation soil and the wall failed as a result of deep-seated sliding. In this case, the critical wall height remained the same for models, with reinforcement spacing equal to 0.2 m and 0.4 m (case 10, figure 4.1-b).

- The behavior of walls with small reinforcement spacing was similar to the behavior of a conventional retaining wall. The identified modes of failure were external or deep-seated mode. The analysis of displacement fields, failure zone distributions, grid distortion, and horizontal displacement distributions confirmed that the reinforced soil was internally stable and moved as a block.
- All walls with large reinforcement spacing experienced internal instability to some degree. The predominant mode of failure was the connection mode. The reinforced mass did not move as a block. Movie analysis of failure zone distributions showed that failure zones evolved first in the reinforced soil, initiating large deformations that led to connection breakage. At the critical state, the predominant part of the reinforced soil was at yield in shear or volume, while the backfill was affected minimally. At failure states, the failure zones propagated within the backfill because of the large deformations at the facing. The analysis of displacement fields, grid distortions, and horizontal displacement distributions showed significant deformations in the reinforced soil.
- The change of critical wall height with respect to soil strength demonstrated the effect of soil strength on wall stability. The critical wall height decreased as soil strength decreased. An important observation was that, with smaller reinforcement spacing, the same or higher critical wall height can be achieved with lower strength soil. The effects of soil strength on failure mechanisms were different for the cases with very stiff foundations and the cases with baseline foundations. For the cases with very stiff foundations, deep-seated failure mode was not identified. The decrease of soil strength changed the mode of failure from external to compound mode, or from compound to connection mode.
- Most of the models experienced connection mode of failure when the reinforcement spacing was equal to 0.6 m or larger. The only exception was observed for the cases with reinforcement spacing of 0.6 m, high strength reinforced and backfill soil, and very stiff foundation, which experienced compound mode of failure.
- The decrease of reinforcement stiffness affected the failure mode and stability of walls with small reinforcement spacing by increasing the wall displacements and the possibility of internal instability. For all cases with DR, the critical wall height was less than the critical wall height of the corresponding cases with BR, and the maximum forces in reinforcement were identified either at the connections or close to them. The maximum horizontal displacements for the cases with DR were approximately 2.5–3 times larger than the maximum horizontal displacements of the corresponding cases with BR.

- Connection strength appeared to have insignificant effects on the behavior of walls with small reinforcement spacing. However, it affected the behavior of walls with large reinforcement spacing, i.e., the increase of connection strength decreased wall displacements, improved wall stability, and changed the failure mode. The analysis of cases with high strength soils, very stiff foundations, and different connection strengths and reinforcement spacing showed that the connection strength effects on wall behavior were significant for the cases with large reinforcement spacing. The increase of connection strength of walls with large reinforcement spacing improved global wall stability (i.e., critical wall height increased), decreased wall displacements, and, as a result of the improved local stability at the wall facing, the mode of failure changed from connection to compound. The wall with structural connection experienced compound mode of failure, while the wall with baseline frictional connection experienced connection mode of failure. The change of connection strength did not affect the behavior of walls with small reinforcement spacing significantly. The model with the low strength frictional connection developed larger reinforcement forces and displacements than both the model with structural connection and the model with high strength frictional connection, but the mode of failure and the critical wall height remained the same.
- Foundation stiffness had significant effects on wall response. A very stiff foundation was investigated and compared to foundations with varying strengths. Decreasing the foundation stiffness or strength decreased the wall stability, changed the mode of failure, and increased the displacements and reinforcement forces. For all cases with very stiff foundations, the bottom reinforcement layers were less stressed. Effects of foundation stiffness on failure mechanisms were investigated by changing the stiffness and strength of foundation soil. Foundation properties had significant effects on wall response. Decreasing foundation stiffness or strength decreased the critical wall height, changed the mode of failure, and increased the displacements and reinforcement forces. The artificially high foundation soil stiffness and strength prevented the development of deep-seated mode of failure and increased wall stability. When the foundation soil was changed from baseline to very stiff soil, the cases with small reinforcement spacing that experienced deep-seated mode of failure changed their mode of failure to compound mode. The walls with large reinforcement spacing were more sensitive to the change of foundation properties.

- Increasing the reinforcement length improved wall stability and decreased wall displacements and reinforcement forces. Analysis of stable states of models representing external, compound, and deep-seated failure modes identified that increasing reinforcement length increased wall stability, and decreased wall displacements and reinforcement forces. Increasing the reinforcement length of models that experience connection mode of failure does not affect wall stability.
- Introducing secondary reinforcement layers in a model with large reinforcement spacing changed the mode of failure from connection to compound, improved global wall stability and local stability at the facing, and decreased the displacements and reinforcement forces. Introducing of secondary reinforcement layers in a model with large reinforcement spacing changed the wall behavior significantly. The following effects were identified: mode of failure changed, global wall stability and local stability at the wall facing increased, and displacements and reinforcement forces decreased. The secondary reinforcement layers improved the wall's global stability by improving the local stability at the facing.
- Analysis of models with different soil dilatancies showed that the mode of failure did not change. The model with zero dilation was less stable and experienced larger deformations and larger reinforcement forces. The failure zones were located in narrower bands in the model with zero dilatancy, compared to cases with baseline dilation.
- A comparison between FLAC predictions and MSEW 1.1 calculations according to AASHTO design method showed good agreement between the results. It indicated that the existing design method was capable to distinguish the modes of failure identified by FLAC analysis especially these due to external instability.
- The slope of slip surfaces that developed at the critical and failure states of all models were measured from FLAC plots of failure zone distributions. The slip surfaces were approximated as planes starting from the top of the backfill. The planar approximation was accurate for models that experienced external or connection failure mode. The slip surfaces of models that experienced compound or deep-seated failure modes were nonplanar, and can be approximated more accurately by circular arcs, as in the slope stability analysis. In most cases, the slip surfaces became nonplanar in the zone close to or within the reinforced soil. The slip surface slopes measured from FLAC plots were lower than the values given by Rankine's and Coulomb's earth pressure theories at both critical and failure states. For all cases, FLAC slip surface slope was closer to the value given by Coulomb's theory, and decreased with the progression of failure.

The results of the parametric study clearly show the influence of reinforcement spacing, connection strength, reinforcement stiffness, and soil properties on the behavior of MSEWs with modular block facing and geosynthetic reinforcement. In general, the MSEWs can sustain higher loads with less deformation when reinforcement spacing is smaller and connection load is higher. Since the emphasis of the current study is on the effects of reinforcement spacing on wall behavior, the study was designed to investigate and quantify these effects with respect to failure. The effects of connection strength and reinforcement stiffness were investigated, but only qualitative evaluation of their effects are possible.

Further parametric studies that implement experimental data from laboratory and large-scale tests must be conducted to quantify the effects of connection strength, reinforcement stiffness, and soil properties such as soil stiffness and dilatancy on the behavior of MSEWs.

The reported numerical simulations supported by laboratory and large-scale tests and further numerical analysis may be used to verify or modify the existing methods of analysis and MSEW design with modular block and close reinforcement spacing.

@Seismicisolation

APPENDIX. TYPICAL INPUT DATA FILE

```

title
Effects of Geosynthetic Reinforcement Spacing on the Behavior of MSEW
;
define set_parameters
;
nstep='t5';
home_dir='c:\chris\'';
fmov=string(home_dir)+'flac'+string(nstep)+'.mov'
command
movie file @fmov
end_command
;
;           WALL DIMENSIONS AND GRID DENSITY PARAMETERS
hw=15
k1=0.6
lr=k1*hw
lra=10
lbc=5
nsl=2
;
;           MATERIAL PROPERTY PARAMETERS
fri_g=45
ni_g=0.3
emod_gi=60000.0
smod_gi=emod_gi/(2.0*(1.0+ni_g))
bmod_gi=emod_gi/(3.0*(1.0-2.0*ni_g))
;
fri_s=45
ni_s=0.3
emod_si=60000.0
smod_si=emod_si/(2.0*(1.0+ni_s))
bmod_si=emod_si/(3.0*(1.0-2.0*ni_s))
;
fri_b=45
ni_b=0.3
emod_bi=60000.0
smod_bi=emod_bi/(2.0*(1.0+ni_b))
bmod_bi=emod_bi/(3.0*(1.0-2.0*ni_b))
;
emod_cb=600000.0
ni_cb=0.15
smod_cb=emod_cb/(2.0*(1.0+ni_cb))

```

```

bmod_cb=emod_cb/(3.0*(1.0-2.0*ni_cb))
;
mod_cab=1e6
stif_gr=smod_si
stre_gr=100
nstif_if=bmod_cb
sstif_if=smod_si
;
nl=hw/0.2
tnsl=nl*nsl
ah=0.2/nsl
nz=lr/ah
nz1=lra/ah
;
nzs=nz+nz1+43
nzy=(nsl+2)*nl+20
ngx = nz + 1
ngy = nzy + 1
;
c_x_1 = 5.2 + lr
c_x_2 = 10.2 + lr + lra
c_x_3 = 5.2 + lr + lra
c_y_1 = 5 + hv
;
z_i_1 = 22 +(lr+lra)/0.1
z_i_2 = z_i_1 + 1
z_i_3 = z_i_1 + 20
z_i_4 = nz + 22
z_i_5 = z_i_4 + 1
z_i_6 = nz + nz1 + 24
z_i_7 = nz + nz1 + 43
z_i_8 = nz + nz1 + 22
z_i_9 = nz + nz1 + 23
z_j_1 = 19+(nsl+2)*nl
z_j_2 = 21+tnsl
z_j_3 = 21+hw/0.1
;
g_i_1 = z_i_1+1
g_i_2 = z_i_3+1
g_i_3 = z_i_5
g_i_4 = z_i_6
g_i_5 = z_i_6 + 1

```

```

g_i_6 = z_i_9
g_j_1 = 20+(nsl+2)*nl
g_j_2 = 22+tnsl
g_j_3 = 22+hw/0.1
cx1=10.5 + lr + lra
end;           "set_paremetes"
;
set_parameters
movie on
;
define e_modulus_ground
;
loop ig (1,z_i_3)
loop jg (1,20)
;
ag=abs(sxx(ig,jg))
agg=sqrt(ag)
ex_1(ig,jg)=20720000*agg
ex_2(ig,jg)=ex_1(ig,jg)/(2.0*(1.0+ni_g))
ex_3(ig,jg)=ex_1(ig,jg)/(3.0*(1.0-2.0*ni_g))
smod_g=ex_2(ig,jg)
bmod_g=ex_3(ig,jg)
;
command
prop bulk=bmod_g shear=smod_g i=ig j=jg
end_command
endloop
endloop
end;           "e_modulus_ground"
;
define e_modulus_resoil
;
loop ir (23,z_i_8)
loop jr (22,wtzj)
;
ar=abs(sxx(ir,jr))
arr=sqrt(ar)
ex_1(ir,jr)=2072*arr
ex_2(ir,jr)=ex_1(ir,jr)/(2.0*(1.0+ni_s))
ex_3(ir,jr)=ex_1(ir,jr)/(3.0*(1.0-2.0*ni_s))
smod_s=ex_3(ir,jr)
bmod_s=ex_2(ir,jr)

```

```

;
command
prop bulk=bmod_s shear=smod_s i=ir j=jr
end_command
end_loop
end_loop
end;           "e_modulus_resoil"
;
define e_modulus_backfill
;
loop ib (z_i_6,z_i_7)
loop jb (22,ba_tzj)
;
ab=abs(min(sxx(ib,jb),szz(ib,jb)))
abb=sqrt(ab)
ex_1(ib,jb)=2072*abb
ex_2(ib,jb)=ex_1(ib,jb)/(2.0*(1.0+ni_b))
ex_3(ib,jb)=ex_1(ib,jb)/(3.0*(1.0-2.0*ni_b))
smod_b=ex_2(ib,jb)
bmod_b=ex_3(ib,jb)
;
command
prop bulk=bmod_b shear=smod_b i=ib j=jb
end_command
end_loop
end_loop
end;           "e_modulus_backfill"
;
window -0.25 cx1 -0.25 cx1
;
;
GROUND: GRID GENERATION & MODELLING
grid ngx, ngy
model mohr i=1,z_i_3 j=1,20
prop dens=2.201 bulk=bmod_gi shear=smod_gi fric=fri_g dil=15 coh=1000 &
i=1,z_i_3 j=1,20
gen 0,0 0,5 5,5 5,0 rat 0.91878121,0.91878121 i=1,21 j=1,21
gen same same 5,2,5 5,2,0 rat 1, 0.981878121 i=21,23 j=1,21
gen same same c_x_3,5 c_x_3,0 rat 1, 0.91878121 i=23,g_i_1 j=1,21
gen same same c_x_2,5 c_x_2,0 rat 1.0883984,0.91878121 i=g_i_1,g_i_2 j=1,21
;

```

```

; GROUND: BOUNDARY CONDITIONS
fix x i=1
fix y j=1
fix x i=g_i_2 j=1,21
;
; GROUND: INITIAL STRESSES
set gravity 9.81
ini sxx -33 var 0,33 j=1,20
ini syy -100 var 0,100 j=1,20
ini szz -33 var 0,33 j=1,20
e_modulus_ground
;
; HISTORIES
his 1 u
his 2 ydis    i=38 j=20
his 3 ex_2    i=38 j=20
his 4 ex_3    i=38 j=20
;
define ground_equilibrium
;
grfname=string(home_dir)+'gr'+string(nstep)+'.sav'
prfname=string(home_dir)+'gr'+string(nstep)+'.pri'
;
command
prop tens 1e5 coh 1e5
solve srat 0.01
prop tens 0 coh 0
prop coh=1000 i=1,z_i_2 j=1,20
solve srat 0.01
end_command
;
e_modulus_ground
end;           "ground_equilibrium"
;
ground_equilibrium
;
ini xdis 0 j=1,21
ini ydis 0 j=1,21
ini x 5.0 y 5.0 i=21 j=21
ini x 5.2 y 5.0 i=23 j=21
ini x c_x_3 y 5.0 i=g_i_1 j=21
;

```

```

save @grfname
;set log on
;set log @prfname
;print xdisp i=25
;set log off
;
define one_layer_parameters
;
;           parameters for block generation
bbgj=22+(layer-1)*(nz+2)
btgj=bbgj+ns1
bbzj=bbgj
btzj=btgj-1
bfgi=17
bfzi=bfgi
;
y1=5+(layer-1)*0.2
y2=y1+0.2
;
;           parameters for wall generation
wbzj=22+(layer-1)*ns1
wtzj=wbzj+ns1-1
wbgj=wbzj
wtgj=wtzj+1
;
;           parameters for backfill generation
ba_bzj=22+(layer-1)*2
ba_tzj=ba_bzj+2
ba_bgj=ba_bzj
ba_tgj=ba_tzj+1
;
end;          "one_layer_parameters"
;
define first_layer_generation
;
command
;           concrete block generation
m e i=bfzi,21 j=bbzj,btzj
gen 5,y1 5,y2 5.2,y2 5.2,y1 i=bfgi,22 j=bbgj,btgj
prop d=2.199 b=bmod_cb s=smod_cb i=bfzi,21 j=bbzj,btzj
;

```

```

;           a layer of wall generation
m m i=23,z_i_8 j=wbzj,wtzj; wall
gen 5.2,y1 5.2,y2 c_x_3,y2 c_x_3,y1 i=23,g_i_6 j=wbgj,wtgj
prop d=2.2 bulk=bmod_si shear=smod_si fric=fri_s dil=15 &
i=23,z_i_8 j=wbzj,wtzj
;
;           a layer of backfill generation
m m i=z_i_6,z_i_7 j=ba_bzj,ba_tzj; backfill
gen c_x_3,y1 c_x_3,y2 c_x_2,y2 c_x_2,y1 rat 1.0883984,1 &
i=g_i_4,g_i_5 j=ba_bgj,ba_tgj
prop dens=2.2 bulk=bmod_bi shear=smod_bi fric=fri_b dil=15 &
i=z_i_6,z_i_7 j=ba_bzj,ba_tzj
;
att as fr g_i_6,wbgj to g_i_6,wtgj bs fr g_i_4,ba_bgj to g_i_4,ba_tgj
fix x i=g_i_5 j=ba_bgj,ba_tgj
;
end_command
;
end;          "first_layer_generation"
;
define one_layer_generation
;
command
;           concrete block generation
m e i=bfzi,21 j=bbzj,btzj
gen x1,y11 x6,y6 x7,y7 x2,y22 i=bfgi,22 j=wbgj,wtgj
prop d=2.199 b=bmod_cb s=smod_cb i=bfzi,21 j=bbzj,btzj
;
;           a layer of wall generation
m m i=23,z_i_8 j=wbzj,wtzj; wall
gen x3,y3 x8,y8 x9,y9 x4,y4 i=23,g_i_6 j=wbgj,wtgj
prop d=2.2 b=bmod_si s=smod_si fric=fri_s dil=15 i=23,z_i_8 j=wbzj,wtzj
;
;           a layer of backfill generation
m m i=z_i_6,z_i_7 j=ba_bzj,ba_tzj
gen x5,y5 x10,y10 c_x_2,y2 c_x_2,y1 rat 1.0883984,1 &
i=g_i_4,g_i_5 j=ba_bgj,ba_tgj
prop d=2.2 b=bmod_bi s=smod_bi fric=fri_b dil=15 &
i=z_i_6,z_i_7 j=ba_bzj,ba_tzj
att as fr g_i_6,wbgj to g_i_6,wtgj bs fr g_i_4,ba_bgj to g_i_4,ba_tgj
fix x i=g_i_5 j=ba_bgj,ba_tgj
end_command

```

```

;
end;           "one_layer_generation"
;
define top_coord_upgrade
;
x1=x(bfgi,btgj)
y11=y(bfgi,btgj)
x2=x(22,btgj)
y22=y(22,btgj)
x3=x(23,wtgj)
y3=y(23,wtgj)
x4=x(g_i_6,wtgj)
y4=y(g_i_6,wtgj)
x5=x(g_i_4,ba_tgj)
y5=y(g_i_4,ba_tgj)
;
end;           "top_coord_upgrade"
;
define define_top_coord
;
x6=x1-y22+y11
y6=y11+x2-x1
x7=x2-y22+y11
y7=y22+x2-x1+1
x8=x7
y8=y7
x9=x4
y9=y7
x10=x4
y10=y7
;
end;           "define_top_coord"
;
;
BEAM & CABLE PROPERTIES
struct prop=2 area=0.002 peri=2 e=mod_cab yield=200 d=2.1
struct prop=2 kbond=stif_gr sbond=stre_gr sfriction=35
struct prop=3 area=0.002 e=mod_cab i=6.67e-10 d=2.1
;
define sos
;
fname=string(home_dir)+'l'+string(nstep) +'_'+string(layer)+'.sav'
fnameend=string(home_dir) +'end'+string(nstep)+'.sav'

```

```

prfname=string(home_dir)+'l'+string(nstep) +'_'+string(layer)+'.pri'
;
command
solve srat 0.01
end_command
;
command
save @fname
;set log on
;set log @prfname
;print xdisp i=25
;set log off
end_command
;
e_modulus_ground
e_modulus_resoil
e_modulus_backfill
;
end;           "sos" = solve & save
;
define wall_construction
;
h_lbc=lbc*0.2
nl1_f=(hw-0.2)/h_lbc
nl1=int(nl1_f)
h_top=hv-0.2-nl1*h_lbc
if h_top=0 then
tnc=nl1
else
tnc=nl1+1
endif
nrl=1
;
layer=1
;
one_layer_parameters
first_layer_generation
;
command
att as fr 23,21 to g_i_1,21 bs fr 23,22 to g_i_6,22
att as fr g_i_1,21 to g_i_2,21 bs fr g_i_6,22 to g_i_5,22
int 1 as fr 19,21 to 24,21 bs long fr bfgi,btgj to 22,btgj

```

```

int 1 f 30 kn nstif_if ks sstif_if coh 0; tbond 30
int 2 as fr 22,bbgj to 22,btgj bs fr 23,wbgj to 23,wtgj
int 2 f 30 kn nstif_if ks sstif_if coh 0; tbond 30
end_command
;
sos
top_coord_upgrade
b1e_no=6
;
command
struct beam begin x1,y11 end x2,y2 seg=5 prop=3
struct node range 1 6 pin
struct cable begin no b1e_no end c_x_1,y2 seg=nz prop=2
int 3 as fr no b1e_no to no 1 bs fr 22,btgj to bfgi,btgj
int 3 f 30 kn nstif_if ks sstif_if coh 0; tbond 30
end_command
;
tot_nu_int=3
;
loop layer (2,nl)
;
top=1+nrl*lbc
bottom=top-lbc+1
;
if top=bottom then
;
one_layer_parameters
define_top_coord
one_layer_generation
;
bbf_no=(nz+6)*(layer-1)+1
bbb_no=bbf_no+5
btf_no=(nz+6)*(layer-2)+1
btb_no=btf_no+5
b_gj=bbgj-2
b_gjb=bbgj-nsl-2
f_1=(layer-2)*5+4
f_2=f_1+1
f_3=f_1+2
f_4=f_1+3
f_5=f_1+4
tot_nu_int=f_5

```

```

;
command
int f_1 as fr no bbf_no to no bbb_no bs fr bfgi,bbgj to 22,bbgj
int f_1 f 30 kn nstif_if ks sstif_if coh 0; tbond 30
int f_2 as fr 22,bbgj to 22,btgj bs fr 23,wbgj to 23,wtgj
int f_2 f 30 kn nstif_if ks sstif_if coh 0; tbond 30
int f_3 as fr bfgi,bbgj to 22,bbgj bs fr bfgi,b_gj to 22,b_gj
int f_3 f 30 kn nstif_if ks sstif_if coh 0; tbond 30
int f_4 as fr 23,wbgj to 23,wtgj bs fr 22,b_gjb to 22,b_gj
int f_4 f 30 kn nstif_if ks sstif_if coh 0; tbond 30
end_command
;
sos
top_coord_upgrade
;
command
stru beam begin x6,y6 end x7,y7 seg 5 prop 3
stru cable begin no btb_no end c_x_1,y9 seg nz prop 2
int f_5 as fr no btb_no to no btf_no bs fr 22,btgj to bfgi,btgj
int f_5 f 30 kn nstif_if ks sstif_if coh 0; tbond 30
end_command
nrl=nrl+1
;
else
;
if layer=bottom then
;
one_layer_parameters
define_top_coord
one_layer_generation
;
bbf_no=(nz+6)*(nrl-2)+1
bbb_no=bbf_no+5
b_gj=bbgj-2
b_gjb=bbgj-nsl-2
f_6=tot_nu_int+1
f_7=f_6+1
f_8=f_6+2
f_9=f_6+3
tot_nu_int=f_9
;

```

```

command
int f_6 as fr no bbf_no to no bbb_no bs fr bfgi,bbgj to 22,bbgj
int f_6 f 30 kn nstif_if ks sstif_if coh 0; tbond 30
int f_7 as fr 22,bbgj to 22,btgj bs fr 23,wbgj to 23,wtgj
int f_7 f 30 kn nstif_if ks sstif_if coh 0; tbond 30
int f_8 as fr bfgi,bbgj to 22,bbgj bs fr bfgi,b_gj to 22,b_gj
int f_8 f 30 kn nstif_if ks sstif_if coh 0; tbond 30
int f_9 as fr 23,wbgj to 23,wtgj bs fr 22,b_gjb to 22,b_gj
int f_9 f 30 kn nstif_if ks sstif_if coh 0; tbond 30
end_command
;
sos
top_coord_upgrade
;
else
;
if layer<top then
;
one_layer_parameters
define_top_coord
one_layer_generation
;
b_gj=bbgj-2
b_gjb=bbgj-nsl-2
f_10=tot_nu_int+1
f_11=f_10+1
f_12=f_10+2
tot_nu_int=f_12
;
command
int f_10 as fr bfgi,b_gj to 22,b_gj bs fr bfgi,bbgj to 22,bbgj
int f_10 f 30 kn nstif_if ks sstif_if coh 0; tbond 30
int f_11 as fr 22,bbgj to 22,btgj bs fr 23,wbgj to 23,wtgj
int f_11 f 30 kn nstif_if ks sstif_if coh 0; tbond 30
int f_12 as fr 23,wbgj to 23,wtgj bs fr 22,b_gjb to 22,b_gj
int f_12 f 30 kn nstif_if ks sstif_if coh 0; tbond 30
end_command
;
sos
top_coord_upgrade
;
else

```

```

;
one_layer_parameters
define_top_coord
one_layer_generation
b_gj=bbgj-2
b_gjb=bbgj-nsl-2
tbf_no=(nz+6)*nrl+1
tbb_no=tbf_no+5
f_13=tot_nu_int+1
f_14=f_13+1
f_15=f_13+2
f_16=f_13+3
tot_nu_int=f_16
;
command
int f_13 as fr bfgi,b_gj to 22,b_gj bs fr bfgi,bbgj to 22,bbgj
int f_13 f 30 kn nstif_if ks sstif_if coh 0; tbond 30
int f_14 as fr 22,bbgj to 22,btgj bs fr 23,wbgj to 23,wtgj
int f_14 f 30 kn nstif_if ks sstif_if coh 0; tbond 30
int f_15 as fr 23,wbgj to 23,wtgj bs fr 22,b_gjb to 22,b_gj
int f_15 f 30 kn nstif_if ks sstif_if coh 0; tbond 30
end_command
;
sos
top_coord_upgrade
;
command
stru beam begin x6,y6 end x7,y7 seg 5 prop 3
stru cable begin no tbb_no end c_x_1,y9 seg nz prop 2
int f_16 as fr no tbb_no to no tbf_no bs fr 22,btgj to bfgi,btgj
int f_16 f 30 kn nstif_if ks sstif_if coh 0; tbond 30
end_command
;
nrl=nrl+1
;
endif
endif
endif
endloop
end;           "wall_construction"
;

```

```
wall_construction  
solve srat 0.01  
save @fnameend  
;  
; = END OF FILE =
```

@Seismicisolation

REFERENCES

Standard Specifications for Highway Bridges, American Association of State Highway and Transportation Officials, Washington, DC, 1998.

Mechanically Stabilized Earth Walls (MSEW), Version 1.1, ADAMA Engineering, Inc., Newark, DE, 1998.

Bathurst, R.J. and Hatami, K., *Seismic Response Analysis of a Geosynthetic-Reinforced Soil Retaining Wall*, Geosynthetic International, 1998, Vol. 5, No. 1–2, pp. 127–166.

Bathurst, R.J. and Hatami, K., *Earthquake Response Analysis of Reinforced-Soil Walls Using FLAC*, *FLAC and Numerical Modeling in Geomechanics*, Detournay, C. and Hart, R., Eds., Proceedings of the International FLAC Symposium on Numerical Modeling in Geomechanics, Minneapolis, MN, 1999, pp. 407–415.

Bathurst, R.J. and Cai, Z., *Pseudo-Static Seismic Analysis of Geosynthetic-Reinforced Retaining Walls*, Geosynthetics International, 1995, Vol. 2, No. 5, pp. 787–831.

Clark, I., personal communications, 1999–2000.

Das, B.M., 1999, *Principles of Foundation Engineering*, Brooks/Cole Publishing Company, 862 pp.

Elias, V. and Christopher, B.R., *Mechanically Stabilized Earth Walls and Reinforced Steep Slopes, Design and Construction Guidelines*, Federal Highway Administration Demonstration Project 82, Report No. FHWA-SA-96-071, Washington, DC, 1997.

Hatami, K. and Bathurst, R.J., *Frequency Response Analysis of Reinforced-Soil Retaining Walls*, Proceedings of the 8th Canadian Conference of Earthquake Engineering, Vancouver, Canada, 1999, pp. 341–346.

Fast Lagrangian Analysis of Continua (FLAC), Version 3.40, Itasca Consulting Group, Inc., Minneapolis, MN, 1998.

Lee, W.F., *Distributions of Lateral Earth Pressure and Reinforcement Tension Inside the Geosynthetic Reinforced Soil Retaining Walls*, Conference Proceedings of Geosynthetics 1999, Boston, MA, 1999, Volume 2, pp. 651–660.

Leshchinsky, D., Kaliakin, V., Bose, P., and Collin, J., *Failure Mechanism in Geogrid-Reinforced Segmental Walls: Experimental Implications, Soils and Foundations*, (Japanese Society of Soil Mechanics and Foundation Engineering), 1994, Vol. 34, No. 4, pp. 33–41.

Leshchinsky, D., *Design Procedures for Geosynthetic Reinforced Steep Slopes*, Technical Report REMR-GT-23, U.S. Army Corps of Engineers, Washington, DC, 1997.

Leshchinsky, D., *Stability of Geosynthetic Reinforced Steep Slopes*, Keynote lecture, Proceedings of the International Symposium on Slope Stability Engineering IS-Shikoku 1999, Japan, 1999, Volume I, Yagi, N., Yamagami, T., and Jiang, J.C., Eds., Balkema, Rotterdam, pp. 49–66.

Ling, H.I., Cardany, C.P., Sun, L-X., and Hashimoto, H., *Finite Element Study of a Geosynthetic-Reinforced Soil Retaining Wall with Concrete-Block Facing*, Geosynthetics International, 2000, Vol. 7, No. 2, pp. 137–162.

Earth Retaining Structures, Reference Manual, Federal Highway Administration, FHWA-NHI-99-015, Washington, DC, 1999.

Geotechnical Engineering Circular No. 2, Earth Retaining Systems, Federal Highway Administration, FHWA-SA-96-038, Washington, DC, 1996.

Wong, K.S., and Duncan, J.M., 1974, *Hyperbolic Stress-Strain Parameters for Nonlinear Finite Element Analysis of Stresses and Movements in Soil Masses*, National Science Foundation, Report No. TE-74-3, 1974, 90 p.

@Seismicisolation

@Seismicisolation

@Seismicisolation



Recycled
Recyclable

HRDI-06/09-03(600)E

@ Seismicisolation